



MISSOURI
S&T

CENTER FOR TRANSPORTATION INFRASTRUCTURE AND SAFETY

Recycled Concrete Aggregate (RCA) for Infrastructure Elements

by

Jeffery S. Volz, SE, PE, PhD (Principal Investigator)

Kamal H. Khayat, PhD (Co-Principal Investigator)

Mahdi Arezoumandi

Jonathan Drury

Seyedhamed Sadati

Adam Smith

Amanda Steele



**NUTC
R312**

**A National University Transportation Center
at Missouri University of Science and Technology**

Disclaimer

The contents of this report reflect the views of the author(s), who are responsible for the facts and the accuracy of information presented herein. This document is disseminated under the sponsorship of the Department of Transportation, University Transportation Centers Program and the Center for Transportation Infrastructure and Safety NUTC program at the Missouri University of Science and Technology, in the interest of information exchange. The U.S. Government and Center for Transportation Infrastructure and Safety assumes no liability for the contents or use thereof.

Technical Report Documentation Page

1. Report No. NUTC R312	2. Government Accession No.	3. Recipient's Catalog No.	
4. Title and Subtitle Recycled Concrete Aggregate (RCA) for Infrastructure Elements	5. Report Date July 2014		6. Performing Organization Code
	8. Performing Organization Report No. Project #00040138		
7. Author/s Jeffery S. Volz, SE, PE, PhD (Principal Investigator), Kamal H. Khayat, PhD (Co-Principal Investigator) Mahdi Arezoumandi, Jonathan Drury, Seyedhamed Sadati Adam Smith, Amanda Steele	9. Performing Organization Name and Address Center for Transportation Infrastructure and Safety/NUTC program Missouri University of Science and Technology 220 Engineering Research Lab Rolla, MO 65409		
12. Sponsoring Organization Name and Address U.S. Department of Transportation Research and Innovative Technology Administration 1200 New Jersey Avenue, SE Washington, DC 20590	10. Work Unit No. (TRAIS)		11. Contract or Grant No. DTRT06-G-0014
	13. Type of Report and Period Covered Final		
14. Sponsoring Agency Code			15. Supplementary Notes
16. Abstract <p>With a growing demand for new construction and the need to replace infrastructure stretched beyond its service life, society faces the problem of an ever-growing production of construction and demolition waste. The Federal Highway Administration (FHWA) estimates that two billion tons of new aggregate are produced each year in the United States. This demand is anticipated to increase to two and a half billion tons each year by 2020. With such a high demand for new aggregates, the concern arises of the depletion of current sources of natural aggregates and the availability of new sources. Similarly, construction waste produced in the United States is expected to increase. From building demolition alone, the annual production of construction waste is estimated to be 123 million tons (FHWA). Currently, this waste is most commonly disposed of in landfills.</p> <p>To address both the concern of increasing demand for new aggregates and increasing production of waste, many states have begun to recognize that a more sustainable solution exists in recycling waste concrete for use as aggregate in new concrete, or recycled concrete aggregate (RCA). This solution helps address the question of how to sustain modern construction demands for aggregates as well as helps to reduce the amount of waste that enters already over-burdened landfills. Many states have begun to implement RCA in some ways in new construction. For instance, forty-one states have recognized the many uses of RCA as a raw material, such as for rip-rap, soil stabilization, pipe bedding, and even landscape materials. Thirty-eight states have gone a step further in integrating RCA into roadway systems for use as aggregate course base material. However, only eleven states have begun using RCA in Portland cement concrete for pavement construction. Furthermore, at the start of this research project, there were no acceptable standards or guidelines in the U.S. for utilizing RCA in structural concrete.</p> <p>The objective of this research was to determine the implications of using RCA in the production of new concrete. Specifically, the study evaluated the fresh and hardened properties, durability, and structural behavior of concrete containing RCA and, based on these results, developed guidelines on its use in infrastructure elements for MoDOT.</p>			
17. Key Words Aggregate, Cement, Concrete, Durability, Fresh Properties, Mix Design, Recycled Concrete Aggregate, Reinforcing Bond, Reinforced Concrete, Shear Behavior, Sustainability.	18. Distribution Statement No restrictions. This document is available to the public through the National Technical Information Service, Springfield, Virginia 22161.		
19. Security Classification (of this report) unclassified	20. Security Classification (of this page) unclassified	21. No. Of Pages 488	22. Price

FINAL Report

**Recycled Concrete Aggregate (RCA) for
Infrastructure Elements**

By

Jeffery S. Volz, SE, PE, PhD (Principal Investigator)

Kamal H. Khayat, PhD (Co-Principal Investigator)

Mahdi Arezoumandi

Jonathan Drury

Syedhamed Sadati

Adam Smith

Amanda Steele

Missouri University of Science and Technology, Rolla, Missouri

July 2014

EXECUTIVE SUMMARY

On behalf of the Missouri Department of Transportation (MoDOT), Missouri University of Science and Technology (Missouri S&T) completed a research study on recycled concrete aggregate (RCA) derived from materials indigenous to the State of Missouri. The report, entitled *Recycled Concrete Aggregate (RCA) for Infrastructure Elements*, consists of a summary report followed by five detailed technical reports. Taken together, these reports document the background, detailed approaches, experimental procedures and processes, results, findings, conclusions, and recommendations of the study.

The research work plan included nine tasks consisting of the following: (1) Task 1: Literature Review, (2) Task 2: RCA Characterization, (3) Task 3: Mix Development & Fresh Concrete Properties, (4) Task 4: Hardened Mechanical Properties, (5) Task 5: Durability Performance, (6) Task 6: Bond and Development Length, (7) Task 7: Full Scale Specimen Tests, (8) Task 8: Recommendations & Specifications for Implementing RCA in Concrete, and (9) Task 9: Value to MoDOT and Stakeholders to Implementing RCA in Concrete.

Based on the results of Tasks 1 through 7, the researchers recommend the implementation of RCA in concrete for construction of transportation-related infrastructure in the State of Missouri. However, the investigators also recommend initially limiting the RCA replacement levels to 50% in order to prevent any decreased performance compared to conventional concrete. Higher RCA replacement levels are possible but will depend on the specific application.

Concrete recycling protects natural resources and eliminates the need for disposal by using readily available concrete as an aggregate source for new concrete, including in-place recycling. Recycled concrete is less expensive than virgin aggregate sources, and its use would remove a sizeable amount of material from landfills, turning a waste product into a viable construction material. This value aligns with both MoDOT's Tangible Result of being environmentally and socially responsible and MoDOT's Research Need for strategies to reduce energy consumption. The results presented in this research report provide the methods, standards, and guidelines necessary to implement RCA in the construction of transportation infrastructure within the State of Missouri, turning a waste product into a viable construction material.

ACKNOWLEDGEMENTS

The authors would like to acknowledge the many individuals and organizations that made this research project possible. First and foremost, the authors wish to extend a very sincere thank you to the Missouri Department of Transportation (MoDOT). In addition to their financial support, the authors appreciate MoDOT's vision and commitment to recycling and using innovative materials in the construction and maintenance of Missouri's transportation network. In particular, the success of this project would not have been possible without the inspiration, guidance, and patience of Ms. Jennifer Harper. The authors also wish to extend a sincere thank you to MoDOT's Technical Advisory Group for their thorough review of the draft final report and many insightful comments and suggestions, namely Ms. Jennifer Harper, Mr. Greg Sanders, and Mr. Brett Trautman. Special thanks also to Mr. Bill Stone for his drive to reduce MoDOT's carbon footprint while maintaining a high-quality transportation system.

The authors would also like to thank the National University Transportation Center (NUTC): Center for Transportation Infrastructure and Safety (CTIS) housed at Missouri University of Science and Technology (Missouri S&T), which provided valuable match funding from the United States Department of Transportation through RITA and the UTC Program. This match funding allowed for more extensive testing and research on the many factors critical to success of the project.

The authors would also like to thank the companies that provided material and equipment contributions necessary for the successful completion of this project, including the Ameren Corporation, BASF Corporation, and Capital Quarries.

Finally, the authors would like to thank Missouri S&T for their valuable contributions to the research. The university awarded two Chancellor's Fellowships to graduate students working on this project. These individuals represent some of the finest graduate students at Missouri S&T. The authors also appreciate the tireless staff of the Department of Civil, Architectural, and Environmental Engineering and the Center for Infrastructure Engineering Studies. Their assistance both inside and out of the various laboratories was invaluable to the successful completion of this project.

TABLE OF CONTENTS

	Page
ACKNOWLEDGEMENTS	iv
LIST OF ILLUSTRATIONS	vii
LIST OF TABLES	viii
SECTION	
1. INTRODUCTION	1
1.1. REPORT ORGANIZATION	1
1.2. BACKGROUND	1
2. PROJECT WORK PLAN	4
2.1. TASK 1: LITERATURE REVIEW	5
2.2. TASK 2: RCA CHARACTERIZATION	5
2.3. TASK 3: MIX DEVELOPMENT & FRESH CONCRETE PROPERTIES	5
2.4. TASK 4: HARDENED MECHANICAL PROPERTIES	7
2.5. TASK 5: DURABILITY PERFORMANCE	8
2.6. TASK 6: BOND AND DEVELOPMENT LENGTH	8
2.7. TASK 7: FULL SCALE SPECIMEN TESTS	10
2.7.1. Subtask 7a: Full-Scale Beam Shear Tests	10
2.7.2. Subtask 7b: Full-Scale Beam Flexural Tests	10
2.8. TASK 8: RECOMMENDATIONS & SPECIFICATIONS FOR IMPLEMENTING RCA IN CONCRETE	11
2.9. TASK 9: VALUE TO MODOT AND STAKEHOLDERS TO IMPLEMENTING RCA IN CONCRETE	11
3. TASK SUMMARIES: FINDINGS, CONCLUSIONS & RECOMMENDATIONS	13
3.1. TASK 1: LITERATURE REVIEW	13
3.2. TASK 2: RCA CHARACTERIZATION	15
3.3. TASK 3: MIX DEVELOPMENT & FRESH CONCRETE PROPERTIES	16
3.4. TASK 4: HARDENED MECHANICAL PROPERTIES	17
3.5. TASK 5: DURABILITY PERFORMANCE	19
3.6. TASK 6: BOND AND DEVELOPMENT LENGTH	20
3.7. TASK 7: FULL SCALE SPECIMEN TESTS	22

3.8. TASK 8: RECOMMENDATIONS & SPECIFICATIONS FOR IMPLEMENTING RCA IN CONCRETE	24
3.9. TASK 9: VALUE TO MODOT AND STAKEHOLDERS TO IMPLEMENTING RCA IN CONCRETE	25
4. BIBLIOGRAPHY	28
5. TESTING STANDARDS	29
APPENDICES	
A. REPORT A: PRELIMINARY MIX DEVELOPMENT	30
B. REPORT B: MECHANICAL AND DURABILITY PROPERTIES OF RCA CONCRETE.....	79
C. REPORT C: BOND BEHAVIOR OF RCA CONCRETE.....	179
D. REPORT D: SHEAR BEHAVIOR OF RCA CONCRETE	322
E. REPORT E: FLEXURAL BEHAVIOR OF RCA CONCRETE.....	437

LIST OF ILLUSTRATIONS

Figure	Page
Figure 1 Beam Splice Test Setup.....	9
Figure 2 Full Scale Beam Test Setup.....	11

LIST OF TABLES

Table	Page
Table 1 Concrete Test Methods and Protocols	6

1. INTRODUCTION

1.1. REPORT ORGANIZATION

The following report documents a research project on recycled concrete aggregate (RCA) performed by Missouri University of Science and Technology (Missouri S&T) on behalf of the Missouri Department of Transportation (MoDOT). The report consists of a Summary Report followed by five detailed technical reports. Section 1 of the Summary Report presents the report organization and background for the study. The project work plan is presented in Section 2 to familiarize the reader with the overall objectives, project tasks, and scope of the research study. Following the project work plan, the summary findings, conclusions, and recommendations are presented task by task in Section 3. Detailed Technical Reports A through E are attached following the Summary Report, which provides the detailed specifics undertaken in this research investigation. The Summary Report is designed to provide the reader with the project highlights in terms of findings, conclusions, and recommendations, while Technical Reports A through E provide the background, detailed approaches, experimental procedures and processes, results, findings, conclusions, and recommendations.

1.2. BACKGROUND

The construction of buildings, bridges, roadways and other infrastructure continues to increase in the twenty-first century, especially in areas with ever-growing populations. Existing structures and highways require repair or replacement as they reach the end of their service life or simply no longer satisfy their intended purpose due to the growing population. As modern construction continues, two pressing issues will become

more apparent to societies: an increasing demand for construction materials, especially concrete and asphalt aggregates, and an increasing production of construction and demolition waste. Already, the Federal Highway Administration (FHWA) estimates that two billion tons of new aggregate are produced each year in the United States. This demand is anticipated to increase to two and a half billion tons each year by 2020. FHWA also estimates that the annual production of construction waste from building demolition alone is approaching 123 million tons.

To address both the concern of increasing demand for new aggregates and increasing production of construction waste, many states have begun to recognize that a more sustainable solution exists in recycling waste concrete for use as aggregate in new concrete. This solution helps address the question of how to sustain modern construction demands for aggregates as well as helps to reduce the amount of waste that enters already over-burdened landfills.

Concrete recycling protects natural resources and eliminates the need for disposal by using readily available concrete as an aggregate source for new concrete, including in-place recycling. However, the successful application of RCA requires a thorough understanding of its effect on the fresh and hardened properties of the resulting concrete. For instance, recycled aggregate usually has higher absorption and lower specific gravity than virgin sources. Both of these issues require adjustments during the mix design process. Concrete made with RCA can also experience increased creep, shrinkage, and permeability – as well as decreased stiffness and compressive strength – compared to concrete produced from virgin aggregate. Nonetheless, proper application of RCA can

decrease the cost of transportation-related infrastructure and remove a significant amount of material from landfills, increasing the sustainability of concrete.

2. PROJECT WORK PLAN

As with most research projects, the project work plan evolved during the course of the study as results became available. The work plan described below reflects the work as completed on the project.

The *objective* of the research was to determine the implications of using RCA in the production of new concrete. Specifically, the study evaluated the fresh and hardened properties, durability, and structural behavior of concrete containing RCA. The *project work plan* included nine (9) tasks necessary to reach this goal and consisted of the following:

1. Task 1: Literature Review
2. Task 2: RCA Characterization
3. Task 3: Mix Development & Fresh Concrete Properties
4. Task 4: Hardened Mechanical Properties
5. Task 5: Durability Performance
6. Task 6: Bond & Development Length
7. Task 7: Full-Scale Specimen Tests
8. Task 8: Recommendations & Specifications for Implementing RCA in
Concrete
9. Task 9: Value to MoDOT and Stakeholders to Implementing RCA in
Concrete

The following sections discuss each of these individual tasks.

2.1. TASK 1: LITERATURE REVIEW

The purpose of this task was to conduct a comprehensive and critical literature review of past experiences and previous research on RCA, with particular attention to the impact that these findings may have on the work plan. Specifically, the literature review focused on studies that investigated RCA properties (*e.g.*, absorption, durability) as well as the behavior of concrete containing RCA including the fresh and hardened properties (*e.g.*, workability, compressive strength, creep, shrinkage), structural properties (*e.g.*, bond, shear), and durability (*e.g.*, freeze-thaw resistance, permeability, scaling).

2.2. TASK 2: RCA CHARACTERIZATION

In this task, the research team evaluated the properties of RCA made from concrete containing virgin aggregates indigenous to the state of Missouri. Critical properties studied included density, relative density (specific gravity), absorption, gradation, and abrasion resistance – properties that are also critical for virgin aggregate sources. A standard MoDOT Class B air-entrained mix served as the baseline concrete and as parent material for the RCA. The test methods and protocols are shown in **Table 1**.

2.3. TASK 3: MIX DEVELOPMENT & FRESH CONCRETE PROPERTIES

The aim of this task was to develop, test, and evaluate a series of mixes containing RCA that were targeted for pavement construction and structural concrete with 28-day compressive strengths of 3,500 to 5,500 psi. The higher absorption typical of RCA tends to increase the “harshness” of the mix and often requires alternative methods of

Table 1 Concrete Test Methods and Protocols

PROPERTY	TEST METHOD	TEST TITLE/DESCRIPTION	TASK
RCA CHARACTERIZATION TESTS			
Density, Relative Density, & Absorption	ASTM C 127	Standard Test Method for Density, Relative Density (Specific Gravity), and Absorption of Coarse Aggregate.	2
Gradation	ASTM C 136	Standard Test Method for Sieve Analysis of Fine and Coarse Aggregates.	2
Abrasion Resistance	ASTM C 131	Standard Test Method for Resistance to Degradation of Small-Size Coarse Aggregate by Abrasion and Impact in the Los Angeles Machine.	2
FRESH CONCRETE PROPERTY TESTS			
Unit Weight	ASTM C 138	Standard Test Method for Density (Unit Weight).	3
Air Content	ASTM C 231	Standard Test Method for Air Content of Freshly Mixed Concrete by the Pressure Method.	3
Rheology	Non-ASTM	Establish Bingham parameters (yield stress and plastic viscosity).	3
Slump, Slump Retention	ASTM C 143	Standard Test Method for Slump of Hydraulic-Cement Concrete.	3
Bleeding	ASTM C 232	Standard Test Methods for Bleeding of Concrete.	3
HARDENED MECHANICAL PROPERTY TESTS			
Compressive Strength	ASTM C 39	Standard Test Method for Compressive Strength of Cylindrical Concrete Specimens.	4
Splitting Tensile Strength	ASTM C 496	Standard Test Method for Splitting Tensile Strength of Cylindrical Concrete Specimens.	4
Flexural Strength	ASTM C 78	Standard Test Method for Flexural Strength of Concrete.	4
Modulus of Elasticity	ASTM C 469	Standard Test Method for Static Modulus of Elasticity.	4
Drying Shrinkage	ASTM C 157	Standard Test Method for Length Change of Hardened Hydraulic-Cement Mortar and Concrete.	4
Fracture Energy	RILEM TC 50-FMC	Determination of the Fracture Energy of Mortar and Concrete by Means of Third Point Bend Test on Notched Beams	4
DURABILITY TESTS			
Resistivity	Non-ASTM	Surface and Bulk Resistivity Measurements	5
Bulk Electrical Conductivity	ASTM C 1760	Standard Test Method for Bulk Electrical Conductivity of Hardened Concrete	5
Permeable Pore Volume & Absorption	ASTM C 642	Standard Test Method for Density, Absorption, and Voids in Hardened Concrete.	5
Scaling Resistance	ASTM C 672	Standard Test Method for Scaling Resistance of Concrete Surfaces Exposed to Deicing Chemicals.	5
Rapid Freeze Thaw Resistance	ASTM C 666, A	Standard Test Method for Resistance of Concrete to Rapid Freezing and Thawing.	5
MILD STEEL BOND AND DEVELOPMENT TESTS			
Third Point Loading Splice Test Specimens	Non-ASTM	Generally regarded as the most realistic test method for development length and splice length, see Fig. 1.	6
FULL SCALE SPECIMEN TESTS			
Shear Test Specimens	Non-ASTM	Full-scale tests to study the shear behavior of beams containing RCA and evaluate the contributions from the concrete, V_c , and transverse (shear) reinforcement, V_s , see Fig. 2.	7
Flexural Test Specimens	Non-ASTM	Full-scale tests to study the flexural behavior of beams containing RCA, see Fig. 2.	7
Non-ASTM – refers to a test method that is not a standard ASTM test. The test is either a generally accepted research practice test or standard undertaken at Missouri S&T for similar studies.			

determining the concrete proportions, such as the Equivalent Mortar Volume (EMV) method of proportioning. The research team developed mixes containing 30%, 50%, 70%, and 100% replacement rates of virgin coarse aggregate with RCA and also evaluated the effect of changes in paste volume and sand-to-coarse aggregate contents on optimum contents of RCA. A standard MoDOT Class B air-entrained concrete served as the baseline mix for the study. The test methods and protocols are shown in **Table 1**.

2.4. TASK 4: HARDENED MECHANICAL PROPERTIES

The objective of the proposed research was to determine the implications of using RCA in the production of new concrete. As such, in this task, the investigators focused on the hardened mechanical properties of concrete containing RCA compared to concrete containing virgin aggregates. The research team used the optimum mix designs from Task 3 to evaluate the impact of different substitution rates and types of RCA on the basic mechanical properties of concrete, such as compressive strength and shrinkage. The primary issue evaluated was whether or not RCA had a negative influence on the resulting concrete properties, and, if so, at what substitution rates do these negative influences begin. Furthermore, how do changes in the properties of RCA impact the substitution rates at which the negative influences begin? For instance, if the RCA maximum aggregate size is reduced from 3/4 in. to 1/2 in. through additional grinding, can the concrete use 30% more RCA before suffering any increase in shrinkage? The test methods and protocols are shown in **Table 1**.

2.5. TASK 5: DURABILITY PERFORMANCE

Previous studies have shown mixed results as to the effect of RCA on the durability performance of concrete. Thus, the aim of this task was to assess the durability performance of concrete containing RCA compared to concrete containing virgin aggregates. Specifically, the research team investigated the effect of RCA on concrete resistivity, conductivity, permeability, absorption, scaling resistance, and freeze-thaw resistance. As with Tasks 3 and 4, the test matrix included different substitution rates of RCA for virgin coarse aggregate. The test methods and protocols are shown in **Table 1**.

2.6. TASK 6: BOND AND DEVELOPMENT LENGTH

The issue to be addressed under this task was to determine whether the current *AASHTO LRFD Bridge Design Specifications*¹ for development length are appropriate for concrete containing RCA. In other words, does RCA enhance, compromise, or not affect the relationship between development length and compressive strength as previously formulated for concrete containing virgin aggregates. This task investigated development length of mild steel in concrete containing RCA compared to concrete containing virgin aggregates.

Two types of tests were used to evaluate the bond performance of mild steel bars in concrete containing RCA. The first test was a direct pull-out test based on protocols recommended in the RILEM Standard 7-II-128.² Although this test does not offer a realistic stress state in terms of bond performance in a flexural member, it does offer a convenient relative comparison of bond between different concrete types. The second test

was a full-scale beam splice specimen, which is generally regarded as the most realistic test method for evaluating bond.^{3,4}

The investigators constructed and instrumented several direct pull-out specimens for testing. Data recorded during the test included load and bar slip. The test variables involved bar size and concrete type (concrete with or without RCA), with the RCA including two replacement levels: 50% and 100%.

The investigators also constructed and instrumented full-scale rectangular beams for splice specimen testing as shown in **Figure 1**. Specimen instrumentation consisted of strain gauges placed at the start of each lap. Data recorded during the tests included load and deflection of the specimen as it was tested to flexural or bond failure. The test variables involved lap length and concrete type (concrete with or without RCA), with the RCA including two replacement levels: 50% and 100%. The test method and protocols are also shown in **Table 1**.

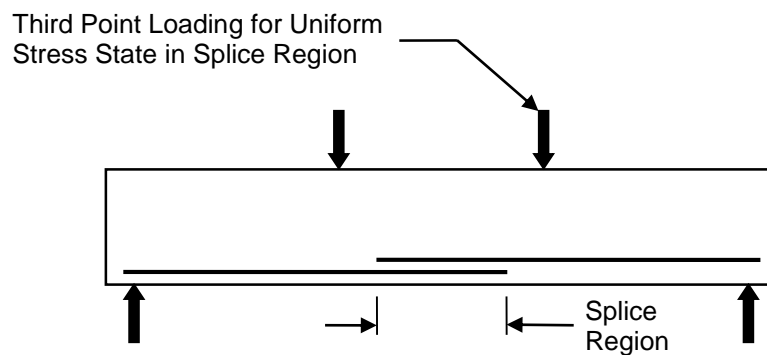


Figure 1 Beam Splice Test Setup

2.7. TASK 7: FULL SCALE SPECIMEN TESTS

This task involved testing of full-scale specimens constructed from concrete containing RCA for comparison with concrete containing virgin aggregates. The full-scale specimens included beam specimens for both shear and flexural testing. This task involved two (2) subtasks. Details regarding the test methods to be investigated are summarized in **Table 1**.

2.7.1. Subtask 7a: Full-Scale Beam Shear Tests. This subtask involved full-scale beam tests to study the shear behavior of concrete containing RCA, which is critical since aggregate properties have such a significant impact on shear strength of concrete. The investigators constructed, instrumented, and tested rectangular beams in the configuration shown in **Figure 2**, which applies a uniform shear over a significant portion of the beam. The variables included amount of longitudinal (flexural) reinforcement and concrete type (concrete with or without RCA). Specimen instrumentation consisted of strain gauges and linear variable displacement transducers (LVDTs). Data recorded during the tests also included load and deflection of the specimen as it was tested to shear failure.

2.7.2. Subtask 7b: Full-Scale Beam Flexural Tests. This subtask involved full-scale beam tests to study the flexural behavior of concrete containing RCA. The investigators constructed, instrumented, and tested rectangular beams in the configuration shown in **Figure 2**, which applies a uniform moment over a significant portion of the beam. The variables included amount of longitudinal (flexural) reinforcement and concrete type (concrete with or without RCA). Specimen instrumentation consisted of

strain gauges and LVDTs. Data recorded during the tests also included load and deflection of the specimen as it was tested to flexural failure.

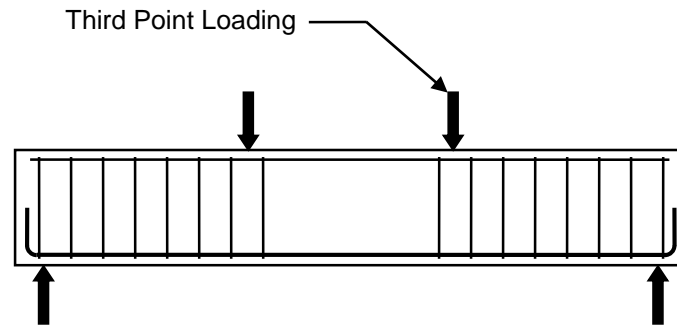


Figure 2 Full Scale Beam Test Setup

2.8. TASK 8: RECOMMENDATIONS & SPECIFICATIONS FOR IMPLEMENTING RCA IN CONCRETE

Based on the results of Tasks 1 through 7, the investigators developed recommendations for the use of RCA in concrete for infrastructure elements. Based on these recommendations and the results of this research study, the investigators also developed a suggested MoDOT specification for the use of RCA in concrete for transportation-related infrastructure.

2.9. TASK 9: VALUE TO MODOT AND STAKEHOLDERS TO IMPLEMENTING RCA IN CONCRETE

The issue to be addressed under this task was to quantify the benefit to MoDOT of applying the results of this research project – specifically, to determine a “value to MoDOT and the residents of Missouri” in the event that RCA is incorporated into construction of the State’s transportation-related infrastructure. Concrete recycling protects natural resources and eliminates the need for disposal by using readily available

concrete as an aggregate source for new concrete, including in-place recycling. Recycled concrete is less expensive than virgin aggregate sources, and its use would remove a sizeable amount of material from landfills, turning a waste product into a viable construction material. This value aligns with both MoDOT's Tangible Result of being environmentally and socially responsible⁵ and MoDOT's Research Need for strategies to reduce energy consumption.⁶

Overall, this task sought to establish a basis for whether or not RCA should be used by MoDOT, based upon the results from Tasks 1 through 8.

3. TASK SUMMARIES: FINDINGS, CONCLUSIONS & RECOMMENDATIONS

The following descriptions summarize the major findings, conclusions, and recommendations for project Tasks 1 through 9. Each sub-section refers to the specific Technical Report A through E where the background, detailed approach, experimental procedures and processes, results, findings, conclusions, and recommendations may be referenced for much greater detail. Report designations (*i.e.*, “Report A”) are provided as a reference such that the specific detailed report located in the appendix may be consulted to gain an improved understanding of how this particular finding or conclusion was established.

3.1. TASK 1: LITERATURE REVIEW

Detailed Technical Reports A through E each provide a thorough literature review related to the topic of study at hand. The reader is referred to the detailed technical reports for topic specific literature reviews on RCA. However, the more notable general findings include the following:

Technical Reports A through E:

- RCA is a double phase material consisting of virgin coarse aggregate with varying amounts of adhered mortar.
- RCA results in a double interfacial transition zone in the new concrete, with the first zone between the original virgin aggregate and the adhered mortar and the second zone between the adhered mortar and the paste of the new concrete mixture.

- The quality of RCA is tied to the properties of the original waste concrete, the new composition, the mixing approach, and the deterioration conditions of the recycled aggregates.
- RCA generally has lower specific gravity and unit weight and considerably higher absorption and porosity compared to natural aggregates as a result of the adhered mortar.
- As the strength of the parent material increases, the quantity of adhered mortar increases due to increased bond between the aggregate and mortar.
- As the maximum aggregate size used in the parent material decreases, the quantity of adhered mortar increases due to increased surface area of the virgin aggregate.
- Although the use of RCA reduces workability due to increased water demand, proper mix proportioning and the use of superplasticizing admixtures will result in workable concrete mixtures.
- In general, as the percentage of RCA increases, compressive strength decreases, but the effect is negligible at replacement rates of 30% or less.
- In general, as the percentage of RCA increases, splitting tensile strength decreases due to the double interfacial transition zone.
- In general, as the percentage of RCA increases, the modulus of elasticity decreases due to the lower modulus of the adhered mortar.
- In general, as the percentage of RCA increases, the amount of shrinkage increases due to the lower restraining capacity of the RCA compared to virgin aggregate, although the effect is negligible at replacement rates of 30% or less.

- Conclusions with regard to durability resistance have been mixed and performance appears to be more a function of the quality of the parent material.
- Research on bond of mild steel in recycled aggregate concrete (RAC) has been very limited, with most studies performing only pull-out tests, tests on small-scale specimens, or limiting the RCA replacement levels below 50%.
- Research on shear strength of recycled aggregate concrete (RAC) has been limited and is generally contradictory, with studies showing either a decrease in shear capacity with increasing RCA replacement levels or no effect at all.
- Research on flexural strength of RAC has been limited but, in general, has shown that as the percentage of RCA increases, the number and size of flexural cracks increases and the deformations are much higher.

3.2. TASK 2: RCA CHARACTERIZATION

A standard MoDOT Class B air-entrained mix served as the parent material for the RCA. The research team cast 20 cubic yards of the MoDOT mix into concrete blocks for processing at a local quarry. The quarry then crushed, screened, and sieved the material to produce a MoDOT D Gradation similar to that of the Potosi limestone used in the parent material. The research team then evaluated the properties of the RCA necessary for developing the recycled aggregate concrete (RAC) mix designs. The findings and conclusions from this task consist of the following:

Technical Reports A & B:

- The RCA met the requirements for a MoDOT D Gradation.

- The bulk density of the RCA measured 89.7 pcf compared to 99.7 pcf for the Potosi limestone.
- The specific gravity of the RCA measured 2.35 compared to 2.72 for the Potosi limestone.
- The absorption of the RCA measured 4.56% compared to 0.98% for the Potosi limestone.
- The Los Angeles Abrasion of the RCA measured 41% compared to 43% for the Potosi limestone.
- The residual mortar content of the RCA measured 46% by weight.

3.3. TASK 3: MIX DEVELOPMENT & FRESH CONCRETE PROPERTIES

This portion of the study involved developing and evaluating a series of mixes containing the RCA produced in Task 2. The MoDOT Class B mix design served as the guideline for developing the mixes, and the study examined replacement levels of 30%, 50%, 70%, and 100%. The findings and conclusions from this task consist of the following:

Technical Reports A & B:

- The research team successfully developed recycled aggregate concrete (RAC) mixes containing 30%, 50%, 70%, and 100% RCA. The mixes met MoDOT requirements for slump and air content for an air-entrained Class B mix.
- As the RCA replacement level increased, the workability of the mixes decreased, requiring additional water reducing admixture and, for the 100% RCA mix, a modification to the fine aggregate percentage to improve workability.

- As the RCA replacement level increased, the unit weight of the concrete mixture decreased due to the lower specific gravity of the RCA.
- As the RCA replacement level increased, bleeding of the fresh concrete increased, although even at 100% replacement, the amount of bleeding was still at an acceptable level for conventional concrete.
- Except for the concrete made with 100% RCA replacement, it was observed that the yield stress was generally higher for the RAC mixtures compared to the baseline.
- Most of the plastic viscosity results obtained for the RCA mixtures (excluding the 50% RCA mix) were higher than the baseline. However, no clear trend existed.

3.4. TASK 4: HARDENED MECHANICAL PROPERTIES

This portion of the study evaluated the hardened mechanical properties of the mixes developed in Task 3. The objective of this task was to determine the implications of using RCA in the production of new concrete. The findings and conclusions from this task consist of the following:

Technical Report B:

- In terms of compressive strength, there was not a significant decrease for the 70% and 100% RCA mixes compared to the baseline mix. However, due to higher air contents, the mixtures made with 30% and 50% RCA replacement had lower compressive strengths compared to the baseline and other RCA mixtures.
- Although the amount of cementitious materials used in the Equivalent Mortar Volume (EMV) mixes was lower than the baseline mixture, this method produced concretes with relatively high compressive strengths.

- The Two Stage Mixing Approach (TSMA) did not result in increased compressive strengths except for a slight increase in the 56-day strength of the 100% RCA mix. No significant difference was observed between the 100% RCA and 100% RCA-TSMA specimens at 91 days.
- In terms of splitting tensile strength and flexural strength, in general, the RCA mixes showed a slight decrease in performance compared to the baseline mix. However, specimens made with the EMV method had very good tensile and flexural performance compared to the baseline mix. However, the TSMA was not effective in enhancing splitting tensile strength, although it did improve flexural performance.
- As the RCA replacement level increased, the modulus of elasticity decreased. However, specimens made with the EMV method had comparable values to the baseline mix, while the TSMA specimens showed the same decrease in performance as the standard RCA mixes.
- In terms of shrinkage, the RCA mixes had comparable values to the baseline mix, which is contrary to most of the data available in the literature. This result may be traced to the internal curing effect of the highly absorptive RCA used in this research. Specimens constructed using the EMV method revealed very low shrinkage compared to the baseline mix, most likely the result of the very low amount of fresh paste and higher coarse aggregate content for these mixes. No improvement in shrinkage behavior of the specimens made with 100% RCA was observed due to the use of the TSMA.

Technical Reports C, D & E:

- The splitting tensile strength decreased 12% for the 50% RCA mix and 29% for the 100% RCA mix compared to the baseline mix.
- The fracture energy decreased 14% for the 50% RCA mix and 22% for the 100% RCA mix compared to the baseline mix.
- It is important to note that for the bond (Report C), shear (Report D), and flexural (Report E) studies, due to the quantity of material required, the recycled aggregate concrete (RAC) was produced by a local ready-mix supplier and not from a laboratory produced mix.

3.5. TASK 5: DURABILITY PERFORMANCE

Previous studies have shown mixed results as to the effect of RCA on the durability performance of concrete. Thus, the aim of this portion of the study was to assess the durability performance of concrete containing RCA compared to concrete containing virgin aggregates. Specifically, the research team investigated the effect of RCA on concrete resistivity, conductivity, permeability, absorption, scaling resistance, and freeze-thaw resistance. The findings and conclusions from this task consist of the following:

Technical Report B:

- Both permeable void volume and absorption of the RCA mixtures was higher than the baseline mixture. The EMV method was effective in reducing the absorption. No significant difference was observed due to using the TSMA.

- Both the surface and bulk electrical resistivity values decreased as a result of increased RCA content. This decrease was greatest at replacement levels of 50% or more and is likely due to the higher porosity of the RCA compared to the virgin aggregate. Both the EMV method and TSMA were not effective in enhancing the electrical resistivity of the 100% RCA mix.
- In terms of deicing salt scaling, mixtures containing up to 70% RCA performed at an acceptable level. However, the 100% RCA mix suffered serious scaling damage. The EMV method was not effective in improving resistance to scaling. However, the specimens made with 100% RCA-TSMA had very good scaling resistance.
- In terms of freeze/thaw resistance, mixtures containing up to 70% RCA performed at an acceptable level. However, the 100% RCA mix had durability factors below the acceptable threshold level of 80%. Both the EMV method and TSMA were effective at improving freeze/thaw resistance for the 100% RCA mix, with durability factors above 80%.
- The use of fly ash increased the durability performance of all RCA mixes.

3.6. TASK 6: BOND AND DEVELOPMENT LENGTH

The mix designs tested for bond and development consisted of the baseline mix and two RCA replacement levels – 50% and 100% – subsequently referred to as RAC-50 and RAC-100, respectively. The baseline mix is subsequently referred to as the virgin aggregate concrete or VAC. Two test methods were used for the bond strength comparisons. The first was a direct pull-out test based on RILEM 7-II-128² “RC6: Bond test for reinforcing steel. 1. Pull-out test.” The second test method consisted of full-scale

beam splice test specimens subjected to third point loading until failure of the splice. The findings and conclusions from this task consist of the following:

Technical Report C:

- All concrete material properties were negatively impacted with increasing replacement of coarse natural aggregates with RCA. The most drastic decreases were seen in splitting tensile strength and fracture energy, both of which play a crucial role in bond strength. The splitting tensile strength decreased 12% and 29% for the RAC-50 and RAC-100 mixes, respectively. The fracture energy decreased 14% and 22% for the RAC-50 and RAC-100 mixes, respectively.
- For the #4 pull-out tests, based on a square root normalization for compressive strength, there was essentially no difference in average peak bond stress between the VAC and RAC-50 mixes. However, there was a slight increase of 6.0% in the RAC-100 over the VAC mix.
- For the #4 pull-out tests, based on a fourth root normalization for compressive strength, there was a slight increase in average peak bond stress between the VAC and both RCA replacement levels, 7.9% for the RAC-50 mix and 12.9% for the RAC-100 mix.
- For the #6 bar pull-out tests, based on a square root normalization for compressive strength, there was essentially no difference in average peak bond stress between the VAC, RAC-50, and RAC-100 mixes.
- For the #6 bar pull-out tests, based on a fourth root normalization for compressive strength, both the RAC-50 and RAC-100 mixes had 7.1% higher bond stress than the VAC mix.

- For the beam splice specimen tests, based on a square root normalization for compressive strength, the RAC-50 specimens had a slight increase in average peak bar stress of 5.9% over the VAC specimens while the RAC-100 specimens suffered a decrease of 16.9%.
- For the beam splice specimen tests, based on a fourth root normalization for compressive strength, both RCA mixes suffered a decrease in average peak bar stress compared to the VAC specimens, 5.0% for the RAC-50 specimens and 19.5% for the RAC-100 specimens.
- Based on an analysis of the test results, particularly those for the more realistic beam splice specimens, RCA replacement levels above 50% result in a noticeable decrease in bond strength which parallels the decrease in splitting tensile strength and fracture energy.

3.7. TASK 7: FULL SCALE SPECIMEN TESTS

The mix designs tested in the full-scale specimens consisted of the baseline mix and two RCA replacement levels – 50% and 100% – subsequently referred to as RAC-50 and RAC-100, respectively. The baseline mix is subsequently referred to as the virgin aggregate concrete or VAC. Most research to date has consisted only of the evaluation of the strength and durability of RCA concrete mixtures, while only a limited number of studies have implemented full-scale testing of specimens constructed with recycled aggregate concrete (RAC) to determine its potential use in the industry. For this research, a laboratory testing program was developed to investigate the shear and flexural performance of reinforced concrete beams constructed with RCA. The experimental

program consisted of 26 tests – 18 for shear and 8 for flexure – performed on full-scale reinforced concrete beams. The findings and conclusions from this task consist of the following:

Technical Report D (shear):

- In terms of crack morphology, crack progression, and load-deflection response, the behavior of the VAC and RAC beams was virtually identical.
- Statistical data analyses – both parametric and nonparametric – showed that there was no statistically significant difference between the normalized shear capacities of the VAC and RAC-50 specimens.
- Statistical data analyses – both parametric and nonparametric – showed that there was a statistically significant difference between the normalized shear capacities of the VAC and RAC-100 specimens, and as a result, the RAC-100 specimens had, on average, 11% lower shear capacity than the VAC.
- For the RAC-50 test beams, the splitting tensile strength, flexural strength, and fracture energy decreased between 1% and 6% compared to the VAC, with the shear strength of the RAC-50 specimens experiencing a decrease of only 1%.
- For the RAC-100 test beams, the splitting tensile strength, flexural strength, and fracture energy decreased between 9% and 22% compared to the VAC, with a corresponding reduction in shear strength of 11%.
- The decrease in shear capacity is most likely due to the double interfacial transition zone that exists when using recycled concrete as aggregate, and the effect is more pronounced as the percentage replacement increases.

- Although limited based on the number of variables tested in this study, it would appear that replacing more than 50% of the virgin aggregate with RCA will result in a noticeable decrease in shear capacity, 11% for the mixes studied in this investigation.

Technical Report E (flexure):

- In terms of crack morphology and crack progression, the RAC beams experienced a larger number, and corresponding closer spacing, of flexural cracks compared to the VAC beams.
- In terms of load deflection behavior, the RAC beams showed lower stiffness both before and after the cracking moments compared to the VAC beams.
- The RAC beams had comparable flexural capacity to the VAC beams.
- Existing design standards conservatively predicted the flexural capacities of the RAC beams.
- Although limited based on the number of variables tested in this study, it would appear that replacing 100% of the virgin aggregate with RCA does not result in any decrease in ultimate flexural capacity compared to VAC mixes.

3.8. TASK 8: RECOMMENDATIONS & SPECIFICATIONS FOR IMPLEMENTING RCA IN CONCRETE

Based on the results of Tasks 1 through 7, the investigators recommend the implementation of RCA in concrete for the construction of transportation-related infrastructure in the State of Missouri. However, the investigators also recommend initially limiting the RCA replacement levels to 50% in order to prevent any decreased performance compared to conventional concrete. In general, when limiting the

replacement level to 50%, there are no special requirements in order to utilize RCA in concrete production. However, the following general recommendations should be followed:

- With regard to the RCA, follow the standard MoDOT requirements for virgin aggregate sources in order to characterize the RCA from the specific parent material source. In particular, evaluate the RCA for contamination from chlorides and for signs of D-cracking. With regard to chloride contamination, acceptable levels will depend on a variety of factors including: (1) overall chloride level of the processed RCA (chloride levels vary within exposed concrete with high levels near the surface and negligible levels away from the surface, and when mixed together, acceptable average levels may result in the processed RCA), (2) specific application with regard to type of concrete (*e.g.*, unreinforced concrete, reinforced concrete, prestressed concrete), and (3) specific application with regard to location (*e.g.*, pavement, foundation, retaining wall, bridge deck). With regard to D-cracking, perform identical tests used to evaluate virgin aggregate sources.
- With regard to mix design, follow the standard MoDOT requirements. The only modifications will likely involve increases in the amount of water-reducer or superplasticizer in order to reach the desired level of workability.

3.9. TASK 9: VALUE TO MODOT AND STAKEHOLDERS TO IMPLEMENTING RCA IN CONCRETE

With a growing demand for new construction and the need to replace infrastructure stretched beyond its service life, society faces the problem of an ever-growing production of construction and demolition waste. The Federal Highway

Administration (FHWA) estimates that two billion tons of new aggregate are produced each year in the United States. This demand is anticipated to increase to two and a half billion tons each year by 2020. With such a high demand for new aggregates, the concern arises of the depletion of current sources of natural aggregates and the availability of new sources. Similarly, construction waste produced in the United States is expected to increase. From building demolition alone, the annual production of construction waste is estimated to be 123 million tons (FHWA). Currently, this waste is most commonly disposed of in landfills.

To address both the concern of increasing demand for new aggregates and increasing production of waste, many states have begun to recognize that a more sustainable solution exists in recycling waste concrete for use as aggregate in new concrete. This solution helps address the question of how to sustain modern construction demands for aggregates as well as helps to reduce the amount of waste that enters already over-burdened landfills. Based on a survey by FHWA in 2002, many states had begun to implement recycled concrete aggregate in some ways in new construction. For instance, forty-one states had recognized the many uses of RCA as a raw material, such as for rip-rap, soil stabilization, pipe bedding, and even landscape materials. Thirty-eight states had gone a step further in integrating RCA into roadway systems for use as aggregate base course material. Unfortunately, only eleven states had begun using RCA in Portland cement concrete for pavement construction.

However, over the intervening 12 years, the use of RCA has increased significantly, particularly within the last 5 years, and the Missouri Department of Transportation (MoDOT) has instituted a very aggressive program to increase the use of

recycled materials in transportation-related construction, including the use of RCA.

Nevertheless, at the start of this research project, there were no acceptable standards or guidelines in the U.S. for utilizing RCA in structural concrete, which became one of the main objectives of this research study.

Concrete recycling protects natural resources and eliminates the need for disposal by using readily available concrete as an aggregate source for new concrete, including in-place recycling. Recycled concrete is less expensive than virgin aggregate sources, and its use would remove a sizeable amount of material from landfills, turning a waste product into a viable construction material. This value aligns with both MoDOT's Tangible Result of being environmentally and socially responsible⁵ and MoDOT's Research Need for strategies to reduce energy consumption.⁶ The results presented in this research report provide the methods, standards, and guidelines necessary to implement RCA in the construction of Missouri's transportation infrastructure, turning a waste product into a viable construction material.

4. BIBLIOGRAPHY

1. AASHTO (2010). *AASHTO LRFD Bridge Design Specifications*, 5th edition, Washington, D.C.
2. RILEM (1994). “RC5: Bond Test for Reinforcing Steel. 1. Pullout test,” *RILEM Technical Recommendations for the Testing and Use of Construction Materials*, 7-II-128, E & FN Spon, London, U.K.
3. Ramirez, J.A. and Russell, B.W. (2008). *Splice Length for Strand/Reinforcement in High-Strength Concrete*, NCHRP Project 12-60 Report, Transportation Research Board, Washington, D.C.
4. ACI Committee 408 (2003). “Bond and Development of Straight Reinforcing Bars in Tension (408R-03),” *Technical Documents*, American Concrete Institute, Farmington Hills, MI.
5. MoDOT Tangible Results – Environmentally and Socially Responsible, <http://www.modot.mo.gov/about/MissionValuesTangibleResults.htm>.
6. Stone, W. (2010). “Update on MoDOT’s Research Activities and Needs,” <http://library.modot.mo.gov/RDT/Forum/y10/BillStoneLunchDiscussion.pdf>.

5. TESTING STANDARDS

1. AASHTO – American Association of State Highway Transportation Officials:
<http://www.transportation.org>
2. ACI – American Concrete Institute: <http://www.concrete.org>
3. ASTM International – American Society of Testing Methods: <http://www.astm.org>
4. PCI – Prestressed/Precast Concrete Institute: <http://www.pci.org>

APPENDIX A

FINAL Report A

TRyy1317

**Project Title: Recycled Concrete Aggregate (RCA) for
Infrastructure Elements**

Report A: Preliminary Mix Development

Prepared for
Missouri Department of Transportation
Construction and Materials

Missouri University of Science and Technology, Rolla, Missouri

May 2014

The opinions, findings, and conclusions expressed in this publication are those of the principal investigators and the Missouri Department of Transportation. They are not necessarily those of the U.S. Department of Transportation, Federal Highway Administration. This report does not constitute a standard or regulation.

ABSTRACT

To begin to analyze Recycled Aggregate Concrete (RAC) behavior using coarse aggregate consisting of Recycled Concrete Aggregate (RCA), a baseline concrete had to be selected and, for this study, a MoDOT Class B concrete was chosen. The baseline mix was then classified based on fresh and hardened concrete properties including slump, air content, compressive strength, splitting tensile strength, modulus of rupture, and modulus of elasticity. Also cast from the baseline mix were numerous unreinforced concrete beams to be crushed to produce the RCA. The crushing process was performed by a local quarry so as to produce a one inch maximum aggregate size (MAS).

The RCA was classified using ASTM aggregate tests including density, relative density, absorption, gradation, and abrasion resistance. From that classification, the RCA was compared to the coarse aggregate used to produce the baseline mix as well as acceptable ranges for aggregate used in MoDOT Class B concretes. The RCA was then used as the coarse aggregate in the production of the RAC trial mixes. The acceptable criteria for the trial mixes were the same as those set for the baseline concrete as it was being designed to replace the baseline concrete. During mixing, it was observed that the RAC produced using forty percent fine aggregate was capable of meeting strength requirements but failed to meet slump requirements. The slump from the forty percent fine aggregate RAC displayed a more viscous behavior than conventional concrete. Using that observation and a combined gradation analysis, a new mix was designed using forty-five percent fine aggregate. The final mix used for the study was a composition similar to a MoDOT Class B mix with the only difference being the fine aggregate content.

TABLE OF CONTENTS

	Page
ABSTRACT	ii
LIST OF ILLUSTRATIONS	vi
LIST OF TABLES	vii
1. INTRODUCTION	1
1.1. BACKGROUND	1
1.2. OBJECTIVES	1
1.3. SCOPE	1
2. LITERATURE REVIEW	3
2.1. RECYCLED CONCRETE AGGREGATE (RCA)	3
2.1.1. Properties of RCA	3
2.1.2. Effect of Parent Concrete Properties on RCA Characteristics	5
2.2. PROPERTIES OF CONCRETE MADE USING RCA	6
2.2.1. Fresh Concrete Properties	6
2.2.2. Mechanical Properties	7
2.2.2.1. Compressive Strength	7
2.2.2.2. Splitting Tensile Strength	8
2.2.2.3. Modulus of Elasticity	9
2.2.3. Direct Volume Replacement (DVR) Mixture Proportioning	9
3. TECHNICAL APPROACH	10
4. PHASE I – DETERMINATION OF RCA MIX DESIGN	11
4.1. EXPERIMENTAL DESIGN	11
4.2. REPLICATE SPECIMENS	12
4.3. MATERIALS	12
4.3.1. Portland Cement	12
4.3.2. Water Reducer/High Range Water Reducer	13
4.3.3. Air Entraining Agent	13
4.3.4. Coarse Aggregate	13
4.3.5. Fine Aggregate	13

4.4. TEST EQUIPMENT AND PROCEDURES	13
4.4.1. Mixing Procedure	13
4.4.1.1. Pre-Mixing Preparation.....	13
4.4.1.2. Mixing Method	13
4.4.2. Strength Specimens	14
4.4.2.1. Cylinder Compressive Strength.....	14
4.4.2.2. Splitting Tensile Strength	15
4.4.3. Slump.....	16
4.4.4. Air Content	16
4.5. RESULTS AND DISCUSSION.....	17
5. PHASE II – PRODUCTION OF RCA.....	19
5.1. EXPERIMENTAL DESIGN	19
5.2. REPLICATE SPECIMENS	20
5.3. MATERIALS.....	21
5.4. TEST EQUIPMENT AND PROCEDURES	21
5.4.1. Mixing Procedure	21
5.4.1.1 Pre-Mixing Preparation.....	21
5.4.1.2. Mixing Method	22
5.4.2. Strength Specimens	22
5.4.2.1 Cylinder Compressive Strength	22
5.4.2.2. Splitting Tensile Strength	23
5.4.3. Slump.....	23
5.4.4. Air Content	23
5.4.5. Modulus Specimens	23
5.4.5.1 Modulus of Elasticity.....	23
5.4.5.2. Modulus of Rupture	24
5.4.6. Gradation	24
5.4.7. Density and Absorption.....	24
5.4.8. Abrasion Resistance	25
5.4.9. Dry-Rodded Unit Weight	25
5.5. RESULTS AND DISCUSSION.....	26

6. PHASE III – DETERMINATION OF RAC MIX DESIGN	29
6.1. EXPERIMENTAL DESIGN	29
6.2. REPLICATE SPECIMENS	29
6.3. MATERIALS	29
6.4. TEST EQUIPMENT AND PROCEDURES	30
6.4.1. Mixing Procedure	30
6.4.1.1 Pre-Mixing Preparation	30
6.4.1.2. Mixing Method	30
6.4.2. Strength Specimens	31
6.4.3. Slump	32
6.4.4. Air Content	32
6.5. RESULTS AND DISCUSSION	32
7. SUMMARY AND CONCLUSIONS	37
BIBLIOGRAPHY	39

LIST OF ILLUSTRATIONS

Figure	Page
Figure 2.1: Magnified View of RCA Matrix	4
Figure 5.1: Concrete Beam Molds with PVC Conduits.....	20
Figure 5.2: RCA Gradation with MoDOT Gradation D Limits.....	26
Figure 5.3: Washed RCA.....	27
Figure 5.4: Close Up View of Washed RCA.....	27
Figure 6.1: Virgin Coarse Aggregate Gradation.....	34
Figure 6.2: RCA Gradation.....	34
Figure 6.3: Combined Gradation Analysis	35

LIST OF TABLES

Table	Page
Table 2.1: Details of Parent Concrete (Padmini et al., 2009)	5
Table 2.2: Details of Recycled Aggregate Concrete (Padmini e al., 2009)	5
Table 4.1: Mix Design Guidelines for a MoDOT Class B Concrete	12
Table 4.2: Mixing Method Sequence (MoDOT Class B)	15
Table 4.3: General Mix Design Parameters	17
Table 4.4: Oven-Dry Mix Design Selected	17
Table 5.1: Virgin Aggregate and RCA Comparison	28
Table 6.1: Mixing Method Sequence (RAC)	31
Table 6.2: General Mix Design Parameters (RAC)	32
Table 6.3: Oven-Dry Mix Design Selected (RAC)	33
Table 6.4: RAC Mix Design Template	36
Table 6.5: RAC Oven-Dry Batch Weights	36

1. INTRODUCTION

1.1. BACKGROUND

Missouri S&T was contracted by MoDOT to determine the feasibility of using recycled concrete aggregate (RCA) in concrete used for structural purposes. Using RCA in concrete has been shown in recent studies to be able to produce adequately strong concrete with an inherent property of high paste content. Although high paste contents can lead to creep and durability problems, in many applications such as sidewalks and interior structural elements these problems are not detrimental to their integrity. The push in recent years to promote sustainable design was also a driving force in trying to use RCA in concrete along with the abundant supply of the current waste material. As a part of the overall study being conducted by Missouri S&T, this part of the study deals with the production of the RCA and the determination of a mix design to be used in future structural elements.

1.2. OBJECTIVES

The objectives of this portion of the study were to produce a typical MoDOT concrete to be processed into RCA and to develop the mix design to be used for future work in the project.

1.3. SCOPE

The scope of this study was limited to moderate strength MoDOT concrete mixes commonly produced and recycled as well as MoDOT approved admixtures for air

entraining and water reduction. Both admixtures used in this study were Master® Builders products.

2. LITERATURE REVIEW

2.1. RECYCLED CONCRETE AGGREGATE (RCA)

2.1.1. Properties of RCA. In recent years, there has been a movement towards sustainable management of construction and demolition (C&D) waste. This movement is producing legal requirements. Due to this, sectors of the construction industry are undertaking various endeavors to minimize waste generation and improve the management of C&D waste (Limbachiya et al., 2007).

The building industry is a major consumer of materials as well as a major producer of waste (Padmini et al., 2009). According to Abbas et al. (2008), concrete accounts for up to 67% by weight of construction and demolition waste. This is not just a problem in the United States. Tam et al. (2007) published numbers in line with these values in many cases throughout the world as well as the fact that the rate of production of waste is ever increasing.

As a result of the increasing rate of demolition, it is becoming essential to effectively reuse demolition waste in order to conserve natural resources. Decreasing natural aggregate sources as well as increasing problems with waste management support the idea of using recycled waste as aggregate for new concrete production (Padmini et al., 2009).

As a result of the problems mentioned, the idea of producing “green” recycled aggregate concrete (RAC) has emerged. RAC is by definition a concrete produced using recycled aggregate. According to Kou et al. (2012), RAC will fulfill the three prerequisites of green materials: i) the material can recycle and reduce natural resources and energy consumption; ii) the material will not affect the environment; and iii) the

material can maintain sustainable development. Although there are obvious positives from using RCA, there are some technical obstacles limiting its use in concrete production. It should be remembered that RCA is actually a small piece of concrete containing original coarse aggregate (OCA) as well as the adhered mortar (AM). For a clear understanding of the RCA matrix, the separate parts must be identified separately (Nagataki et al., 2000). This concept is visible in **Figure 2.1**.

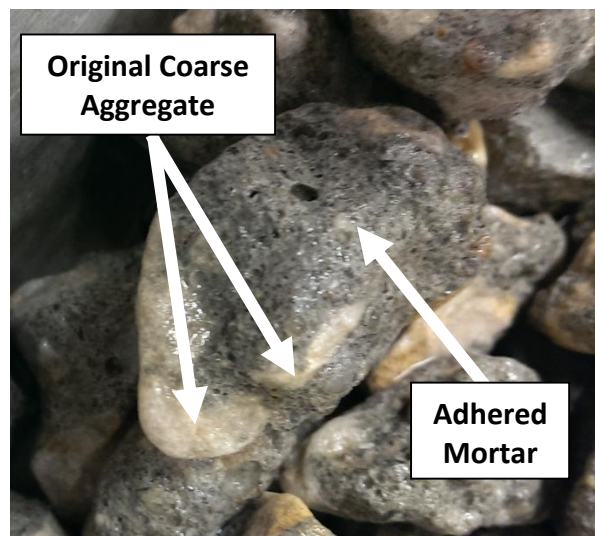


Figure 2.1: Magnified View of RCA Matrix

Li et al. (2012) proposed that the quality of RAC is tied to the properties of the original waste concrete, the new composition, the mixing approach, and the deterioration conditions of the recycled aggregates. Initial investigations of RAC looked into mechanical and durability properties. It was observed that although the use of RCA was viable, a decrease in performance of the RAC should be regarded as a normal outcome. Also, Nagataki et al. (2000) reported that the quality of the RCA was not always dependent upon the properties of the adhered mortar.

2.1.2. Effect of Parent Concrete Properties on RCA Characteristics. Padmini et al. (2009) performed studies to analyze the effects between the parent concrete properties on both the RCA as well as the RAC. Three different gradations of natural aggregates with differing maximum aggregate sizes were used to produce concrete. For each gradation, three different concrete compressive strengths were studied. Also, for each of those nine mixes, three different workabilities were studied to produce a total of twenty-seven mixes which are detailed in **Table 2.1**. Then, using a jaw crusher and adjusting its opening size to match the maximum size of the aggregate used in the parent concrete, recycled aggregates were produced to be used in making RAC specimens. The details of the concrete specimens made using RCA are included in **Table 2.2**.

Table 2.1: Details of Parent Concrete (Padmini et al., 2009)

Target mean strength (MPa)	Water-cement ratio	Workability (CF)	Mix proportion by weight and compressive strength with crushed granite aggregate of maximum size					
			10 mm		20 mm		40 mm	
			Mix	Compressive strength (MPa)	Mix	Compressive strength (MPa)	Mix	Compressive strength (MPa)
PC-121	0.58	0.75	1:1.9:3.1	35	1:2.0:4.1	37	-	31
		0.85	1:1.8:3.0		1:1.9:3.9		1:1.9:4.8	
		0.95	1:1.8:2.9		1:1.8:3.8		-	
PC-234	0.43	0.75	1:1.2:2.3	49	1:1.3:3.0	50	-	45
		0.85	1:1.2:2.2		1:1.2:2.9		1:1.3:3.7	
		0.95	1:1.1:2.1		1:1.2:2.8		-	
PC-345	0.34	0.75	1:0.9:1.7	56	1:0.9:2.3	57	-	52
		0.85	1:0.8:1.7		1:0.9:2.2		1:0.9:2.9	
		0.95	1:0.8:1.8		1:0.8:2.2		-	

Table 2.2: Details of Recycled Aggregate Concrete (Padmini et al., 2009)

Designation of recycled aggregate	Strength of parent concrete from which RA is derived (MPa)	Combinations of recycled aggregate concrete cast (three workabilities for each mix)		
		M15	M25	M35
		RA10-1	35	RAC 10-1-1
RA10-2	49	RAC 10-2-1	RAC 10-2-2	RAC 10-2-3
RA10-3	56	RAC 10-3-1	RAC 10-3-2	RAC 10-3-3
RA20-1	37	RAC 20-1-1	RAC 20-1-2	RAC 20-1-3
RA20-2	50	RAC 20-2-1	RAC 20-2-2	RAC 20-2-3
RA20-3	58	RAC 20-3-1	RAC 20-3-2	RAC 20-3-3
RA40-1	31	RAC 40-1-1	RAC 40-1-2	RAC 40-1-3
RA40-2	45	RAC 40-2-1	RAC 40-2-2	RAC 40-2-3
RA40-3	52	RAC 40-3-1	RAC 40-3-2	RAC 40-3-3

Note: RA10-1 indicates that recycled aggregate of maximum sized 10 mm derived from parent concrete of mix 1.

The results of the study indicated that:

1. As the strength of the parent concrete was increased, specific gravities increased marginally and the quantity of adhered mortar increased due to increased bond between the aggregate and the mortar.
2. The reduced specific gravity of recycled aggregate results in reduced amount of coarse aggregate in RCA.
3. The water absorption of the recycled aggregate was significantly higher than the parent aggregate, which was due to: i) type of parent aggregate, ii) strength of parent concrete, and iii) the maximum aggregate size used in the parent concrete.
4. The percentage of water absorption increased with increasing strength of parent concrete due to the higher content of adhered mortar on such recycled aggregates
5. Water absorption increased with decreasing maximum aggregate size used in the parent concrete due to the higher surface area available for mortar to adhere to said aggregates for equal volume of aggregates.

2.2. PROPERTIES OF CONCRETE MADE USING RCA

2.2.1. Fresh Concrete Properties. Hoffmann et al. (2012) reported that a relatively high amount of water is needed in concrete production to reach good workability due to high water absorption of the RCA if the aggregate is not pre-soaked. From that, and the known high absorption of the RCA, it is evident that accurate water

amounts in the concrete can only be obtained from accurate moisture content measurements prior to mixing.

Domingo et al. (2009) reported that increasing the presence of RCA in the mix decreased the workability of the concrete, which may be traced to the shape, texture, and absorption of the RCA. They stated that due to that, it is necessary to use pre-saturated RCA or a larger amount of superplasticizing additives. Sagoe et al. (2001) however reported that plant processed RCA resulted in relatively smooth, spherical particles which lead to improved concrete workability when compared to natural aggregates.

Although it is generally accepted that using RCA reduces the workability of the concrete, it has been observed that through proper mix proportioning and the use of superplasticizing additives, workability goals can be met.

2.2.2. Mechanical Properties. In regards to the performance of the concrete, the workability of the concrete may yield a look into the mechanical behavior, but to see the complete picture it is necessary to test the hardened concrete. Although the relation between certain mechanical properties of normal concrete are moderately understood, those same relations may not hold true for new concretes. For that reason each property must be investigated individually

2.2.2.1. Compressive Strength. While making concrete for structural uses, the compressive strength is one of the main parameters that should be taken into account. For that reason, many researchers have worked to investigate the effect of replacing natural aggregates with recycled aggregates on compressive strength. It is generally believed that the concrete compressive strength decreases with the increase of RCA in the mixture.

However, typically it is observed that replacements of less than thirty percent produce a negligible effect on compressive strength.

Etxeberria et al. (2007) reported that concrete made with a complete replacement of natural coarse aggregate with RCA resulted in a twenty to twenty-five percent reduction in compressive strength for a given w/c ratio and cement. They also reported that a complete replacement of the coarse aggregate required a high amount of cement to obtain high compressive strengths and was therefore not economically feasible. They stated that when producing medium strength concretes, a maximum of twenty-five percent replacement was economical. Other researchers including Domingo et al. (2009) and Sim and Park (2011) reported increases in concrete strengths with increasing RCA replacement percentages.

Due to the controversies present in the literature review with the issue of compressive strength, very few conclusions can be made. It can be concluded that the w/c is one of the main contributors affecting the compressive strength. Also, with the increased absorption of the RCA, water management will be very important. Through proper water management, the effective w/c can be kept constant.

2.2.2.2. Splitting Tensile Strength. Kou et al. (2012) observed that regardless of the type of recycled aggregate used, the splitting tensile strength of the specimens before the age of twenty-eight days decreased as a function of increasing the RCA replacement ratio. However, they observed that for some types of RCA used, an increase in the splitting tensile strength at the age of ninety days was observed. Xiao et al. (2012) also reported decreasing splitting tensile strength with increasing RCA replacement ratios but did not report any trend of increases.

2.2.2.3. Modulus of Elasticity. Hoffmann et al. (2012) reported that the elastic modulus generally decreases with an increase of recycled aggregate content and with the content of crushed concrete, bricks, and tiles. Pereira et al. (2012) observed that although increasing the RCA replacement ratio resulted in a decrease of elastic modulus of the RAC, using proper type and amount of superplasticizer can increase the elastic modulus to values higher than those of reference concrete specimens with no superplasticizer.

Generally, it is believed that the modulus of elasticity decreases as the RCA replacement increases. The reason may be linked to the high volume of adhered mortar with comparatively low modulus of elasticity that is attached to the original aggregate in the RCA (Xiao et al., 2012).

2.2.3. Direct Volume Replacement (DVR) Mixture Proportioning. Knaack and Kurama (2011) used the direct volume replacement method for producing normal strength concrete mixtures with RCA. The DVR method considers the RCA as a single phase material. A predetermined volume of virgin aggregate is replaced by an equal volume of coarse RCA. The mix proportioning is similar to the method presented in ACI 211 (ACI Committee 211, 1991) for proportioning normal, heavyweight, and mass concrete. Based on the results of their study, it was reported that the workabilities of fresh concrete made with this method were similar to those of the virgin aggregate concrete.

3. TECHNICAL APPROACH

This study was performed in three phases: determination of RCA mix design, production of RCA, and determination of new mix designs implementing RCA. The production of RCA involved producing a selected MoDOT approved concrete mix and determining and using a method to produce a MoDOT approved aggregate gradation from the recycled concrete. Developing a mix design utilizing RCA involved working with multiple mixes until the preselected properties were met.

4. PHASE I – DETERMINATION OF RCA MIX DESIGN

4.1. EXPERIMENTAL DESIGN

A number of decisions needed to be made before the start of the study. The initial concrete to use, virgin aggregate sources, admixture types and dosages, test types, and testing equipment all needed to be decided upon.

The main design consideration impacting the final product was which MoDOT concrete mix to be used in the study. The concrete to be used was important because it dictated the mechanical properties of the aggregate to be produced but it also impacted the validity of the whole study. With the aim of this study to impact sustainability, the concrete to be chosen needed to be in an abundant supply and likely to be a source of recycling in the future. A MoDOT Class B concrete was ultimately selected to be studied. It was selected because it is a very common mix design used, it had a moderate strength requirement of around 4,500 psi, and it was a concrete that had been produced before at Missouri S&T.

By selecting a MoDOT Class B concrete, many mix design choices were simultaneously decided upon. The MoDOT Class B mix dictates strict guidelines for the type and amount of aggregates and cement, the water-cement ratio, the minimum air content, and type and amount of admixtures. The guidelines for a MoDOT Class B concrete can be seen in **Table 4.1**. Based on those guidelines, the virgin coarse aggregate was selected to be Potosi dolomite, Missouri river sand was selected to be the fine aggregate, a water-cement ratio of 0.45, and MB-AE 90 and Glenium 7500 were selected.

Table 4.1: Mix Design Guideline for a MoDOT Class B Concrete

Class B Concrete w/Air	
Cementitious Amount, lbs	535
w/c Ratio	0.40
Amount of Fine Aggregate (by volume), %	45
Design Air Content, %	6.0
Air Entrainment	
	Typical Dosage
Daravair 1400	0.5 - 3.0 fl. oz./100lbs of cement
MB-AE 90	0.25 - 4.0 fl. oz./100lbs of cement
AEA 92	0.1 - 4.0 fl. oz./100lbs of cement
Type A Water Reducer	
	Typical Dosage
Daracem 65	3.0 - 9.0 fl. oz./100lbs of cement
ADVA 140M	5.0 - 9.0 fl. oz./100lbs of cement
WRDA 82	3.0 - 5.0 fl. oz./100lbs of cement
Glenium 7500	5.0 - 8.0 fl. oz./100lbs of cement

The properties of the virgin concrete and RCA to be produced that were of interest to the study included slump, air content, compressive strength gain over time, shear strength gain over time, aggregate density, aggregate absorption, aggregate gradation, and aggregate abrasion resistance. ASTM standard test methods were chosen for each property to be determined.

4.2. REPLICATE SPECIMENS

For each laboratory trial mixture, the research team performed one slump test, one air content test, fifteen compressive strength tests, and ten tensile strength tests.

4.3. MATERIALS

4.3.1. Portland Cement. Type I/II cement was used for all trial batches in the laboratory as well as large scale specimens.

4.3.2. Water Reducer/High Range Water Reducer. The WR/HRWR used in the study was Master® Builders Glenium 7500.

4.3.3. Air Entraining Agent. The AE used in the study was Master® Builders MB-AE 90.

4.3.4. Coarse Aggregate. The coarse aggregate used in this portion of the study was virgin limestone aggregate from the Potosi Quarry (Potosi, MO).

4.3.5. Fine Aggregate. The fine aggregate used in this portion of the study was virgin natural sand from Missouri River Sand (Jefferson City, MO).

4.4. TEST EQUIPMENT AND PROCEDURES

4.4.1. Mixing Procedure.

4.4.1.1. Pre-Mixing Preparation. Prior to mixing of the concrete batches, the individual components were weighed and placed in their own separate containers. All aggregate types were tested for moisture content per ASTM C 566 (ASTM 2013) and adjusted properly. The mixing water was separated into four containers. The water container sizes were one half, three eighths, one sixteenth, and one sixteenth in relation to the total mix water. The two smallest containers were used to mix in the air entrainer and water reducing admixtures.

4.4.1.2. Mixing Method. The concrete batches for the strength specimens, slump, and air content were mixed using the same procedure. The mixing conformed to ASTM C 192 (ASTM 2007a). The drum mixer was first moistened by putting cement and water into the drum and allowing it to rotate. Once all surfaces inside the mixer were moist, the slurry was drained from the mixer. Next, the mixing drum was turned on and

all of the coarse aggregates and all of the fine aggregates were added to the drum with half of the allotted mix water. After approximately three minutes, when the mix water had been mostly absorbed into the aggregate, all of the cement was added to the mixing drum along with three eighths of the total mix water. The concrete mixture was then allowed to mix for two minutes. At that point, the WR/HRWR along with the water it had been mixed with was added to the concrete. Thirty seconds after that the AE along with the water it had been mixed with was added to the concrete and the mixture was left to mix for three minutes. After those three minutes, the mixture was allowed to rest in the still drum mixer and then mixed for two more minutes. Immediately after the final two minute mixing, slump and air content tests were begun and, if the results were deemed acceptable, strength specimens were cast. The complete mixing sequence is shown in

Table 4.2.

4.4.2. Strength Specimens.

4.4.2.1. Cylinder Compressive Strength. Fifteen replicate specimens per mixture were molded. Each cylinder mold was treated with a bond break solution prior to placing any concrete inside the molds. The placing, consolidation, and finishing of the cylinder specimens was done as outlined in ASTM C 192 (ASTM 2007a). Following the finishing of the cylinder specimens, the specimens were placed on a flat surface, covered with plastic, and allowed to cure for twenty-four hours in the laboratory. After the day of curing in the lab, the specimens that were not to be tested at day one were moved into a moist cure room conforming to ASTM C 192 (ASTM 2007a).

Three replicate specimens were tested each test day to determine the average strength per day. Prior to the testing of the cylinders, the two ends of the cylinder had to

be made parallel. To prepare the cylinder, sulfur caps were added to the cylinder in accordance with ASTM C 617 (ASTM 2012a). With the cylinders prepared properly, the specimens were placed into a Forney testing machine and loaded at a rate corresponding to a stress rate on the specimen of thirty-five plus or minus seven pounds per square inch (35 ± 7 psi), which is the limit set forth in ASTM C 39 (ASTM 2011a). The maximum load carried by the specimen was recorded and the strength of each cylinder was then calculated to be that load divided by the cross-sectional area of the cylinder.

Table 4.2: Mixing Method Sequence (MoDOT Class B)

Elapsed Time (mm:ss)	Action
0:00	Turn on the mixing drum Insert plenty of water into the mixer Insert a scoop of cement into the mixer
3:00	Drain the excess slurry Insert all of the aggregate and half of the total mix water
6:20	Insert all of the cement Insert three eighths of the total mix water
8:30	Insert the WR/HRWR along with the water it was mixed with
9:00	Insert the AE along with the water it was mixed with
12:00	Stop the drum from rotating
15:00	Re-start the mixer
17:00	Stop mixing the concrete Remove the concrete and begin testing

4.4.2.2. Splitting Tensile Strength. Ten replicate specimens were molded using the same procedure as that used for the compressive strength specimens. Also, the curing

procedure for these specimens was identical to that for the compressive strength specimens. All cylinders cast were cured identically.

Two replicate specimens were tested each test day to determine the average splitting tensile strength per day. The splitting tensile strength test was performed in accordance with ASTM C 496 (ASTM 2011b). The cylinder was loaded with a diametrical compressive force along its length. That compressive load induces a tensile force along the plane containing the applied load. The splitting tensile strength specimens were also tested in a Forney testing machine. To determine the strength value for each specimen, the maximum carried load was divided by pi times the diameter squared.

4.4.3. Slump. For each concrete mixture produced, two tests were run on the fresh concrete. The first test run was the slump test. The slump test is used to measure the workability of the concrete mixture. In accordance with ASTM C 143 (ASTM 2012b), the slump test is run by placing and compacting, through rodding, concrete into a standardized conical mold and then raising the mold. The slump of the concrete is determined by measuring the distance the top face of concrete has fallen from its original position.

4.4.4. Air Content. The method chosen to determine the air content of the concrete mixtures produced was the pressure method as prescribed in ASTM C 231 (ASTM 2010a). In this method, a container is filled with compacted concrete and sealed such as to remove all air outside of the concrete. Pressurized air is then forced into the container and a calibrated dial is read to determine the air content present in the given concrete mixture. This method is very effective and accurate when using a properly calibrated machine as well as using the appropriate aggregate correction factors, as

determined per ASTM C 231 (ASTM 2010a). The aggregate correction factor accounts for each aggregate's innate tendency to accept air when the pressure pot has air forced into the container.

4.5. RESULTS AND DISCUSSION

After producing numerous design batches in the laboratory and running the strength and fresh concrete tests, it was decided that the appropriate admixtures required to produce a concrete conforming to the guidelines of a MoDOT Class B mix were 8.0 oz./cwt of Glenium 7500 and 0.5 oz./cwt of MB-AE 90. The Class B mix design and selected oven-dry (OD) mix design can be seen in **Tables 4.3** and **4.4**, respectively.

Table 4.3: General Mix Design Parameters

MoDOT Class B Mix Design	
Cementitious Amount, lbs	535
w/c Ratio	0.40
Amount of Fine Aggregate (by volume), %	40
Design Air Content, %	6.0
Design Slump, in.	5.0

Table 4.4: Oven Dry Mix Design Selected

OD Design Batch Weights	
Design Weight (lb/yd ³)	
Cement	535
Water	241
Missouri River Sand	1225
1" Potosi Dolomite	1915
Recycled Concrete Aggregate	0
Admixtures Dosage (fl.ozs/cwt)	
HRWR, Glenium 7500	8.0
AE, MB-AE 90	0.5

The selected mix produced an average air content value of six percent and a slump slightly larger than five and a half inches while also producing average strength values slightly larger than the required 4,500 psi on average.

5. PHASE II – PRODUCTION OF RCA

5.1. EXPERIMENTAL DESIGN

Once the mix design for the virgin aggregate concrete had been decided upon, the problem of producing the aggregate from the cast concrete specimens had to be addressed. Many ideas were discussed in the design meetings from using laboratory jaw crushers as seen in some of the literature review to using a mechanical jackhammer to pulverize the concrete specimens. Ultimately, the decision was made to approach Capital Quarries to see if it was possible to use their facilities to produce the RCA. The benefit of using the quarry was that after crushing the specimens, the material could be sieved to produce a MoDOT D Gradation similar to that of the Potosi limestone used as the virgin aggregate. If Capital Quarries agreed to crush the specimens, what size and shape the specimens needed to be for the quarry to crush them had to be addressed at that time. Capital Quarries agreed to crush and screen the concrete and said that concrete beams would be acceptable for crushing as long as there was no steel present in the elements.

After deliberating on a method to cast beams with no steel present and also be able to pick the beams up and transport them, it was decided to imbed two PVC conduits into each beams to create holes through the finished member. Those holes were used to place temporary steel bars in to create pick-points on the concrete beams. The layout of the molds with the conduits present can be seen in **Figure 5.1**. As shown in the figure, the long beam molds were used to cast two beams each by providing a break at their midpoint. This was done to make the beams safer to transport as well as easier for the quarry to handle. The conduit that was cast into the concrete beams was designed to be removed prior to crushing.



Figure 5.1: Concrete Beam Molds with PVC Conduits

With Capital Quarries agreeing to process the RCA, the next consideration was how much aggregate would be obtained from each cubic yard of concrete crushed and how many tons of aggregate would be required. It was determined that the production weight of RCA should be approximately thirty tons and assuming twenty-five percent loss in processing the beams, that would require twenty cubic yards of concrete beams. Rolla Ready Mix (RRM) was selected as the concrete provider for the large concrete pours due to the required amount of material.

5.2. REPLICATE SPECIMENS

In the laboratory, the space allocated for the RCA research project allowed the casting of five long concrete beams along with enough space for any small scale specimens that would be required for the research for each pour. Due to those space

limitations, five different concrete pours producing four cubic yards of concrete beams each were scheduled. Along with the beams to be crushed, numerous small scale specimens were cast including compressive strength specimens, splitting tensile strength specimens, modulus of elasticity specimens, and modulus of rupture specimens. Also for each test, slump and air content were performed to confirm that the concrete being used was what was supposed to be delivered and also met the MoDOT Class B concrete requirements. Once the RCA had been produced, the aggregate was tested four times for gradation, density, absorption, dry-rodded unit weight, and abrasion resistance.

5.3. MATERIALS

For the RCA production phase (Phase II), the research team used the same materials as those used to produce the laboratory mixes of Phase I. Refer to Section 4.3 for a complete discussion of the various concrete constituents, including the Portland cement type, WR/HRWR admixture, AE admixture, and coarse and fine aggregates.

5.4. TEST EQUIPMENT AND PROCEDURES

5.4.1. Mixing Procedure.

5.4.1.1. Pre-mixing Preparation. Prior to ordering concrete from Rolla Ready Mix, the mix design was adjusted by removing a controlled amount of water from the batch weights. This step was done to help control the amount of mix water arriving from the batch plant. The WR/HRWR and AE admixtures were also prepared as these would be added to the concrete mixture when it arrived at the lab.

5.4.1.2. Mixing Method. When the concrete truck arrived at the lab, a slump test was performed on the concrete to determine if the appropriate w/c ratio was present in the concrete. If the mix was too dry, water was added until the expected slump occurred. At that point, the WR/HRWR was added to the truck and the concrete was allowed to mix for approximately one minute. After that, the AE agent was added to the truck and the concrete was allowed to mix for approximately five minutes. After that time, the concrete was ready to be placed in the appropriate molds.

5.4.2. Strength Specimens.

5.4.2.1. Cylinder Compressive Strength. Numerous replicate specimens were molded for each batch of concrete delivered by RRM during construction of the RCA parent material. Each cylinder mold was treated with a bond break solution prior to placing any concrete inside the molds. The placing, consolidation, and finishing of the cylinder specimens was done as outlined in ASTM C 192 (ASTM 2007a). Following the finishing of the cylinder specimens, the specimens were placed on a flat surface, covered with plastic, and allowed to cure for twenty-four hours in the laboratory. After the day of curing in the lab, the specimens were de-molded and placed next to their respective beams and allowed to cure in the same conditions.

Three replicate specimens were tested to determine the compressive strength of the concrete on selected days. The specimens were sulfur capped in accordance with ASTM C 617 (ASTM 2012a) and the compressive strength test was performed in accordance with ASTM C 39 (ASTM 2011a). Once the compressive strength reached a minimum of 2,000 psi, the beams were de-molded and stored until the most recent beam had reached the required 4,500 psi compressive strength. At such time, the beams were

transported to the quarry for processing and the remaining compressive strength specimens were tested to characterize the parent concrete for the RCA.

5.4.2.2. Splitting Tensile Strength. Numerous replicate specimens were molded using the same procedure as that used for the compressive strength specimens. Also, the curing procedure for these specimens was identical to that for the compressive strength specimens. All cylinders cast were cured identically.

Two replicate specimens were tested to determine the splitting tensile strength of the concrete on selected days. The splitting tensile strength test was performed in accordance with ASTM C 496 (ASTM 2011b). Refer to Section 4.4.2.2 for a detailed discussion of the testing procedure. After the beams were transported to the quarry for processing, the remaining splitting tensile strength specimens were tested to characterize the parent concrete for the RCA.

5.4.3. Slump. The slump test was used during the beam pours to determine the amount of water present in the mix by comparing the slump measured with the slump expected as well as to check that the standards for a MoDOT Class B concrete were being met. The slump test was performed in accordance with ASTM C 143 (ASTM 2012b). Refer to Section 4.4.3 for a detailed discussion of the testing procedure.

5.4.4. Air Content. The air content was determined for each of the beam pours in accordance with ASTM C 231 (ASTM 2010a). Refer to Section 4.4.4 for a detailed discussion of the testing procedure.

5.4.5. Modulus Specimens.

5.4.5.1. Modulus of Elasticity. The modulus of elasticity was performed in accordance with ASTM C 469 (ASTM 2010b). The modulus of elasticity measures the

relationship between stress and strain below the proportional limit. Prior to running the test, a linear measuring device is installed on the specimen to measure the strain. The test is then started by conditioning the specimen through loading and partially unloading the specimen. The test is then run by loading the specimen again and unloading it completely. The linear approximation of the data is then reported as the modulus of elasticity. This test was run once for each pour at the time of the concrete beams being processed at the quarry for the purpose of characterizing the parent concrete for the RCA.

5.4.5.2. Modulus of Rupture. The modulus of rupture was run in accordance with ASTM C 78 (ASTM 2010c). The modulus of rupture is a test to determine the flexural strength of an unreinforced beam using a third-point loading scheme. The test is considered valid if the specimen breaks between the top two loading points in the area of constant moment. This test was run three times for each pour at the time of the concrete beams being processed at the quarry for the purpose of characterizing the parent concrete for the RCA.

5.4.6. Gradation. The gradation analysis was performed in accordance with ASTM C 33 (ASTM 2007b). A washed gradation was performed on the RCA prior to each beam pour. The washed gradation is used to better classify the fine particles present in a gradation. The gradation is a breakdown of percent of particles falling between certain sizes and is run by stacking mesh baskets and shaking them until the particles have fallen to the tightest screen.

5.4.7. Density and Absorption. The density and absorption tests were run in accordance with ASTM C 127 (ASTM 2012c). The density is the mass per unit volume of a material. The absorption is defined by ASTM C 127 (ASTM 2012c) as the increase

in mass of a material due to water penetration over a given length of time. These two tests are run together as the absorption is a function of the oven-dry density and the saturated surface dry density.

The absorption is calculated by allowing an oven-dry sample of aggregate to be submerged in water for a given period of time. At such time, the sample is removed and the surface water is removed. With the sample completely full of water but having no water on its surface, the increase in mass from the oven-dry state is the mass of the absorbed water. That water mass divided by the oven-dry mass is the absorption.

The differing densities are calculated by weighing the sample in the air and underwater at varying degrees of saturation. The relationships between the differing masses are used to calculate the differing densities.

5.4.8. Abrasion Resistance. The abrasion resistance test chosen was the Los Angeles abrasion (LAA) test and it was performed in accordance with ASTM C 535 (ASTM 2012d). The LAA is run by rotating a specific gradation of material inside a steel drum along with steel ball bearings of specific weight and size. The material is rotated for a given number of turns and then the new gradation is sieved over a No. 12 sieve. The LAA loss by abrasion value for the given aggregate is then equal to percent of mass passing through the No. 12 sieve rounded to the nearest whole percent.

5.4.9. Dry-Rodded Unit Weight. The bulk density test was run in accordance with ASTM C 29 (ASTM 2009). The bulk density is the measure of the weight of a given aggregate packed into a container of a given volume, divided by that volume. The larger the bulk density, the tighter the aggregate are packed together. Another possibility is that it could be due to a very dense aggregate.

5.5. RESULTS AND DISCUSSION

The concrete beams were all processed at Capital Quarries just north of Rolla, MO. During the processing, the aggregate was sieved to yield a gradation acceptable by MoDOT Gradation D requirements as shown in **Figure 5.2**.

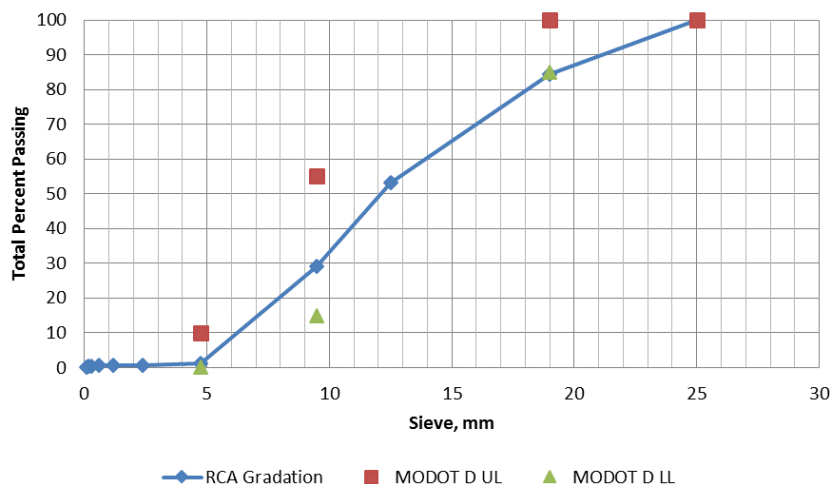


Figure 5.2: RCA Gradation with MoDOT Gradation D Limits

The aggregate product had more adhered mortar present than expected based on literature review and the moderate to low strength of the parent concrete. Photographs of the RCA that was produced can be seen in **Figures 5.3** and **5.4**.

When comparing the properties of the RCA to the virgin aggregate used in the parent concrete, the Potosi limestone, most of the data was as expected. The oven-dry bulk specific gravity was larger for the virgin aggregate. The bulk density was also higher for the virgin aggregate which, since the gradations are nearly identical and the specific gravity is larger, is quite obvious. Also, the absorption for the RCA was much higher than the virgin aggregate as expected. The interesting comparison comes from the LAA

abrasion test. The RCA was slightly more resistant to abrasion than the virgin aggregate.

All of this data is presented in **Table 5.1**.



Figure 5.3: Washed RCA



Figure 5.4: Close Up View of Washed RCA

Table 5.1: Virgin Aggregate and RCA Comparison

	Virgin Aggregate	RCA
Bulk Density	99.7 pcf	89.7 pcf
Bulk Specific Gravity, OD	2.72	2.35
Absorption	0.98%	4.56%
LAA Loss	43%	41%

6. PHASE III – DETERMINATION OF RAC MIX DESIGN

6.1. EXPERIMENTAL DESIGN

The main purpose in developing a design RAC mix for the study was to propose a design that could be implemented into use by MoDOT. The secondary purpose of the mix design development was to be able to replace the selected parent concrete with the proposed RCA. With those two purposes in mind, it was obvious that the mix design proposed needed to have a similar make-up and similar required properties as the parent concrete selected previously. For that reason, the requirements set forth for the RAC mix design were the same as for the MoDOT Class B mix and the starting point for the mix design was to replace the virgin coarse aggregate completely (volumetrically) with RCA. Again, the same admixtures were used to maintain consistency between the mix designs.

6.2. REPLICATE SPECIMENS

For each trial mixture, there were two slump tests (before and after addition of WR/HRWR), one air content test, fifteen compressive strength specimens, and ten tensile strength specimens produced.

6.3. MATERIALS

To develop the recycled aggregate concrete (RAC) mix design (Phase III), the research team used the same materials as those used to produce the laboratory and plant mixes of Phases I and II except for the coarse aggregate. The Potosi limestone coarse aggregate was substituted with the recycled concrete aggregate (RCA) produced during Phase II. Refer to Section 4.3 for a complete discussion of the Portland cement type,

WR/HRWR admixture, AE admixture, and fine aggregate. Refer to Section 5.5 for details on the RCA.

6.4. TEST EQUIPMENT AND PROCEDURES

6.4.1. Mixing Procedure.

6.4.1.1. Pre-Mixing Preparation. Prior to mixing of the concrete batches, the individual components were weighed and placed in their own separate containers. All aggregate types were tested for moisture content per ASTM C 566 (ASTM 2013) and adjusted properly. The mixing water was separated into four containers. The water container sizes were one half, three eighths, one sixteenth, and one sixteenth in relation to the total mix water. The two smallest containers were used to mix in the air entrainer and water reducing admixtures into.

6.4.1.2. Mixing Method. The concrete batches for the strength specimens, slump, and air content were mixed using the same procedure. The mixing conformed to ASTM C 192 (ASTM 2007a). The drum mixer was first moistened by putting cement and water into the drum and allowing it to rotate. Once all surfaces inside the mixer were moist, the slurry was drained from the mixer. Next, the mixing drum was turned on and all of the coarse aggregate and all of the fine aggregate were added to the drum with half of the allotted mix water. After approximately six minutes, when the mix water had been mostly absorbed into the aggregate, all of the cement was added to the mixing drum along with three eighths of the total mix water. The concrete mixture was then allowed to mix for two minutes. At that point, the WR/HRWR along with the water it had been mixed with was added to the concrete. Thirty seconds after that the AE along with the

water it had been mixed with was added to the concrete and the mixture was left to mix for three minutes. After those three minutes, the mixture was allowed to rest in the still drum mixer and then mixed for two more minutes. Immediately after the final two minute mixing, slump and air content tests were begun and, if the results were deemed acceptable, strength specimens were cast. The complete mixing sequence is shown in

Table 6.1.

Table 6.1: Mixing Method Sequence (RAC)

Elapsed Time (mm:ss)	Action
0:00	Turn on the mixing drum Insert plenty of water into the mixer Insert a scoop of cement into the mixer
3:00	Drain the excess slurry Insert all of the aggregate and half of the total mix water
9:20	Insert all of the cement Insert three eighths of the total mix water
11:30	Insert the WR/HRWR along with the water it was mixed with
12:00	Insert the AE along with the water it was mixed with
15:00	Stop the drum from rotating
18:00	Re-start the mixer
20:00	Stop mixing the concrete Remove the concrete and begin testing

6.4.2. Strength Specimens. The same number of specimens and procedures outlined in Section 4.4.2 were also used during the laboratory mixes of Phase III. Refer to Sections 4.4.2.1 and 4.4.2.2 for detailed discussions of the testing procedures for compressive strength and splitting tensile strength, respectively.

6.4.3. Slump. The slump test was performed for each laboratory mix in accordance with ASTM C 143 (ASTM 2012b). Refer to Section 4.4.3 for a detailed discussion of the testing procedure.

6.4.4. Air Content. The air content was determined for each laboratory mix in accordance with ASTM C 231 (ASTM 2010a). Refer to Section 4.4.4 for a detailed discussion of the testing procedure.

6.5. RESULTS AND DISCUSSION

After producing multiple batches of RAC using the same exact mix design used for the parent concrete, it was evident that the slump was not behaving as required. Since the HRWR amount being used was already at the maximum suggested for a MoDOT Class B concrete, the AE amount was increased from half a percent up to one percent. That initial RAC mix design was made multiple times, but the mix was behaving poorly. The mix appeared “sticky” or more viscous than any of the parent mixes from the trial batches in both the mixing drum as well as during the slump test. The slump test required nearly three times the amount of time to settle for the initial RAC mix as compared to the parent mixes. The Class B mix design and selected oven-dry (OD) mix design are shown in **Tables 6.2** and **6.3**, respectively.

Table 6.2: General Mix Design Parameters (RAC)

MoDOT Class B Mix Design	
Cementitious Amount, lbs	535
w/c Ratio	0.40
Amount of Fine Aggregate (by volume), %	40
Design Air Content, %	6.0
Design Slump, in.	5.0

Table 6.3: Oven Dry Mix Design Selected (RAC)

OD Design Batch Weights	
Design Weight (lb/yd ³)	
Cement	535
Water	241
Missouri River Sand	1249
1" Potosi Dolomite	0
Recycled Concrete Aggregate	1662
Admixtures Dosage (fl.ozs/cwt)	
HRWR, Glenium 7500	8.0
AE, MB-AE 90	1.0

After observing the RAC mix behavior, the mix was reproduced while varying the amount of admixtures. Noticing that admixture adjustments did little to change the behavior of the mixture, it was decided to look into different mechanisms that could lead to a “sticky” mix. The mechanism that was investigated was the behavior of the particles and their relation to each other. That mechanism was selected because the “sticky” mix appeared to have particles rolling over each other. To look into the interactive particle behavior, the gradations between the two coarse aggregates from the study were analyzed. The two gradations are shown in **Figures 6.1** and **6.2**, respectively.

As can be seen from comparing the two plots, the RCA gradation has fewer small particles on the limiting sieves even though both aggregates meet MoDOT Gradation D limits. Also, there are almost no fine particles present in the RCA. Without the presence of enough fine particles, the aggregate will behave like marbles unable to maintain a dense packing formation.

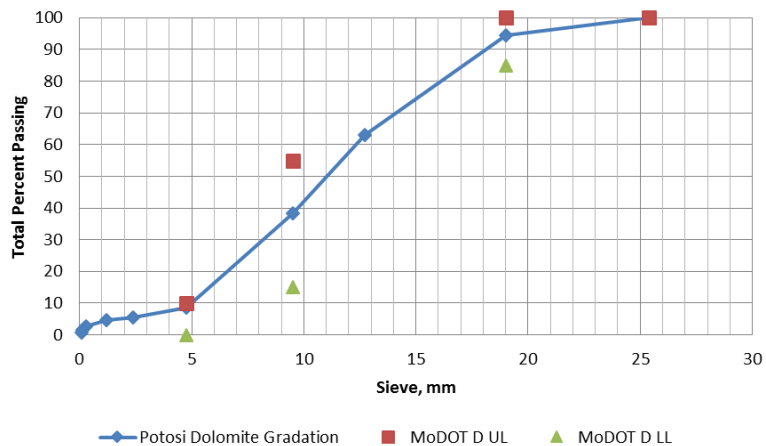


Figure 6.1: Virgin Coarse Aggregate Gradation

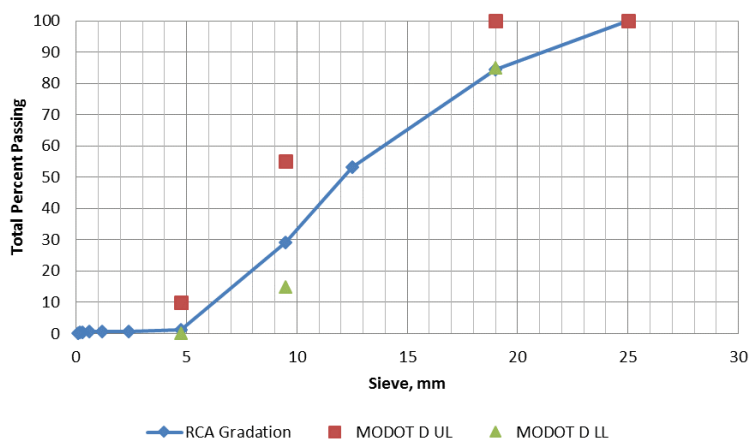


Figure 6.2: RCA Gradation

To better understand the behavior present in the “sticky” mix, a combined gradation was plotted. Along with the combined gradation, a plot of each gradation separately, fine aggregate and coarse aggregate, along with a modified combined gradation was also determined. These four plots are shown in **Figure 6.3**.

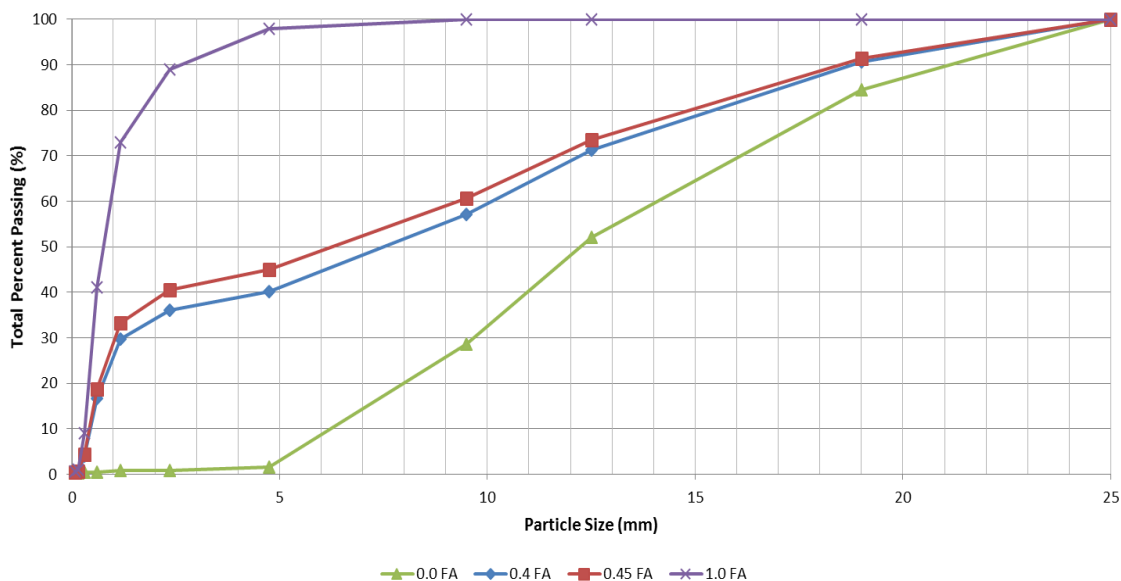


Figure 6.3: Combined Gradation Analysis

With this plot, it becomes visually evident that increasing the fine aggregate by only five percent, from forty percent to forty-five percent, the mix increases its fine aggregate volume by nearly fifteen percent and has little change in its coarse aggregate volume. Using this modified fine aggregate percentage, the MoDOT Class B mix was modified and batched using the initial RAC mix design with 8.0 oz./cwt HRWR and 1.0 oz./cwt AE. That batch appeared to have a more normal viscosity in comparison to those seen in the parent concrete mixes but with excessive slump. After refinement, the HRWR was reduced to produce the final RAC mix to be used for the remainder of the study. The final RAC mix design is detailed in **Tables 6.4** and **6.5**.

Table 6.4: RAC Mix Design Template

"Modified" MoDOT Class B Mix Design	
Cementitious Amount, lbs	535
w/c Ratio	0.40
Amount of Fine Aggregate (by volume), %	45
Design Air Content, %	6.0
Design Slump, in.	5.0

Table 6.5: RAC Oven-Dry Batch Weights

OD Design Batch Weights	
Design Weight (lb/yd ³)	
Cement	535
Water	241
Missouri River Sand	1405
1" Potosi Dolomite	0
Recycled Concrete Aggregate	1524
Admixtures Dosage (fl.ozs/cwt)	
HRWR, Glenium 7500	6.0
AE, MB-AE 90	1.0

7. SUMMARY AND CONCLUSIONS

The determination of the initial mix design was mainly governed by the choice to use a MoDOT Class B concrete. From that, the initial mix design was developed with the only questions to answer being which virgin aggregates to use, which admixtures to use, and what amount of admixture to use.

With the parent concrete mix designed, the task of processing the soon to be hardened concrete specimens into piles of aggregate lay ahead. The processing was handled by Capital Quarries. The only barrier to overcome with the large specimens that were being cast to be crushed was how to cast them without any steel embedments yet facilitate handling. The solution involved embedding PVC conduits into the beams to allow bars to be slid in and out of the concrete when movement by chains was required. Then, when the beams were processed into RCA, the small scale specimens that were cast alongside them were tested to analyze the RAC and the parent concrete on the day of processing because that is the day that the properties stopped gaining strength and rigidity. The RCA was characterized and it was found to be lighter and more porous than the virgin coarse aggregate, but it was slightly tougher when tested using the Los Angeles abrasion test.

Lastly, the development of the RCA mix design to be used for the remainder of the RCA study was developed. The mix design was initially developed exactly as a MoDOT Class B concrete with RCA as the coarse aggregate, but it was soon discovered that there were problems. The mix was behaving far more viscously than any of the previous concrete mix designs. After analyzing the particle characteristics for each aggregate source and the combined aggregates used to produce the RAC, it was

determined that a lack of fines was causing viscosity issues in the concrete. The fine aggregate percent by volume was increased from forty percent up to forty-five percent. With that change, the HRWR was able to be reduced to three quarters of that used in the parent concrete while producing similar strength, air content, and slump. That final mix design was then to be used for the remainder of the study of RAC.

BIBLIOGRAPHY

- Abbas, G. F., Fournier, B., Isgor, O. B., Razaqpur, A. G., Foo, S., “Quantification of the Residual Mortar Content in Recycled Concrete Aggregates by Image Analysis”, Material Characterization, Vol. 60, 2009, pp. 716-728.
- ACI. (1991). “Standard Practice for Selecting Proportions for Normal, Heavyweight, and Mass Concrete,” *ACI 211.1-91*, American Concrete Institute, Farmington, MI.
- ASTM. (2007a). “Standard Practice for Making and Curing Concrete Test Specimens in the Laboratory” *ASTM C 192/C 192M – 07*, ASTM International, West Conshohocken, PA.
- ASTM. (2007b). “Standard Specification for Concrete Aggregates” *ASTM C 33/C 33M – 07*, ASTM International, West Conshohocken, PA.
- ASTM. (2009). “Standard Test Method for Bulk Density and Voids in Aggregate” *ASTM C 29/C 29M – 09*, ASTM International, West Conshohocken, PA.
- ASTM. (2010a). “Standard Test Method for Air Content of Freshly Mixed Concrete by the Pressure Method” *ASTM C 231/C 231M – 10*, ASTM International, West Conshohocken, PA.
- ASTM. (2010b). “Standard Test Method for Static Modulus of Elasticity and Poisson’s Ratio of Concrete in Compression” *ASTM C 469/C 469M – 10*, ASTM International, West Conshohocken, PA.
- ASTM. (2010c). “Standard Test Method for Flexural Strength of Concrete” *ASTM C 78/C 78M – 10*, ASTM International, West Conshohocken, PA.
- ASTM. (2011a). “Standard Test Method for Compressive Strength of Cylindrical Specimens” *ASTM C 39/C 39M – 11*, ASTM International, West Conshohocken, PA.
- ASTM. (2011b). “Standard Test Method for Splitting Tensile Strength of Cylindrical Concrete Specimens” *ASTM C 496/C 496M – 11*, ASTM International, West Conshohocken, PA.
- ASTM. (2012a). “Standard Practice for Capping Cylindrical Concrete Specimens” *ASTM C 617/C 617M – 12*, ASTM International, West Conshohocken, PA.
- ASTM. (2012b). “Standard Test Method for Slump of Hydraulic-Cement Concrete” *ASTM C 143/C 143M – 12*, ASTM International, West Conshohocken, PA.

- ASTM. (2012c). “Standard Test Method for Density, Relative Density, and Absorption of Coarse Aggregates” *ASTM C 127/C 127M – 12*, ASTM International, West Conshohocken, PA.
- ASTM. (2012d). “Standard Test Method for Resistance to Degradation of Large-Size Coarse Aggregate by Abrasion and Impact in the Los Angeles Machine” *ASTM C 535/C 535M – 12*, ASTM International, West Conshohocken, PA.
- ASTM. (2013). “Standard Test Method for Total Evaporable Moisture Content of Aggregate by Drying” *ASTM C 566/C 566M – 13*, ASTM International, West Conshohocken, PA.
- Domingo-Cabo, Lazaro, C., Lopez-Gayarre, F., Serrano-Lopez, M. A., Serna, P., Castano-Tabares, J. O., “Creep and Shrinkage of Recycled Aggregate Concrete”, Construction and Building Materials, Vol. 23, 2009, pp. 2545-2553.
- Etxeberria, M., Vazquez, E., Mari, A., Barra, M., “Influence of Amount of Recycled Coarse Aggregates and Production Process on Properties of Recycled Aggregate Concretes”, Cement and Concrete Research, Vol. 37, 2007, pp. 735-742.
- Hoffmann, C., Schubert, S., Leemann, A., Motavalli, M., “Recycled Concrete and Mixed Rubble Aggregates: Influence of Variations in Composition on the Concrete Properties and Their use as Structural Material”, Construction and Building Materials, Vol. 35, 2012, pp. 701-709.
- Knaack, A. M. and Kurama, Y. C., “Design of Normal Strength Concrete Mixtures with Recycled Concrete Aggregates”, ASCE Structures Congress, 2011.
- Kou, S., Poon, C., Wan, H., “Properties of Concrete Prepared with Lo-X-Grade Recycled Concrete Aggregate”, Construction and Building Materials, Vol. 36, 2012, pp. 881-889.
- Li, W., Xiao, J., Sun, Z., Kawashima, S., Shah, S. P., “Interfacial Transition Zones in Recycled Concrete with Different Mixing Approaches”, Construction and Building Materials, Vol. 35, 2012, pp. 1045-1055.
- Limbackiya, M. C., Marrocchino, E., Koulouris, A., “Chemical –Mineralogical Characterization of Coarse Recycled Concrete Aggregate”, Waste Management, Vol. 27, 2007, pp. 201-208.
- Nagataki, S., Gokce, A., Saeki, T., “Effects of Recycled Aggregate Characteristics on Performance Parameters of Recycled Aggregate Concrete”, Proceedings of Fifth CANMET/ACI International Conference on Durability of Concrete, Barcelona, June 2012, pp. 51-71.

- Padmini, A. K., Ramamurthy, K., Mathews, M. S., "Influence of Parent Concrete on the Properties of Recycled Aggregate Concrete", Construction and Building Materials, Vol. 23, Issue 2, Feb. 2009, pp. 829-836.
- Pereira, P., Evangelista, L., Brito, J., "The Effect of Superplasticizers on the Workability and Compressive Strength of Concrete Made with Fine Recycled Concrete Aggregates", Construction and Building Materials, Vol. 28, 2012, pp. 722-729.
- Sagoe, K., Brown, T., Taylor, A. H., "Performance of Concrete Made with Commercially Produced Coarse Recycled Concrete Aggregate", Cement and Concrete Research, Vol. 31, 2001, pp. 707-712.
- Sim, J. and Park, C., "Compressive Strength and Resistance to Chloride Ion Penetration and Carbonation of Recycled Aggregate Concrete with Varying Amount of Fly Ash and Fine Recycled Aggregate", Waste Management, Vol. 31, 2011, pp. 2352-2360.
- Tam, V. W. Y., Tam, C. M., Wang, Y., "Optimization on Proportion for Recycled Aggregate in Concrete Using Two-Stage Mixing Approach", Construction and Building Materials, Vol. 21, 2007, pp. 1928-1939.
- Xiao, J., Xie, H., Yang, Z., "Shear Transfer Across a Crack in Recycled Aggregate Concrete", Cement and Concrete Research, Vol. 42, 2012, pp. 700-709.

APPENDIX B

FINAL Report B

TRyy1317

**Project Title: Recycled Concrete Aggregate (RCA) for
Infrastructure Elements**

Report B: Mechanical and Durability Properties of RCA Concrete

Prepared for
Missouri Department of Transportation
Construction and Materials

Missouri University of Science and Technology, Rolla, Missouri

May 2014

The opinions, findings, and conclusions expressed in this publication are those of the principal investigators and the Missouri Department of Transportation. They are not necessarily those of the U.S. Department of Transportation, Federal Highway Administration. This report does not constitute a standard or regulation.

ABSTRACT

The present project investigates the properties of sustainable concrete materials made with recycled concrete aggregate (RCA) as a partial replacement of coarse aggregate. Seven RCA-made experimental mixtures, as well as two mixtures made with virgin aggregates were used in this study. The study has focused on properties of a MoDOT Class B concrete mixture.

Several concrete mixtures with different amounts of RCA replacement varying from 30% to 100% were investigated. Two additional types of RCA concrete mixtures, mixed and proportioned according to different procedures, were also incorporated in the study. A mixture with 100% RCA replacement mixed according to the two stage mixing approach (TSMA) was studied to investigate the effect of TSMA on both the mechanical and durability properties of RCA-produced concrete. In addition, the equivalent mortar volume (EMV) method was used successfully to develop a mixture with approximately 30% RCA replacement.

Different fresh, mechanical, and durability properties were investigated in this study. Based on the results, it is concluded that it is possible to produce sustainable concrete mixtures using high volumes of RCA as replacement for virgin coarse aggregate in MoDOT Class B concrete.

TABLE OF CONTENTS

	Page
ABSTRACT.....	ii
LIST OF ILLUSTRATIONS.....	v
LIST OF TABLES.....	vii
1. INTRODUCTION.....	1
1.1. BACKGROUND.....	1
1.2. OBJECTIVE AND SCOPE OF WORK.....	2
1.3. RESEARCH METHODOLOGY.....	2
1.4. REPORT OUTLINE.....	4
2. LITERATURE REVIEW ON RECYCLED AGGREGATE.....	5
2.1. GENERAL.....	5
2.2. USE OF RECYCLED AGGREGATE AS COARSE AGGREGATE.....	7
2.2.1. Background.....	7
2.3. PREVIOUS STUDIES RELATED TO RAC.....	8
2.3.1. Fresh Properties.....	8
2.3.2. Mechanical Properties.....	8
2.3.2.1. Compressive Strength.....	8
2.3.2.2. Splitting Tensile Strength.....	9
2.3.2.3. Flexural Strength.....	10
2.3.2.4. Modulus of Elasticity.....	10
2.3.2.5. Shrinkage.....	11
2.3.3. Durability.....	12
2.3.3.1. Chloride Ion Permeability.....	12
2.3.3.2. Freeze/thaw Resistance.....	12
2.4. CONCLUDING REMARKS.....	13
3. EXPERIMENTAL PROGRAM.....	14
3.1. MATERIAL PROPERTIES.....	14
3.2. MIXTURE PROPORTIONS.....	19
3.2.1. Conventionally Proportioned Mixtures.....	19

3.2.2. Two Stage Mixing Approach	19
3.2.3. Equivalent Mortar Volume Mixture Proportioning Method	20
3.3. TEST MATRIX	28
3.4. SAMPLING AND CURING	31
4. RESULTS AND DISCUSSION	33
4.1. FRESH PROPERTIES	33
4.1.1. General	33
4.1.2. Bleeding.....	34
4.1.3. Rheological Properties	35
4.2. MECHANICAL PROPERTIES	38
4.2.1. General	38
4.2.2. Compressive Strength.....	39
4.2.3. Splitting Tensile Strength.....	42
4.2.4. Flexural Strength	44
4.2.5. Modulus of Elasticity	48
4.3. DURABILITY	51
4.3.1. General	51
4.3.2. Drying Shrinkage	53
4.3.3. Surface Resistivity.....	56
4.3.4. Bulk Electrical Conductivity	62
4.3.5. Permeable Void Volume	66
4.3.6. Absorption.....	68
4.3.7. Deicing Salt Scaling.....	71
4.3.8. Freeze/thaw Resistance	74
5. FINDINGS, CONCLUSIONS, AND RECOMMENDATIONS.....	80
5.1. FINDINGS AND CONCLUSIONS	80
5.2. RECOMMENDATIONS.....	83
BIBLIOGRAPHY	85

LIST OF ILLUSTRATIONS

Figure	Page
Figure 2.1 Schematic Sketch of RCA and ITZs (Xiao et al. 2012)	7
Figure 3.1 RCA Particles before Separating the Mortar (left) and after Separating the Residual Mortar (right)	16
Figure 3.2 Particle Size Distribution of the Fine Aggregate.....	17
Figure 3.3 Particle Size Distribution of the Coarse Aggregate.....	18
Figure 3.4 Individual Percentage Retained on Each Sieve	18
Figure 4.1 Bingham Model for Rheological Properties of Concrete (ICAR manual)	36
Figure 4.2 Yield Stress Analysis (ICAR manual).....	36
Figure 4.3 ICAR Rheometer Interface.....	37
Figure 4.4 Splitting Tensile Strength Test Setup	42
Figure 4.5 Simply Supported Beam for Determining the Flexural Strength (ASTM C78).....	46
Figure 4.6 Modulus of Elasticity Test Setup	49
Figure 4.7 Variations in Relative Humidity and Temperature of the Environmental Chamber	54
Figure 4.8 Measuring the Length of the Shrinkage Specimens	54
Figure 4.9 Drying Shrinkage Deformation of the Specimens.....	56
Figure 4.10 Schematic View of the Surface Resistivity Measurement Principles (Proseq SA 2013).....	57
Figure 4.11 Surface Resistivity Measurement	59
Figure 4.12 Correlation Between the Surface Resistivity and RCA Replacement Ratio ..	62
Figure 4.13 Measuring Bulk Electrical Resistivity. Top foam (top left), Lower Foam (top right), and Specimen Resistivity (bottom photo)	64
Figure 4.14 Correlation between the Bulk Resistivity and RCA Replacement Ratio	65
Figure 4.15 Correlation between the Surface and Bulk Electrical Resistivity Measurements	66
Figure 4.16 Correlation between the Absorption Values Measured after Immersion and Boiling	71

Figure 4.17 Rating Scale for Scaling Resistance (ASTM C672).....	73
Figure 4.18 Silicon Made Dike for Ponding the Surface of the Specimen with a Chloride Solution.....	74
Figure 4.19 Appearance of the Specimen Surfaces after 50 Cycles of Deicing-salt Scaling Test	77
Figure 4.20 Freeze/thaw Testing, Procedure A, Freezing and Thawing in Water (left), Measurement of Pulse Velocity (right).....	78
Figure 4.21 Variations in Durability Factor with Freeze/thaw Cycles	78

LIST OF TABLES

Table	Page
Table 3.1 Physical Properties and Chemical Compositions of Cement.....	14
Table 3.2 Chemical Compositions of Ameren UE Fly Ash (Wolfe 2011).....	15
Table 3.3 Physical Properties of the Aggregates	17
Table 3.4 Test Matrix for Making Concrete Mixtures.....	30
Table 3.5 Mixture Proportions of Concrete used in the Study	31
Table 3.6 Test Methods and Standard used in the Study	32
Table 4.1 Slump Value, Air Content, and Unit Weight of Fresh Concrete Mixtures.....	33
Table 4.2 Results of Bleeding Measurements.....	35
Table 4.3 Rheological Properties of the Concrete Mixtures.....	38
Table 4.4 Fresh Properties of Mixtures used for Mechanical Property Sampling.....	39
Table 4.5 Compressive Strength Results	40
Table 4.6 Splitting Tensile Strength Results.....	43
Table 4.7 Comparing the Splitting Tensile Strength Data with ACI 318 Equation	45
Table 4.8 Flexural Strength Results.....	47
Table 4.9 Comparing the Flexural Strength Measurements with ACI 318 Equation.....	48
Table 4.10 Modulus of Elasticity Measurements	49
Table 4.11 Comparing the Modulus of Elasticity Measurements with ACI 318 Equation	52
Table 4.12 Comparing the Modulus of Elasticity Measurements with AASHTO Equation	52
Table 4.13 Fresh Properties of Mixtures used for Durability Sampling.....	53
Table 4.14 Correlation between the Surface Resistivity and Likelihood of Corrosion	58
Table 4.15 Correlation between the Surface Resistivity and Rate of Corrosion	59
Table 4.16 Surface Electrical Resistivity Measurements	60
Table 4.17 Correlation between the Surface Resistivity and Chloride Ion Permeability ..	61
Table 4.18 Bulk Electrical Resistivity Measurements.....	64
Table 4.19 Permeable Void Volume Measurements	68
Table 4.20 Durability Classification Based on Permeable Void Volume (CCAA 2009)..	69

Table 4.21 Absorption after Immersion.....	70
Table 4.22 Absorption after Immersion and Boiling.....	70
Table 4.23 Deicing Salt Scaling Data.....	75
Table 4.24 Variations in Durability Factor of Specimens	79

1. INTRODUCTION

1.1. BACKGROUND

Sustainable solutions for the concrete industry are taking into account the durability, environmental impacts, and costs of the project (Kim 2013). Due to the increasing rate of demolition, it is essential to effectively reuse demolition waste in order to conserve the nonrenewable natural resources. Decreasing natural resources, as well as increasing problems with waste management, ecological hazards, landfill limitations and increasing distances between the natural resources and consumption markets, support the idea of recycled wastes to be used for new concrete production (Padmini et al., 2009). Besides, reducing the carbon footprint in such a highly consumed material is a key factor in decreasing the total emissions produced by the construction industry (McIntyre 2009).

As a result of variable characteristics of recycled aggregates compared to virgin aggregate sources, there currently exists a conservative approach, limiting the use of recycled concrete aggregate (RCA) in field implementations (Surya 2013). RCA is mostly being used in granular bases, embankments, sound barriers, fills, and so on. (Kim 2013, Gabr 2012). Laboratory investigations on properties of concrete made with RCA has proved to be an issue of great interest during the past decades. However, there is a limited number of field implementations of RCA in structural applications, which is mainly due to a lack of proper selection criteria. The present study aims at investigating the feasibility of producing sustainable concrete materials for infrastructure applications. The research is mainly focusing on MoDOT Class B concrete mixtures.

1.2. OBJECTIVE AND SCOPE OF WORK

The main *objective* of this research study was to evaluate the fresh, mechanical, and durability properties of concrete mixtures made with RCA as virgin coarse aggregate replacement.

The following scope of work was implemented in order to achieve the objective of the research study:

- Perform a literature review;
- Develop a research plan;
- Develop mix designs for both conventional and RCA concrete;
- Evaluate the fresh properties of the reference and RCA concrete;
- Evaluate the mechanical properties of the reference and RCA concrete;
- Evaluate the durability properties of the reference and RCA concrete;
- Compare test results to current guidelines and previous research findings;
- Develop conclusions and recommendations; and
- Prepare this report to document the details, results, findings, conclusions, and recommendations of this study.

1.3. RESEARCH METHODOLOGY

The proposed research methodology included five (5) tasks necessary to successfully complete the study. They are as follows:

Task #1: The purpose of this task was to conduct a comprehensive and critical literature review of past experiences and previous research on RCA, with particular attention to the impact that these findings could have on the research plan. Specifically,

the literature review focused on studies that investigated RCA properties (*e.g.*, absorption, durability) as well as the behavior of concrete containing RCA including the fresh and hardened properties (*e.g.*, workability, compressive strength, flexural strength, shrinkage), and durability (*e.g.*, freeze-thaw resistance, permeability, scaling).

Task #2: Develop reference and RCA-made concrete mix designs. The purpose of this task was to develop concrete mixtures incorporating RCA as a partial or full replacement of virgin coarse aggregate. Alternative mixing procedures and experimental mix proportioning methods were also used for developing mixtures in this phase. Conventional concrete mix designs served as controls during this study.

Task #3: Perform material and component testing. A number of fresh and hardened concrete property tests were completed to evaluate the performance of the RCA made mixtures and determine the validity of using these tests to predict the performance of concretes containing recycled concrete aggregate.

Task #4: Analyze test data. The material, component, and test results were analyzed to evaluate the behavior of the developed mixtures compared to conventional virgin aggregate concrete. The test data included:

Fresh properties: Slump, air content, bleeding, and rheological properties.

Mechanical properties: Compressive strength, splitting tensile strength, flexural strength, modulus of elasticity, shrinkage.

Durability: Permeable void volume, absorption, surface electrical resistivity, bulk electrical resistivity, freeze/thaw durability, and deicing salt scaling.

Task #5: Develop findings, conclusions, and recommendations. This task synthesized the results of the previous tasks into findings, conclusions, and recommendations on mechanical and durability properties of RCA-constructed concrete.

1.4. REPORT OUTLINE

This report includes five chapters. This section will discuss the information that will be presented in more detail throughout this document.

Chapter 1 acts as an introduction to the report. This introduction contains a brief background of recycled aggregate. It also discusses the research objective, scope of work, and research plan.

Chapter 2 includes information from previous research performed on the characterization of recycled aggregate and its applications as a coarse aggregate in concrete.

Chapter 3 includes information about the experimental program. The experimental program consisted of producing concrete mixtures with different amounts of RCA replacement and using different mixing methods. This chapter also includes the properties of the material used in study, as well as details of the mixture proportioning methods used in research.

Chapter 4 presents the test results and the different analyses used to investigate the fresh properties, mechanical performance, and durability of the produced specimens.

Chapter 5 concludes this document, summarizing the findings and conclusions of this study and proposing recommendations and future research.

2. LITERATURE REVIEW ON RECYCLED AGGREGATE

2.1. GENERAL

With the introduction of waste legislation in the form of regulations and directives in many parts of world, a significant movement towards the sustainable management of construction and demolition (C&D) waste is becoming a legal requirement. In response, different sectors of the construction industry are undertaking various initiatives to minimize waste generation and improve the management of C&D waste to maximize economic and environmental benefits, generally by placing emphasis on increasing recycling for reuse (Limbachiya et al 2007).

The building industry in particular is a major consumer of materials and at the same time a major producer of waste (Padmini et al. 2009). According to Abbas et al. (2009) concrete accounts for up to 67% by weight of construction and demolition waste. The amount of demolition waste dumped at landfill sites in the United Kingdom is said to be in excess of 20 million tons per annum. The bulk of this material is concrete (50%–55%) and masonry (30%–40%) with only small percentages of other materials such as metals, glass and timber (Tam et al. 2007). In the Netherlands, about 14 million tons of building and demolition waste per annum are produced, in which about 8 million tons are recycled, mainly for unbound road base courses (Tam et al. 2007). It is also estimated that approximately 200 million tons of waste concrete are currently produced annually in the mainland of China (Xiao et al. 2012).

Due to the increasing rate of demolition, it is essential to effectively reuse demolition waste in order to conserve the nonrenewable natural resources. As a result of the mentioned problems, the idea of producing *green* recycled aggregate concrete (RAC),

which is by definition a concrete in which recycled aggregate is used, has emerged.

Recycled aggregate concrete will satisfy the three prerequisites of green materials (i) it can recycle and reduce natural resources and energy consumption; (ii) it will not affect the environment; and (iii) it can maintain sustainable development. However, there are some technical obstacles limiting the use of RCA in concrete production. In evaluation of the recycled aggregate characteristics, it should be kept in mind that each recycled concrete aggregate particle is still a piece of concrete composed of the original coarse aggregate (OCA) and the adhered mortar (AM). The recombined form of these concrete particles with a new matrix is called recycled aggregate concrete. For a clear understanding of the recycled aggregate and to predict its possible effects on concrete, the constituents of these composite particles must be identified separately (Nagataki et al. 2000).

It is a believed concept that the quality of RAC is tied to the properties of the original waste concrete, the new composition, the mixing approach, and the deterioration conditions of the recycled aggregates. Initial investigations on the use of recycled aggregate usually focused on incorporating recycled coarse aggregate and its influence on mechanical and durability properties of the RAC. It was an adopted concept that although the use of recycled coarse aggregate may be viable, a decrease in the performance of the RAC should be regarded as a normal outcome which can be mitigated through various approaches such as increasing cement content in mixture, etc. (Bagragi et al. 1990).

2.2. USE OF RECYCLED AGGREGATE AS COARSE AGGREGATE

2.2.1. Background. RCA is typically regarded as a double phase material consisting of the original virgin aggregate and the adhered residual mortar. The RAC will have more constituents: RCA aggregate, fresh mortar, and virgin coarse aggregates. Thus, there are two types of interfacial transition zones (ITZs) in RACs: one, the old ITZ between the original virgin coarse aggregate and the adhered mortar; and the second one between the new mortar and the RCA. (**Figure 2.1**)

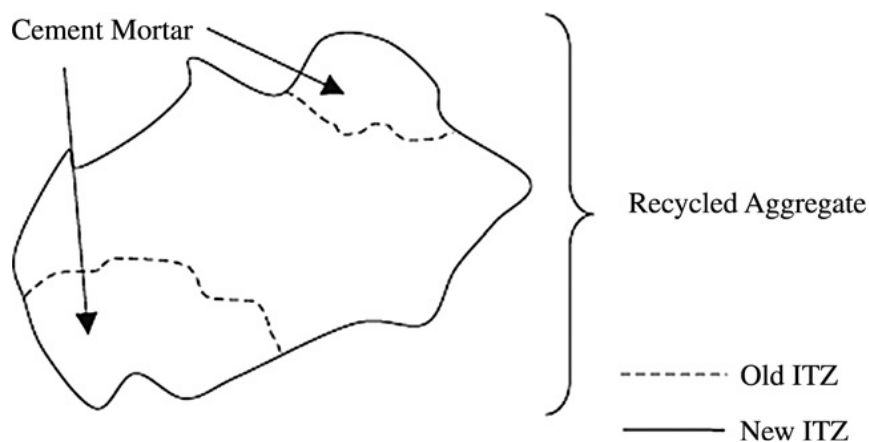


Figure 2.1 Schematic Sketch of RCA and ITZs (Xiao et al. 2012)

As a result of usually high amounts of adhered mortar content in recycled aggregates, these types of aggregates have high water absorption, low density, low specific gravity, and high porosity compared to natural aggregates (Kou et al. 2012). Some technical problems, including weak interfacial transition zones between cement paste and aggregate, porosity and traverse cracks within demolition concrete, high level of sulphate and chloride contents, impurity, poor grading, and high variations in quality, render the use of recycled aggregate difficult. It is usually believed that adhered mortar is

the main cause of the lower properties of the recycled aggregates compared to the virgin natural aggregates.

2.3. PREVIOUS STUDIES RELATED TO RAC

2.3.1. Fresh Properties. As a result of usually high amounts of adhered mortar existing in RCA particles, the density of these aggregates are lower than those of virgin aggregates, which in turn results in a decrease in unit weight of concrete made with these types of aggregates. However, the conclusions on the workability properties of the recycled aggregate concretes are not always revealing inferior properties in these types of concrete mixtures.

Surface texture of the RCA particles may have positive or negative effects on workability of the mixture. Domingo et al. (2009), reported that a greater presence of recycled aggregates decreases the workability of the concrete which may be traced to the shape, texture, and absorption characteristics of recycled aggregates. They stated that is the reason why it is necessary to use saturated recycled aggregate or a greater amount of superplasticizers to maintain the workability.

On the other hand, Sagoe et al. (2001), reported that plant processing of recycled aggregate produces relatively smoother spherical particles, which leads to improved concrete workability in comparison with some natural aggregate concretes with equivalent grading and ratio of fine to coarse aggregate.

2.3.2. Mechanical Properties.

2.3.2.1. Compressive Strength. It is usually reported that the RCA replacement level has a significant effect on compressive strength of concrete. It is believed that using

RCA has a negative impact on strength properties of concrete. This is mainly due to the inferior properties of the residual mortar phase of the RCA particles. However, this effect is usually negligible for replacement levels up to 30%. Nixon (1978) also found that the compressive strength of RAC is somewhat lower compared with the strength of control mixes of conventional concrete. Hansen (1986) concluded that the compressive strength of RAC is largely controlled by a combination of the water to cement ratio of the original concrete and the water to cement ratio of the RAC when other factors are essentially identical.

Sagoe et al. (2001) observed no significant difference in the compressive strength of the specimens made with up to 100% replacement of coarse recycled aggregate with the reference concrete made with basalt coarse aggregates. The recycled aggregates were saturated before mixing.

Variations in compressive strength is mostly a function of the quality of RCA, which may result in various compressive strength values; no change in the strength, decrease, or even increase in the compressive strength when compared with the reference specimens. However, it is usually reported that decrease in w/cm and increase in cementitious materials content result in enhanced compressive strength of RAC (Xiao et al. 2012).

2.3.2.2. Splitting Tensile Strength. It is generally reported that RCA replacement results in a decrease in splitting tensile strength of concrete. Ravindrarajah et al. (1985) reported that the splitting tensile strength of RAC was consistently 10% lower than that of conventional concrete. Tabsh and Abdelfatah (2009) reported that about 25%–30% drop in the tensile strength was observed in concrete made with RCA.

Kou et al. (2012), observed that regardless of the type of the recycled aggregate used, the splitting tensile strength of the specimens decreased as a function of increasing RCA replacement ratio before the age of 28 days. However, for some types of the RCAs used, an increase in the splitting tensile strength at the age of 90 days is observed. Sagoe et al. (2001), reported that there is no significant difference between the splitting tensile strength of the reference and the recycled aggregate concrete specimens. On the other hand, Limbachiya (2012) and Yong and Teo (2009) reported that while replacing up to 50% of coarse aggregate with RCA, there was no difference in splitting tensile and flexural strengths between the RAC and the reference, but at complete replacement results were improved for RCA due to better interlocking.

2.3.2.3. Flexural Strength. It is usually reported that the RCA replacement does not have significant negative effects on flexural strength of concrete. Xiao and Li (2005), Hu (2007), and Cheng (2005) have reported that RCA replacement only has marginal effects on flexural strength of concrete. Ravindrarajah and Tam (1985) have also reported that increasing the RCA content does not have a significant effect on flexural strength. Topçu and Sengel (2004) have reported that the flexural strength is decreasing due to the increase in RCA replacement level.

2.3.2.4. Modulus of Elasticity. It is generally believed that the modulus of elasticity is decreasing as the RCA replacement ratio is increasing. This is believed to be due to the comparatively lower modulus of elasticity of the residual mortar attached to the RCA particles which will decrease the stiffness of the aggregate skeleton in RCA-made concrete (Xiao et al. 2012). Similar results were also reported by Hoffmann et al. (2012)

and Cabo et al. (2009), who observed that the modulus of elasticity is decreasing as a function of increasing the RCA replacement ratio.

2.3.2.5. Shrinkage. Kou et al. (2007), Kou and Poon (2012), Hansen and Boegh (1985), Fathifazl et al. (2011), Nassar and Soroushian (2012), and Gomez (2002) have studied the shrinkage behavior of the RCA-made concrete mixtures and observed that the shrinkage is increasing directly with an increase in RCA content. However, this increase is negligible up to 20% replacement ratio (Kou et al. 2007). This increase in shrinkage deformation is most probably due to the lower restraining capacity of the RCA particles due to an increase in the total mortar content and a decrease in the total stiff virgin aggregate portion in the mixture (Xiao et al. 2012).

Domingo-Cabo et al. (2009), found that the shrinkage of RAC increased after 28 days. The RAC with a RCA replacement level of 20% showed a similar shrinkage to the conventional concretes in the early stage. For a period of 6 months, the shrinkage in RAC was 4% higher. In the case of a RCA replacement level of 50%, the shrinkage was 12% greater than that of the conventional concrete after 6 months. Moreover, Sagoe et al. (2001), reported that the drying shrinkage of RAC was about 25% higher than that of conventional concrete, possibly due to the lower restraining capacity of RCA particles compared to natural aggregate.

Kou et al. (2012) reported that drying shrinkage of RAC increases as the coarse recycled aggregate replacement ratio increases. They also observed that recycled aggregates with lower water absorption capacities results in lower shrinkage rates.

Kim and Bentz (2008) investigated the drying shrinkage in concrete mixtures made with RCA. They have reported that the RCA particles can be used as a means of

internal curing in concrete, which is useful in reducing the drying shrinkage. Similar results were reported by Hu et al. (2013) who reported that incorporating fine RCA is useful in decreasing the drying shrinkage through internal curing.

2.3.3. Durability.

2.3.3.1. Chloride Ion Permeability. It is usually reported that the chloride ion permeability of concrete made with RCA is inferior to that of conventional concrete. However, in the case of high quality RCA, it is observed that there is little difference between the chloride ion penetration of RAC and conventional concretes.

Sim and Park (2011) observed that in the case of concrete made with coarse RCA and partial replacement of fine recycled aggregates, there is no significant difference between the total charges passed through the specimens of up to 100% fine recycled aggregate replacement. However, as the curing time increases, the more fine recycled aggregate replacement results in a decrease in the total charge passed. Based upon their results, it seems that increasing the curing period as well as incorporating proper types and amounts of supplementary cementitious materials (SCMs), the chloride ion permeability may be controlled.

Kou et al. (2012), reported that the chloride ion permeability increases as a result of an increase in the coarse RCA replacement. However, the negative effect is more significant in the case of low grade RCA. Similar results were reported by Otsuki et al. (2001) and Shayan and Xu (2003).

2.3.3.2. Freeze/thaw Resistance. It is generally believed that the RCA-made concrete mixtures are more susceptible to damage due to the freeze/thaw cycles (Xiao et al. 2012). Medina 2013, Richardson (2011), Ajdukiewicz (2002), and Limbachyia (2000)

have investigated the frost durability of the RCA-made concrete mixtures and reported that given the similar strength grade, there is not a significant difference in freeze/thaw resistance of the RCA-made and conventional concrete mixtures.

2.4. CONCLUDING REMARKS

Due to the lower quality of RCA particles compared to virgin aggregates, it is usually expected that the mechanical properties and durability of concrete made with RCA will be lower than conventional concrete. However, depending on the fresh concrete composition and source of RCA, this decrease might be negligible, and even in some cases better performance is expected.

3. EXPERIMENTAL PROGRAM

3.1. MATERIAL PROPERTIES

All the mixtures investigated in this study were proportioned with a binary blend of Type I/II Portland cement produced by Holcim, Inc. and Class C fly ash. Physical properties and chemical compositions of the cement are presented in **Table 3.1**.

Table 3.1 Physical Properties and Chemical Compositions of Cement

Physical properties	
Property	Type I/II Cement
Fineness:	
Blaine, m ² /kg	379
Specific gravity	3.15
Chemical compositions	
Component	% of weight
SiO ₂	19.8
Al ₂ O ₃	4.5
Fe ₂ O ₃	3.2
CaO	64.2
MgO	2.7
SO ₃	3.4
Na ₂ O	0.52 equivalent
LOI	2.6

Table 3.2 includes the typical chemical analysis of the Class C fly ash from the Ameren Labadie Power Plant (Labadie, MO) that was used in making the concrete mixtures.

The fine aggregate was natural sand from Missouri River Sand (Jefferson City, MO), while two types of coarse aggregates were used; virgin coarse aggregate, which was a state-approved Potosi dolomite with a 1 in. maximum nominal aggregate size, and

the laboratory produced RCA used as a partial replacement of the coarse aggregate. The RCA was produced from crushing the non-reinforced concrete beams produced at the High-Bay structural engineering laboratory at Missouri University of Science and Technology. The parent concrete was a mixture with $w/c=0.4$ made with the same virgin aggregate used in this study. The cement content in the parent concrete was 535 lb/yd^3 . Dry-rodded unit weight, absorption, specific gravity, and Los Angeles abrasion resistance of the materials were determined according to ASTM standards for both the virgin and recycled aggregates.

Table 3.2 Chemical Compositions of Ameren UE Fly Ash [M.H. Wolfe 2011]

Chemical compositions	
Component	Range (%)
SiO ₂	30.45 - 36.42
Al ₂ O ₃	16.4 - 20.79
Fe ₂ O ₃	6.78 - 7.73
CaO	24.29 - 26.10
MgO	4.87 - 5.53
SO ₃	2.18 - .36
Na ₂ O	1.54 - 1.98
K ₂ O	0.38 - 0.57
TiO ₂	1.42 - 1.56
P ₂ O ₅	1.01 - 1.93
MnO	0.028 - 0.036
SrO	0.40 - 0.44
BaO	0.68 - 0.9
LOI	0.24 - 1.15

The residual mortar content of the RCA was determined based on the method proposed by Abbas et al. (2009). In this method, RCA particles are submerged in a saturated solution of sodium sulphate being subjected to cycles of freezing and thawing.

Due to the combined effect of the chemical solution and thermal stresses, the mortar phase of the RCA particles is separated from the old virgin aggregates. Two series of samples were used for measuring the residual mortar content of the RCA. Each of these samples contained four individual groups of aggregates remaining on the 3/4, 1/2, 3/8, and #4 sieves. The residual mortar content of each sample was calculated based on the weight of the separated mortar and grain size distribution of the RCA as suggested by Abbas et al. (2009).

Figure 3.1 shows one of the RCA sample series before the cycles and after removing the residual mortar.



Figure 3.1 RCA Particles before Separating the Mortar (left) and after Separating the Residual Mortar (right)

The residual mortar content is then computed as a percentage of the weight of the RCA particles. **Table 3.3** presents a summary of the properties of the fine and coarse aggregates. The gradation curve of the aggregates is compared to the ASTM C33 standard in **Figures 3.2** and **3.3**. **Figure 3.4** plots the amount of coarse aggregates retained on each of the sieves. This curve is indicative of the grain size distributions. The ideal

shape of this diagram is a symmetric bell shaped one. As it is observed, both the coarse aggregates (virgin and RCA) have acceptable distributions. It should be noted that the Los Angeles abrasion results are the average values calculated for two series of samples obtained from the coarse aggregate piles.

Table 3.3 Physical Properties of the Aggregates

Aggregate	Specific gravity	Dry rodded unit weight (pcf)	Absorption (%)	LA abrasion (%)	Residual mortar (% of wt.)
Fine	2.641	-	0.5	-	-
Potosi dolomite	2.72	99.7	0.98	43	-
RCA	2.35	89.7	4.56	41	46

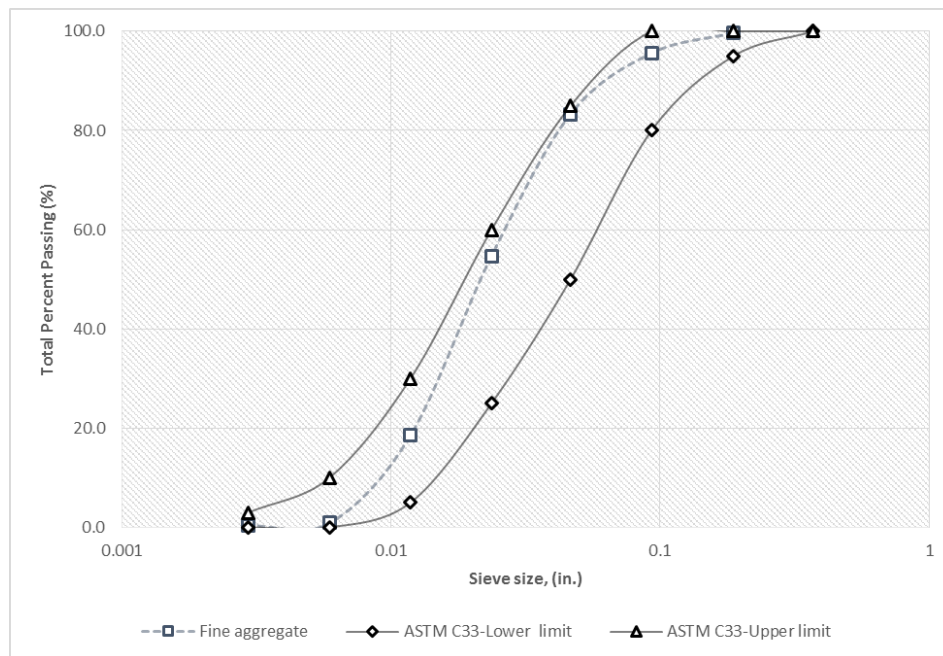


Figure 3.2 Particle Size Distribution of the Fine Aggregate

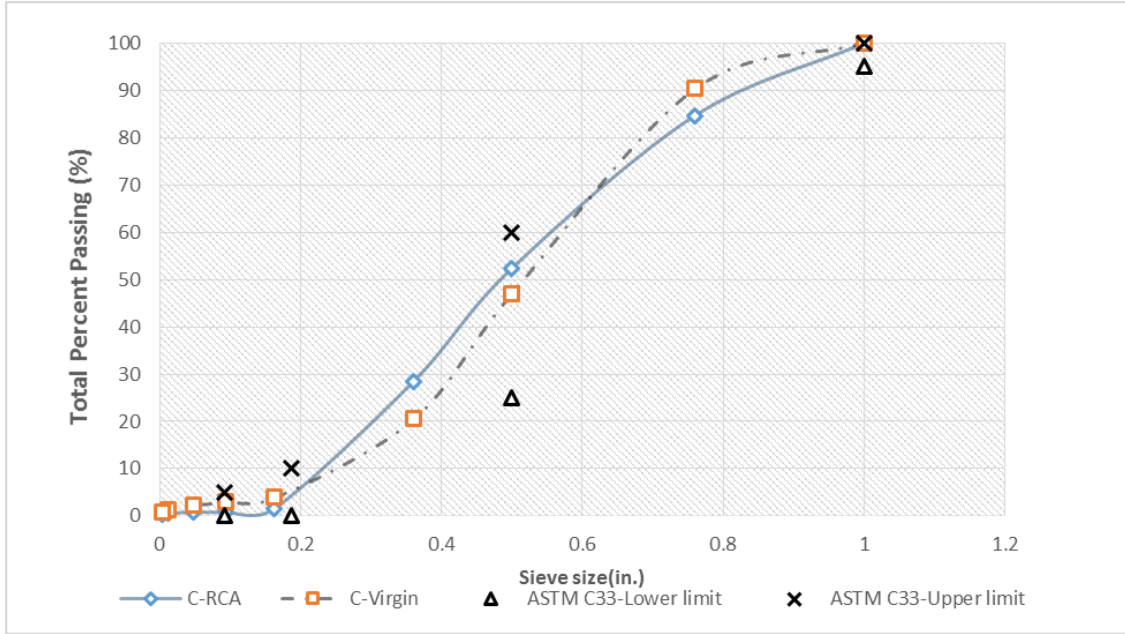


Figure 3.3 Particle Size Distribution of the Coarse Aggregate

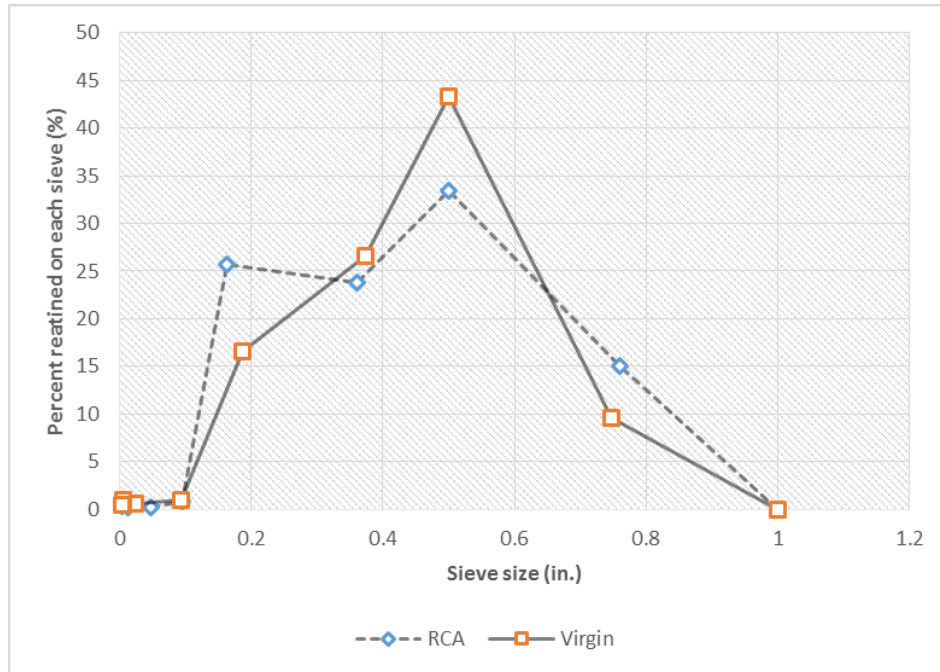


Figure 3.4 Individual Percentages Retained on Each Sieve

3.2. MIXTURE PROPORTIONS

3.2.1. Conventionally Proportioned Mixtures. The study focused on MoDOT Class B concrete mixtures. Seven of the investigated mixtures had a fixed water to cementitious materials ratio (w/cm) of 0.45 and a sand to total aggregate ratio of 42.5%, by volume. The total amount of the cementitious materials used in making the reference and the experimental mixtures was 535 lb/yd³ except for the mixture proportioned according to the equivalent mortar volume (EMV) method. This method is introduced in Section 3.2.3. Twenty five percent of the weight of the cement was replaced with Class C fly ash to reduce the carbon footprint in these sustainable concrete mixtures. A total number of five conventionally proportioned concrete mixtures were produced in the laboratory, including the reference, and mixtures with different amounts of coarse RCA content varying from 30% up to 100% replacement by volume of the coarse aggregate. These mixtures were produced according to the conventional mixing sequence introduced by ASTM C192. It should be noted that two other concrete mixtures were also produced based on the two stage mixing approach (TSMA) and the EMV method. These two methods are introduced in Sections 3.2.2 and 3.2.3, respectively.

Two other concrete mixtures with the w/c of 0.4 and the same cement content with no fly ash replacement were also investigated in this research. These concrete mixtures were the same for casting the structural elements. One of these mixtures is made with no recycled aggregates and the second one was a mixture with full replacement of the coarse aggregate with RCA.

3.2.2. Two Stage Mixing Approach. A second type of mixture made with 100% RCA replacement was produced using the Two Stage Mixing Approach (TSMA). The

main idea of the TSMA is to encapsulate the RCA particles with a low w/cm, of high quality cement paste in order to enhance the surface properties of the RCA as well as the interfacial transition zone (ITZ) formed between the RCA particle and the fresh surrounding hydrated cement paste (Otsouki et al. 2003, Ryu 2002, Tam et al. 2005, 2007, 2008, and 2009, Elhakam et al. 2012, Li et al. 2012). In order to produce the concrete with TSMA, the coarse RCA was loaded in the mixer along with a quarter of the water and the air entraining admixture. After one minute of mixing, the cementitious materials were added with mixing continuing for one minute. Then, half of the remaining water was introduced and allowed to mix for one minute to coat the RCA particles with a rich cement paste. The rest of the materials were then loaded followed by two minutes of mixing.

3.2.3. Equivalent Mortar Volume Mixture Proportioning Method. Fathifazl et al. (2009), have introduced a mixture proportioning method for making concrete with coarse RCA as a replacement for virgin coarse aggregates. Considering the residual mortar content of RCA as part of the total mortar content of the RCA-made concrete is the basis of this method of mixture proportioning. In the proposed method, the RCA-made concrete mixture is proportioned to have the same total mortar volume as a companion concrete mixture made entirely with fresh virgin (here also referred as natural) aggregates, with the companion mixture made with the same type of coarse aggregate as that in the RCA. Mixture proportioning based on the proposed method essentially involves proper determination of the amounts of RCA and fresh mortar in the RCA-made concrete. The method proceeds as follows (Fathifazl et al. 2009):

At the first step, a companion concrete mixture should be proportioned based on conventional concrete mixture proportioning methods, only with natural aggregate being used in the composition. It is assumed that the natural aggregate (NA) used in this mixture has the same gradation and maximum size as the RCA. This mixture is called natural aggregate concrete (NAC).

The next step is to design a second mixture containing both the natural aggregate and RCA. This mixture is called the RCA-concrete. The volume of NA in the RCA-concrete mixture is shown by $V_{NA}^{RCA-concrete}$.

The natural aggregate content ratio, R, is defined as:

$$R = \frac{V_{NA}^{RCA-concrete}}{V_{NA}^{NAC}} \quad (3-1)$$

Where $V_{NA}^{RCA-concrete}$ = volume of natural aggregate in RCA-concrete and V_{NA}^{NAC} = volume of natural aggregate in NAC.

R=0 refers to a concrete mixture with no NA (*i.e.*, 100% RCA) in composition, and R=1 corresponds to a mixture made with 100% NA (*i.e.*, no RCA). For the RCA-concrete and its NAC to have the same properties, the proposed method requires that the two following conditions to be satisfied:

1. The total mortar content in the NAC should be equal to the total mortar content of the RCA-concrete mixture. The total mortar content of the RCA-concrete mixture can be determined by the summation of residual mortar content attached to the RCA particles available in RCA-concrete mixture and the fresh mortar content of the same mixture.

2. The total NA content in the NAC to be equal to the total NA content of the RCA-concrete mixture. The total NA content of the RCA-concrete mixture can be determined by the summation of original virgin aggregate available in the RCA particles used in RCA-concrete mixture and the NA content of the RCA-concrete mixture.

These two conditions are summarized in the following Equations:

$$V_{TM}^{RCA-concrete} = V_M^{NAC} \quad (3-2)$$

$$V_{TNA}^{RCA-concrete} = V_{NA}^{NAC} \quad (3-3)$$

Where $V_{TM}^{RCA-concrete}$ = total mortar (TM) volume in RCA-concrete, V_M^{NAC} = mortar volume in the companion concrete made entirely with natural aggregate, and $V_{TNA}^{RCA-concrete}$ = total natural aggregate (TNA) volume in RCA-concrete.

Therefore, Equations (3-2) and (3-3) can be reformed as:

$$V_{TM}^{RCA-concrete} = V_{RM}^{RCA-concrete} + V_{NM}^{RCA-concrete} \quad (3-4)$$

$$V_{TNA}^{RCA-concrete} = V_{OVA}^{RCA-concrete} + V_{NA}^{RCA-concrete} \quad (3-5)$$

Where $V_{RM}^{RCA-concrete}$ = residual mortar (RM) volume in RCA-concrete, $V_{NM}^{RCA-concrete}$ = volume of the fresh or new mortar (NM) in RCA-concrete; and $V_{OVA}^{RCA-concrete}$ = original virgin aggregate volume in RCA concrete.

It is assumed that the differences between the strength and density of the residual mortar and the fresh mortar on the one hand and the differences between the original

virgin aggregate (OVA) and fresh NA type and/or shape may have negligible effect on the overall properties of RCA-concrete compared to the companion NAC. It is also assumed that the severely damaged mortar will not survive the crushing process during RCA production. This ensures the quality of the residual mortar attached to the RCA particles.

In order to ensure the conditions stated in Equation (3-5), amount of original virgin aggregate in RCA-concrete should be quantified:

$$V_{OVA}^{RCA-concrete} = V_{RCA}^{RCA-concrete} \times (1 - RMC) \times \frac{SG_b^{RCA}}{SG_b^{OVA}} \quad (3-6)$$

Where $V_{RCA}^{RCA-concrete}$ = volume of RCA in RCA-concrete and SG_b^{RCA} and SG_b^{OVA} = bulk specific gravities of RCA and original virgin aggregate (OVA) available in the RCA particles, respectively. Again it should be noted that the RMC is the residual mortar content of the RCA.

The required volumes of RCA and fresh natural aggregate in the RCA-concrete can be determined using the Equations (3-1), (3-2), (3-5), and (3-6):

$$V_{RCA}^{RCA-concrete} = \frac{V_{NA}^{NAC} \times (1 - R)}{(1 - RMC) \times \frac{SG_b^{RCA}}{SG_b^{OVA}}} \quad (3-7)$$

$$V_{RCA}^{RCA-concrete} = V_{NA}^{NAC} \times R \quad (3-8)$$

$$W_{OD-RCA}^{RCA-concrete} = V_{RCA}^{RCA-concrete} \times SG_b^{RCA} \times 1000 \quad (3-9)$$

$$W_{OD-NA}^{RCA-concrete} = V_{NA}^{RCA-concrete} \times SG_b^{NA} \times 1000 \quad (3-10)$$

Where $W_{OD-RCA}^{RCA-concrete}$ = required oven-dry weight of RCA in RCA-concrete,
 $W_{OD-NA}^{RCA-concrete}$ = required oven-dry weight of natural aggregate in RCA-concrete, and
 SG_b^{NA} = bulk specific gravity of natural aggregate.

Next step is to determine the amount of required water, cement, and fine aggregate proportions in RCA-concrete mixture. The residual mortar content available in RCA-concrete should be quantified to satisfy the condition expressed in Equation (3-2).

$$V_{RM}^{RCA-concrete} = V_{RCA}^{RCA-concrete} \times \left[1 - (1 - RMC) \times \frac{SG_b^{RCA}}{SG_b^{OVA}} \right] \quad (3-11)$$

The amount of fresh mortar in RCA-concrete can be determined using Equations (3-2), (3-4), and (3-11):

$$V_{NM}^{RCA-concrete} = V_M^{NAC} - V_{RM}^{RCA-concrete} \quad (3-12)$$

Where $V_{NM}^{RCA-concrete}$ is the new (fresh) mortar content in RCA-concrete, V_M^{NAC} is the total mortar content of natural aggregate concrete, and $V_{RM}^{RCA-concrete}$ is the volume of residual mortar in RCA-concrete.

The corresponding quantities of water, cement, and fine aggregate in RCA-concrete can be determined using the following Equations:

$$W_w^{RCA-concrete} = W_w^{NAC} \times \frac{V_{NM}^{RCA-concrete}}{V_M^{NAC}} \quad (3-13)$$

$$W_c^{RCA-concrete} = W_c^{NAC} \times \frac{V_{NM}^{RAC-concrete}}{V_M^{NAC}} \quad (3-14)$$

$$W_{OD-FA}^{RCA-concrete} = W_{OD-FA}^{NAC} \times \frac{V_{NM}^{RAC-concrete}}{V_M^{NAC}} \quad (3-15)$$

Where $W_w^{RCA-concrete}$ and W_w^{NAC} are the weights of water in RCA-concrete and natural aggregate concrete, $W_c^{RCA-concrete}$ and W_c^{NAC} are the weights of cement in RCA-concrete and natural aggregate concrete, and $W_{OD-FA}^{RCA-concrete}$ and W_{OD-FA}^{NAC} are the oven dried weights of fine aggregate in RCA-concrete and NAC respectively.

An upper limit exists for the RCA content in the RCA-concrete mixture in the EMV method. This limit is a function of residual mortar content of the RCA. The theoretical lower and upper limits of residual mortar content, 0 and 100%, respectively, should be examined to determine the effect of residual mortar content on RCA-concrete mixture proportioning. Given the fact that the maximum amount of any coarse aggregate, including RCA, which can be placed in a unit volume of concrete, is equal to the dry-rodded unit volume of that aggregate. Therefore, the upper limit of RCA content in RCA concrete is the dry-rodded volume of RCA ($V_{DR-RCA}^{RAC-concrete}$). Hence, the maximum volume of RCA that can be added to a unit volume of RCA-concrete can be calculated as:

$$V_{maxRCA}^{RCA-concrete} = \frac{SG_{DR}^{RCA}}{SG_b^{RCA}} \quad (3-16)$$

Where $V_{maxRCA}^{RAC-concrete}$ = maximum volume of RCA that can be added to a unit volume of RCA-concrete, SG_{DR}^{RCA} = dry-rodded specific gravity of RCA, and SG_b^{RCA} = bulk specific gravity of RCA.

The absolute volume of natural aggregate in natural aggregate concrete, in Equation (3-7) can be related to its dry-rodded volume as:

$$V_{NA}^{NAC} = V_{DR-NA}^{NAC} \times \frac{SG_{DR}^{NA}}{SG_b^{NA}} \quad (3-17)$$

Where V_{NA}^{NAC} = volume of natural aggregate in NAC, SG_{DR}^{NA} = dry-rodded specific gravity of natural aggregate, and SG_b^{NA} = bulk specific gravity of natural aggregate.

By substituting Equations (3-16) and (3-17) in Equation (3-7), the minimum replacement ratio (R_{min}) can be calculated as:

$$R_{min} = 1 - \frac{(1 - RMC)}{V_{DR-NA}^{NAC}} \times \frac{SG_{DR}^{RCA}}{SG_{DR}^{OVA}} \times \frac{SG_b^{NA}}{SG_b^{OVA}} \geq 0 \quad (3-18)$$

Where RMC = residual mortar content of the RCA, V_{DR-NA}^{NAC} = dry-rodded volume of natural aggregate in natural aggregate concrete, SG_{DR}^{RCA} = dry-rodded specific gravity of RCA, SG_{DR}^{OVA} = dry-rodded specific gravity of original virgin aggregate available in RCA particles, SG_b^{NA} = bulk specific gravity of natural aggregate, and SG_b^{OVA} = bulk specific gravity of original virgin aggregate.

By assuming identical shape and size grading for RCA and NA, it can be written that:

$$\frac{SG_{DR}^{RCA}}{SG_{DR}^{NA}} = \frac{SG_b^{RCA}}{SG_b^{NA}} \quad (3-19)$$

Assuming the fresh natural aggregate that is used as replacement of RCA to be similar to the original virgin aggregate in RCA, the ratio $\frac{SG_b^{NA}}{SG_b^{OVA}}$ in Equation (3-18) would become one. Therefore, by substituting Equation (3-19) into Equation (3-18), one obtains:

$$R_{min} = 1 - \frac{(1 - RMC)}{V_{DR-NA}^{NAC}} \times \frac{SG_b^{RCA}}{SG_b^{NA}} \geq 0 \quad (3-20)$$

It should be noted that the negative value for R_{min} implies that one can make a concrete mixture with 100% RCA, without the need for any fresh natural aggregate.

As the residual mortar content increases and approaches 100%, the required volume of RCA in RCA-concrete in Equation (3-7) hyperbolically increases and approaches infinity ($V_{RCA}^{RCA-concrete} / V_{NA}^{NAC} \rightarrow \infty$). However, if the $(1-R)$ in the numerator of Equation (3-7) is set equal to its denominator, $((1 - RMC) \times \frac{SG_b^{RCA}}{SG_b^{OVA}})$, the resulting equation would be valid for any residual mortar content. The physical interpretation of the latter action is replacement of residual mortar volume in RCA with fresh natural aggregate ($V_{NA}^{RCA-concrete} = V_{RM}^{RCA-concrete}$) to compensate for the deficiency of the total

natural aggregate in RCA-concrete compared to the companion natural aggregate concrete. Therefore:

$$R = \frac{V_{RM}^{RCA-concrete}}{V_{RCA}^{RCA-concrete}} \quad (3-21)$$

Where $V_{RM}^{RCA-concrete}$ = volume of residual mortar in RCA-concrete, and

$V_{RCA}^{RCA-concrete}$ = volume of RCA in RCA-concrete.

By substituting Equations (3-21) and (3-11) into Equation (3-7), the required RCA and natural aggregate volumes can be found as:

$$V_{RCA}^{RCA-concrete} = V_{NA}^{NAC} \quad (3-22)$$

$$V_{NA}^{RCA-concrete} = V_{NA}^{NAC} \times [1 - (1 - RMC) \times \frac{SG_b^{RCA}}{SG_b^{OVA}}] \quad (3-23)$$

Where $V_{NA}^{RCA-concrete}$ = required volume of natural aggregate in RCA-concrete.

Again it should be highlighted that the EMV method is completely detailed by Fathifazl et al. (2009).

3.3. TEST MATRIX

Table 3.4 summarizes the test matrix used in this part of the research for evaluating the effect of RCA replacement level on properties of concrete.

In the case of laboratory produced mixtures, three different concrete batches were produced to meet the required volume for sampling purposes. Two successive batches of

4.5 cubic feet were used to make samples for the mechanical properties and the durability performance. An extra batch of 2.5 cubic feet was also produced for investigating the fresh properties.

The design air content of the batches used for mechanical properties and durability sampling was $6\pm 1\%$. Although MoDOT considers a maximum slump value of 6.0 in. while using water reducer admixtures, the targeted slump value was set to 7 ± 1 in. to facilitate testing the fresh properties with the ICAR rheometer. The amount of required admixtures was determined by making trial batches of two cubic feet for all of the investigated mixtures.

Table 3.5 summarizes the mixtures used in the study to evaluate the properties of the concrete made with RCA.

Regarding the mixture proportioning for the EMV method, it should be noted that this mixture was initially produced with the RCA replacement levels determined by Fathifazl et al. (2009). However, the produced mixture was a harsh mixture with low content of fresh mortar and workability problems. Therefore, the RCA replacement ratio was decreased in mixture proportioning. Several mixtures with different replacement levels were investigated for fresh properties in the laboratory in order to find the maximum practical replacement ratio to make a workable concrete in the laboratory. Finally, the $R = 0.834$ was selected to plug in the equations. This yields approximately 30% replacement of RCA by volume of the coarse aggregate. The total amount of fresh mortar used in producing the EMV mixture was 15% less than the reference mixture. This means that the total amount of cementitious materials used for reducing the EMV mixture was 15% less than the reference mixture (i.e. 454 lb/yd^3). The sand content and the water

amount was decreased by 15% as well. However, the w/cm of the fresh mortar was 0.45 same as the reference mixture.

Table 3.4 Test Matrix for Making Concrete Mixtures

w/cm	Mixing method	Coarse RCA replacement (% of volume)				
		0	30	50	70	100
0.45	Conventional	✓	✓	✓	✓	✓
	EMV		✓			
	T SMA					✓
0.4	Conventional	✓				✓

Similar to the other laboratory produced mixtures, 25% of the required Portland cement was replaced with Class C fly ash for the EMV mixture. The total amount of coarse aggregate content of this mixture was 2078 lb/yd³ which is 13% more than the reference mixture. This simultaneous increase in coarse aggregate content and decrease in fresh mortar content results in inferior workability of the EMV mixture compared to the reference concrete mixture.

Table 3.5 Mixture Proportions of Concrete used in the Study

Mixture type	Laboratory produced mixtures							Sampled from truck	
	Ref.	30% RCA	30% EMV	50% RCA	70% RCA	100% RCA	100% TSMA	0 % RCA	100% RCA
Cementitious materials (lb/yd ³)	535	535	458	535	535	535	535	535	535
Cement type I (lb/yd ³)	401	401	344	401	401	401	401	535	535
Class C fly ash, replacement by mass (%)	25	25	25	25	25	25	25	-	-
Fly ash (lb/yd ³)	134	134	114	134	134	134	134	-	-
w/cm	0.45	0.45	0.45	0.45	0.45	0.45	0.45	0.4	0.4
Water content (lb/yd ³)	240.75	240.75	206	240.75	240.75	240.75	240.75	214	214
Sand/Aggregate, by volume (%)	42.5	42.5	36.5	42.5	42.5	42.5	42.5	40	45
Sand content (lb/yd ³)	1301	1301	1122	1301	1301	1301	1301	1253	1410
RCA replacement ratio by volume (%)	0	30	30	50	70	100	100	0	100
Coarse virgin aggregate content (lb/yd ³)	1835	1284	1518	917	550	-	-	1958	-
Coarse RCA content (lb/yd ³)	-	475	560	791	1108	1583	1583	-	1548

3.4. SAMPLING AND CURING

A variety of samples were taken from each type of the laboratory produced concrete mixtures to investigate the fresh properties, mechanical performance and durability according to **Table 3.6**. A vibrating table was used for consolidating the fresh concrete in molds.

Table 3.6 Test Methods and Standard used in the Study

PROPERTY	TEST METHOD	TEST TITLE/DESCRIPTION
FRESH CONCRETE PROPERTY TESTS		
Unit Weight	ASTM C 138	Standard Test Method for Density (Unit Weight).
Air Content	ASTM C 231	Standard Test Method for Air Content of Freshly Mixed Concrete by the Pressure Method.
Bleeding	ASTM C 232	Standard Test Methods for Bleeding of Concrete.
Rheological properties		ICAR rheometer
HARDENED MECHANICAL PROPERTY TESTS		
Compressive Strength, 4×8 in. cylinders, (1, 7, 28, 56, and 91 d)	ASTM C 39	Standard Test Method for Compressive Strength of Cylindrical Concrete Specimens.
Splitting Tensile Strength, 4×8 in. cylinders, (7, 28, and 56 d)	ASTM C 496	Standard Test Method for Splitting Tensile Strength of Cylindrical Concrete Specimens.
Flexural Strength, 6×6×20 in. beams (28 and 56 d)	ASTM C 78	Standard Test Method for Flexural Strength of Concrete.
Modulus of Elasticity, 4×8 in. cylinders, (28, 56 d)	ASTM C 469	Standard Test Method for Static Modulus of Elasticity.
Shrinkage, 3×3×11.25 in. prisms	ASTM C 157	Standard Test Method for Length Change of Hardened Hydraulic-Cement Mortar and Concrete
DURABILITY TESTS		
Permeable void ratio, 4×8 in. cylinders, (28, 56, and 91 d)	ASTM C 642	Standard Test Method for Density, Absorption, and Voids in Hardened Concrete
Elect. Resistivity, 4×8 in. cylinders, (28, 56, and 91d)	ASTMC 1760	Standard Test Method for Bulk Electrical Conductivity of Hardened Concrete
Surface Resistivity, 4×8 in. cylinders, (28, 56, and 91d)	AASHTO TP 95	Surface Resistivity Indication of Concrete's Ability to Resist Chloride Ion Penetration
Freeze Thaw Resistance, Procedure A, 3×4×16 in. prisms	ASTM C 666	Standard Test Method for Resistance of Concrete to Rapid Freezing and Thawing.
Deicing-salt Scaling Resistance, 3×10×11 in. panels	ASTM C 672	Standard Test Method for Scaling Resistance of Concrete Surfaces Exposed to Deicing Chemicals.

Samples were kept under wet burlap and covered by plastic sheets for 24 hours before demolding. After demolding the specimens, the curing process started. Specimens were placed in lime-saturated water with temperature of 70 ± 5 °F up to the age of testing.

4. RESULTS AND DISCUSSION

4.1. FRESH PROPERTIES

4.1.1. General. A batch of 2.5 ft³ was produced for investigating the fresh properties of the concrete mixtures containing various amounts of RCA. All these batches were made with the constant w/cm of 0.45. Total number of six concrete mixtures were investigated in this phase. The studied fresh properties included bleeding potential and rheological properties. All these mixtures were produced with the same initial slump value and air content except for the EMV mixture. Due to the high amount of coarse aggregate and decrease in the fresh mortar content in this mixture, the slump value was lower than the other mixtures. Therefore, this mixture was not used for investigating the rheological properties. It should also be noted that the mixture made with 50% RCA replacement had slightly lower air content compared to the targeted range of 6±1%. However, given the fact that no sampling for durability or mechanical property testing was scheduled at this phase, this mixture was used for investigating the rheological properties and bleeding potential. **Table 4.1** summarizes the slump value and air content of the investigated mixtures.

Table 4.1 Slump Value, Air Content, and Unit Weight of Fresh Concrete Mixtures

Mixture type	Ref.	30% RCA	30% EMV	50% RCA	70% RCA	100% RCA
Slump (in.)	7.0	7.0	1.5	7.0	7.0	7.5
Air content (%)	5.5	5.8	4.8	4.0	5.5	5.2
Unit weight (pcf)	149.8	145.3	149.8	147.0	143.9	142.0

4.1.2. Bleeding. Bleeding is a form of segregation where some of the water in the concrete tends to rise to the surface of the freshly placed material. This arises due to the inability of the solid components of the concrete to hold all of the mixing water when they settle downwards (water being the lightest of all the mix constituents). Bleeding of the water continues until the cement paste has stiffened enough to end the sedimentation process (Mehta and Monteiro 2006). If the bleed water is remixed during the finishing of the top surface, a weak top surface will result. To avoid this, the finishing operations can be delayed until the bleed water has evaporated. Conversely, if evaporation of the surface water is faster than the rate of bleed, plastic shrinkage cracking may occur.

Bleeding potential of the mixtures was investigated according to the ASTM C 232 test method. A cylindrical container of approximately 0.5 ft³ capacity with internal diameter of 10±0.25 in. and internal height of 11±0.25 in. was used for the test. Fresh concrete was cast into the container in three layers. The container was then placed on a flat and vibration free surface while covered with a wet towel to avoid evaporation. Accumulated water was collected from the surface of the specimen in different time intervals. In order to facilitate the collection of the bleed water, container was tilted by placing an approximately 1.5 in. thick block under one side of the cylinder two minutes before each recording. Results of the bleeding test are reported in **Table 4.2**.

No significant bleeding was observed in most of the mixtures. The mixture made with 100% RCA replacement had the maximum registered bleeding equal to 0.18 gm/in² of the surface area of the specimen.

Table 4.2 Results of Bleeding Measurements

Mixture type	Ref.	30% RCA	30% EMV	50% RCA	70% RCA	100% RCA
Accumulated bleeding water (gr)	0.0	0.8	0.0	6.5	3.1	14.0
Accumulated bleeding water (gm/in ²)	0.0	0.01	0.0	0.08	0.04	0.18
Last observation time (min)	120	120	130	120	130	180

4.1.3. Rheological Properties. Fresh concrete can be considered as a fluid. This means that fresh concrete can start to flow due to shear stress. Flow characteristics of fresh concrete are described using the “Bingham” equation:

$$\tau = \tau_0 + \mu D \quad (4-1)$$

Where:

τ = shear stress (Pa)

τ_0 = yield stress (Pa)

μ = plastic viscosity (Pa/s)

D = shear rate (1/s)

Yield stress is defined as the minimum shear stress required to start the flow of a fluid and the viscosity is the measure of internal resistance to flow. **Figure 4.1** is a schematic pattern of rheological properties of a Bingham (non-Newtonian) fluid like concrete.

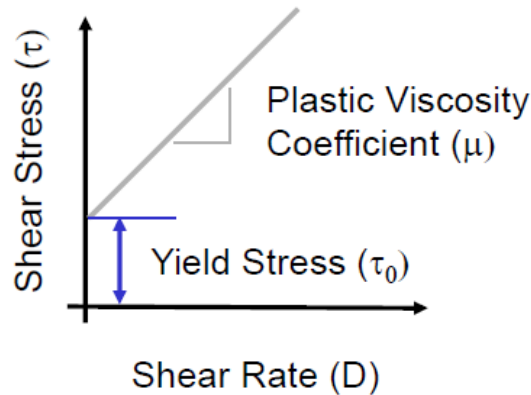


Figure 4.1 Bingham Model for Rheological Properties of Concrete (ICAR manual)

Concrete, however, is not a simple fluid because it displays thixotropic behavior, which means that the shear stress required to initiate flow is high when the concrete has been in an “at rest condition”, but a lower shear stress is needed to maintain flow once it has begun. Such behavior is shown in **Figure 4.2** where variations in shear stress is depicted versus time for a slowly applied shear strain. From the start point, the shear stress is increasing up to reach to a maximum called “static yield stress”. This maximum point is the initiation of flow and after this point the shear rate required for continuing the flow will decrease. The required shear stress for continuing the flow will stabilize after a few seconds. This stabilized shear rate is known as the “dynamic yield stress”.

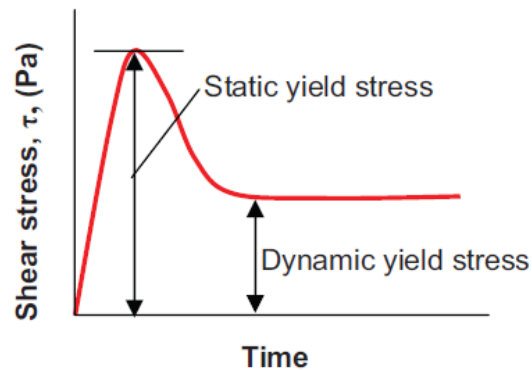


Figure 4.2 Yield Stress Analysis (ICAR manual)

A portable ICAR rheometer was used for determining the rheological properties of concrete mixtures. Both the stress growth and the flow curve tests were performed for the mixtures at different time intervals. **Figure 4.3** presents the interface of the ICAR software used for the rheological testing.

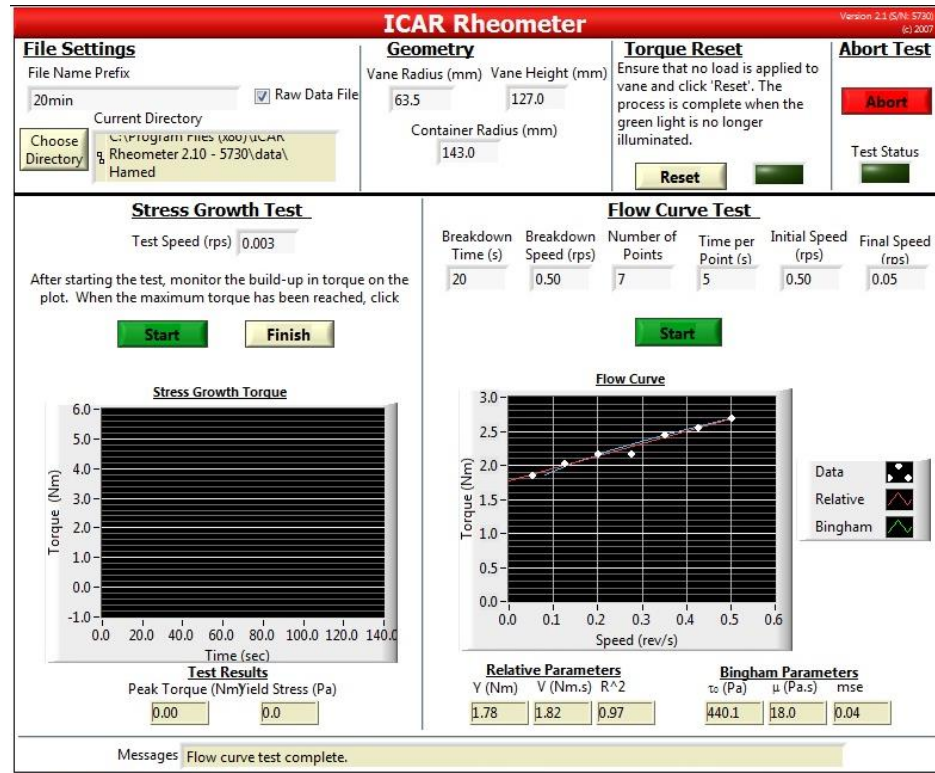


Figure 4.3 ICAR Rheometer Interface

As a rule of thumb, the ICAR rheometer is suitable for use with concrete mixtures with slump values higher than 4 to 5 in. Therefore it was not possible to use this rheometer to measure the rheological properties of the EMV mixture. **Table 4.3** includes the data obtained from the ICAR rheometer. The maximum yield stress was determined with the stress growth test. The flow curve test was performed to investigate the plastic viscosity and the yield stress of the samples.

Except for the concrete made with 100% RCA replacement, it was observed that the dynamic yield stress is generally higher in the case of RCA mixtures while compared to the reference. Most of the plastic viscosity results obtained for the RCA mixtures (besides that of the 50% mixture) is higher than the reference mixture. However, no clear trend of effect of RCA replacement ratio on rheological properties was observed. Similar results were reported by Hu et al. (2013).

Table 4.3 Rheological Properties of the Concrete Mixtures

Mixture	Max yield stress (Pa)	Plastic viscosity (Pa.s)	Yield stress (Pa)
Ref.	3272.4	37.3	659.3
30% RCA	4668.9	49.0	369.4
50% RCA	3523.9	28.3	639.0
70% RCA	3338.6	40.7	535.8
100% RCA	1829.8	47.4	252.2

4.2. MECHANICAL PROPERTIES

4.2.1. General. For each of the mixtures, a batch of 4.5 ft³ concrete was produced to take samples of the mechanical properties. The targeted slump value and air content of the produced mixtures were 7.0 ± 1.0 in. and $6.0 \pm 1.0\%$ respectively. However, the air content of the mixture made with 50% RCA was slightly higher than the targeted range.

Table 4.4 includes the fresh properties of the mixtures.

Table 4.4 Fresh Properties of Mixtures used for Mechanical Property Sampling

Mixture type	Laboratory produced mixtures (w/cm=0.45)							Sampled from truck (w/c=0.4)	
	Ref.	30% RCA	30% EMV	50% RCA	70% RCA	100% RCA	100% TSMA	0 % RCA	100% RCA
Slump (in.)	5.0	8.0	3.5	7.0	7.5	8.0	6.5	5.5	8.5
Air content (%)	6.4	7.0	5.0	8.0	5.8	5.3	5.0	8.5	6.5
Unit weight (pcf)	147.4	144.2	148.9	141.1	142.5	141.2	141.7	147.2	137.5

4.2.2. Compressive Strength. Table 4.5 includes a summary of the compressive strength results of the specimens up to 91 days of age. For each testing age, three 4×8 in. cylindrical specimens were used for determining the compressive strength according to ASTM C39. A sulfur based capping compound was used for treating the specimen surfaces at all test ages.

With regard to the results presented in **Table 4.5** it was inferred that in the case of specimens made with w/cm=0.45 with varying RCA content from zero to 100% replacement, the maximum results were observed for the reference mixture made with virgin aggregates. A slight decrease was observed when using RCA as a replacement for coarse aggregate. However, the decrease was more in the case of specimens made with 30% and 50% RCA replacement. This may be mostly due to the higher air content of these two mixtures compared to the mixtures made with 70% and 100% RCA replacement. Another important point to mention, is that the RCA particles were made from parent concrete of w/c=0.4. This means that the fresh mortar with w/cm=0.45 may be the weaker mortar phase governing the strength.

These findings are in line with data obtained by Ryu (2002) who used three types of RCA to make concrete mixtures of $w/c = 0.25$ and 0.55 . It was observed that the compressive strength of the concrete specimens with w/c of 0.55 were the same regardless of the RCA type. However, a similar trend was not observed in the case of specimens with $w/c = 0.25$. Based on the results it was proposed that the strength of the concrete depends on the relative quality of the old and new ITZ formed in concrete made with RCA. In the case of low w/c , the strength of the concrete is governed by the quality of the RCA and the old ITZ in its structure. However, when the w/c is high, the new ITZ formed between the RCA and cement paste may be much weaker and govern the strength characteristics of the concrete.

Table 4.5 Compressive Strength Results

Mixture type	Laboratory produced mixtures ($w/cm=0.45$)							Sampled from truck ($w/c=0.4$)	
	Ref.	30% RCA	30% EMV	50% RCA	70% RCA	100% RCA	100% TSMA	0 % RCA	100% RCA
Age	Average values for three specimens (psi)								
1 Day	2740	2300	2630	2130	2330	2480	2860	4170	3580
7 Days	4180	3670	4660	3650	4440	4510	4610	4980	4660
28 Days	5150	4670	5630	4470	5610	5540	5230	5810	5290
56 Days	5580	5230	6660	4720	5930	5610	6180	6550	5480
91 Days	6220	5360	6375	5040	6100	6200	6165	7880	6100

Given the 23% decrease in compressive strength due to full RCA replacement in concrete mixtures made with $w/c=0.4$, it may be concluded that the high quality concrete

mixtures are more sensitive to RCA replacement. There was no significant difference in compressive strength of the reference and the 100% RCA mixtures with $w/cm=0.45$. This might be partly due to the 1.0% lower air content in the 100% RCA mixture as well.

Regardless of the first day compressive strength, there was no significant difference in compressive strength of the 100% RCA specimens made with 0.4 and 0.45 w/cm . It should be noted that the air content of the specimens made with $w/c=0.4$ was 1.2% higher than the other case. Pozzolanic reaction due to 25% replacement of cement with Class C fly ash in specimens made with $w/cm = 0.45$ might be another reason for this observation.

The TSMA seems not to be beneficial in increasing the compressive strength of the 100% mixture. The 56 day compressive strength of the TSMA mixture is approximately equal to the 91 day strength of the 100% RCA specimens. However, the 91 day results are similar. This finding is contradictory to the observations of Outsuki et al. (2001) who reported up to a 13% increase in compressive strength as a result of the double mixing method. Tam et al. (2005, 2007, 2009) have reported beneficial effects of TSMA for improving the compressive strength of RCA-made concrete mixtures.

The specimens made with the EMV method had the best performance among all the laboratory produced mixtures. Besides the first day strength, the compressive strength of these specimens were higher than the reference mixture for all the test ages up to 91 days. However, a slight decrease in 91 day compressive strength of the EMV specimens were observed while compared to 56 day results, which might be due to experimental errors, etc. Similar beneficial effects were reported by Fathifazl et al (2009).

All the obtained results were higher than the minimum requirement of 3000 psi at 28 days for MoDOT Class B concrete mixtures.

4.2.3. Splitting Tensile Strength. Table 4.6 includes a summary of the splitting tensile strength results of the mixtures. For each testing age, three 4×8 in. cylindrical specimens were used to determine the splitting tensile strength according to ASTM C496 and the mean values were reported. The splitting tensile test setup is shown in **Figure 4.4**.

Compressive loads (P) are applied on the top and bottom of the specimens where two strips of plywood are placed to apply load along a vertical plane through the specimens. The load at failure is recorded as the peak load, and the tensile strength is calculated using the following equation.

$$F_t = \frac{P}{\pi DL} \quad (4-2)$$

Where F_t = splitting tensile strength (psi), P = Ultimate load at failure (lb), D = Sample diameter (in.), and L = Sample length (in.).



Figure 4.4 Splitting Tensile Strength Test Setup

Specimens made with 30% and 50% RCA replacement had the lowest splitting tensile strength values at early age of 7 days. This might be related to the higher air content of these mixtures compared to the other specimens. Besides the results obtained for specimens of the EMV and 100% RCA-TSMA mixtures, there was not a great spread in data obtained for splitting tensile strength of the reference mixture and those made with RCA at 56 days. Mixture made with 100% RCA-TSMA had the lowest splitting tensile strength results at 28 and 56 days of age. On the other hand, the splitting tensile strength of the EMV specimens were 5% and 20% higher than the reference specimen at 28 and 56 days respectively.

Table 4.6 Splitting Tensile Strength Results

Mixture type	Laboratory produced mixtures (w/cm=0.45)							Sampled from truck (w/c=0.4)	
	Ref.	30% RCA	30% EMV	50% RCA	70% RCA	100% RCA	100% TSMA	0 % RCA	100% RCA
Age	Average values for three specimens (psi)								
7 Days	440	345	450	360	410	425	420	415	380
28 Days	480	450	505	430	470	425	405	500	415
56 Days	505	480	605	470	520	480	440	605	435

Again it was observed that for the specimens made with w/c=0.4, the splitting tensile strength decreased drastically due to full RCA replacement. This decrease was only 4% in the case of specimens made with w/cm=0.45. In the case of specimens made with 100% RCA replacement, tensile strength of the specimens made with w/c=0.4 was not

higher than those for the specimens made with $w/cm=0.45$. This might be due to higher air content of concrete made with $w/c=0.4$ as well as the pozzolanic effect of 25% Class C fly ash used in $w/cm=0.45$ specimens. Results are in line with data obtained by Sagoe et al. (2001), who reported that there is no significant difference between the splitting tensile strength of the reference and the recycled aggregate concrete specimens. The EMV results are similar to those reported by Fathifazl et al. (2011) who observed the positive impact of the EMV method on splitting tensile strength of concrete. However, the data obtained from TSMA was contradictory to that reported by Tam et al. (2005, 2007).

The splitting tensile strength of normal weight concrete can be estimated using the following equation provided by ACI 318:

$$f_{ct} = 6.7 \sqrt{f'_c} \quad (4-3)$$

Where:

f'_c = compressive strength of concrete (psi)

f_{ct} = splitting tensile strength (psi).

The predicted values using the suggested ACI equations and the variations from the test results are reported in **Table 4.7**.

It was observed that in most of the cases, the ACI equation overestimates the splitting tensile strength. The most accurate predictions were in the case of the reference mixture with $w/cm = 0.45$.

4.2.4. Flexural Strength. The flexural strength, also known as modulus of rupture, was measured on $6 \times 6 \times 21$ in. beams in accordance with ASTM C78. Two specimens were tested for each concrete mixture at each testing age and the mean values

were reported as flexural strength of the concrete. A four-point bending setup was used for testing the flexural strength. **Figure 4.5** depicts a schematic view of the test setup used for loading the beams. Two rigid supports were located approximately 1.5 in. away from each side of the specimen. The load was applied on the concrete beam and the failure load (P) was recorded. The flexural strength is then calculated using the following equation:

$$R = \frac{Pl}{bh^2} \quad (4-4)$$

Where R = modulus of rupture (psi), P = the ultimate load (lb), l = span length equal to 18 in., b = average beam width at fracture (in.), and h = average beam height at fracture (in.).

Table 4.7 Comparing the Splitting Tensile Strength Data with ACI 318 Equation

Mixture type	Laboratory produced mixtures (w/cm=0.45)							Sampled from truck (w/c=0.4)	
	Ref.	30% RCA	30% EMV	50% RCA	70% RCA	100% RCA	100% TSMA	0 % RCA	100% RCA
Age	Predicted value by ACI 318 (psi)								
7 Days	433	406	457	405	446	450	455	473	457
Variation (%)	-1.6	17.6	1.6	12.4	8.9	5.9	8.3	13.9	20.4
28 Days	481	458	503	448	502	499	485	511	487
Variation (%)	0.2	1.7	-0.5	4.2	6.8	17.3	19.6	2.1	17.4
56 Days	500	485	547	460	516	502	527	542	496
Variation (%)	-0.9	0.9	-9.6	-2.1	-0.8	4.5	19.7	-10.4	14.0

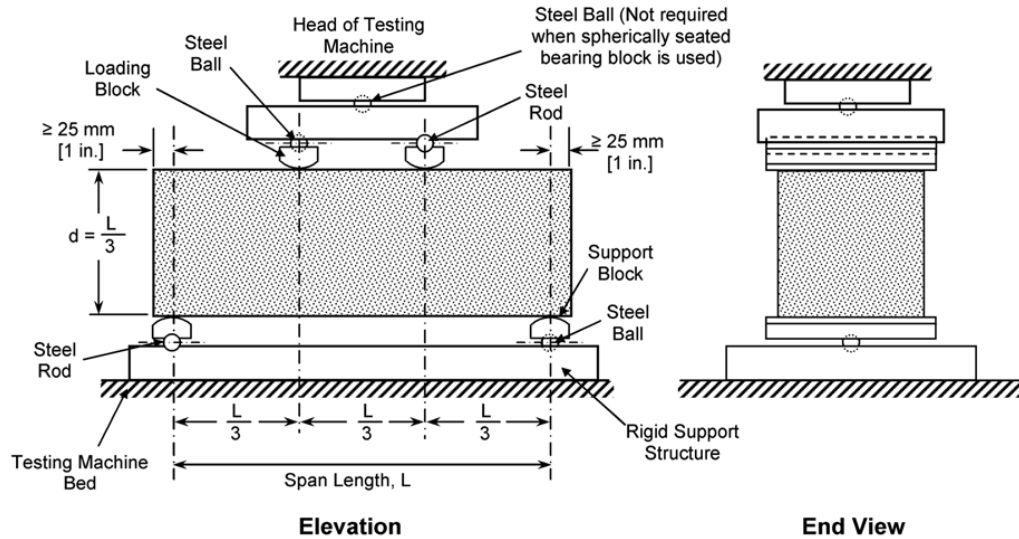


Figure 4.5 Simply Supported Beam for Determining the Flexural Strength (ASTM C78)

Table 4.8 includes the modulus of rupture data obtained from testing different specimens. Flexural strength of the specimens made with 30% and 50% RCA were lower than the reference specimens. This might be mostly due to the higher air content, especially in the case of 50% RCA specimens. The flexural strength of the specimens made with 70% and 100% RCA replacement were pretty close to the reference mixture. Similar results were published by Xiao and Li (2005) and Ravindrarajah and Tam (1985) who reported that increasing the RCA content does not have a significant effect on flexural strength. The high quality of RCA along with the rough surface texture which increases the aggregate interlock might be considered as the main reasons for these observations.

Contrary to the splitting tensile strength results, TSMA was effective in increasing the flexural strength of the specimens by 25% and 6% at 28 and 56 days respectively. Specimens made with the EMV method had very good flexural performance as well. The

28 day results obtained for this mixture was 24% higher than the reference mixture.

However, both the mixtures had similar performance at 56 days.

Table 4.8 Flexural Strength Results

Mixture type	Laboratory produced mixtures (w/cm=0.45)							Sampled from truck (w/c=0.4)	
	Ref.	30% RCA	30% EMV	50% RCA	70% RCA	100% RCA	100% TSMA	0 % RCA	100% RCA
Age	Average values for two specimens (psi)								
28 Days	590	635	730	610	630	605	760	645	680
56 Days	765	695	780	630	760	775	820	890	690

The flexural strength of normal weight concrete can be estimated using the following equation provided by ACI 318:

$$R = 7.5 \sqrt{f'_c} \quad (4-5)$$

Where

f'_c = compressive strength of concrete (psi)

R = flexural strength (psi)

The predicted values using the suggested ACI equations are reported in **Table 4.9**. It was observed that for all the concrete mixtures in both the test ages, the ACI equation underestimates the flexural strength.

Table 4.9 Comparing the Flexural Strength Measurements with ACI 318 Equation

Mixture type	Laboratory produced mixtures (w/cm=0.45)							Sampled from truck (w/c=0.4)	
	Ref.	30% RCA	30% EMV	50% RCA	70% RCA	100% RCA	100% TSMA	0 % RCA	100% RCA
Age	Predicted value by ACI 318 (psi)								
28 Days	538	513	563	501	562	558	542	572	545
Variation (%)	-8.8	-19.3	-22.9	-17.8	-10.8	-7.7	-28.6	-11.4	-19.8
56 Days	560	542	612	515	578	562	590	607	555
Variation (%)	-26.8	-22.0	-21.5	-18.2	-24.0	-27.5	-28.1	-31.8	-19.5

4.2.5. Modulus of Elasticity. Table 4.10 includes a summary of the static modulus of elasticity (Young's modulus) results. For each testing age, three 4×8 in. cylindrical specimens were used for determining the static modulus of elasticity according to ASTM C469. Figure 4.6 shows the test setup used for measuring the modulus of elasticity.

The loading cycles were repeated three times for each sample. The vertical strain of the specimen corresponding to each stress level was measured using a LVDT system. The results were then used for determining the modulus of elasticity based on the following equation:

$$E = \frac{S_2 - S_1}{\varepsilon_2 - 0.000050} \quad (4-6)$$

Where E = Chord modulus of elasticity (psi), S_2 = Stress corresponding to 40% of the ultimate load capacity, S_1 = Stress corresponding to a longitudinal strain of 0.000050, and ϵ_2 = longitudinal strain caused by the stress S_2 .



Figure 4.6 Modulus of Elasticity Test Setup

Table 4.10 Modulus of Elasticity Measurements

Mixture type	Laboratory produced mixtures (w/cm=0.45)							Sampled from truck (w/c=0.4)	
	Ref.	30% RCA	30% EMV	50% RCA	70% RCA	100% RCA	100% TSMA	0 % RCA	100% RCA
Age	Average values for three specimens (ksi)								
28 Days	4780	4600	5350	4350	5030	4830	4670	6300	4700
56 Days	5700	5000	5480	4820	5100	5100	4630	6410	5020

It was observed that the modulus of elasticity is decreasing due to the use of RCA. This is due to the lower stiffness of the RCA particles compared to the virgin aggregate. Similar results were also reported by Hoffmann et al. (2012), and Cabo et al. (2009) who observed that the modulus of elasticity is decreasing as a function of an increase in the RCA replacement ratio.

Variations in modulus of elasticity is in line with the compressive strength results, with the lowest results observed in the case of specimens made with 30% and 50% RCA replacement. These specimens had the highest air contents in the fresh mixture. No improvement was observed in specimens made with 100% RCA-TSMA. While comparing to the reference mixture, the specimens made with the EMV method had 12% higher modulus of elasticity results at 28 days. However, the modulus of elasticity of the reference mixture was 4% higher than the EMV specimens at 56 days. No significant difference was observed between the modulus of elasticity of the 100% RCA specimens with $w/c=0.4$ and $w/cm=0.45$. It was also observed that the mixture with lower w/c was more sensitive to RCA replacement. A 22% decrease in 56-day modulus of elasticity was observed in the case of the mixture with $w/c=0.4$. This decrease was limited to 12% in the case of specimens made with $w/cm=0.45$.

Modulus of elasticity results are compared to the following equations provided by ACI 318 and AASHTO codes for estimating the modulus of elasticity based on the compressive strength:

ACI 318 :

$$E = 57000 \sqrt{f'_c} \quad (4-7)$$

Where E is the modulus of elasticity (psi) and f'_c is the compressive strength (psi).

AASHTO code:

$$E = 33000W_c^{3/2}\sqrt{f'_c} \quad (4-8)$$

Where E is the modulus of elasticity (ksi), W_c is the unit weight of concrete (kcf=1000 pcf), and f'_c is the compressive strength (ksi).

Table 4.11 summarizes the ACI 318 estimations for the modulus of elasticity based on the compressive strength results at 28 and 56 days of age. It was observed that the ACI equation underestimates the modulus of elasticity for all the tested specimens at different ages. Shown in **Table 4.12** are the estimated values for the modulus of elasticity based on the equation provided by AASHTO. Similar to the ACI 318 equation, the equation provided by AASHTO underestimates the modulus of elasticity results. However, the difference between the ACI predictions and the laboratory measurements was less.

4.3. DURABILITY

4.3.1. General. For each of the experimental mixtures, the same volume of concrete (4.5 ft³) was produced for the durability test sampling. The volume of these batches was selected to be the same as the batches for the mechanical properties to ensure the minimum possible difference in quality of the produced concrete. The mixture for durability investigations was produced directly after finishing the sampling of specimens for mechanical properties. The shrinkage specimens were cast from this batch. Therefore, the shrinkage results are presented along with the durability tests. Shown in **Table 4.13** are the fresh properties of the mixtures for durability sampling.

**Table 4.11 Comparing the Modulus of Elasticity Measurements
with ACI 318 Equation**

Mixture type	Laboratory produced mixtures (w/cm=0.45)							Sampled from truck (w/c=0.4)	
	Ref.	30% RCA	30% EMV	50% RCA	70% RCA	100% RCA	100% TSMA	0 % RCA	100% RCA
Age	ACI 318 estimation for MOE (ksi)								
28 Days	4091	3895	4277	3811	4269	4243	4122	4345	4146
Variation (%)	-14	-15	-20	-12	-15	-12	-12	-31	-12
56 Days	4258	4122	4652	3916	4389	4269	4481	4613	4220
Variation (%)	-25	-18	-15	-19	-14	-16	-3	-28	-16

**Table 4.12 Comparing the Modulus of Elasticity Measurements
with AASHTO Equation**

Mixture type	Laboratory produced mixtures (w/cm=0.45)							Sampled from truck (w/c=0.4)	
	Ref.	30% RCA	30% EMV	50% RCA	70% RCA	100% RCA	100% TSMA	0 % RCA	100% RCA
Age	AASHTO estimation for MOE (ksi)								
28 Days	3882	3545	4165	3470	3882	3727	3576	4122	3517
Variation (%)	-19	-23	-22	-20	-23	-23	-23	-35	-25
56 Days	4002	3764	4584	3608	4258	3731	3916	4760	3538
Variation (%)	-30	-24	-16	-25	-17	-27	-15	-26	-30

Table 4.13 Fresh Properties of Mixtures used for Durability Sampling

Mixture type	Laboratory produced mixtures (w/cm=0.45)							Sampled from truck (w/c=0.4)	
	Ref.	30% RCA	30% EMV	50% RCA	70% RCA	100% RCA	100% TSMA	0 % RCA	100% RCA
Slump (in.)	6.0	7.0	4.0	5.5	8.0	8.5	6.0	5.5	8.5
Air content (%)	7.2	7.2	5.5	6.6	5.6	5.4	5.5	8.5	6.5
Unit weight (pcf)	146.0	143.6	148.5	144.2	143.1	141.0	140.5	147.2	137.5

4.3.2. Drying Shrinkage. Three 3.0×3.0×11.25 in. prisms were used for monitoring drying shrinkage of each of the concrete mixtures according to ASTM C157. The concrete specimens were demolded 24 hours after casting and placed in the lime-saturated water of 70±5 °F for seven days. The samples were then kept in an environmental chamber with a temperature of 70±5 °F and a relative humidity of 50±5% located at the Hy-Point facility. However, the temperature and/or relative humidity of the chamber were out of the mentioned ranges in periods of time. **Figure 4.7** shows the variations of the relative humidity and temperature of the environmental chamber.

A length comparator with digital indicator was used for measuring the length of the specimens immediately after removing them from the curing tank as shown in **Figure 4.8**.

This initial length was registered and used as the reference for determining the shrinkage deformation of the specimens. The same device was used for measuring the length of specimens at different time intervals after moving them to the environmental chamber. **Figure 4.9** presents the shrinkage deformation of the specimens.

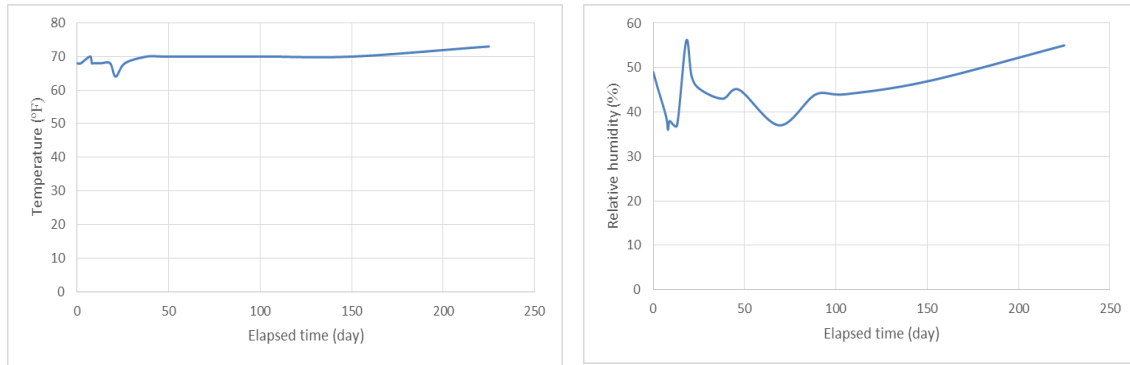


Figure 4.7 Variations in Relative Humidity and Temperature of the Environmental Chamber



Figure 4.8 Measuring the Length of the Shrinkage Specimens

It was observed that all the mixtures made with $w/cm=0.45$ had approximately similar shrinkage performance. An increase in shrinkage was observed in case of specimens made with 70% RCA. It is usually reported that the shrinkage is increasing as a function of an increase in RCA content. This is believed to be related to the lower stiffness and restraining capacity of the RCA particles due to the residual mortar and a decrease in

the total stiff virgin aggregate portion in the mixture as stated by Xiao et al. (2012). On the other hand, Kim and Bentz (2008) and Hu et al. (2013) have observed that the RCA has beneficial effects on shrinkage properties. This might be due to the internal curing using absorptive RCA particles. Similar trends were observed in the case of laboratory made specimens with $w/cm=0.45$. Based on the obtained results, there is not a significant difference in shrinkage behavior of most of the specimens made with different percentages of RCA and $w/cm=0.45$. It should be noted that the absorption of the coarse RCA used in this study is 4.56% and aggregates were completely saturated at the beginning of the mixing process. The specimens made with the EMV method had good shrinkage performance which is due to the low fresh mortar content of this mixture. It also should be taken into account that the increased amount of coarse aggregate in this mixture has a positive impact on reducing the shrinkage. Deformations registered in the case of the laboratory made specimens made with 100% RCA-TSMA is slightly higher than the 100% RCA mixture (both with $w/cm=0.45$). No improvement in shrinkage behavior was observed as a result of using the two stage mixing method.

It also should be noted that the specimen made with virgin aggregates and $w/c=0.4$ had better shrinkage deformation compared to the mixture made with $w/cm=0.45$. However, a similar trend was not observed in the case of specimens made with 100% RCA. This might be due to use of Class C fly ash in specimens made with $w/cm =0.45$.

Differences in the shrinkage deformation of the specimens made with $w/c=0.4$ was more significant than those made with $w/cm=0.45$. This means that concrete made with lower w/c may be more sensitive to RCA replacement.

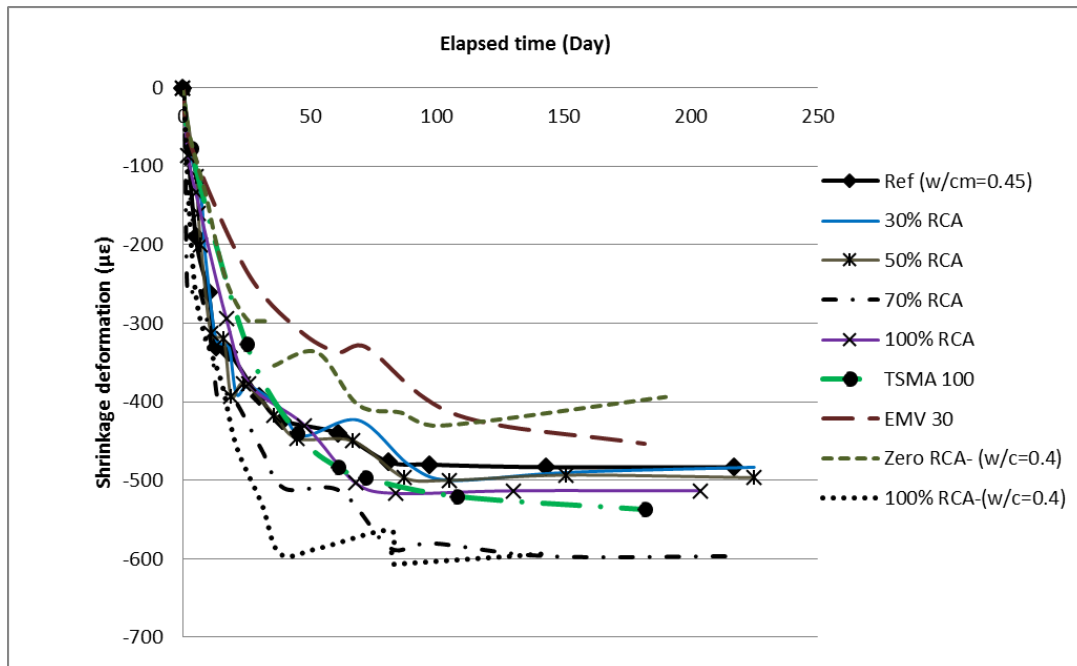


Figure 4.9 Drying Shrinkage Deformation of the Specimens

4.3.3. Surface Resistivity. Resistivity is a material property that quantifies the degree to which an object prevents the passage of an electrical current. While the solid material in concrete has a relatively high resistivity, the pores are partially to fully saturated with a concentrated alkaline solution that has a relatively low resistivity. Thus, electrical current flows primarily through the pore solution, giving an indirect measure of the quality of the microstructure.

The Resipod resistivity meter produced by Proceq Co. with a uniform electrode spacing of 1.5 in. was used to measure the surface resistivity of the cylindrical concrete specimens. The Resipod is a resistivity meter operating on the principle of the Wenner probe. The Wenner probe consists of four equally spaced, co-linear electrodes that are placed in contact with a concrete cylinder specimen. An alternating current is applied to the outermost electrodes and the voltage between the middle two electrodes is used to

determine the resistance as shown in **Figure 4.10**.

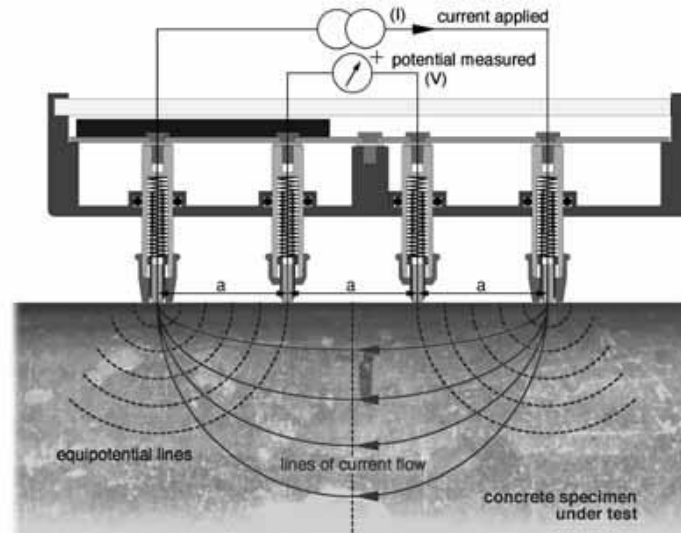


Figure 4.10 Schematic View of the Surface Resistivity Measurement Principles (Proseq SA 2013)

The current is carried by the ions available in the pore solution. The sample resistivity is calculated from the resistance, the distance between the electrodes and the dimensions of the cylinder using the following equation:

$$\rho = 2\pi aV / I \quad (4-9)$$

Where:

ρ = surface resistivity (k Ω cm)

a = electrode spacing (1.5 in.)

V = potential difference (V)

I = applied electric current

A correction factor equal to 1.1 was applied to the measurements for compensating the effect of lime curing according to AASHTO TP-95.

Considering the less time and effort required for conducting the surface resistivity

test, many agencies are moving towards this method to replace alternative time consuming methods such as the rapid chloride ion permeability test (RCPT), chloride ponding, etc., (Chini et al. 2003). This method is also applicable for field measurements for predicting the likelihood of corrosion due to chloride diffusion as well as estimating the corrosion rate once depassivation of the steel has taken place. **Table 4.14** includes the empirical criteria suggested by Proceq Co. (2013) for measured resistivity which can be used to determine the likelihood of corrosion on flat surfaces in the field. **Table 4.15** includes the criteria introduced by Proceq Co. (2013) to predict the corrosion rate based on the surface resistivity on flat surfaces while referring to depassivated steel.

Table 4.14 Correlation between the Surface Resistivity and Likelihood of Corrosion

Concrete Resistivity	Likelihood of Corrosion
≥ 100 k Ω cm	Negligible risk of corrosion
$=50-100$ k Ω cm	Low risk of corrosion
$=10-50$ k Ω cm	Moderate risk of corrosion
≤ 10 k Ω cm	High risk of corrosion

Three 4×8 in. cylindrical specimens were used for determining the surface resistivity. The same specimens were used for tests at different ages to monitor the variations in electrical resistivity with time. Specimens were kept in lime saturated water up to the test time. Before starting the test, specimens were thoroughly washed to ensure performing measurements on a clean surface. **Figure 4.11** shows the surface resistivity measurement process.

Table 4.15 Correlation between the Surface Resistivity and Rate of Corrosion

Concrete Resistivity	Estimated corrosion rate
>20 k Ω cm	Low corrosion rate
10-20 k Ω cm	Low to moderate corrosion rate
5-10 k Ω cm	High corrosion rate
<5 k Ω cm	Very high corrosion rate

**Figure 4.11 Surface Resistivity Measurement**

A good connection between the electrodes and the concrete surface is the most important factor affecting the reliability of measurements. Therefore, the test surfaces were kept wet during the test period to have a good connection. For each specimen, four separate readings were taken around the circumference of the cylinder at 90-degree increments (0°, 90°, 180°, and 270°). Measurements were repeated several times at each angle to find the most reliable reading.

Table 4.16 summarizes the results of the surface resistivity at different ages. It was

observed that for all the specimens, the resistivity is continuously increasing with time. This is due to the continuing hydration process that reduces the voids and pore space inside the concrete microstructure.

Table 4.16 Surface Electrical Resistivity Measurements

Mixture type	Laboratory produced mixtures (w/cm=0.45)						
	Ref.	30% RCA	30% EMV	50% RCA	70% RCA	100% RCA	100% TSMA
Age	Average values for three specimens (kΩcm)						
28 Days	6.3	7.4	6.0	7.6	7.0	5.0	5.2
56 Days	9.5	8.6	8.1	8.4	8.8	6.8	6.1
91 Days	11.6	11.8	9.1	11.6	9.1	8.1	7.2

It was observed that at 28 days of age, most of the RCA-made mixtures had higher resistivity values compared to the reference specimens. However, the surface resistivity measured for the reference specimens was higher than the RCA specimens at 56 days. There was no significant difference in surface resistivity of the reference mixture and the mixtures made with 30% and 50% of RCA at 91 days. But, the specimens made with 70% and 100% RCA replacement had significantly lower resistivity at this age. TSMA was not effective in enhancing the surface resistivity of concrete made with 100% RCA. The EMV mixture had less resistivity compared to the reference and the 30% RCA mixture as well.

Chini et al. (2003) have conducted a comprehensive study in collaboration with the Florida Department of Transportation (FDOT) to correlate the surface resistivity to other

electrical resistivity test methods such as the rapid chloride ion permeability test (RCPT). Several types of concrete mixtures made with different types and amounts of pozzolans have been studied in different ages. **Table 4.17** proposed by Chini et al. (2003) compares the surface resistivity results with the RCPT values.

Table 4.17 Correlation between the Surface Resistivity and Chloride Ion Permeability

Chloride ion permeability	RCPT test	Surface resistivity (kΩcm)	
	Charge passed (Coulomb)	28 Days	91 Days
High	>4000	<12	<11
Moderate	2000-4000	12-21	11-19
Low	1000-2000	21-37	19-37
Very low	100-1000	37-254	37-295
Negligible	<100	>254	>295

With regard to the criteria introduced at **Table 4.17** the following conclusions may be made:

28 day test results: all the specimens, including the reference and the RCA-made concrete mixtures have “High” chloride ion permeability index.

91 day test results: The reference specimens and those made with up to 50% RCA replacement have “Moderate” chloride ion permeability. However, increasing the RCA content to 70% and 100% results in decreasing the electrical surface resistivity and increasing the chloride ion permeability to the “High” level. Similar results were observed for the specimens made with 100% RCA-TSMA and the EMV method with “High” level of chloride ion permeability.

Figure 4.12 depicts the variations in surface resistivity as a function of RCA replacement level for the reference specimens and those made with up to 100% RCA replacement.

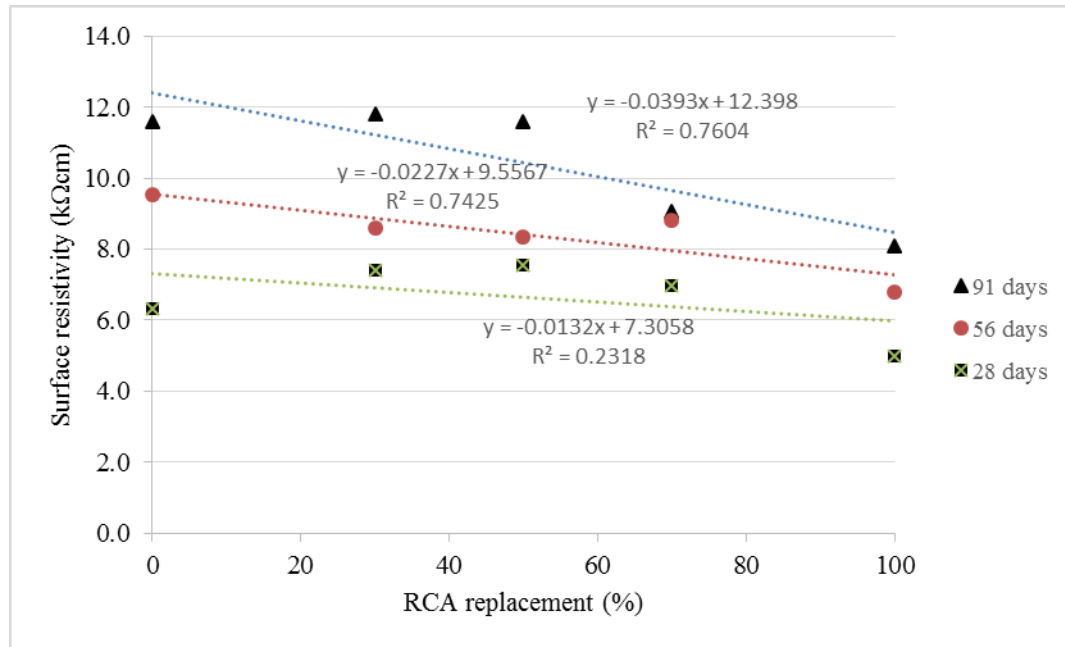


Figure 4.12 Correlation between the Surface Resistivity and RCA Replacement Ratio

A good linear relation exists between the RCA content and the resistivity at 56 and 91 days. It was observed that the surface resistivity decreases at a higher rate at 91 days compared to 56 and 28 days.

4.3.4. Bulk Electrical Conductivity. Besides the surface resistivity, the bulk electrical conductivity of the specimens were measured using the Resipod test setup. The same samples used for the surface resistivity test were used for measuring the bulk conductivity according to ASTM C1760. In order to conduct this test, it is required to put pieces of wet foam on top and bottom of the specimen, between the concrete surface and

the metal plates of the test setup. The foam pieces ensure proper electrical contact to the cylinder. However, depending on the moisture condition, these foam pieces will also have some electrical resistivity that should be taken into account to determine the true value of the sample's bulk resistivity. **Figure 4.13** shows the three steps required for bulk resistivity measurements.

First, the resistivity of the upper foam should be determined (R_{upper}). Then, the bottom foam should be placed between the plates, with the specimen on the top plate to simulate the effect of the weight of the specimen on foam thickness and porosity. The resistivity of the bottom foam should be recorded (R_{lower}). Finally, the bulk resistivity of the sample with foam at top and bottom should be measured ($R_{measured}$). Using the following equation, the net bulk resistivity of the sample should be calculated:

$$R_{cylinder} = R_{measured} - R_{upper} - R_{lower} \quad (4-10)$$

Table 4.18 summarizes the results of the bulk electrical resistivity measurements. Similar to the surface resistivity measurements, most of the RCA made specimens had better performance while compared to the reference mixture at 28 days. However, the EMV specimens had inferior performance compared to 30% RCA specimens at 91 days. It was observed that the bulk resistivity is decreasing as a result of an increase in RCA content with the maximum values for the reference, and the minimum results for the 100% RCA replacement at 56 and 91 days. The TSMA was not effective in enhancing the bulk resistivity of the 100% RCA concrete mixture. The electrical resistivity of the EMV mixture was similar to the 30% RCA mixture and less than the reference at 56 days.



Figure 4.13 Measuring Bulk Electrical Resistivity. Top Foam (top left), Lower Foam (top right), and Specimen Resistivity (bottom photo)

Table 4.18 Bulk Electrical Resistivity Measurements

Mixture type	Laboratory produced mixtures (w/cm=0.45)						
	Ref.	30% RCA	30% EMV	50% RCA	70% RCA	100% RCA	100% TSMA
Age	Average values for three specimens (kΩcm)						
28 Days	6.3	7.4	6.7	7.4	6.7	5.3	5.2
56 Days	10.5	9.0	9.0	8.8	9.0	7.3	7.0
91 Days	13.1	12.4	10.2	11.7	10.3	9.4	8.2

Figure 4.14 compares the bulk resistivity measurements of the reference specimens with those of specimens made with various RCA contents ranging from 30% to 100% at different ages. A linear relationship was determined between the RCA content and bulk resistivity.

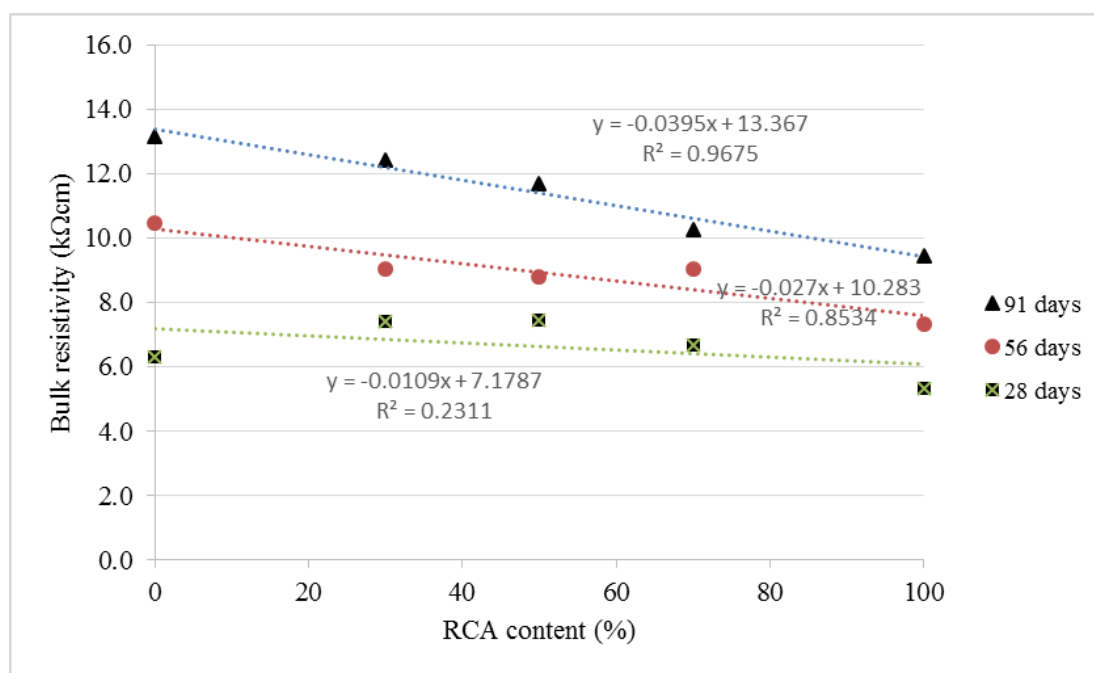


Figure 4.14 Correlation between the Bulk Resistivity and RCA Replacement Ratio

It was observed that the effect of RCA content is more significant at later ages with approximately 0.04 kΩcm decrease in bulk resistivity as a function of each percent increase in RCA replacement at 91 days. The decrease rate was approximately 0.03 kΩcm and 0.01 kΩcm at 56 and 28 days respectively.

Figure 4.15 depicts the correlation between the bulk electrical resistivity and the surface resistivity of the same specimens measured at different ages. A linear correlation exists between these two measured parameters with very little spread in data.

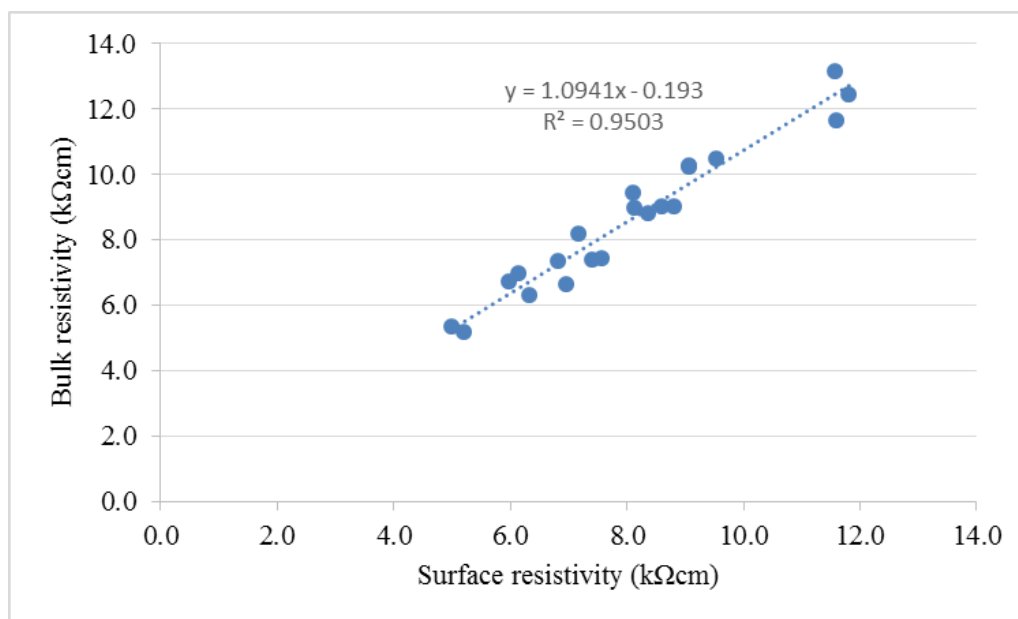


Figure 4.15 Correlation between the Surface and Bulk Electrical Resistivity Measurements

4.3.5. Permeable Void Volume. The ASTM C642 method measures the volume of permeable voids of a concrete sample as a percentage of the volume. This method determines the water absorption after immersion in water at room temperature and after immersion in boiling water for five hours. The high temperature affects both the viscosity and the mobility of the water molecules which may enable the greater displacement of water within the pore system of the hardened concrete (CCAA 2009). Two samples were used for determining the permeable void volume. These samples were half cylinders measuring 4 in. in diameter and 4 in. in height. These samples were obtained by cutting a 4×8 in. cylinder into two pieces. This way, each specimen had finished, formed, and cut surfaces exposed to water penetration. Samples were dried in an oven at a temperature of 220 ± 40 °F up to a constant mass. The oven dried mass of the samples was measured after cooling down to room temperature (A). The specimens were then immersed in water in

room temperature up to a time when the specimen was completely saturated and the saturated surface dried (SSD) mass of the specimen was constant. After registering this weight (B), the specimens were immersed in boiling water for five hours, followed by a 14 hours period of rest to cool down to room temperature. The SSD weight after boiling was measured in this step (C). Finally, the submerged weight of specimens was determined (D). The following equations were used for measuring the absorption, density, and permeable void volume of the specimens:

$$\text{Bulk dry density } (g_1) = [A/(C-D)] \times \rho \times 100 \quad (4-11)$$

$$\text{Apparent density } (g_2) = [A/(A-D)] \times \rho \times 100 \quad (4-12)$$

$$\text{Permeable void volume } (\%) = (g_2 - g_1) / g_2 \times 100 \quad (4-13)$$

Where ρ is the density of water equal to 1 gm/cm^3

Table 4.19 includes a summary of the mean values calculated for the permeable void volume of the specimens. It was generally observed that the permeable void volume is increasing as a function of an increase in RCA content. This is due to the higher amount of permeable mortar introduced to the mixture through RCA particles.

The permeable void volume has been used by VicRoads (CCAA 2009) to classify concrete durability as shown in **Table 4.20**. It should be noted that vibrated cylindrical specimens were used for determining the permeable void volume in this study.

It was observed that both the mixtures with no RCA replacement, and the mixture proportioned according to the EMV method had permeable void volumes close to 11%, which means that these mixtures had “Excellent” performance. The mixtures made with 30% and 50% RCA replacement had permeable void volumes close to 12% can be

categorized as mixtures with “Good” performance for all test ages. The mixture made with 70% RCA replacement had the permeable void volume close to 13.5%. This means that this mixture had “Normal” permeable void volume. Specimens made with 100% RCA replacement had “Marginal” performance with results ranging between 15% and 16% for all ages. However, the specimens made with 100% RCA-TSMA had “Normal” performance at 91 days of age.

Table 4.19 Permeable Void Volume Measurements

Mixture type	Laboratory produced mixtures (w/cm=0.45)							Sampled from truck (w/c=0.4)	
	Ref.	30% RCA	30% EMV	50% RCA	70% RCA	100% RCA	100% TSMA	0 % RCA	100% RCA
Age	Average values for two specimens (%)								
28 Days	11.27	12.29	11.62	12.29	13.38	15.12	15.23	11.5	15.75
56 Days	11.36	12.34	11.18	12.29	14.58	15.07	14.32	-	-
91 Days	11.49	12.77	11.03	12.37	13.64	14.87	13.85	10.49	15.28

4.3.6. Absorption. Absorption of the concrete samples is measured for both the saturated and boiled conditions according to the ASTM C642 test method. The following equations are used for calculating the absorption of the samples after immersion and after boiling:

$$\text{Absorption after immersion} = [(B-A)/A] \times 100 \quad (4-14)$$

$$\text{Absorption after immersion and boiling} = [(C-A)/A] \times 100 \quad (4-15)$$

Where “A” is the oven dry weight, “B” is the SSD weight after immersion, and “C” is the SSD weight after immersion and boiling.

Table 4.20 Durability Classification based on Permeable Void Volume (CCAA 2009)

Durability classification indicator	Vibrated cylinders (Permeable void %)	Rodded cylinders (Permeable void %)	Cores (Permeable void %)
Excellent	< 11	< 12	< 14
Good	11-13	12-14	14-16
Normal	13-14	14-15	16-17
Marginal	14-16	15-17	17-19
Bad	> 16	> 17	> 19

Tables 4.21 and **4.22** summarize the measured absorption values. For both the immersed and boiled specimens, it was observed that absorption is increasing as a function of increase in RCA replacement ratio. Samples made with $w/c=0.4$ had relatively lower absorption values compared to samples made with $w/c=0.45$.

It was also observed that the absorption values registered for the specimens made with the EMV method were less than the reference specimens and those made with 30% RCA. The TSMA was shown to be beneficial in reducing the absorption values registered at 56 and 91 days.

Figure 4.16 depicts the correlation between the absorption values determined after immersion in boiling water versus the absorption values determined after immersion in water at room temperature. A strong linear relation between the absorption values

determined after immersion and those determined after boiling exists.

Table 4.21 Absorption after Immersion

Mixture type	Laboratory produced mixtures (w/cm=0.45)							Sampled from truck (w/c=0.4)	
	Ref.	30% RCA	30% EMV	50% RCA	70% RCA	100% RCA	100% TSMA	0 % RCA	100% RCA
Age	Average values for two specimens (%)								
28 Days	5.00	5.55	5.02	5.49	6.02	6.87	6.95	4.75	6.42
56 Days	5.06	5.53	4.74	5.67	6.28	7.11	6.61	-	-
91 Days	4.92	5.92	4.84	5.66	6.16	7.16	6.77	4.24	6.29

Table 4.22 Absorption after Immersion and Boiling

Mixture type	Laboratory produced mixtures (w/cm=0.45)							Sampled from truck (w/c=0.4)	
	Ref.	30% RCA	30% EMV	50% RCA	70% RCA	100% RCA	100% TSMA	0 % RCA	100% RCA
Age	Average values for two specimens (%)								
28 Days	5.06	5.67	5.13	5.67	6.18	7.15	7.26	4.62	6.60
56 Days	5.14	5.69	4.89	5.63	6.44	7.15	6.79	-	-
91 Days	5.15	5.96	4.82	5.68	6.32	7.02	6.74	4.14	6.49

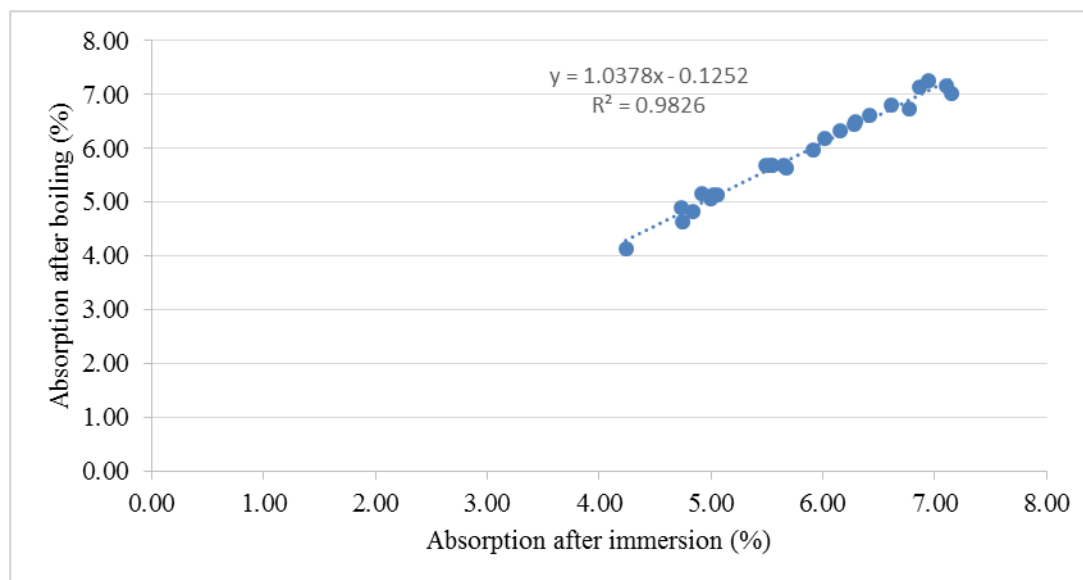


Figure 4.16 Correlation between the Absorption Values Measured after Immersion and Boiling

Immersion in boiling water results in an increase in absorption rate. The average values recorded for absorption after boiling are approximately 3.8% higher than average values registered after immersion in water at room temperature. Similar trends were observed by Thomas et al. (2013), Kou and Poon (2012) and Olorunsogo and Padayachee (2002) who observed an increase in absorption rates after boiling in concrete specimens made with virgin aggregates.

4.3.7. Deicing Salt Scaling. Deicing salts used for ice and snow on concrete contribute to surface scaling and spalling. The scaling and spalling in these cases is physical deterioration. Deicing salts induce mortar flaking, scaling and surface spalling of non-air-entrained concrete during frost conditions, and are thought to be one of the significant causes of this surface deterioration. In addition to leaving the surface deteriorated and rough, this phenomenon can also increase the permeability of the concrete (Mehta and Monteiro 2006). In order to investigate the scaling potential in

concrete mixtures, the ASTM C672 test is developed. Slabs with minimum surface area of 72 in.² and minimum thickness of three inches are recommended for this test. A dike is placed on the finished surface of the specimen. This dike is used for ponding the surface of the specimen with a solution of calcium chloride with a concentration of 5.34 oz./gal. Specimens should then be subjected to 50 daily cycles of freezing and thawing. The specimen surface will be washed and the damage will be assessed after each five cycles. The level of deterioration will be rated in a qualitative manner from zero up to four according to the criteria introduced in **Figure 4.17**. Examples of surface appearance corresponding to each of the ratings are also depicted in **Figure 4.17**.

Three slab specimens measuring 3×10×11 in. in dimension were cast for each mixture for deicing salt scaling test. Specimens were cured in lime saturated water for 28 days. It should be noted that according to the standard, the moist curing period is two weeks. But, this period was extended to four weeks to ensure hydration of the fly ash in the concrete mixtures.

The moist curing was followed by a two week period of curing specimens in an environment with constant temperature and relative humidity level. Silicon was used to cast the aforementioned dike on top of the specimens as shown in **Figure 4.18**. Specimens were then transported to the MoDOT material laboratory in Jefferson City, Missouri.

Table 4.23 includes the results of the deicing salt scaling test of the laboratory made specimens.

Rating	0	1
Condition of Surface	No scaling	Very slight scaling
Typical surface appearance		
Rating	2	3
Condition of Surface	Slight to moderate scaling	Moderate scaling
Typical surface appearance		
Rating	4	5
Condition of Surface	Moderate to severe scaling	Severe scaling
Typical surface appearance		

Figure 4.17 Rating Scale for Scaling Resistance (ASTM C672)



Figure 4.18 Silicon made Dike for Ponding the Surface of the Specimen with a Chloride Solution

It is observed that the scaling resistance of the RCA-made concrete specimens is less than the reference mixture. For the reference mixture ($w/c=0.45$) very slight scaling was observed by the end of test cycles. The specimens made with 30%, 50%, and 70% RCA had slight to moderate scaling issues at the same time.

Specimens made with 100% RCA had moderate to severe scaling. However, the specimens made with 100% RCA-TSMA have very slight scaling. It was observed that the EMV specimens are not resistant enough against scaling. For these specimens, moderate to severe scaling was observed by the end of 50 cycles.

Figure 4.19 includes sample photos taken from one out of three panels tested for each mixture at the end of 50 cycles of deicing salt scaling test.

4.3.8. Freeze/thaw Resistance. Saturated concrete is susceptible to damage due to freeze/thaw cycles. The water available in concrete pores can occupy 9% more space while frozen. If there is no space for this volume expansion, freezing may cause distress in

the concrete. Distress to critically saturated concrete from freezing and thawing will start with the first freeze-thaw cycle and will continue throughout successive winter seasons resulting in repeated loss of concrete surface (Mehta and Monteiro 2006).

Table 4.23 Deicing Salt Scaling Data

Mixture		Number of cycles									
		5	10	15	20	25	30	35	40	45	50
Laboratory produced specimens (w/cm=0.45)	Ref.	0	0	0	1	1	1	1	1	1	1
	30% RCA	1	1	1	1	2	2	2	2	2	2
	EMV 30%	1	2	3	3	3	3	4	4	4	4
	50% RCA	1	1	1	1	2	2	2	2	2	2
	70% RCA	0	0	1	1	1	2	2	2	2	2
	100% RCA	2	3	3	4	4	4	4	4	4	4
	T SMA 100	1	1	1	1	1	1	1	1	1	1

Disruptive pressures will be developed in a saturated specimen of paste unless every capillary cavity in the paste is not farther than three or four thousandths of an inch from the nearest escape boundary. Such closely spaced boundaries are provided by the correct use of a suitable air-entraining agent. This creates a large number of closely spaced, small air bubbles in the hardened concrete. The air bubbles relieve the pressure build-up caused by ice formation by acting as expansion chambers (Mehta and Monteiro 2006). Prismatic samples measuring 3×4×16 in. were used to perform the freeze/thaw testing according to ASTM C666, Procedure A. For this procedure, specimens were cured in lime saturated water for a period of four weeks before being subjected to freezing and thawing cycles. It is important to note that the period of water curing of the standard test is

14 days; however, given the 25% fly ash replacement, the initial duration of water curing was increased to 28 days. This test subjects the specimens to 300 freezing and thawing cycles. Every 36 cycles, the specimens are removed and properties of the concrete are measured. The ultrasonic pulse velocity test was used for determining the dynamic modulus of elasticity of the specimens and its variation with the increase in freeze/thaw cycles as shown in **Figure 4.20**. **Figure 4.21** plots the variations of the durability factor of the specimens tested according to procedure A as a function of freeze/thaw cycles.

The durability factor reflects the residual dynamic modulus of elasticity of the concrete. A drop in durability factor reflects the presence of internal cracking of the concrete due to damage from repetitive cycles of freezing and thawing. Values of durability factor greater than 80% after 300 cycles of freezing and thawing reflect adequate frost durability.

The highest durability factor was observed in the case of the reference mixture. All the specimens made with up to 70% of RCA replacement had durability factors higher than 80%. This indicates the proper frost resistance of these concrete mixtures. However, the mixture made with 100% RCA had durability factor of 78.5% by the end of the test cycles. This means that the specimens made with 100% RCA replacement might be susceptible to damage due to freeze/thaw cycles. The specimens made with the EMV method had lower durability factor compared to the 30% RCA mixture. The specimens made with 100% RCA-TSMA mixture had acceptable durability factor of 83.7%.

Summary of results is included in **Table 4.24**.

<p>Reference (rating=1)</p>		<p>30% RCA (rating=2)</p>	
<p>30% RCA EMV (Rating=4)</p>		<p>50% RCA (rating=2)</p>	
<p>70% RCA (rating=2)</p>		<p>100% RCA (rating=4)</p>	
<p>100% RCA TSMA (rating=1)</p>			

Figure 4.19 Appearance of the Specimen Surfaces after 50 Cycles of Deicing Salt Scaling Test



Figure 4.20 Freeze/thaw Testing, Procedure A, Freezing and Thawing in Water (left); Measurement of Pulse Velocity (right)

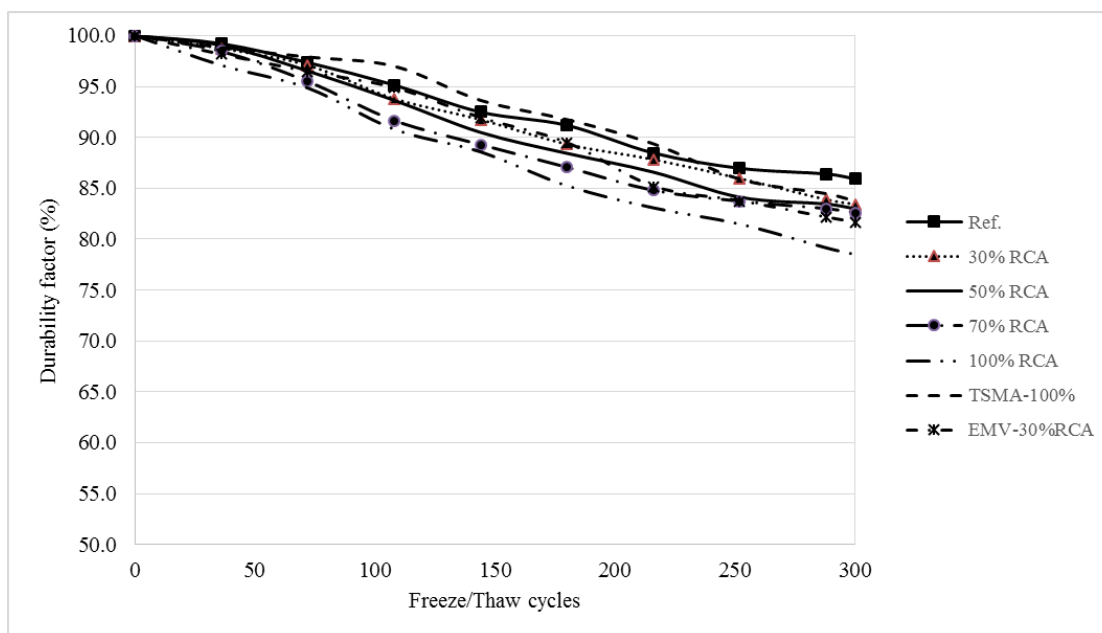


Figure 4.21 Variations in Durability Factor with Freeze/thaw Cycles

Table 4.24 Variations in Durability Factor of Specimens

Mixture type	Laboratory produced mixtures (w/cm=0.45)						
	Ref.	30% RCA	30% EMV	50% RCA	70% RCA	100% RCA	100% TSMA
Average values for three specimens (%)							
# Cycle	300	300	300	300	300	300	300
DF (%)	85.9	83.4	81.6	83.0	82.6	78.5	83.7

5. FINDINGS, CONCLUSIONS, AND RECOMMENDATIONS

The main objective of this research study was to evaluate the fresh properties, mechanical performance, and durability of concrete made with RCA. The research was focused on MoDOT Class B concrete with normal strength level. The idea was to investigate the feasibility of producing highly consumed sustainable concrete mixtures with RCA as partial or full replacement of coarse aggregate. Several mixtures with different amounts of RCA and with different mixture proportioning methods and mixing sequences were produced.

5.1. FINDINGS AND CONCLUSIONS

Based on the results of the performed study, the following findings and conclusions are presented:

- There was not a significant difference between the fresh properties of the reference and the concrete mixtures made with RCA replacements up to 100%. However, the EMV mixture was a harsh mixture with significantly lower workability compared to the other mixtures. This result is likely due to the higher coarse aggregate content and lower fresh mortar in the EMV mixture.
- The RCA made in the study was a laboratory-based material. The mixture proportion of the parent concrete used for producing the RCA was similar to that of a MoDOT-PCCP mixture with a $w/c=0.4$. This results in producing a high quality RCA.

- There was not a significant difference in compressive strength of the concrete mixtures made with RCA replacements up to 70% and 100%. However, due to the higher air content, the mixtures made with 30% and 50% RCA replacement had lower compressive strength compared to the reference and other mixtures.
- Although the amount of cementitious materials used in the EMV mix was lower than the reference mixture, this method resulted in producing concrete with high compressive strength. The TSMA was not helpful in increasing the compressive strength up to 28 days. However, the 56 day compressive strength of this mixture seems to be improved compared to the 100% RCA traditional mixture. No significant difference was observed between the 100% RCA and 100% RCA-TSMA specimens at 91 days. It should also be noted that using the TSMA will increase the mixing time, which will potentially increase the costs of concrete production.
- There was not a significant difference in splitting tensile strength and flexural strength of the mixtures made with RCA. Specimens made with the EMV method had very good tensile and flexural performance compared to the reference mixture. The TSMA was not effective in enhancing the splitting tensile strength. However, flexural strength was improved with TSMA.
- Modulus of elasticity is shown to be affected by RCA replacement ratio. The modulus of elasticity decreases as a function of an increase in RCA content. The EMV mixture had very good modulus of elasticity results. The TSMA was not effective in increasing the modulus of elasticity.

- Contrary to most of the data available in the literature, increasing the RCA did not have a significant negative impact on shrinkage of concrete mixtures. This might be traced in the internal curing effect of the highly absorptive RCA particles. The specimens made with the EMV method had very low shrinkage deformations. This result is due to the lower fresh paste incorporated in this mixture, as well as an increased amount of coarse aggregate in the blend. No improvement in shrinkage behavior of the specimens made with 100% RCA was observed due to the use of the TSMA.
- Permeable void volume and absorption of the RCA mixtures is higher than the reference mixture. The EMV method was effective in reducing the absorption. No significant difference was observed due to using the TSMA.
- Both the surface and bulk electrical resistivity values decrease as a result of increases in RCA content. A decrease in electrical resistivity is more pronounced in replacement levels above 50%. This is due to the more porous mortar phase introduced to the mixture through the RCA particles. Care must be taken while using RCA in aggressive environments when working with reinforced concrete structures. The EMV method was not effective in enhancing the electrical resistivity. The TSMA was not beneficial in increasing the resistivity of the 100% RCA specimens as well.
- Performance of the specimens made with up to 70% RCA replacement seems to be acceptable while being subjected to deicing salt scaling. The mixture made with 100% RCA replacement, however, seems to be susceptible to damage. The EMV method was not effective in enhancing the scaling

resistance. However, the specimens made with 100% RCA-TSMA had very good scaling resistance.

- Durability factor values obtained for specimens made with up to 70% RCA were higher than the acceptable threshold level of 80%. The specimens made with 100% RCA seem to be susceptible to damage due to freeze thaw cycles. Mixtures made with the EMV method and the TSMA had acceptable frost resistance with durability factors higher than 80%.

5.2. RECOMMENDATIONS

It is possible to produce sustainable concrete mixtures with high replacement levels of RCA to be used in MoDOT Class B mixtures. Based on the results presented in this report, the following topics are proposed for further investigating the properties of RCA concrete for infrastructure applications:

- Using other supplementary cementitious materials, such as ground granulated blast furnace slag (GGBS), silica fume, glass powder, etc. as a replacement for Portland cement with the aim of further decreasing the carbon foot print in RCA produced concrete mixtures. Combinations of some supplementary cementitious materials can offset some of the drop in concrete performance resulting from using RCA, thus enabling greater replacements of the virgin aggregate using RCA.
- Investigating the feasibility of using fine RCA in sustainable concrete production.

- Investigating the feasibility of producing high volume recycled aggregate concrete mixtures for other applications (e.g. pavements, etc.).
- Investigating what tests are necessary to adequately characterize RCA sources for use in concrete.

BIBLIOGRAPHY

- AASHTO TP 95, (2011), Standard Method of Test for Surface Resistivity Indication of Concrete's Ability to Resist Chloride Ion Penetration.
- Abbas A., Fathifazl G., Isgor O. B., Razaqpur A. G., Fournier B., and Foo S., (2008), Proposed method for determining the residual mortar content of recycled concrete aggregates, *Journal of ASTM International*, Vol. 5, No. 1, 12.
- Abbas. A., Fathifazl. G., Fournier. B., Isgor. O. B., Zavadil. R., Razaqpur. A. G., and Foo. S., (2009), Quantification of the residual mortar content in recycled concrete aggregates by image analysis, *Materials Characterization*, 60, 716-728.
- Abd Elhakam. A., Mohamed. A., and Awad. E., (2012), Influence of self-healing, mixing method and adding silica fume on mechanical properties of recycled aggregates concrete, *Construction and Building Materials*, Volume 35, 421–427.
- Ajdukiewicz. A., and Kliszczewicz. A. (2002), Influence of recycled aggregates on mechanical properties of HS/HPC, *Cement and Concrete Composites*, Volume 24, Issue 2, 269–279.
- ASTM C 1760, (2012), Standard Test Method for Bulk Electrical Conductivity of Hardened Concrete.
- ASTM C127, (2012), Standard Test Method for Density, Relative Density (Specific Gravity), and Absorption of Coarse Aggregate.
- ASTM C138/C138M, (2012) Standard Test Method for Density (Unit Weight), Yield, and Air Content (Gravimetric) of Concrete.
- ASTM C143/C143M, (2012), Standard Test Method for Slump of Hydraulic-Cement Concrete.
- ASTM C157/C157M, (2008), Standard Test Method for Length Change of Hardened Hydraulic-Cement Mortar and Concrete.
- ASTM C192 / C192M, (2013), Standard Practice for Making and Curing Concrete Test Specimens in the Laboratory.
- ASTM C231/C231M, (2010), Standard Test Method for Air Content of Freshly Mixed Concrete by the Pressure Method.
- ASTM C232/C232M, (2012), Standard Test Methods for Bleeding of Concrete.

- ASTM C29/C29M, (2010), Standard Test Method for Bulk Density (“Unit Weight”) and Voids in Aggregate.
- ASTM C33/C33M, (2013), Standard Specification for Concrete Aggregates.
- ASTM C39/C39M, (2012), Standard Test Method for Compressive Strength of Cylindrical Concrete Specimens.
- ASTM C469/C469M, (2010), Standard Test Method for Static Modulus of Elasticity and Poisson’s Ratio of Concrete in Compression.
- ASTM C496/C496M, (2011), Standard Test Method for Splitting Tensile Strength of Cylindrical Concrete Specimens.
- ASTM C535, (2012), Standard Test Method for Resistance to Degradation of Large-Size Coarse Aggregate by Abrasion and Impact in the Los Angeles Machine.
- ASTM C642, (2006), Standard Test Method for Density, Absorption, and Voids in Hardened Concrete.
- ASTM C666/C666M, (2003), (Reapproved 2008) Standard Test Method for Resistance of Concrete to Rapid Freezing and Thawing.
- ASTM C672 / C672M, (2012), Standard Test Method for Scaling Resistance of Concrete Surfaces Exposed to Deicing Chemicals.
- ASTM C78/C78M, (2010), Standard Test Method for Flexural Strength of Concrete (Using Simple Beam with Third-Point Loading).
- Bagragi N. K., Vidyahara H. S., and Ravandeh K., (1990), Mix Design Procedure for Recycled Aggregate Concrete, *Construction and Building Materials*, Vol 4, No 4, 188-193.
- Building Code Requirements for Structural Concrete (ACI 318), (2011), An ACI Standard and Commentary Reported by ACI Committee 318.
- César Medina. C., Isabel S. R. M., and Frías. M., (2013), Freeze-thaw durability of recycled concrete containing ceramic aggregate, *Journal of Cleaner Production*, Volume 40, 151–160.
- Cheng GY. (2005), Experimental study on the basic performance of recycled aggregate concrete with different displacement ratio, *Chinese Concrete Journal*, 11, 67–70 [only available in Chinese].

- Chini, A.R., Muszynski, L.C., and Hicks, J., (2003), Determination of acceptance permeability characteristics for performance-related specifications for portland cement concrete, final report submitted to Florida Department of Transportation, 116-118.
- Domingo-Cabo A., Lázaro C., López-Gayarre F., Serrano-López M. A., Serna P., and Castaño-Tabares J.O., (2009), Creep and shrinkage of recycled aggregate concrete, *Construction and Building Materials*, 23, 2545–2553.
- Fathifazl G., Abbas A., Razaqpur A. G., Isgor O. B., Fournier B., and Foo S., (2009), New mixture proportioning method for concrete made with coarse recycled concrete aggregate, *Journal of Materials in Civil Engineering*, Vol 10, Issue 21, 601-611.
- Fathifazl. G., Razaqpur. A.G., Isgor. O. B., Abbas. A., Fournier. B., and Foo. S., (2011), Creep and drying shrinkage characteristics of concrete produced with coarse recycled concrete aggregate, *Cement and Concrete Composites*, 33, 1026–1037.
- Gabr A. R. and D.A. Cameron, (2012), Properties of recycled concrete aggregate for unbound pavement construction, *Journal of Materials in Civil Engineering*, 24, 754-764.
- Gómez-Soberón J. M. V., (2002), Porosity of recycled concrete with substitution of recycled concrete aggregate: An experimental study, *Cement and Concrete Research*, Volume 32, Issue 8, 1301-1311.
- Hansen T.C., and Boegh E., (1985), Elasticity and drying shrinkage of recycled aggregate concrete, *ACI Journal*, 82(5), 648-652.
- Hansen. T.C., (1986), Recycled aggregate and recycled aggregate concrete, second state of- the-art report, developments from 1945–1985. *Materials and Structures*, 19(3), 201–246.
- Hoffmann. C., Schubert. S., Leemann. A., and Motavalli. M., (2012), Recycled concrete and mixed rubble as aggregates: Influence of variations in composition on the concrete properties and their use as structural material, *Construction and Building Materials*, 35, 701–709.
- Hu J., Wang Z., and Kim Y., (2013), Feasibility study of using fine recycled concrete aggregate in producing self-consolidating concrete, *Journal of Sustainable Cement Based Materials*, Vol. 2, No. 1, 20-34.
- Hu MP. (2007), Mechanical properties of concrete prepared with different recycled coarse aggregates replacement rate. *Chinese Concrete Journal*, 2:52–4 [only available in Chinese].

- ICAR rheometer manual (2013), Germann Instrumens, Inc., www.germann.org.
- Kim H., and Bentz D., (2008), Internal curing with crushed returned concrete aggregates for high performance concrete. NRMCA concrete technology forum: Focus on sustainable development, Denver, United States, 1-12.
- Kim. K., Shin. M., and Soowon Cha, (2013), Combined effects of recycled aggregate and fly ash towards concrete sustainability, *Construction and Building Materials*, Volume 48, Pages 499–507.
- Kou SC, Poon, C.S., and Chan, D., (2007), Influence of fly ash as cement replacement on the properties of recycled aggregate concrete. *Journal of Materials in Civil Engineering*, 19(9), 709-717.
- Kou. S., Poon. C., and Wan. H., (2012), Properties of concrete prepared with low-grade recycled aggregates, *Construction and Building Materials*, 36, 881–889.
- Kou. S.C., and Poon. C.S., (2012), Enhancing the durability properties of concrete prepared with coarse recycled aggregate, *Construction and Building Materials*, Volume 35, 69-76.
- Li. W., Xiao. J., Sun. Z., Kawashima. S., and Shah. S.P., (2012), Interfacial transition zones in recycled aggregate concrete with different mixing approaches, *Construction and Building Materials*, 35, 1045–1055.
- Limbachiya M. C., Leelaware, T., and Dhir R.K., (2000), Use of recycled concrete aggregate in high-strength concrete. *Materials and Structures*, 33(10), 574-580.
- Limbachiya M. C., Marrocchino E., and Koulouris A., (2007), Chemical–mineralogical characterization of coarse recycled concrete aggregate, *Waste Management*, 27, 201–208.
- Limbachiya. M., Seddik. M., and Ouchangur, Y., (2012), Performance of portland/silica fume cement concrete produced with recycled concrete aggregate, *ACI Materials Journal*, 109 (1), 91-100.
- McIntyre. J., Spatari. S., and MacLean. H.L., (2009), Energy and greenhouse gas emissions trade-offs of recycled concrete aggregate use in nonstructural concrete: A north American case study, *Journal of Infrastructure Systems*, 15, 361-370.
- Mehta P. K. and Monteiro P. J. M. (2006), *Concrete, microstructure, properties, and materials, 3rd Edition*”, McGraw-Hill.

- Nagataki S., Gokce A., and Saeki T., (2000), Effects of recycled aggregate characteristics on performance parameters of recycled aggregate concrete, *Proceedings of Fifth CANMET/ACI International Conference on Durability of Concrete*, Barcelona, Spain, 51-71.
- Nassar, R. U. D., and Soroushian, P., (2012), Use of milled waste glass in recycled aggregate concrete, *Proceeding of the ICE Construction Materials*, 165(5), 304-315.
- Nixon. P. J., (1978), Recycled concrete as an aggregate for concrete—a review. *Materials and Structures*, 11(5), 371–8.
- Olorunsogo. F. T., and Padayachee. N., (2002), Performance of recycled aggregate concrete monitored by durability indexes, *Cement and Concrete Research*, Volume 32, Issue 2, 179-185.
- Otsuki. N., Miyazato. S., and Yodsudjai. W., (2003), Influence of recycled aggregate on interfacial transition zone, strength, chloride penetration and carbonation of concrete, *Journal of Materials in Civil Engineering*, 15, 443-451.
- Padmini. A.K., Ramamurthy.K. , Mathews. M.S., (2009), Influence of parent concrete on the properties of recycled aggregate concrete, *Construction and Building Materials*, Volume 23, Issue 2, 829–836.
- Proceq (2013), Resipod Family Operating instructions, concrete durability testing, Proceq SA. www.proceq.com.
- Ravindrarajah S. R., and Tam C.T., (1985), Properties of concrete made with crushed concrete as coarse aggregate. *Magazine of Concrete Research*, 37(130), 29–38.
- Research Report Cement Concrete and Aggregates Australia, Chloride Resistance of Concrete, (2009), 3-34. <http://www.concrete.net.au/publications/publication>.
- Richardson. A., Coventry. K., and Bacon. J., (2011), Freeze/thaw durability of concrete with recycled demolition aggregate compared to virgin aggregate concrete, *Journal of Cleaner Production*, Volume 19, Issues 2–3, Pages 272–277.
- Ryu. J.S., (2002), Improvement on strength and impermeability of recycled concrete made from crushed concrete coarse aggregate, *Journal of Materials Science Letter*, 21, 1565-1567.
- Sagoe-Crentsil K., Brown T., and Taylor A. H., (2001), Performance of Concrete made with commercially produced coarse recycled concrete aggregate, *Cement and Concrete Research*, 31, 707-712.

- Shayan A., and Xu A., (2003), Performance and Properties of Structural Concrete Made with Recycled Concrete Aggregate, *ACI Materials Journal*, V. 100, No. 5, 371-380.
- Sim J., and Park C., (2011), Compressive strength and resistance to chloride ion penetration and carbonation of recycled aggregate concrete with varying amount of fly ash and fine recycled aggregate, *Waste Management*, 31, 2352–2360.
- Surya M., Rao K. V., and Lakshmy P., (2013), Recycled aggregate concrete for transportation infrastructure, *Procedia - Social and Behavioral Sciences*, Volume 104, 1158–1167.
- Tabsh S. W., and Abdelfatah A. S., (2009), Influence of recycled concrete aggregates on strength properties of concrete, *Construction and Building Materials*, 23, 1163–1167.
- Tam V. W. Y., and C.M. Tam, (2008), Diversifying two-stage mixing approach (TSMA) for recycled aggregate concrete: TSMA_s and TSMA_{sc}, *Construction and Building Materials*, 22, 2068–2077.
- Tam V. W. Y., Gao X.F., and Tam C.M., (2005), Microstructural analysis of recycled aggregate concrete produced from two-stage mixing approach, *Cement and Concrete Research*, 35, 1195–1203.
- Tam V. W. Y., Gao X.F., C.M. Tam, and Ng K.M., (2009), Physio-chemical reactions in recycle aggregate concrete, *Journal of Hazardous Materials*, 163, 823–828.
- Tam V. W. Y., Tam C.M., and Wang Y., (2007), Optimization on proportion for recycled aggregate in concrete using two-stage mixing approach, *Construction and Building Materials*, 21, 1928–1939.
- Thomas. C., Setién. J., Polanco. J.A., Alaejos. P., and Sánchez de Juan. M., (2013), Durability of recycled aggregate concrete, *Construction and Building Materials*, Volume 40, 1054-1065.
- Topçu IB, and Sengel S. (2004), Properties of concretes produced with waste concrete aggregate, *Cement and Concrete Research*, 34(8), 1307–1312.
- Wolfe M. H., (2011), Bond strength of high-volume fly ash concrete, a thesis presented to the faculty of the graduate school of the Missouri University Of Science And Technology in partial fulfillment of the requirements for the degree master of science in civil engineering., 18-19.
- Xiao JZ, and Li JB. (2005), Study on relationships between strength indexes of recycled concrete. *Chinese Journal of Building Materials*, 9(2):197–201 [only available in Chinese].

Xiao. J., Li. W., Fan. Y., and Huang. X., (2012), An overview of study on recycled aggregate concrete in China (1996–2011), *Construction and Building Materials*, 31, 364–383.

Yong, P. C. and Teo, D.C.L., (2009), Utilization of recycled aggregate as coarse aggregate in concrete, *UNIMAS E-Journal of Civil Engineering*, 1(1), 1-6.

APPENDIX C

FINAL Report C

TRyy1317

**Project Title: Recycled Concrete Aggregate (RCA) for
Infrastructure Elements**

**Report C: Bond Behavior of Mild Reinforcing Steel in
RCA Concrete**

Prepared for
Missouri Department of Transportation
Construction and Materials

Missouri University of Science and Technology, Rolla, Missouri

May 2014

The opinions, findings, and conclusions expressed in this publication are those of the principal investigators and the Missouri Department of Transportation. They are not necessarily those of the U.S. Department of Transportation, Federal Highway Administration. This report does not constitute a standard or regulation.

ABSTRACT

With a growing demand for new construction and the need to replace infrastructure stretched beyond its service life, society faces the problem of an ever-rising production of construction and demolition waste. Furthermore, existing sources of natural raw materials are increasingly burdened in order to support this new construction. In recent decades, engineers have turned to a more sustainable solution of recycling the concrete from construction and demolition waste to help reduce the overall burden on sources of quality natural concrete aggregates.

The objective of this study was to determine the effect of replacing coarse natural aggregates with recycled concrete aggregates (RCA) on the bond strength between deformed mild reinforcing steel and surrounding concrete. Two different RCA replacement levels were considered, 50% and 100%, and were compared to a standard Missouri Department of Transportation (MoDOT) mix design.

To evaluate bond strength, 18 direct pull-out specimens were tested with both #4 (No. 13) and #6 (No. 19) reinforcing bars and 9 full-scale beam specimens were tested with non-confined contact lap splices located at mid-span. The construction and testing procedure of the direct pull-out specimens was based on the RILEM 7-II-128 *RC6: Bond test for reinforcing steel. 1. Pull-out test* (RILEM, 1994). The full-scale beam splice specimens were based on a non-standard test procedure that is considered to be the most realistic stress state response for bond.

Analysis of the test data indicates that replacing more than 50% of coarse natural aggregates results in diminished bond strength over concrete containing only virgin natural aggregates. This result suggests that the existing equation for development and

splice length as reported in AASHTO LRFD and ACI 318 may require additional modification factors to account for the diminished bond strength when associated with replacement of coarse aggregates with RCA at levels greater than 50%.

TABLE OF CONTENTS

	Page
ABSTRACT	ii
LIST OF ILLUSTRATIONS	vii
LIST OF TABLES	xi
1. INTRODUCTION	1
1.1. BACKGROUND AND JUSTIFICATION	1
1.1.1. General	1
1.1.2. Benefits of Recycled Aggregate Concrete	1
1.1.3. Concerns with Recycled Aggregate Concrete	1
1.2. OBJECTIVES AND SCOPE OF WORK	4
1.3. RESEARCH PLAN	5
1.4. OUTLINE	6
2. LITERATURE REVIEW	8
2.1. BOND CHARACTERISTICS	8
2.2. COMMON BOND TESTS	11
2.3. RCA CONCRETE BOND RESEARCH	13
3. MIX DESIGNS AND CONCRETE PROPERTIES	18
3.1. INTRODUCTION	18
3.2. CONCRETE PROPERTIES	18
3.2.1. Fresh Concrete Properties	18
3.2.2. Compressive Strength of Concrete	19
3.2.3. Modulus of Rupture of Concrete	21
3.2.4. Modulus of Elasticity of Concrete	21
3.2.5. Splitting Tensile Strength of Concrete	21
3.2.6. Fracture Energy of Concrete	22
3.3. RAC MIX DESIGNS	23
3.3.1. Pre-Recycled Concrete Mix Design	23
3.3.2. VAC Control Mix Design and Concrete Properties	26
3.3.3. RAC-50% Mix Design and Concrete Properties	28

3.3.4. RAC-100% Mix Design and Concrete Properties.....	30
3.4. CONCRETE MECHANICAL PROPERTIES	33
3.4.1. Modulus of Rupture Results.....	33
3.4.2. Modulus of Elasticity Results.....	34
3.4.3. Splitting Tensile Strength Results	34
3.4.4. Fracture Energy Results	35
3.4.5. Comparison of Mechanical Properties	36
4. EXPERIMENTAL PROGRAM.....	38
4.1. INTRODUCTION	38
4.2. RCA PRODUCTION	38
4.3. DIRECT PULL-OUT SPECIMENS	40
4.3.1. Direct Pull-Out Specimen Design	40
4.3.2. Direct Pull-Out Specimen Fabrication	42
4.3.3. Direct Pull-Out Specimen Test Set-Up	44
4.3.4. Direct Pull-Out Specimen Test Procedure	45
4.4. BEAM SPLICE SPECIMENS	46
4.4.1. Beam Splice Specimen Design.....	46
4.4.2. Beam Splice Specimen Fabrication.....	47
4.4.3. Beam Splice Specimen Test Set-Up.....	52
4.4.4. Beam Splice Specimen Test Procedure.....	54
5. TEST RESULTS AND EVALUATIONS	55
5.1. DIRECT PULL-OUT TEST RESULTS.....	55
5.2. BEAM SPLICE TEST RESULTS.....	58
5.3. REINFORCING BAR TENSION TEST RESULTS	65
5.4. ANALYSIS OF RESULTS	68
5.4.1. Methodology	68
5.4.2. Analysis and Interpretation of Direct Pull-Out Results.....	70
5.4.3. Analysis and Interpretation of Beam Splice Results	78
6. FINDINGS, CONCLUSIONS AND RECOMMENDATIONS	89
6.1. INTRODUCTION	89
6.2. FINDINGS.....	89

6.2.1. Material Properties Testing	89
6.2.2. Direct Pull-Out Testing	90
6.2.3. Beam Splice Testing.....	90
6.3. CONCLUSIONS	91
6.3.1. Direct Pull-Out Testing	91
6.3.2. Beam Splice Testing.....	91
6.4. RECOMMENDATIONS.....	92
APPENDIX A: DIRECT PULL-OUT TEST DATA PLOTS.....	94
APPENDIX B: BEAM SPLICE TEST DATA PLOTS	100
APPENDIX C: PHOTOGRAPHS OF BEAM SPLICE FAILURES.....	104
APPENDIX D: STATISTICAL ANALYSIS OF RESULTS	114
BIBLIOGRAPHY.....	127

LIST OF ILLUSTRATIONS

Figure	Page
Figure 1.1: States using RCA as Aggregate.....	3
Figure 1.2: States using RCA as Base Aggregate.....	3
Figure 1.3: States using RCA in PC Concrete.....	4
Figure 2.1: Bond Force Transfer Mechanisms (ACI 408, 2003).....	8
Figure 2.2: Formation of Goto Cracks (ACI 408, 2003).....	9
Figure 2.3: Formation of Hoop Stresses and Resulting Splitting Cracks (ACI 408, 2003).....	9
Figure 2.4: Pull-Out Failure (ACI 408, 2003).....	10
Figure 2.5: Schematic Direct Pull-Out Test (ACI 408, 2003).....	11
Figure 2.6: Schematic Beam-End Test (ACI 408, 2003).....	12
Figure 2.7: Schematic Beam Anchorage Test (ACI 408, 2003).....	13
Figure 2.8: Schematic Beam Splice Test (ACI 408, 2003).....	13
Figure 3.1: Compressive Strength Test.....	20
Figure 3.2: Splitting Tensile Failure Mode.....	22
Figure 3.3: Control Mix Strength Gain with Time.....	28
Figure 3.4: RAC-50 Mix Strength Gain with Time.....	30
Figure 3.5: RAC-100 Mix Strength Gain with Time.....	33
Figure 3.6: Comparison of Normalized Mechanical Properties.....	37
Figure 4.1: Formwork for Casting Pre-Recycled Concrete.....	39
Figure 4.2: Schematic of #4 (No. 13) Bar Direct Pull-Out Specimen.....	41
Figure 4.3: Schematic of #6 (No. 19) Bar Direct Pull-Out Specimen.....	41
Figure 4.4: Completed Direct Pull-Out Specimens in Molds.....	44
Figure 4.5: Test Set-Up for Direct Pull-Out Specimen.....	45
Figure 4.6: LVDT Set-Up for Direct Pull-Out Specimen.....	45
Figure 4.7: Schematic of Beam Splice Specimen Profile.....	48
Figure 4.8: Schematic of Beam Splice Specimen Plan.....	48
Figure 4.9: Spliced Length with Attached Strain Gauges.....	49
Figure 4.10: Completed Cage for Beam Splice Specimen.....	49

Figure 4.11: Steel Cages in Forms	50
Figure 4.12: Casting of Beam Splice Specimens	51
Figure 4.13: Schematic of Beam Splice Loading	53
Figure 4.14: Beam Splice Specimens in Load Test Frame	53
Figure 4.15: LVDT Set-Up for Beam Splice Test	54
Figure 5.1: Peak Bond Stresses for VAC Pull-Out Specimens	57
Figure 5.2: Peak Bond Stresses for RAC-50 Pull-Out Specimens	57
Figure 5.3: Peak Bond Stresses for RAC-100 Pull-Out Specimens	58
Figure 5.4: Typical Plot of Slip versus Applied Load	59
Figure 5.5: Peak Loads for VAC Beam Splice Specimens	61
Figure 5.6: Peak Loads for RAC-50 Beam Splice Specimens	62
Figure 5.7: Peak Loads for RAC-100 Beam Splice Specimens	62
Figure 5.8: Peak Stresses for VAC Beam Splice Specimens	63
Figure 5.9: Peak Stresses for RAC-50 Beam Splice Specimens	63
Figure 5.10: Peak Stresses for RAC-100 Beam Splice Specimens	64
Figure 5.11: Typical Load versus Deflection Plot (VAC-3)	66
Figure 5.12: Typical Load versus Strain Plot (VAC-3)	66
Figure 5.13: Beam Splice Crack Propagation at Failure (RAC50-1)	67
Figure 5.14: Beam Splice Specimen Bottom View at Failure (RAC50-1)	67
Figure 5.15: Average #4 Pull-Out Bond Stresses by Square Root Normalization	74
Figure 5.16: Boxplot of #4 Pull-Out Bond Stresses by Square Root Normalization	74
Figure 5.17: Average #4 Pull-Out Bond Stresses by Fourth Root Normalization	75
Figure 5.18: Boxplot of #4 Pull-Out Bond Stresses by Fourth Root Normalization	75
Figure 5.19: Average #6 Pull-Out Bond Stresses by Square Root Normalization	76
Figure 5.20: Boxplot of #6 Pull-Out Bond Stresses by Square Root Normalization	76
Figure 5.21: Average #6 Pull-Out Bond Stresses by Fourth Root Normalization	77
Figure 5.22: Boxplot of #6 Pull-Out Bond Stresses by Fourth Root Normalization	77
Figure 5.23: Comparison of #4 (No.13) and #6 (No. 19) Square Root Normalized Pull-out Results	78
Figure 5.24: Comparison of #4 (No.13) and #6 (No. 19) Fourth Root Normalized Pull-out Results	79
Figure 5.25: Average Beam Splice Peak Stresses by Square Root Normalization	82

Figure 5.26: Boxplot of Peak Stresses by Square Root Normalization	82
Figure 5.27: Average Beam Splice Peak Stresses by Fourth Root Normalization.....	83
Figure 5.28: Boxplot of Peak Stresses by Fourth Root Normalization.....	83
Figure 5.29: Comparison of Prediction Ratios for Beam Splice Results.....	87
Figure 5.30: Comparison of Beam Splice Results to Database	88
Figure A.1: Bond Stresses for #4 Pull-Out Specimens, Square Root Normalization.....	95
Figure A.2: Bond Stresses for #4 Pull-Out Specimens, Fourth Root Normalization	95
Figure A.3: Bond Stresses for #6 Pull-Out specimens, Square Root Normalization	96
Figure A.4: Bond Stresses for #6 Pull-Out Specimens, Fourth Root Normalization	96
Figure A.5: Applied Load vs. Slip Plot for #4 (No. 13) VAC-PO4	97
Figure A.6: Applied Load vs. Slip Plot for #6 (No. 19) VAC-PO6	97
Figure A.7: Applied Load vs. Slip Plot for #4 (No. 13) RCA50-PO4.....	98
Figure A.8: Applied Load vs. Slip Plot for #6 (No. 19) RCA50-PO6.....	98
Figure A.9: Applied Load vs. Slip Plot for #4 (No. 13) RCA100-PO4.....	99
Figure A.10: Applied Load vs. Slip Plot for #6 (No. 19) RCA100-PO6.....	99
Figure B.1: Applied Load vs. Strain for VAC Specimens.....	101
Figure B.2: Applied Load vs. Strain for RAC-50 Specimens.....	101
Figure B.3: Applied Load vs. Strain for RAC-100 Specimens.....	102
Figure B.4: Applied load vs. Midspan Deflection for VAC	102
Figure B.5: Applied load vs. Midspan Deflection for RAC-50	103
Figure B.6: Applied load vs. Midspan Deflection for RAC-100.....	103
Figure C.1: Side View of VAC-1	105
Figure C.2: Bottom View of VAC-1.....	105
Figure C.3: Side View of VAC-2	106
Figure C.4: Bottom View of VAC-2.....	106
Figure C.5: Side View of VAC-3	107
Figure C.6: Bottom View of VAC-3.....	107
Figure C.7: Side View of RAC50-1.....	108
Figure C.8: Bottom View of RAC50-1	108
Figure C.9: Side View of RAC50-2.....	109
Figure C.10: Bottom View of RAC50-2.....	109

Figure C.11: Side View of RAC50-3.....	110
Figure C.12: Bottom View of RAC50-3.....	110
Figure C.13: Side View of RAC100-1.....	111
Figure C.14: Bottom View of RAC100-1.....	111
Figure C.15: Side View of RAC100-2.....	112
Figure C.16: Bottom View of RAC100-2.....	112
Figure C.17: Side View of RAC100-3.....	113
Figure C.18: Bottom View of RAC100-3.....	113

LIST OF TABLES

Table	Page
Table 3.1: Fresh Concrete Properties of Pre-Recycled Concrete	24
Table 3.2: Compressive Strength Results of Pre-Recycled Concrete.....	25
Table 3.3: Splitting Tensile Strength Results of Pre-Recycled Concrete	25
Table 3.4: Modulus of Rupture Results of Pre-Recycled Concrete.....	26
Table 3.5: Modulus of Elasticity Results of Pre-Recycled Concrete.....	26
Table 3.6: Control Mix Design Specifications	27
Table 3.7: Control Design Mix Proportions, Oven-Dry Basis.....	27
Table 3.8: Control Splitting Tensile Strength Results	28
Table 3.9: RAC-50 Mix Design Specifications	29
Table 3.10: RAC-50 Design Mix Proportions, Oven-Dry Basis	30
Table 3.11: RAC-50 Splitting Tensile Strength Results.....	31
Table 3.12: RAC-100 Mix Design Specifications	32
Table 3.13: RAC-100 Design Mix Proportions, Oven-Dry Basis	32
Table 3.14: RAC-100 Splitting Tensile Strength Results.....	32
Table 3.15: Modulus of Rupture Results	34
Table 3.16: Modulus of Elasticity Results.....	35
Table 3.17: Splitting Tensile Strength Results	35
Table 3.18: Fracture Energy Results.....	36
Table 5.1: Testing Matrix for Direct Pull-Out Specimens.....	55
Table 5.2: Pull-Out Test Results.....	56
Table 5.3: Testing Matrix for Beam Splice Specimens	59
Table 5.4: Beam Splice Test Results	61
Table 5.5: #6 Reinforcing Bar Tension Test Results.....	67
Table 5.6: Beam Splice Test Day Compressive Strengths	70
Table 5.7: Normalized Bond Stresses for Pull-Out Specimens	73
Table 5.8: Normalized Developed Stresses for Beam Splice Specimens.....	81
Table 5.9: Comparison of Measured to Theoretical Stress in Beam Splice Specimens	85
Table 5.10: Prediction Ratios for Beam Splice Results.....	87

Table D.1: Parametric Analysis of #4 (No.13) Pull-Out Results with Square Root Normalization between VAC and RAC-50	115
Table D.2: Non-parametric Analysis of #4 (No.13) Pull-Out Results with Square Root Normalization between VAC and RAC-50	115
Table D.3: Parametric Analysis of #4 (No.13) Pull-Out Results with Square Root Normalization between VAC and RAC-100	116
Table D.4: Non-parametric Analysis of #4 (No.13) Pull-Out Results with Square Root Normalization between VAC and RAC-100	116
Table D.5: Parametric Analysis of #6 (No.19) Pull-Out Results with Square Root Normalization between VAC and RAC-50	117
Table D.6: Non-Parametric Analysis of #6 (No.19) Pull-Out Results with Square Root Normalization between VAC and RAC-50	117
Table D.7: Parametric Analysis of #6 (No.19) Pull-Out Results with Square Root Normalization between VAC and RAC-100	118
Table D.8: Non-Parametric Analysis of #6 (No.19) Pull-Out Results with Square Root Normalization between VAC and RAC-100	118
Table D.9: Parametric Analysis of #4 (No.13) Pull-Out Results with Fourth Root Normalization between VAC and RAC-50	119
Table D.10: Non-parametric Analysis of #4 (No.13) Pull-Out Results with Fourth Root Normalization between VAC and RAC-50	119
Table D.11: Parametric Analysis of #4 (No.13) Pull-Out Results with Fourth Root Normalization between VAC and RAC-100	120
Table D.12: Non-parametric Analysis of #4 (No.13) Pull-Out Results with Fourth Root Normalization between VAC and RAC-100	120
Table D.13: Parametric Analysis of #6 (No.19) Pull-Out Results with Fourth Root Normalization between VAC and RAC-50	121
Table D.14: Non-Parametric Analysis of #6 (No.19) Pull-Out Results with Fourth Root Normalization between VAC and RAC-50	121
Table D.15: Parametric Analysis of #6 (No.19) Pull-Out Results with Fourth Root Normalization between VAC and RAC-100	122
Table D.16: Non-Parametric Analysis of #6 (No.19) Pull-Out Results with Fourth Root Normalization between VAC and RAC-100	122
Table D.17: Parametric Analysis of Beam Splice Results with Square Root Normalization between VAC and RAC-50	123
Table D.18: Non-Parametric Analysis of Beam Splice Results with Square Root Normalization between VAC and RAC-50	123
Table D.19: Parametric Analysis of Beam Splice Results with Square Root Normalization between VAC and RAC-100	124

Table D.20: Non-Parametric Analysis of Beam Splice Results with Square Root Normalization between VAC and RAC-100	124
Table D.21: Parametric Analysis of Beam Splice Results with Fourth Root Normalization between VAC and RAC-50	125
Table D.22: Non-Parametric Analysis of Beam Splice Results with Fourth Root Normalization between VAC and RAC-50	125
Table D.23: Parametric Analysis of Beam Splice Results with Fourth Root Normalization between VAC and RAC-100	126
Table D.24: Non-Parametric Analysis of Beam Splice Results with Fourth Root Normalization between VAC and RAC-100	126

1. INTRODUCTION

1.1. BACKGROUND AND JUSTIFICATION

1.1.1. General. The construction of buildings, bridges, and roadways continues to increase in the twenty-first century, especially in areas with ever-growing populations. Existing structures and highways require repair or replacement as they reach the end of their service life or simply no longer satisfy their intended purpose due to the growing population. As modern construction continues, two pressing issues will become more apparent to societies: an increasing demand for construction materials, especially concrete and asphalt aggregates, and an increasing production of construction and demolition waste. Already, the Federal Highway Administration (FHWA) estimates that two billion tons of new aggregate are produced each year in the United States. This demand is anticipated to increase to two and a half billion tons each year by 2020. With such a high demand for new aggregates, the concern arises of the depletion of the current sources of natural aggregates and the availability of new sources. Similarly, the construction waste produced in the United States is expected to increase. From building demolition alone, the annual production of construction waste is estimated to be 123 million tons (FHWA). Currently, this waste is most commonly disposed of in landfills.

To address both the concern of increasing demand for new aggregates and increasing production of waste, many states have begun to recognize that a more sustainable solution exists in recycling waste concrete for use as aggregate in new concrete, or recycled concrete aggregates (RCA). The solution helps address the question of how to sustain modern construction demands for aggregates as well as helps to reduce the amount of waste that enters already over-burdened landfills.

Based on a survey by FHWA in 2002, many states had begun to implement recycled concrete aggregates in some ways in new construction. As shown in **Figure 1.1**, most states had recognized the many uses of RCA as a raw material, such as for rip-rap, soil stabilization, pipe bedding, and even landscape materials. As shown in **Figure 1.2**, many states had gone a step further in integrating RCA into roadway systems for use as aggregate base course material. However, as shown in **Figure 1.3**, only a small number of states had begun using RCA in Portland cement concrete for pavement construction. However, over the intervening 12 years, the use of RCA has increased significantly, particularly within the last 5 years, and the Missouri Department of Transportation (MoDOT) has instituted a very aggressive program to increase the use of recycled materials in transportation-related construction. However, there are currently no acceptable standards or guidelines in the U.S. for utilizing RCA in structural concrete.

1.1.2. Benefits of Recycled Aggregate Concrete. The use of recycled aggregate concrete (RAC) offers a sustainable solution for the continued growth of modern infrastructure. Primarily, RAC concrete diverts construction and demolition waste from the solid waste stream while easing the demand from non-renewable natural aggregate sources. Much research has been performed that shows up to 100% of the coarse aggregates in new concrete can be replaced with RCA.

1.1.3. Concerns with Recycled Aggregate Concrete. RCAs are composed of both the original, or virgin, aggregate, as well as mortar which remains adhered to the surface of the aggregate. In the production of RCA, the removal of all this residual mortar would prove costly and detrimental to the integrity of the virgin aggregates within the concrete. Therefore, residual mortar is inevitable. Research has shown that this residual

mortar causes high water absorption, low density, low specific gravity, and high porosity in RCAs compared to natural aggregates (Kou et al. 2012). These effects in the recycled aggregate can decrease hardened concrete properties of RAC. According to Abbas et al. (2008), the amount of residual mortar on the RCA can significantly affect the mechanical and durability properties of RAC. To reduce the negative impacts of this residual mortar, new mix design methods such as the equivalent mortar volume method can be used.

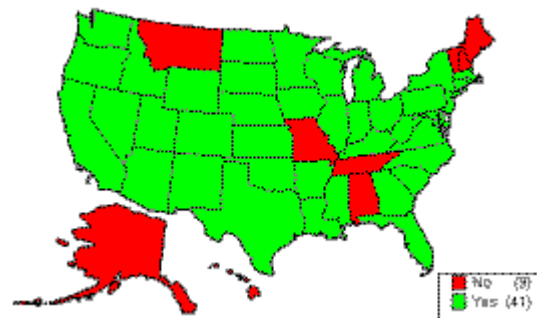


Figure 1.1: States using RCA as Aggregate

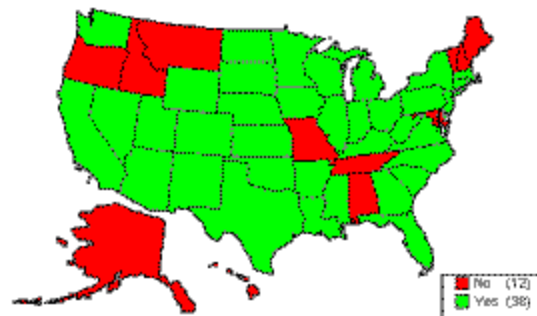


Figure 1.2: States using RCA as Base Aggregate

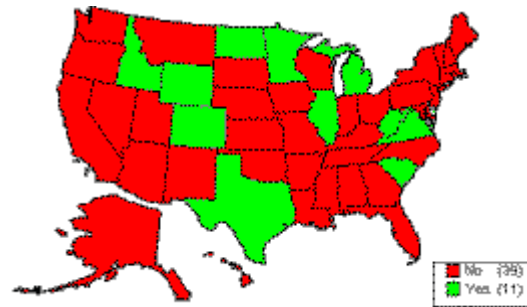


Figure 1.3: States using RCA in PC Concrete

Due to the variety of sources of RCA and the various functions, environment, and wear of the concrete structures and pavements from which the RCA can be obtained, characterizing this aggregate can be very difficult. Controlled studies must be performed to account for each of these variables on a regional basis, such as for each state's Department of Transportation, so that the aggregates within the area can be adequately characterized.

1.2. OBJECTIVES AND SCOPE OF WORK

The main objective of this study was to determine the effect of replacing coarse virgin aggregates with RCA on concrete bond strength with deformed reinforcing steel bars. This experimental study consisted of comparing the bond performance of two RCA mixes designed at different replacement levels to a Missouri Department of Transportation (MoDOT) standard mix design at the same strength level. Additionally, the effect of bar size on the bond strength of RCA concrete compared with virgin aggregate concrete was also evaluated.

The following scope of work was implemented in an effort to reach these objectives: (1) review of the applicable literature; (2) develop a research plan; (3) design

and construct test fixtures; (4) design and construct test specimens; (5) test specimens to failure and record applicable data; (6) analyze results and conduct comparisons between RAC and control mix designs; (7) develop conclusions and recommendations; (8) prepare this report in order to document the information obtained during this study.

1.3 RESEARCH PLAN

For this experimental program, the bond performance of RCA concrete designed at different replacement levels will be investigated and compared with a standard MoDOT mix design. The RCA mix design procedure to be investigated is the direct replacement method. This design method is a volumetric procedure that replaces a percentage of the virgin coarse aggregate directly with the RCA. For this bond study, the three replacement levels that will be considered are 0%, 50%, and 100%. The 0% replacement mix will serve as the control and will contain only virgin aggregates. For the 50% RCA mix, half of the total volume of coarse virgin aggregates will be substituted with RCA. For the 100% mix, the total volume of coarse virgin aggregates will consist of RCA. For all RCA mixes, the virgin aggregates used to make the RCA will be MoDOT approved 1" Potosi Dolomite. To control the amount of variables in this study, the RCA will be produced from beams that are cast and cured by the researchers in a controlled laboratory environment. The crushing procedure and pre-crushed and post-crushed environmental conditions of the aggregates will be constant.

To investigate the bond performance, two bond test types will be performed: direct pull out tests and large scale beam splice tests. Direct pull out tests will be performed based on the RILEM 7-II-128 *RC6: Bond test for reinforcing steel. 1. Pull-out*

test (RILEM, 1994). While direct pull out tests do not provide a realistic flexural type stress-state response in the specimen, they provide a basis of comparison among other direct pull out results and are commonly used for bond performance comparison. A total of 18 direct pull-out specimens were constructed and tested to bond failure using this test method. The full scale beam splice test will be based on a non-standardized procedure that has been developed in previous bond research. The beam splice test provides the most realistic response for bond performance in flexural stress state. A total of 9 full-scale beam splice specimens were constructed and tested to bond failure.

1.4 OUTLINE

This report consists of six chapters and four appendices. Chapter 1 contains a brief explanation of the current uses, benefits, and concerns of RAC as well as the objective and scope of work of this study.

Chapter 2 provides a discussion of the bond force transfer between concrete and embedded deformed steel bars, bond failure mechanisms, accepted tests for characterizing bond strength, and a review of the literature for RAC bond research.

Chapter 3 details the mix designs that were developed for this study as well as the test methods used to determine fresh and hardened concrete properties that were found at the time of testing the bond specimens.

Chapter 4 details the design, fabrication, test setup, and test procedure for the direct pull-out and full-scale beam splice specimens.

Chapter 5 provides the recorded test data, the methodology used to normalize the data, normalized results, and a comparison among RCA replacement levels and across bar size.

Chapter 6 summarizes the findings, conclusions, and recommendations from this study.

2. LITERATURE REVIEW

2.1. BOND CHARACTERISTICS

In reinforced concrete, the transfer of forces between deformed steel bars and the adjacent concrete occurs by three primary modes: 1) chemical adhesion between the bar and concrete, 2) friction forces, transverse forces, and relative slip, and 3) bearing of the ribs or deformations against the surrounding concrete. For deformed bars, adhesion is lost after the initial slip. This slip initiates bearing of the ribs against the surrounding concrete surface. Frictional forces along the surface of the bar remain small compared to these bearing forces, and bearing plays the biggest role in bond behavior. To balance the forces on the surface of the deformed bar, which are shown in **Figure 2.1**, compressive and shear stresses develop in the contacting concrete surfaces. These stresses develop into tensile stresses which in turn can lead to cracking of the concrete (ACI 408, 2003).

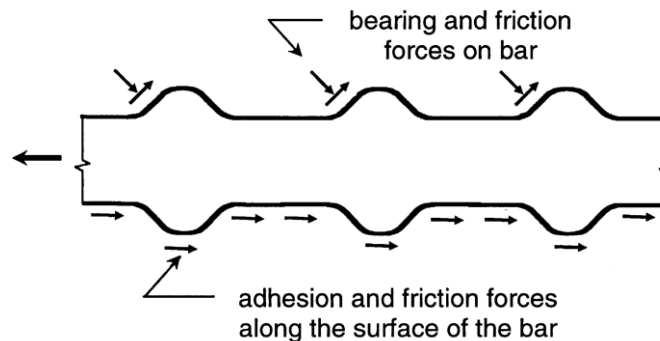


Figure 2.1: Bond Force Transfer Mechanisms (ACI 408, 2003)

Goto cracks can form as a result of the tension stresses induced by the compression forces at the bearing contact surfaces extending from the ribs. The formation of these cracks is shown in **Figure 2.2**. These cracks can result in a conical failure surface

for bars in tension that extend outside of the concrete. However, Goto cracks do not play a significant role in bond anchorage or reinforcement development (ACI 408, 2003).

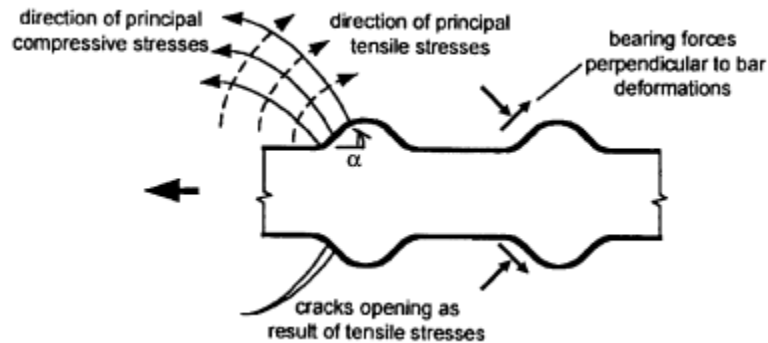


Figure 2.2: Formation of Goto Cracks (ACI 408, 2003)

Transverse cracks, form when the minimum concrete cover or bar spacing is small. The transverse cracks form as a result of hoop tensile stresses in the surrounding concrete induced by the bearing action of the ribs. With small cover, these cracks can reach the outside surface of the concrete and form splitting cracks as shown in **Figure 2.3**.

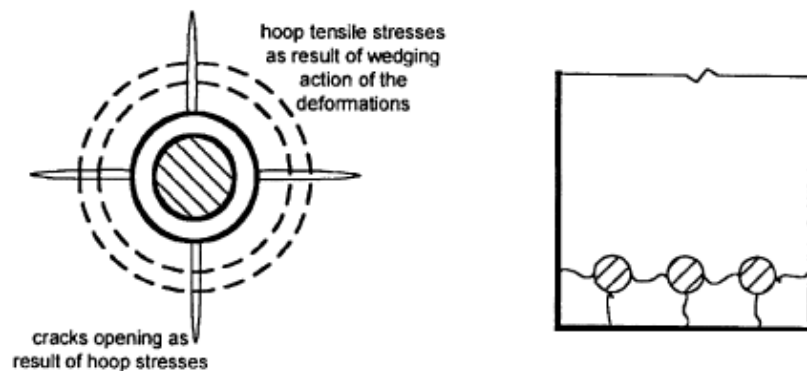


Figure 2.3: Formation of Hoop Stresses and Resulting Splitting Cracks (ACI 408, 2003)

When concrete cover and bar spacing is sufficiently large or enough transverse reinforcement is provided to prevent splitting failure, the bond failure may be a pull out type. This failure results in the shearing along the top surfaces of the reinforcing bar's ribs as shown in **Figure 2.4**. Most bond failures result as a combination of both concrete splitting and pull out type failure modes (ACI 408, 2003). It is also possible that if anchorage of the bar into the concrete is adequate or sufficient confinement is provided to delay crack propagation, the steel bar may yield or strain harden prior to bond failure. Thus, bond failure only occurs when stresses in the steel do not exceed its tensile strength.

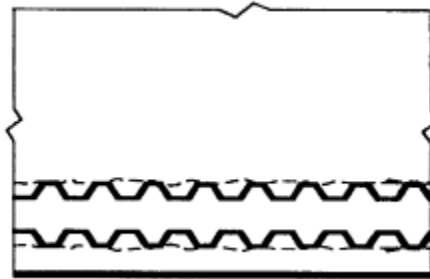


Figure 2.4: Pull-Out Failure (ACI 408, 2003)

Based on the above discussion, it is obvious that bond behavior is largely controlled by the following factors: mechanical properties of the surrounding concrete, concrete cover and bar spacing, presence or absence of confinement, surface condition of the bar, and the geometry of the bar (namely deformation shape, rib height, and bar diameter).

2.2. COMMON BOND TESTS

Many testing methods have been developed to measure bond strength between concrete and reinforcing steel bars. The configuration of each test method has an important role in the bond response. Four of the most common test configurations are pull out specimens, beam-end specimens, beam anchorage specimens, and splice specimens (full beams). The direct pull-out test method is the most commonly used due to the ease of fabricating and testing of these specimens. However, this method produces the least realistic bond response of the four listed. As the bar of a pull-out specimen is loaded in tension, the surrounding concrete is in compression. In most practical applications of reinforced concrete, both the bar and the surrounding concrete experience tension. A concern with pull-out specimens is this additional confinement from the induced compression at the anchorage zone. Due to the unrealistic nature of the stress state produced, pull-out specimens are not recommended as the only means of determining bond strength, but can serve as a useful comparison (ACI 408, 2003). A schematic of the pull-out test is shown in **Figure 2.5**.

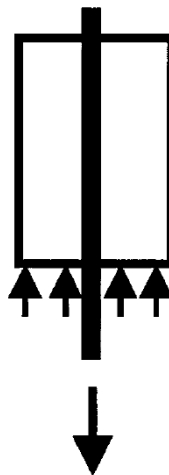


Figure 2.5: Schematic Direct Pull-Out Test (ACI 408, 2003)

The beam-end specimen, also known as the modified cantilever, more accurately represents reinforced concrete behavior. In this method, the bar and the surrounding concrete experience tension. This is achieved by loading the bar in tension and applying a compressive force a distance approximately equal to the embedded length of the bar away from the end of the bar. These specimens are relatively easy to fabricate and test, and offer bond strength measurements more accurate to full-scale tests. A schematic of the beam-end test is shown in **Figure 2.6**.

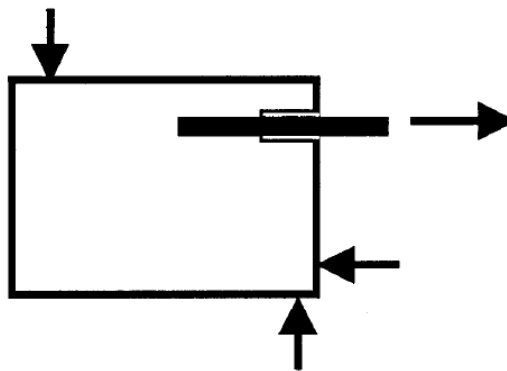


Figure 2.6: Schematic Beam-End Test (ACI 408, 2003)

Beam anchorage specimens are full-scale specimens with a configuration designed to simulate flexural cracks with a known bonded length. While these specimens provide a realistic bond response, they can be challenging to fabricate (ACI 408, 2003). A schematic of the anchorage test is shown in **Figure 2.7**.

Splice specimens are an alternative full-scale bond test. These splice beams are tested under four-point loading such that the splice is located in a constant moment region, similarly to the modulus of rupture test. Splice specimens are much easier to fabricate and will produce similar results as the anchorage specimens. Due to the simplicity of fabricating these specimens and the realistic bond response, splice

specimens have provided the bulk of data used in developing current empirical design equations (ACI 408, 2003). A schematic of the beam splice test is shown in **Figure 2.8**.

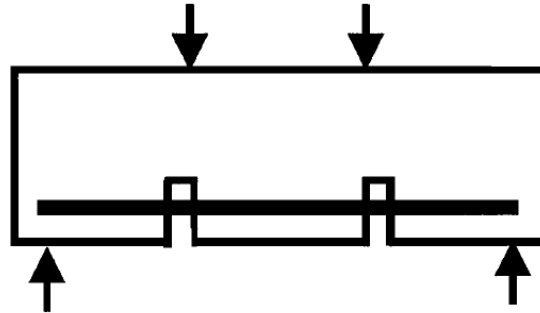


Figure 2.7: Schematic Beam Anchorage Test (ACI 408, 2003)

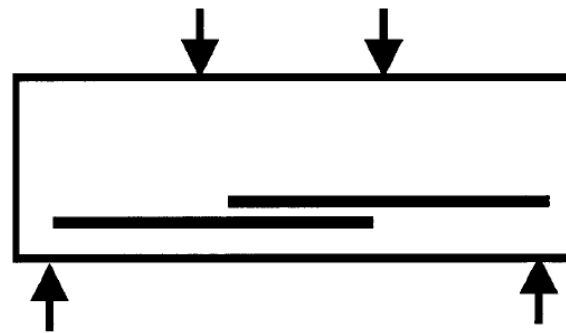


Figure 2.8: Schematic Beam Splice Test (ACI 408, 2003)

2.3. RCA CONCRETE BOND RESEARCH

Much of the existing literature on recycled concrete aggregates (RCA) focuses on the mechanical and durability characteristics of concretes made with RCA. Few studies have been conducted to evaluate the structural performance of RCA concrete, and of those even fewer have concentrated on the bond characteristics of RCA concrete. In a study by Ajdukiewicz and Kliszczewicz (2002), pull-out specimens designed per RILEM recommendations were used to evaluate bond performance of 0% and 100% RCA

replacement. The mix designs used in this study were developed by conventional direct replacement of natural aggregates with RCA. They found that there is no significant difference between bond strength of deformed bars embedded in concrete with coarse RCA replacement and concrete containing only natural coarse aggregates. In this study, the greatest difference in bond strength was observed when smooth bars were used. There was a 20% decrease in bond strength when both coarse and fine aggregates were replaced with RCA, and an 8% decrease when natural sand and coarse RCA was used. (Ajdukiewicz and Kliszczewicz 2002) Typically, though, RCA fines are not recommended for use in new concretes.

Studies have shown that replacing natural sand with fine RCA will drastically increase the water demand and reduce the mix workability. Likewise, the drying shrinkage increases significantly from concrete made with coarse RCA only (20% to 50% more) to concretes made with both fine and coarse RCA (70% to 100% more). Further studies have shown that the mechanical properties are more negatively impacted with the addition of RCA fines. The decrease in compressive strength, tensile strength, and modulus of elasticity are much more pronounced when both fine and coarse RCA are present than when only coarse RCA is present (ACI 555R 2001).

Xiao and Falkner (2005) investigated the bond performance of concretes with 0%, 50%, and 100% replacement of coarse natural aggregates only with RCA using 36 direct pull-out specimens. The conclusions from this study were similar to those by Ajdukiewicz and Kliszczewicz (2002), namely that no difference was observed between the bond strength of deformed bars at 0% RCA replacement and 50% or 100% RCA

replacement. When smooth bars were used, a maximum decrease in bond strength of 12% was observed in the RCA concrete (Xiao and Falkner 2005).

Generally, the mix design method used with RCA concrete has a significant impact on bond strength to mild steel reinforcing bars. Currently, there is no standard procedure for mix design using RCA. The conventional method used in much of the current literature is a direct replacement of coarse aggregate with RCA. However, research has shown that the mortar attached to RCA negatively influences the mechanical and durability properties of RCA concrete (Shayan, 2003). To compensate for this residual mortar on RCA particles, Abbas (2008) has proposed a mix design procedure coined the “Equivalent Mortar Volume” (EMV) method. The key aspect of the EMV method is that the residual mortar of RCA is included in the total mortar volume of the mix, and the amount of new mortar and total amount of coarse aggregate are adjusted to account for this difference (Abbas, 2008).

Existing research has shown that bond strength of RCA designed by the conventional method is lower than bond strength of RCA designed by the EMV method. In 2008, Fathifazl utilized beam-end test specimens to evaluate bond performance under a more realistic stress state response with both conventional and EMV mix designs. Using beam-end specimens with a Canadian standard No. 30 ($d_b = 1.18$ in. or 29.9 mm) deformed reinforcing bars, Fathifazl found that the bond strength (normalized by the square root of compressive strength) of concrete specimens designed using conventional methods of coarse aggregate replacement were 24% lower than their companion natural aggregate specimens. The study showed that bond strength of specimens designed using

the EMV method were only 6% lower than their companion natural aggregate specimens. (Fathifazl, 2008)

In order to investigate the effect of bar size, Fathifazl compared the bond strengths of beam-end specimens containing either a Canadian standard No. 15 ($d_b = 0.63$ in. or 16.0 mm) or No. 30 ($d_b = 1.18$ in. or 29.9 mm) deformed bar. RCA made from two different sources and with different original virgin aggregate material was used. He found that, regardless of the original virgin aggregate material in the RCA and mix design method, the specimens containing No. 15 bars had higher bond strengths than those containing No. 30 bars. These findings are in consensus with ACI 408 that length to develop a reinforcing bar increases as bar diameter increases. This relationship is reflected in the development length equation presented in ACI 318. Furthermore, he found that when designed by the conventional method of direct replacement of natural aggregates for RCA, specimens containing No. 15 bars had 35% higher bond strengths than the specimens containing No. 30 bars. However, when designed by the EMV method, specimens containing No. 15 bars had bond strengths of at least 41% higher than those containing No. 30 bars (Fathifazl 2008).

In 2011, Butler, West, and Tighe evaluated bond performance using 100% direct replacement of coarse aggregates with RCA using 24 beam-end test specimens. This study showed that natural aggregate beam-end specimens had bond strengths 9% to 21% higher than RCA beam-end specimens. Furthermore, they investigated a correlation between the RCA aggregate crushing value (ACV) and bond strength of concretes made with RCA. Using natural aggregates and two different sources of RCA, they found that as ACV increases, the bond strength decreases. For both RCA sources, the ACV of the RCA

was 26% to 43% higher than natural aggregates. Previous research had shown that as the ACV increases, fracture energy of the resulting concrete decreases, and since bond is also related to fracture energy, the researchers reasoned that the ACV would offer a method to predict bond strength when using RCA. Additionally, they observed a strong relationship between ACV and splitting tensile strength, namely that as ACV increases, splitting tensile strength decreases (Butler et al. 2011).

Bond failures where splitting cracks control the peak load is governed by the tensile response of the concrete. The tensile response depends on the splitting tensile capacity and fracture energy, or capacity of the concrete to dissipate energy as a crack opens. As described in ACI 408R (2003), concrete with higher fracture energies provide improved bond capacities even if the concrete has similar tensile strengths.

3. MIX DESIGNS AND CONCRETE PROPERTIES

3.1. INTRODUCTION

The following section contains the procedures used to determine the fresh properties as well as the hardened mechanical properties of the concrete used in this study. A discussion of the mix designs used and their respective properties is also reported in this section.

3.2. CONCRETE PROPERTIES

3.2.1. Fresh Concrete Properties. For all three mixes used in this study the fresh concrete properties that were found were slump, unit weight, and air content. The slump test was performed in accordance with ASTM C 143 (2010) *Standard Test Methods for Slump of Hydraulic Cement Concrete*. The inside of a standard slump cone was wetted and placed on a damp surface. Concrete was added to the cone in three equal lifts and rodded 25 times each lift with the appropriately dimensioned steel rod. Excess concrete was struck off at the top of the cone using the rod, and any superfluous concrete was removed from around the base of the mold. The mold was lifted at a constant rate over five seconds, and the cone was inverted next to the slumped concrete. The slump measurement was taken from the rod placed over the top of the inverted cone to the center of the slumped concrete.

The unit weight of the concrete was determined in accordance with ASTM C 138 (2010) *Standard Test Method for Density (Unit Weight), Yield, and Air Content (Gravimetric) of Concrete*. A steel measure of known volume was weighed then filled with concrete in three equal lifts. Each lift was rodded 25 times and tapped with a rubber

mallet to help consolidate the concrete. Once filled, a steel plate was placed flat on the top of the measure, covering approximately $\frac{3}{4}$ of the open area. The plate was pulled back across the covered area to screed off excess concrete. The plate was then placed flat in the same position and pushed forward to screed the rest of the open area of the measure. Next, the steel plate was tilted at an angle and used to screed the top surface of the measure until it was level and smooth. A wet sponge was used to wipe away excess concrete from the outside of the measure and along the top rim. The measure was then weighed, and the unit weight was determined.

The air content of the fresh concrete was determined in accordance with ASTM C 231 (2010) *Standard Test Method for Air Content of Freshly Mixed Concrete by the Pressure Method* using a type B pressure meter. After the unit weight was determined the same measure filled with concrete was used to determine air content. The pressure meter lid was wetted and secured over the top of the measure. The air chamber positioned on top of this lid was sealed off, and the appropriate initial pressure was added to the chamber. Next, water was gently injected into one petcock until it flowed without air bubbles from the opposite petcock ensuring the space between the lid and the surface of the concrete was filled with water. The stream of water was inspected for the presence of mortar, which would invalidate the test. The petcocks were then closed, and the air from the chamber was injected into the concrete-filled bottom measure while simultaneously tapping the measure with a rubber mallet. The air content was then recorded from the gauge on the pressure meter.

3.2.2. Compressive Strength of Concrete. The compressive strength, f'_c , of the concrete was determined as per ASTM C39 (2011) *Standard Test Method for*

Compressive Strength of Cylindrical Concrete Specimens. For each set of direct pull-out and beam splice specimens, accompanying cylinders were made to determine the compressive strength. The cylindrical molds used had a diameter of 4 in. (10.2 cm) and height of 8 in. (20.3 cm). These cylinders were left to cure in the same condition next to the bond test specimens. The compressive strength of the concrete was tested at 1, 3, 7, 14, 28, and 60 days as well as on the days of testing the bond specimens. Prior to testing, the cylinders were capped with a sulfur compound to give a uniform stress distribution during testing. The load rate was 565lb/sec (2.5kN/sec) as per the ASTM C39 standard. **Figure 3.1** shows a capped cylinder in the loading machine. Three specimens were tested with the average representing one strength data point. The compressive strength of each mix design was determined from companion cylinders to the bond test specimens on the day of testing.



Figure 3.1: Compressive Strength Test

3.2.3. Modulus of Rupture of Concrete. The modulus of rupture, f_r , was determined according to ASTM C 78 (2010) *Standard Test Method for Flexural Strength of Concrete*. Small beams with dimensions 6 in. x 6 in. x 24 in. (15 cm x 15 cm x 60 cm) were cast to find the modulus of rupture. To test these beams, simple third point loading was used with a span length of 18 in. (45 cm). Upon reaching the peak load of the test, the modulus of rupture was calculated by the following equation:

$$f_r = \frac{PL}{bd^2} \quad (3.1)$$

where P is the peak load, L is the beam length, and b and d are the beam width and depth, respectively, measured at the fractured surface of the beam after failure. Three specimens were tested with the average representing one strength data point.

3.2.4. Modulus of Elasticity of Concrete. The modulus of elasticity, E_c , of the concrete was determined according to ASTM C 469 (2010) *Standard Test Method for Static Modulus of Elasticity and Poisson's Ratio of Concrete in Compression*. Cylinders with a 6 in. (15.2 cm) diameter and 12 in. (30.5 cm) height were used to determine the modulus of elasticity. The modulus of elasticity for each mix design was determined from companion cylinders to the bond test specimens on the day of testing.

3.2.5. Splitting Tensile Strength of Concrete. The splitting tensile strength, f_{tsp} , of the concrete was determined according to ASTM C496 (2011) *Standard Test Method for Splitting Tensile Strength of Cylindrical Concrete Specimens*. The splitting tensile strength was found on the day of bond specimen testing for each mix design. To find this strength, 6 in. x 12 in. (15.2 cm x 30.5 cm) cylinders were used. Upon reaching the peak load of this test, the splitting tensile strength was found by the following equation:

$$f_{tsp} = \frac{2P}{\pi LD} \quad (3.2)$$

where P is the peak load, L is the cylinder length, and D is the cylinder diameter. **Figure 3.2** shows the failure mode from the splitting tensile test. Three specimens were tested with the average representing one strength data point. The splitting tensile strength of each mix design was determined from companion cylinders to the bond test specimens on the day of testing.

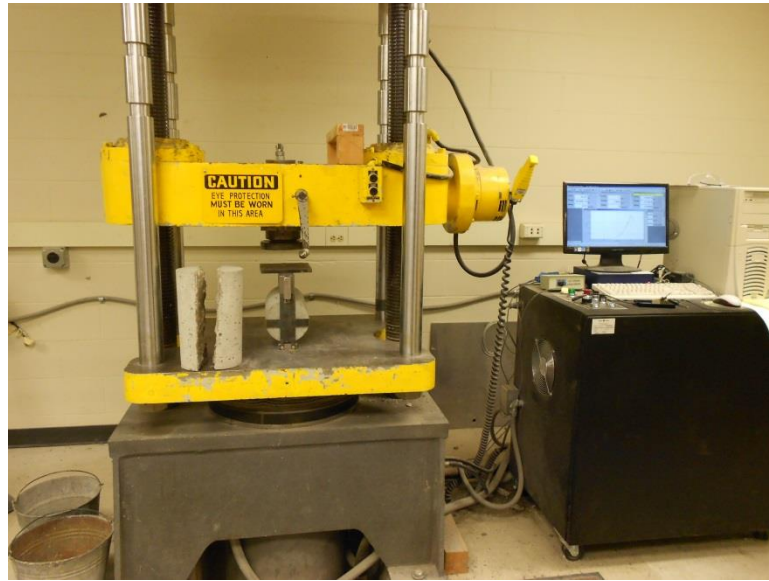


Figure 3.2: Splitting Tensile Failure Mode

3.2.6. Fracture Energy of Concrete. The fracture energy, G_f , was determined according to RILEM TC 50-FMC *Determination of the Fracture Energy of Mortar and Concrete by Means of Three-Point Bend Tests on Notched Beams*. Notched beams with dimensions 6 in. x 6 in. x 24 in. (15 cm x 15 cm x 60 cm) were cast in small batches for each mix design. Under three-point loading, the span was 18 in. (45 cm). The notch was cast into the concrete at midspan with a depth of 1.5 in. (4 cm) and width of 0.25 in. (0.6 cm). A gauge was applied at the notch to measure the crack mouth opening displacement, and displacement was measured at midspan by linear variable differential transformers

(LVDTs). The fracture energy was calculated by dividing the total energy dissipated by the projected surface area of the crack as in the following equation:

$$G_f = \frac{W}{bd-a_o} \quad (3.3)$$

where W is the total energy dissipated, b and d are the beam width and depth respectively, and a_o is the depth of the notch. Three specimens were tested with the average representing one fracture energy data point.

3.3. RAC MIX DESIGNS

For this study, three mix designs were produced and evaluated for bond performance. A MoDOT Class B air-entrained mix design was used as a baseline for reference throughout the study. The specified cement content in this mix was 535 lb., the water-to-cement ratio was 0.40, the target slump was 6 in., and the design air content was 6%. The specified amount of fine aggregate as a volume of total aggregates was 40%. For this mix, the typical dosage range of the MoDOT-approved air entrainment MB-AE 90 was 0.25-4.0 fl.oz./100 lb. of cement (0.16-2.61 mL/kg of cement). The typical dosage of the Type A water reducer Glenium 7500 is 5.0 - 8.0 fl.oz./100 lb of cement (0.33-5.22 mL/kg of cement). Two RAC mixes were produced as modified Class B mix designs. The direct replacement method of RCA for coarse aggregate was used to design the RAC mixes. Two RCA replacement levels were considered: 50% and 100% volumetric replacement.

3.3.1. Pre-Recycled Concrete Mix Design. In order to control the number of variables in this experimental study, the recycled aggregates were produced by the researchers in a controlled laboratory environment. Unreinforced concrete beams were

cast in five separate pours, and fresh and hardened concrete properties were determined from companion small-scale specimens from each pour. An equal volume of concrete was produced in each pour. The mix design used for the RCA production was the same Class B mix design used for the control in this study. MoDOT's specifications for this mix and the oven-dry design batch weights are provided in Section 3.3.2.

To better understand the aggregate properties of the RCA, the concrete properties including air content, unit weight, compressive strength, splitting tensile strength, modulus of rupture, and modulus of elasticity were determined for each pour where the RCA parent beams were cast. The fresh concrete properties are shown below in **Table 3.1**. The hardened concrete properties are shown in **Tables 3.2** through **3.5**. For these hardened properties, an overall average value is presented. This value was assumed to be the average value for all of the concrete used to create the RCA since each pour contributed an equal volume to the total concrete crushed.

Table 3.1: Fresh Concrete Properties of Pre-Recycled Concrete

Pour	Slump (in.)	Air (%)
1	8	5.5
2	7	5.75
3	6	6.5
4	8	7
5	6	5.5

Conversion: 1 in. = 2.54 cm

Table 3.2: Compressive Strength Results of Pre-Recycled Concrete

Pour	Specimen	Compressive Strength, psi	Average Compressive Strength, psi	Overall Average Compressive Strength, psi
1	1	6571	6415	5385
	2	6501		
	3	6173		
2	1	4045	4267	
	2	4363		
	3	4392		
3	1	5472	5353	
	2	5311		
	3	5277		
4	1	4780	5293	
	2	5553		
	3	5547		
5	1	5690	5598	
	2	5619		
	3	5484		

Conversion: 1 psi = 6.9 kPa

Table 3.3: Splitting Tensile Strength Results of Pre-Recycled Concrete

Pour	Specimen	Tensile Strength (psi)	Average Tensile Strength (psi)	Overall Average Tensile Strength (psi)
1	1	564	587	522
	2	611		
2	1	554	516	
	2	478		
3	1	555	525	
	2	494		
4	1	520	513	
	2	507		
5	1	592	467	
	2	342		

Conversion: 1 psi = 6.9 kPa

Table 3.4: Modulus of Rupture Results of Pre-Recycled Concrete

Pour	Specimen	MOR (psi)	Average MOR (psi)	Overall Average MOR (psi)
1	1	716	745	570
	2	775		
2	1	572	505	
	2	438		
3	1	538	565	
	2	593		
4	1	532	501	
	2	471		
5	1	582	535	
	2	488		

Conversion: 1 psi = 6.9 kPa

Table 3.5: Modulus of Elasticity Results of Pre-Recycled Concrete

Pour	MOE (psi)	Overall Average MOE (psi)
1	6,000,000	5,520,000
2	5,100,000	
3	5,700,000	
4	5,150,000	
5	5,650,000	

Conversion: 1 psi = 6.9 kPa

3.3.2. VAC Control Mix Design and Concrete Properties. A MoDOT Class B air-entrained mix was used for the control mix in this study. The target strength was 4000 psi (27.58 MPa). The MoDOT mix specifications are summarized in **Table 3.6**, and the oven-dry design batch weights are shown in **Table 3.7**. The fresh properties of the concrete were determined after the addition of the chemical admixtures on the day of casting the bond test specimens. The slump was 8 in. (20.3 cm), the air content was 13%, and the unit weight was 144.4 lb/yd³ (2313 kg/m³). However, the 13% air content value was believed to be incorrect due to a faulty air meter as the mix design and remaining

fresh properties were identical to the Class B mix design used as the parent material for the RAC. As a result, an air content of 6% was assumed for the control concrete.

The compressive strength, splitting tensile strength, and modulus of elasticity of the mix were determined from companion cylinders that were cast from the same concrete batch as the bond test specimens. **Figure 3.3** shows the compressive strength gain over time. At 90 days, the compressive strength was found to be 4650 psi (32.06 MPa), just over the target strength. On the day of testing, the compressive strength was 4000 psi (27.58 MPa). The splitting tensile strength on the day of testing the bond specimens was 397 psi (2.74 MPa). The results are shown in **Table 3.8**. Likewise, the modulus of elasticity of the concrete found on the day of testing the bond specimens was 4,300,000 psi (29.65 GPa).

Table 3.6: Control Mix Design Specifications

Cementitious Amount, lb/yd ³	535
w/c Ratio	0.4
Amount of Fine Aggregate (by volume), %	40
Design Air Content, %	6.0
Target Slump, in.	6.0

Conversion: 1 lb./yd³ = 0.59 kg/m³
1 in. = 2.54 cm

Table 3.7: Control Design Mix Proportions, Oven-Dry Basis

Cement	535 lb/yd ³
Water	214.0 lb/yd ³
Coarse Aggregate	1958.2 lb/yd ³
Fine Aggregate	1252.7 lb/yd ³
Air Entrainment MB-AE 90	1 fl.ozs/cwt
Water Reducer Glenium 7500	6 fl.ozs/cwt

Conversion: 1 lb./yd³ = 0.59 kg/m³
1 oz. = 29.6 ml

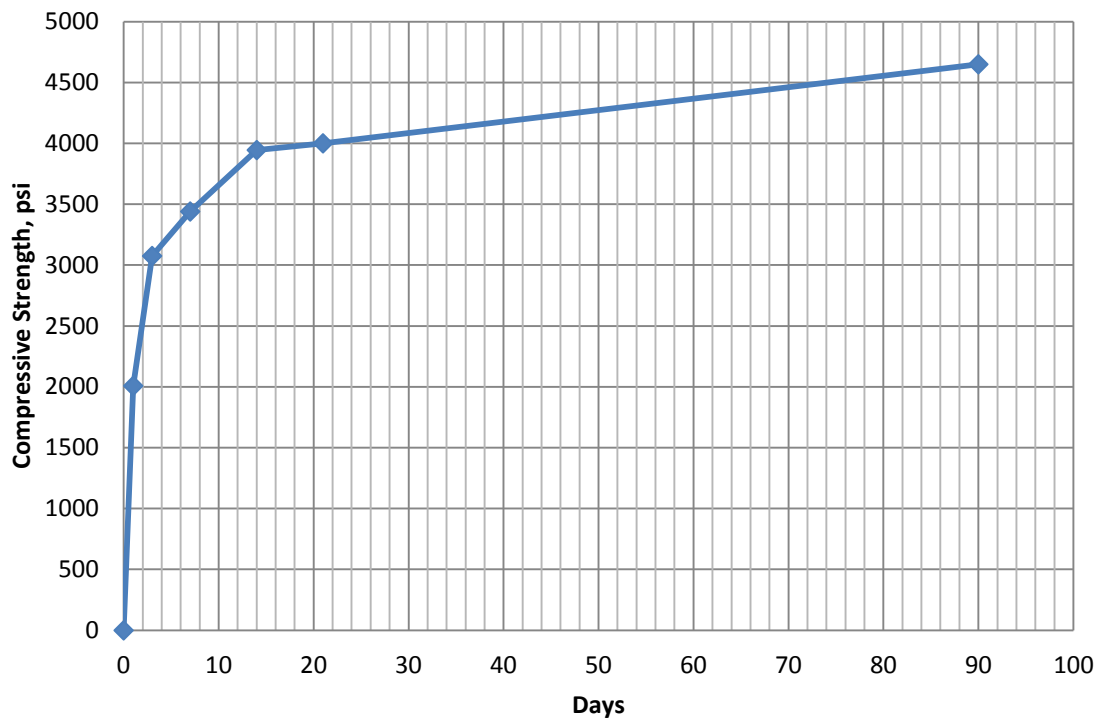


Figure 3.3: Control Mix Strength Gain with Time
Conversion: 1 psi = 6.9 kPa

Table 3.8: Control Splitting Tensile Strength Results

Specimen	Splitting Tensile Strength (psi)	Average Splitting Tensile Strength (psi)
Control-1	369	397
Control-2	423	
Control-3	397	

Conversion: 1 psi = 6.9 kPa

3.3.3. RAC-50% Mix Design and Concrete Properties. The first mix incorporating RCA was a 50% direct replacement design, subsequently referred to as RAC-50. Half of the total volume of coarse aggregate in the control MoDOT Class B mix was directly substituted with the laboratory-produced RCA. In order to maintain consistency with the control specimens, the MoDOT Class B mix specifications were

used to design the 50% direct replacement mix. The achieved 28-day strength of this mix during trial batching was 5500 psi (37.92 MPa), so this was used for the design of bond test specimens.

The mix specifications are summarized in **Table 3.9**, and the oven-dry design batch weights are shown in **Table 3.10**. The fresh properties of the concrete were determined after the addition of the chemical admixtures on the day of casting the bond test specimens. The slump was 6.5 in. (16.5 cm), the air content was 8%, and the unit weight was 139.8 lb/yd³ (2239 kg/m³).

The compressive strength, splitting tensile strength, and modulus of elasticity of the mix were determined from companion cylinders that were cast from the same concrete batch as the bond test specimens. **Figure 3.4** shows the compressive strength gain over time. At 60 days, the compressive strength was 3800 psi (26.20 MPa). On the day of testing, the compressive strength was 3560 psi (24.54 MPa). The splitting tensile strength on the day of testing the bond specimens was 344 psi (2.37 MPa). The results are shown in **Table 3.11**. Likewise, the modulus of elasticity of the concrete on the day of testing the bond specimens was 3,750,000 psi (25.86 GPa).

Table 3.9: RAC-50 Mix Design Specifications

Cementitious Amount, lb/yd ³	535
w/c Ratio	0.4
Amount of Fine Aggregate (by volume), %	40
Design Air Content, %	6.0
Target Slump, in.	6.0

Conversion: 1 lb./yd³ = 0.59 kg/m³

1 in. = 2.54 cm

Table 3.10: RAC-50 Design Mix Proportions, Oven-Dry Basis

Cement	535 lb/yd ³
Water	214.0 lb/yd ³
Coarse Natural Aggregate	979.1 lb/yd ³
Coarse Recycled Aggregate	845.9 lb/yd ³
Fine Aggregate	1252.7 lb/yd ³
Air Entrainer MB-AE 90	1 fl.ozs/cwt
Water Reducer Glenium 7500	4 fl.ozs/cwt

Conversion: 1 lb./yd³ = 0.59 kg/m³
1 oz. = 29.6 ml
1 lb. = 0.45 kg

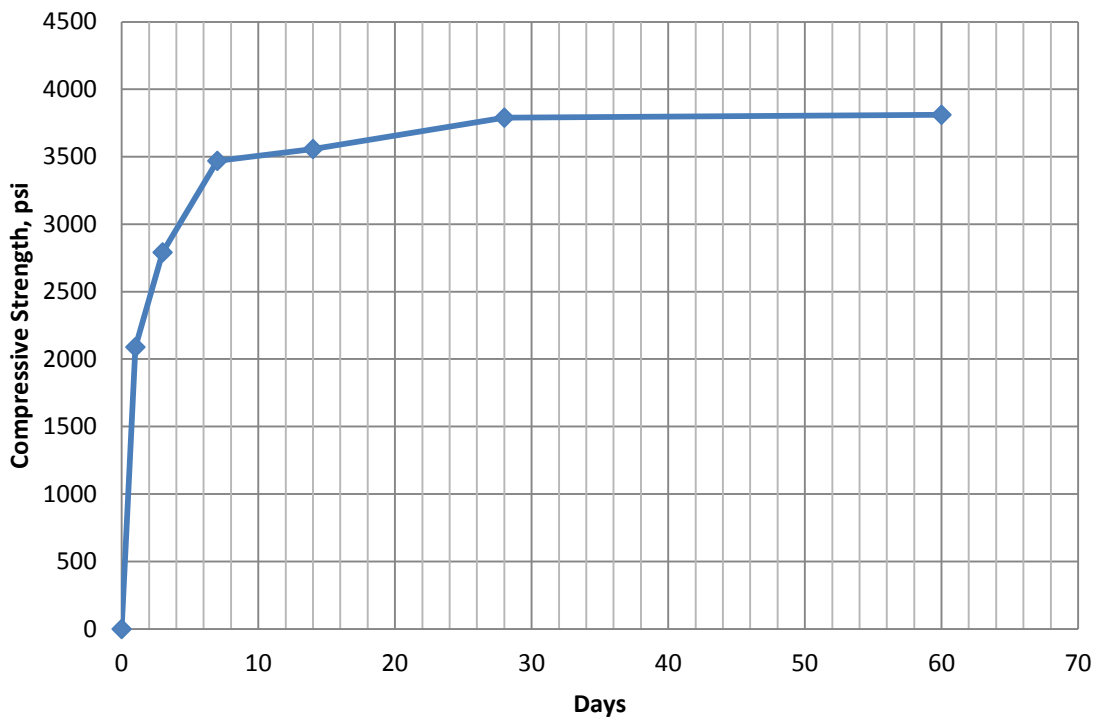


Figure 3.4: RAC-50 Mix Strength Gain with Time

Conversion: 1 psi = 6.9 kPa

3.3.4. RAC-100% Mix Design and Concrete Properties. The second mix incorporating RCA was a 100% direct replacement design, subsequently referred to as RAC-100. The total volume of coarse aggregate in the control MoDOT Class B mix was

directly substituted with the laboratory-produced RCA. In order to maintain consistency with the control specimens, the MoDOT Class B mix specifications were used to design the 100% direct replacement mix. However, during laboratory trial batching, it was noticed from the slump test that the mixes lacked cohesion. To remediate this lack of cohesion, the mix was modified by increasing the amount of fine aggregate volume by 5% of total aggregates. This change notably improved the cohesion of the mix. The achieved 28-day strength of this mix during trial batching was 5500 psi (37.92 MPa), so this was used for the design of bond test specimens.

Table 3.11: RAC-50 Splitting Tensile Strength Results

Specimen	Splitting Tensile Strength (psi)	Average Splitting Tensile Strength (psi)
RAC-50-1	341	344
RAC-50-2	347	

Conversion: 1 psi = 6.9 kPa

The mix specifications are summarized in **Table 3.12**, and the oven-dry design batch weights are shown in **Table 3.13**. The fresh properties of the concrete were determined after the addition of the chemical admixtures on the day of casting the bond test specimens. The slump was 8.5 in. (21.6 cm), the air content was 7%, and the unit weight was 137.2 lb/yd³ (2198 kg/m³).

The compressive strength, splitting tensile strength, and modulus of elasticity of the mix were determined from companion cylinders that were cast from the same concrete batch as the bond test specimens. **Figure 3.5** shows the compressive strength gain over time. At 60 days, the compressive strength was 5300 psi (36.54 MPa). On the day of testing, the compressive strength was 4840 psi (33.37 MPa). The splitting tensile

strength found on the day of testing the bond specimens was 320 psi (2.21 MPa). The results are shown in **Table 3.14**. Likewise, the modulus of elasticity of the concrete found on the day of testing the bond specimens was 4,000,000 psi (27.58 GPa).

Table 3.12: RAC-100 Mix Design Specifications

Cementitious Amount, lb/yd ³	535
w/c Ratio	0.36
Amount of Fine Aggregate (by volume), %	45
Design Air Content, %	6.0
Target Slump, in.	6.0

Conversion: 1 lb./yd³ = 0.59 kg/m³
1 in. = 2.54 cm

Table 3.13: RAC-100 Design Mix Proportions, Oven-Dry Basis

Cement	535 lb/yd ³
Water	192.6 lb/yd ³
Coarse Aggregate	1650.5 lb/yd ³
Fine Aggregate	1441.6 lb/yd ³
Air Entrainer MB-AE 90	1 fl.ozs/cwt
Water Reducer Glenium 7500	6 fl.ozs/cwt

Conversion: 1 lb./yd³ = 0.59 kg/m³
1 oz. = 29.6 ml
1 lb. = 0.45 kg

Table 3.14: RAC-100 Splitting Tensile Strength Results

Specimen	Splitting Tensile Strength (psi)	Average Splitting Tensile Strength (psi)
RAC-100-1	320	320
RAC-100-2	320	
RAC-100-3	319	

Conversion: 1 psi = 6.9 kPa

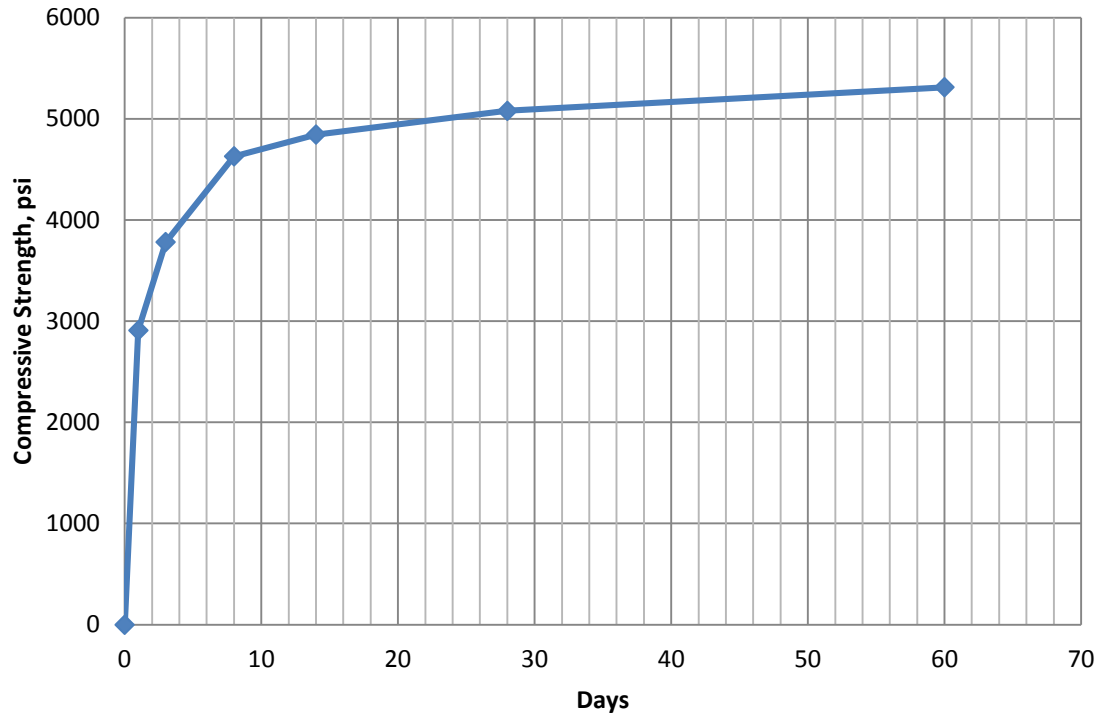


Figure 3.5: RAC-100 Mix Strength Gain with Time
Conversion: 1 psi = 6.9 kPa

3.4. CONCRETE MECHANICAL PROPERTIES

3.4.1. Modulus of Rupture Results. The modulus of rupture, f_r , of the VAC and 100% RCA mixes is shown in **Table 3.15** along with the corresponding compressive strengths on the day of testing. The modulus of rupture for each mix was determined from small batches, and companion cylinders were cast to find the compressive strength. In order to compare the test results across mix designs, the moduli of rupture were normalized by dividing the test value by the square root of the concrete compressive strength. This method of normalization is based on the accepted relationship between modulus of rupture and compressive strength as presented in ACI 318R (2011):

$$f_r = 7.5\lambda\sqrt{f'_c} \quad (3.4)$$

where λ is a correction factor for lightweight concrete.

Table 3.15: Modulus of Rupture Results

Mix	f_c (psi)	f_r (psi)	Normalized f_r	COV	Average Normalized f_r
VAC	5416	501	6.81	9.3%	6.39
	4959	420	5.96		
RAC-100	4546	339	5.03	8.5%	5.69
	4417	391	5.88		
	4944	400	5.69		
	4350	407	6.17		

Conversion: 1 psi = 6.9 kPa

3.4.2. Modulus of Elasticity Results. The average modulus of elasticity, E_c , of the VAC, 50% RCA, and 100% RCA mixes is shown in **Table 3.16** along with the corresponding compressive strengths on the day of testing. The modulus of elasticity of each mix was determined from companion cylinders cast on the same day as the beam splice specimens. To compare the results across mix designs, the moduli of elasticity were normalized by dividing the test value by the square root of the concrete compressive strength. This method of normalization is based on the accepted relationship between modulus of elasticity and compressive strength as presented in ACI 318R (2011):

$$E_c = w_c^{1.5} 33 \sqrt{f'_c} \quad (3.5)$$

where w_c is the unit weight of the concrete.

3.4.3. Splitting Tensile Strength Results. The average splitting tensile strength, f_{tsp} , of the VAC, 50% RCA, and 100% RCA mixes is shown in **Table 3.17** along with corresponding compressive strengths on the day of testing. The splitting tensile strength of each mix was determined from companion cylinders cast on the same day as the beam splice specimens. To compare the results across mix designs, the splitting tensile strengths were normalized by dividing the test value by $f'_c^{2/3}$. This method of

normalization is based on the relationship between splitting tensile strength and compressive strength as presented in CEB-FIP (1990):

$$f_{tsp} = 1.57f_c^{2/3} \quad (3.6)$$

Table 3.16: Modulus of Elasticity Results

Mix	f_c (psi)	Average MOE (ksi)	Average Normalized MOE
VAC	4000	4300	67.99
RAC-50	3560	3750	62.85
RAC-100	4840	4000	57.50

Conversion: 1 psi = 6.9 kPa

Table 3.17: Splitting Tensile Strength Results

Mix	f_c (psi)	Average f_{tsp} (psi)	Average Normalized f_{tsp}
VAC	4000	397	1.58
RAC-50	3560	325	1.39
RAC-100	4840	320	1.12

Conversion: 1 psi = 6.9 kPa

3.4.4. Fracture Energy Results. The average fracture energy, G_f , of the VAC, 50% RCA, and 100% RCA mixes is shown in **Table 3.18** along with the corresponding compressive strengths on the day of testing. The fracture energy for each mix was determined from small batches, and companion cylinders were cast to find the compressive strength. To compare the results across mix designs, the fracture energies were normalized by dividing the test value by $f_c^{0.7}$. This method of normalization is based on the relationship between fracture energy and compressive strength as presented in CEB-FIP (1990):

$$G_f = G_{fo} \left(\frac{f_c}{f_{cmo}} \right)^{0.7} \quad (3.7)$$

where G_{fo} is a constant base value fracture energy dependent on the maximum aggregate size and f_{cmo} is a constant equal to 1450 psi (10 MPa).

Table 3.18: Fracture Energy Results

Mix	f_c (psi)	Average G_f (lbf/ft)	Average Normalized G_f
VAC	5394	20.9	0.0510
RAC-50	6598	20.8	0.0440
RAC-100	4945	15.3	0.0397

Conversion: 1 psi = 6.9 kPa
1 lbf/ft = 6.9 N/m

3.4.5. Comparison of Mechanical Properties. Figure 3.6 shows a graphical comparison of the mechanical properties of the three mixes. All properties are negatively impacted with increasing replacement of coarse natural aggregates with RCA. The most drastic decreases were seen in splitting tensile strength and fracture energy. The splitting tensile strength decreased 12% and 29% for 50% RCA replacement and 100% RCA replacement, respectively. The fracture energy decreased 14% and 22% for 50% RCA replacement and 100% RCA replacement, respectively. In bond failures where splitting cracks control, the peak load is governed by the tensile response of the concrete, which depends on the splitting tensile capacity and fracture energy. Thus, as shown in the reduced splitting tensile strength and fracture energy of high volume RCA concrete, it is expected that the bond carrying capacity will be negatively impacted as well.

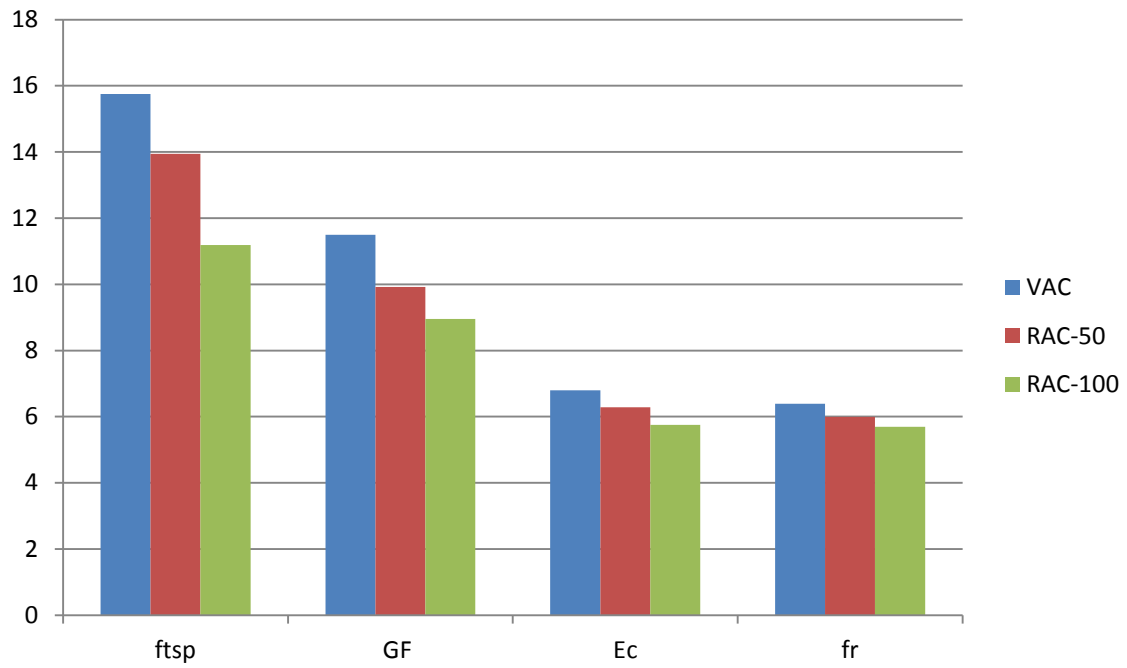


Figure 3.6: Comparison of Normalized Mechanical Properties

Note: Normalized values of $f_{tsp} * 10$ and $E_c * 10^{-1}$

4. EXPERIMENTAL PROGRAM

4.1. INTRODUCTION

To evaluate the bond performance of RAC, both direct pull-out and full-scale beam splice specimens were used. RILEM 7-II-128 *RC6: Bond test for reinforcing steel* was used to develop the direct pull-out type specimens and test method. Likewise, recommendations from ACI 408R-03 *Bond and Development of Straight Reinforcing Bars in Tension* as well as procedures reported in previous research of bond performance were used to develop the full-scale beam splice specimens and test method.

4.2. RCA PRODUCTION

The RCA used throughout the study was produced in the laboratory environment. This step precluded variables such as varying levels of chloride and organic contamination, varying and/or unknown sources of virgin aggregates, and different levels of residual mortar deterioration of the recycled aggregates. By using this laboratory-produced RCA, the amount of residual mortar on the aggregates was a “worst-case” condition with a very high content by volume.

In order to make the RCA, the parent concrete beams were cast and cured in the laboratory. Thirty 1 ft. x 1.5 ft. x 5 ft. (0.30 m x 0.46 m x 1.52 m) and twenty 1 ft. x 1.5 ft. x 7 ft. (0.30 m x 0.46 m x 2.13 m) un-reinforced beams were cast in a total of five separate pours. Short beams were produced to improve the ease of transportation to the crushing site. To build the formwork for these beams, 10 ft. (3.05 m) and 14 ft. (4.27 m) steel and wood forms were used with a plywood divider in the middle to create the smaller beams. Polyvinyl chloride (PVC) tubes were inserted at two locations through the

middle of each formwork such that a steel rod could be temporarily placed through the beams after the formwork was removed and used to lift the beams onto a truck bed. This step was done to eliminate the need to use steel hooks which might have damaged the crushing equipment. **Figure 4.1** shows the prepared formwork for the parent concrete beams.

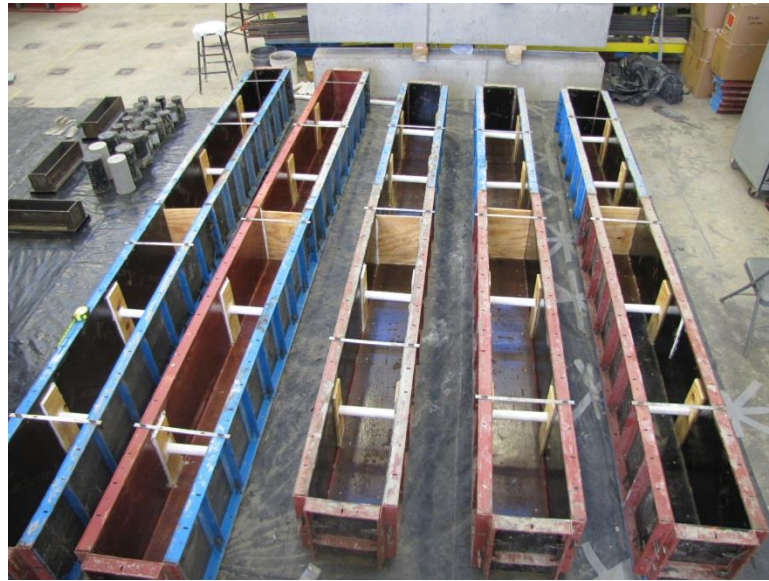


Figure 4.1: Formwork for Casting Pre-Recycled Concrete

Once all these beams were cast and allowed to reach a minimum compressive strength of 4000 psi (27.58MPa), they were transported to the crushing site. For this study, rock crushers at the Rolla, Missouri quarry of Capitol Quarries (Jefferson City, Missouri) were used to crush down the parent concrete beams to the desired MoDOT Gradation D distribution. A mobile crushing plant with both primary and secondary steel jaw crushers was used to process the material.

4.3. DIRECT PULL-OUT SPECIMENS

4.3.1. Direct Pull-Out Specimen Design. RILEM 7-II-128 RC6: *Bond test for reinforcing steel* describes the pull-out specimen as a steel reinforcing bar embedded in a concrete cube with a volume of $10d_s$ by $10d_s$ by $10d_s$, where d_s is the bar diameter. A direct tensile load is applied to the end of the steel bar until the bonded region fails. During testing, both the slip of the embedded bar and applied load are measured. The test specification calls for a bonded length of $5d_s$ and an un-bonded length of $5d_s$ at the end closest to the applied load. Some changes were made to RILEM recommended test specimen design based on results from previous research (Wolfe, 2011).

The direct pull out specimen used in this experimental program was a reinforcing steel bar embedded in a cylindrical volume of concrete with a diameter of 12 in. (30.5 cm). This deviation from the RILEM standard was made to reduce the potential for a splitting failure by maintaining a constant, large concrete cover for the reinforcing bar. The bonded length was $5d_s$ and the un-bonded length was $5d_s$ as per the RILEM testing standard. This un-bonded length is necessary in the design of the direct pull-out specimens to prevent a conical failure surface from forming within the concrete volume at the location of bearing (ACI 408, 2003).

In this testing program, both ASTM A615-09, Grade 60 #4 (No. 13) and #6 (No. 19) deformed steel bars were used in direct pull out specimens. The total length of each bar measured 40 in. (101.6 cm). A length of $3/8$ in. (.95 cm) remained exposed at the end of the bonded portion to facilitate the measure of slip during testing using a linear voltage differential transformer (LVDT). The bonded and un-bonded lengths were 2.5 in. (6.4 cm) for the #4 (No.13) direct pull-out specimens and 3.75 in. (9.5 cm) for the #6 (No. 19)

direct pull out specimens. A schematic of the #4 (No. 13) and #6 (No. 19) specimens are shown in **Figures 4.2** and **4.3**, respectively.

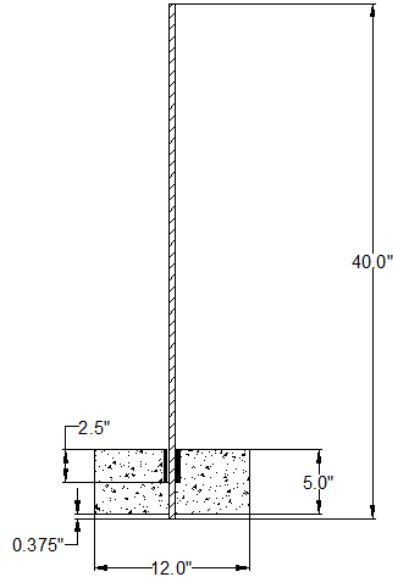


Figure 4.2: Schematic of #4 (No. 13) Bar Direct Pull-Out Specimen

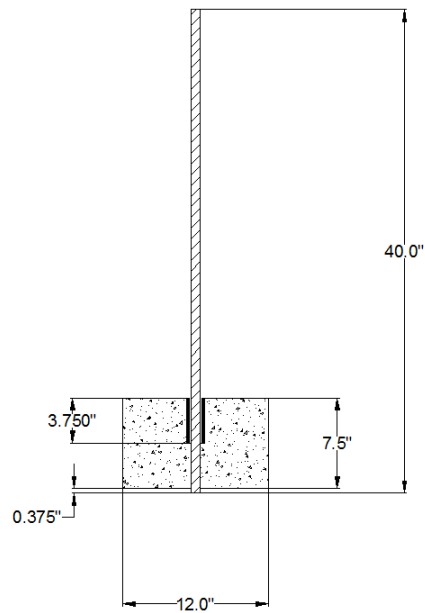


Figure 4.3: Schematic of #6 (No. 19) Bar Direct Pull-Out Specimen

4.3.2. Direct Pull-Out Specimen Fabrication. The molds for the direct pull out specimens were constructed from segments of 12 in. (30.5 cm) diameter cardboard tube concrete forms (QuickTube). Strips measuring 5 in. (12.7 cm) and 7.5 in. (19.1 cm) in length were cut for the #4 (No. 13) bar and #6 (No. 19) bar specimens, respectively. The bases of the molds were constructed from 3/8 in. (.95 cm) plywood cut to 14 in. x 14 in. (35.6 cm x 35.6 cm) squares. The 3/8 in. (0.95 cm) base thickness was chosen to allow a 3/8 in. (0.95 cm) length exposed at the end of the bonded portion to facilitate the measure of slip during testing. A hole was drilled in the center of the base pieces 1/16 in. (0.16 cm) larger than the nominal diameter of the bar in order for the 3/8 in. (0.95 cm) length of the bar to remain exposed. The cardboard segments of QuickTube were then aligned along the base pieces with the drilled-out hole at the center. A bead of waterproof, adhesive silicon was applied at the junction of the plywood base and cardboard segment in order to attach the pieces of the mold and to prevent cement paste from leaking during the casting and curing of the specimens.

Both the #4 (No.13) and #6 (No. 19) steel reinforcing bars were sectioned into 40 in. (101.6cm) long segments for the pull out specimens. PVC pipes were used to form the bond breaker within the concrete cylinder. For the #4 (No. 13) bars, PVC pipe with an inner diameter of 3/4 in. (1.91cm) was used, and for the #6 (No. 19) bars, PVC pipe with an inner diameter of 1 in. (2.54 cm) was used. The PVC pipe segments were cut 1/4 in. (0.64 cm) longer than the required un-bonded length. This step was done so that this 1/4 in. (0.64 cm) length would remain beyond the concrete cylinder on the bearing surface. This extra length was used to help ensure that concrete did not inadvertently fall between the PVC bond breaker and steel bar during casting and finishing of the specimens.

To attach the bond breaker to the bars, a single layer of bubble wrap was taped around the portion to remain un-bonded. This wrap helped to align the PVC concentrically with the steel bar and to also help keep concrete from filling the space within the bond breaker. The segments of PVC were slid over the bubble wrap, and a small bead of waterproof silicone was carefully applied around the top and bottom of the bond breaker to prevent concrete infiltration.

The top pieces of the direct pull out molds were made from 3/8 in. plywood cut to 14 in. x 14 in. (35.6 cm x 35.6 cm) squares. A hole measuring 1/16 in. (0.16 cm) larger than the outside diameter of the PVC pipe was drilled at the center of each top piece. Prior to casting the specimens, the reinforcing bars were placed into the completed forms and leveled to ensure they were plumb with the cylindrical mold base. An outline of the cylindrical base was sketched on the bottom side of the top piece when the steel bar was shown to be plumb through the use of levels. Three wood blocks were then screwed onto the bottom of the top piece of plywood tangentially along the outline of the cardboard tubing to snugly secure the top in place.

To cast the specimens, the steel bar was first inserted into the hole in the bottom of the mold. The bar was held perpendicular as concrete was filled to the top of the mold. A vibrator was used to lightly consolidate the concrete as needed, and the surface of the concrete was finished with a trowel. Once finished, the top piece of the mold was gently slid down over the bar and fitted around the extruded PVC bond breaker. The pull out specimens and the companion compression and splitting tensile specimens were left to cure until the specified peak strength was reached prior to testing. The cardboard and

plywood components of the molds were removed on the day of testing. The completed pull-out specimens curing in their molds are shown in **Figure 4.4**.



Figure 4.4: Completed Direct Pull-Out Specimens in Molds

4.3.3. Direct Pull-Out Specimen Test Set-Up. A 200 kip-capacity (890kN) loading frame manufactured by Tinius Olson was used to test the direct pull out specimens. After the specimens were de-molded, they were inverted and positioned through the top platform of the load frame as shown in **Figure 4.5**. A steel bearing plate was used, and a neoprene pad was placed directly between the concrete surface and steel plate to ensure uniform bearing on the concrete. The steel bar was fed through grips on the middle platform of the testing frame. A smaller steel plate was placed on the top of the concrete cylinder and an LVDT was clamped to a magnetic stand at the top of the specimen. The head of the LVDT was placed on the 3/8 in. (0.95 cm) exposed end of the steel bar to measure the slip during testing. The LVDT set-up is shown in **Figure 4.6**.

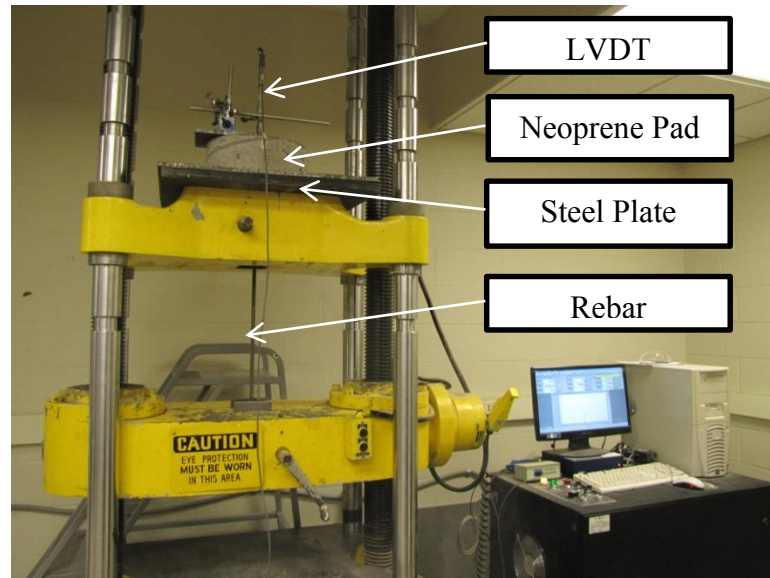


Figure 4.5: Test Set-Up for Direct Pull-Out Specimen



Figure 4.6: LVDT Set-Up for Direct Pull-Out Specimen

4.3.4. Direct Pull-Out Specimen Test Procedure. The computer software controlling the Tinius Olson was programmed to apply a displacement controlled load rate of 0.10 in. (0.3 cm) per minute. A preload of approximately 100 lb. (0.44kN) was applied to the rebar by manually moving the middle platform. This was done to help the

middle fixture properly grip the steel bar. After this preload was applied, the test was initiated. A distinct peak in the load versus slip output plot was watched for during testing. After this peak was detected, the test was continued while the load began to decrease with increasing slip. The test was allowed to run this way in order to determine if there was any additional bond capacity and to be sure that the captured peak load was a true bond failure.

4.4. BEAM SPLICE SPECIMENS

4.4.1. Beam Splice Specimen Design. The beam splice test used in this experimental program is a non-ASTM testing procedure for full scale beams. The design and fabrication of the specimens was based on previous research of bond performance (Looney, 2012 and Wolfe, 2011). The beams used in this study were 10 ft. (3.05m) long with a cross section of 12 in. x 18 in. (0.30m x 0.46m). The longitudinal reinforcement consisted of three ASTM A615-09, Grade 60 #6 (No. 19) deformed steel bars, which were contact lap-spliced at the midspan of the beams. The splice length used for these beams was a reduced value of the development length equation recommended in ACI 318-11 “Building Code Requirements for Structural Concrete”, shown as **Equation 4.1**. Based on previous research by Looney (2012), 70% of this calculated development length was used for the beam splice specimen design. Looney found that this reduction was sufficient to avoid yielding of the bar in a flexural failure mode and to ensure a bond failure mechanism. The equation for development length is:

$$l_d = \left[\frac{3}{40} \frac{f_y}{\lambda \sqrt{f'_c}} \frac{\psi_t \psi_e \psi_s}{\left(\frac{c_b + K_{tr}}{d_b} \right)} \right] * d_b \quad 4.1$$

where, l_d = development length
 f_y = specified yield strength of reinforcement
 λ = lightweight concrete modification factor
 f'_c = specified compressive strength of concrete
 Ψ_t = reinforcement location modification factor
 Ψ_e = reinforcement coating modification factor
 Ψ_s = reinforcement size modification factor
 c_b = smallest of distance from center of a bar to nearest concrete surface or one-half the center-to-center bar spacing
 K_{tr} = transverse reinforcement index
 d_b = nominal diameter of the reinforcing bar

A standard hook was specified at the ends of each longitudinal reinforcing bar to achieve sufficient development. As per ACI 318-11, this hook included a 90-degree bend with the minimum recommended bend diameter of 4.5 in.(11.4cm) and an extension of $12d_b$ at the free end of the bar (ACI 318, 2011).

Transverse reinforcement against shear failure consisted of #3 (No. 10), ASTM A615-09, Grade 60, U-shaped stirrups. To ensure that a shear failure would not occur before bond failure, a stirrup spacing less than the ACI 318-11 maximum stirrup spacing was used. The stirrups were not placed within the lap spliced region in order to avoid the interaction of confinement of the concrete within the splice zone. **Figures 4.7 and 4.8** detail the cross-sectional and plan views of the beam splice specimens, respectively. As shown in the schematic below, 180-degree hooks were used at the free ends of the U-stirrups. To help stabilize and align the cages, #4 (No. 13) bars were used as top bars and placed inside of these hooks.

4.4.2. Beam Splice Specimen Fabrication. The reinforcing bars were sectioned and bent to the appropriate lengths. Before the cages were assembled, a wire brush was used to clear the rust and mill scale at the ends of the longitudinal bars that were to be spliced. This was done to reduce test variability by reducing the influence of the rust and

mill scale on the bond performance. Saw-horses were then used to lay out the bottom reinforcement. Stirrups were placed along the longitudinal bars at the appropriate locations and the top bars were laid in the stirrup hooks. Levels were used to ensure that the stirrups were plumb with the longitudinal reinforcement, and then wire ties were used to connect every joint of the cages. To ensure appropriate concrete cover on the sides of the cages, two very short pieces of #8 (No. 25) bars, about 1 in. (2.54 cm) in diameter, were tied to the outside to serve as spacers. Likewise, 1.5 in (3.81 cm) steel chairs were tied to the bottom of the cages in order to provide sufficient cover.

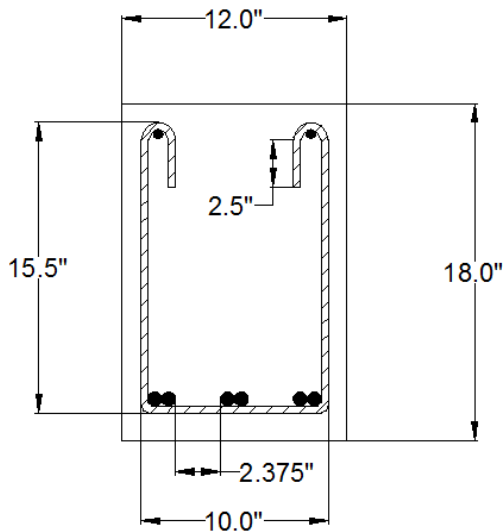


Figure 4.7: Schematic of Beam Splice Specimen Profile

Note: Stirrups omitted from within splice length.

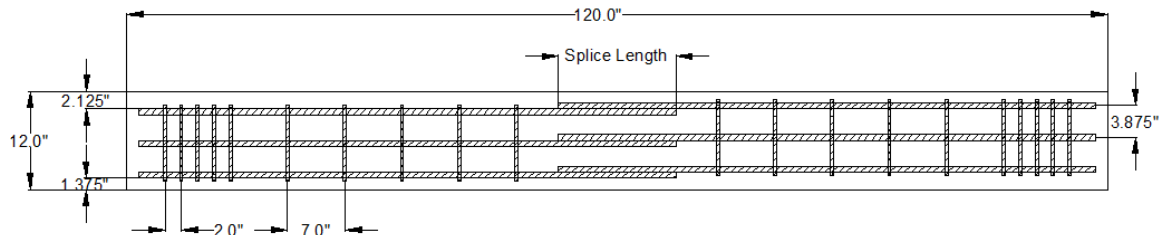


Figure 4.8: Schematic of Beam Splice Specimen Plan

Upon completion of the steel cages, strain gauges were installed at both ends of the contact lap splice to measure strain in the steel during testing. Before the strain gages were attached to the steel, the location along the bar was prepared by grinding a smooth surface, cleaning the area with an acid, and then neutralizing the area. **Figure 4.9** shows the spliced region with installed strain gauges, and **Figure 4.10** shows the finished cages.



Figure 4.9: Spliced Length with Attached Strain Gauges



Figure 4.10: Completed Cage for Beam Splice Specimen

Steel-framed forms were used to construct the beam splice specimens. The walls of these forms were constructed of wood and were held together by steel pins and wire ties. The forms measured 14ft. (4.27m) in length, but in order to reduce this length to the required 10ft. (3.05m) wood block-outs were constructed. After the forms were assembled, form release oil was applied to the walls of the forms to facilitate de-molding of the beams. The finished cages were then placed inside of the forms, and hooks were welded onto the top bars to allow for ease of transportation of the beams after curing.

Figure 4.11 shows the completed cages inside the concrete forms.

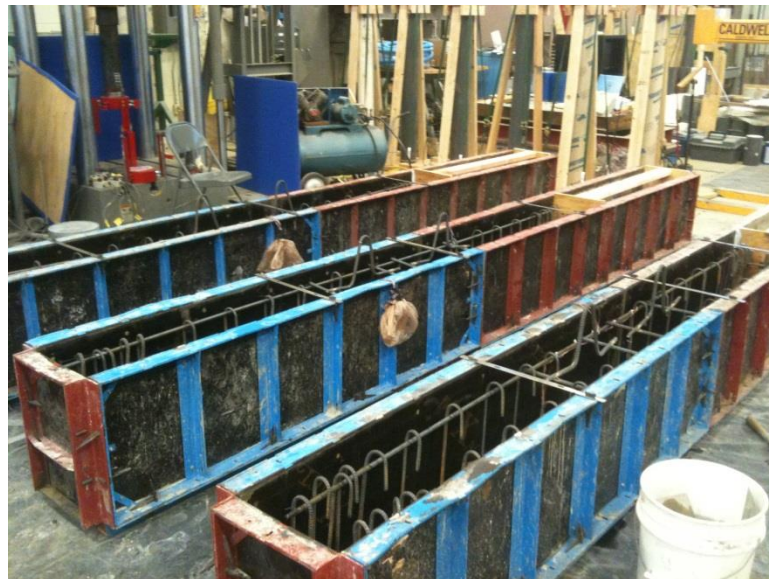


Figure 4.11: Steel Cages in Forms

The mix design was sent to the local Rolla Ready Mix plant, and the concrete was delivered to the lab. A small amount of the water was withheld from each mix design during delivery so that the water content could be slightly adjusted at the lab. Upon arrival of the truck, the slump of the concrete was performed in order to verify that the mix was correct prior to the addition of the chemical admixtures. Once this check was

performed, the air entraining dose and high range water reducer were added along with the additional water required to bring the water-to-cement ratio up to the required mix design. The concrete was allowed to mix at higher speed to produce the desired mix. Once this mixing was complete, the slump and air content were measured to ensure the mix behaved as anticipated. Once this was verified, fresh concrete was placed into an overhead crane bucket which was used to fill the concrete forms. The filling of the forms is shown in **Figure 4.12**. Simultaneously, a wheelbarrow was filled with fresh concrete and used to cast the companion splitting tensile and compression cylinders.



Figure 4.12: Casting of Beam Splice Specimens

The concrete was consolidated in layers in the beam forms. Once the forms were filled, wood blocks were used to screed the surface of the beams. Finishing towels were then used to smooth and level the beam top surface. Care was taken to avoid damage to the strain gauge wires that extended from the middle edge of the concrete beams.

The following day, the beams were removed from their forms after a compression test confirmed that the concrete had developed sufficient strength after 24 hours. Before the day of testing, the beams were prepared by lines being drawn at the locations of the supports and load points. Additionally, an aluminum angle was anchored into the concrete on the side of the beam at the midspan so that the deflection there could be monitored.

4.4.3. Beam Splice Specimen Test Set-Up. Third-point loading was used in order to create a constant, maximum moment in the middle third of the beam, helping to induce bond failure at the splice location at midspan. **Figure 4.13** shows a schematic of the third-point loading condition used to test the beam splice specimens. Through the use of jacks and wheeled-platforms, the beam was positioned onto roller supports beneath two 140 kip-capacity (623kN) hydraulic actuators in the load test frame shown below in **Figure 4.14**. Care was taken to ensure that the beam was positioned along the center line of the test frame. Spreader beams were used to transfer the applied load from the actuators to the concrete test beam. Rollers were placed on top of the beam at the location of the third points. Well sorted masonry sand was placed beneath these rollers and leveled to prevent any roughness along the top of the concrete beam from causing gaps beneath the base of the rollers. The actuators were lowered, and the bottom spreader beam was lined up along the center of the test specimen through the use of levels and T-squares. A 4 ft. (1.22 m) long mirror was kept nearby so that the rupture at the bottom of the beam could be safely inspected upon failure.

The LVDT was attached to a stand next to the beam. The pin of the LVDT was placed on the aluminum angle that had been previously anchored at the midspan of the

beam so that midspan deflection could be measured and recorded. This set-up is shown in **Figure 4.15**. The LVDT along with all six strain gauges were connected to data acquisition channels.

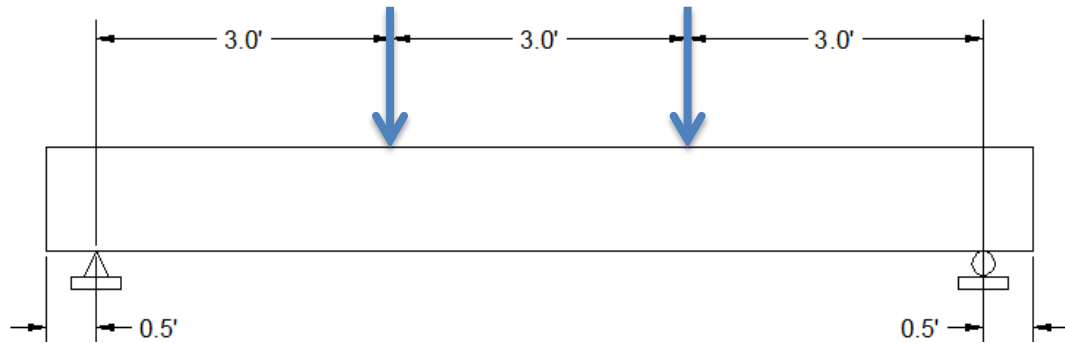


Figure 4.13: Schematic of Beam Splice Loading



Figure 4.14: Beam Splice Specimens in Load Test Frame



Figure 4.15: LVDT Set-Up for Beam Splice Test

4.4.4. Beam Splice Specimen Test Procedure. The data acquisition system was initiated to record data from the strain gauges and LVDT as well as the applied load from the actuators. The test was performed on a displacement-controlled basis; the load was applied in a series of loading steps where each step corresponded to a midspan deflection of 0.02 in. (0.05 cm). After each applied step, the crack patterns were traced in order to track the crack propagation.

The beam was loaded until failure occurred. This bond failure was marked by a very sudden rupture in the concrete along the bottom of the beam in the spliced region. Often, pieces of the concrete cover in the spliced region fell from the beam. This rupture was accompanied by a rapid and drastic drop-off in the load and increase in midspan deflection. Once this failure occurred, testing was completed and data collection was terminated.

5. TEST RESULTS AND EVALUATIONS

5.1. DIRECT PULL-OUT TEST RESULTS

The direct pull-out specimens were constructed to provide a relative measure of performance among the three mix designs. Both RAC mix designs were compared with the MoDOT Class B control mix. For this experimental program, a total of 18 pull-out specimens were tested. To investigate the effect of bar size on the relative bond performance, three specimens were constructed with #4 (No. 13) bars and three with #6 (No. 19) bars for each mix design. The testing matrix is shown below in **Table 5.1**.

Table 5.1: Testing Matrix for Direct Pull-Out Specimens

Mix	Reinforcing Bar Size	Number of Specimens
VAC	#4 (No. 13)	3
	#6 (No. 19)	3
RAC-50	#4 (No. 13)	3
	#6 (No. 19)	3
RAC-100	#4 (No. 13)	3
	#6 (No. 19)	3

Throughout the testing of these specimens, the slip of the bar and the applied load were recorded. When all testing was completed, the maximum applied load was determined for each pull-out specimen, and an average maximum value was found. The maximum bond stress was found by dividing the peak load carried by the bonded surface area of the bar. **Table 5.2** shows the results from the testing. Within each of the specimen names, VAC represents virgin aggregate concrete (the control), RAC50 represents recycled aggregate concrete designed with 50% RCA replacement, and RAC100

represents recycled aggregate concrete designed with 100% RCA replacement. The letters PO signify that these were pull-out specimens, and the number 4 or 6 indicates what bar size was used in the specimen. The final number in the specimen name indicates which of the three tests that specimen was identified as.

The coefficient of variation (COV) of each set of data is also given in **Table 5.2**. For each test set, the variation is relatively low; the maximum within all of the collected test data is 7.3%. These low COV values indicate consistency in the results and reliability in the test as a measure of relative bond performance. Plots of the peak bond stresses for VAC, RAC-50, and RAC-100 specimens are shown in **Figures 5.1, 5.2, and 5.3**, respectively.

Table 5.2: Pull-Out Test Results

Mix	Bar Size	Specimen	Max. Applied Load (lb)	Bond Stress (psi)	Average Bond Stress (psi)	Bond Stress COV
VAC	#4(No. 13)	VAC-PO4-1	10344	2634	2730	5.3%
		VAC-PO4-2	10435	2657		
		VAC-PO4-3	11379	2898		
	#6 (No. 19)	VAC-PO6-1	27172	3075	2965	3.3%
		VAC-PO6-2	25869	2928		
		VAC-PO6-3	25563	2893		
RAC-50	#4(No. 13)	RAC50-PO4-1	12760	3249	3183	6.0%
		RAC50-PO4-2	13083	3332		
		RAC50-PO4-3	11657	2968		
	#6 (No. 19)	RAC50-PO6-1	31109	3521	3432	5.4%
		RAC50-PO6-2	28430	3218		
		RAC50-PO6-3	31440	3558		
RAC-100	#4(No. 13)	RAC100-PO4-1	13968	3557	3281	7.3%
		RAC100-PO4-2	12236	3116		
		RAC100-PO4-3	12451	3171		
	#6 (No. 19)	RAC100-PO6-1	30302	3429	3384	1.2%
		RAC100-PO6-2	29597	3350		
		RAC100-PO6-3	29804	3373		

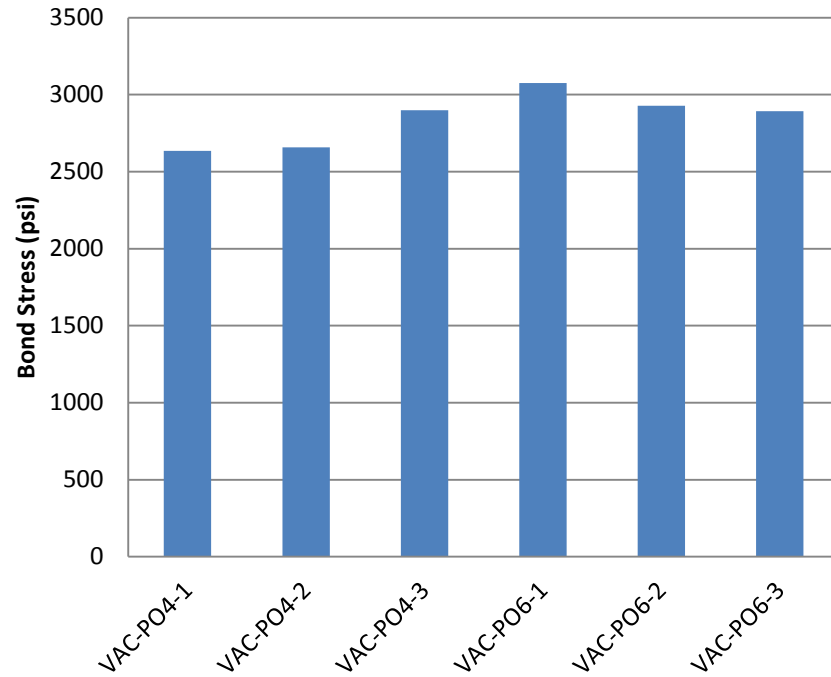


Figure 5.1: Peak Bond Stresses for VAC Pull-Out Specimens
Conversion: 1 psi = 6.9 kPa

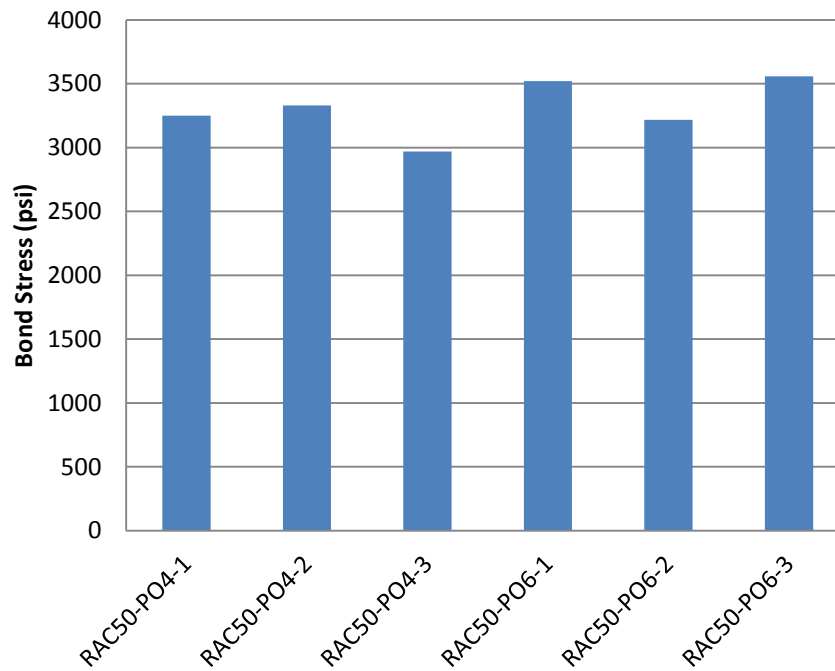


Figure 5.2: Peak Bond Stresses for RAC-50 Pull-Out Specimens
Conversion: 1 psi = 6.9 kPa

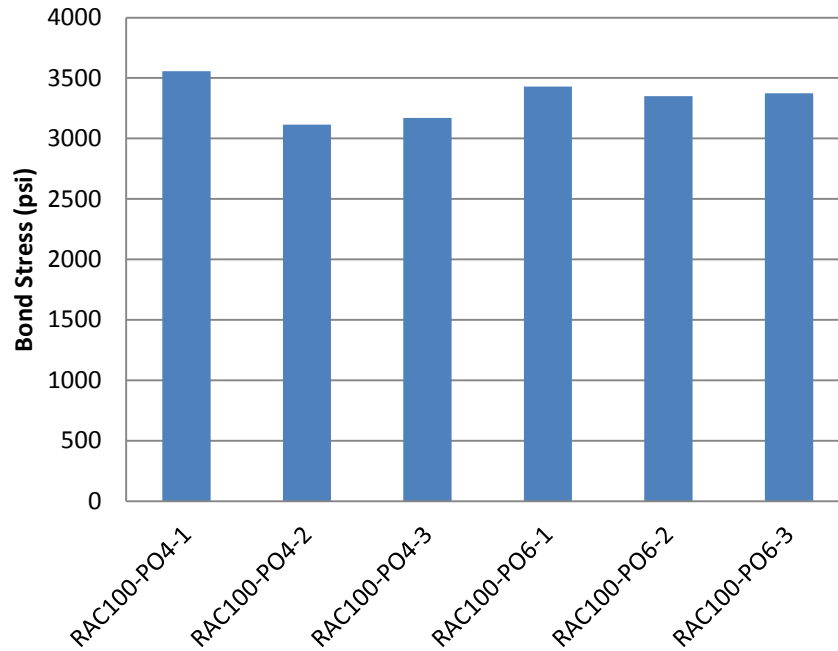


Figure 5.3: Peak Bond Stresses for RAC-100 Pull-Out Specimens
Conversion: 1 psi = 6.9 kPa

For each tested specimen, the bar slip was plotted against the applied load. The plots for most of these specimens indicated that a pull-out failure did occur, as evidenced in the gradual shedding of load after the peak. A typical load-slip plot is shown in **Figure 5.4** from specimen RAC50-PO4-2. The load-slip plots for all tested direct pull-out specimens are included in Appendix A.

5.2. BEAM SPLICE TEST RESULTS

Beam splice specimens were included in this experimental program to provide a test method to evaluate bond performance under a realistic flexural stress-state response. Three beam splice specimens were constructed for each mix design in this study as shown in the test matrix in **Table 5.3**. Both RCA mixes were compared to the

performance of the control specimens. The beams were all constructed with a splice in the longitudinal reinforcement located at midspan.

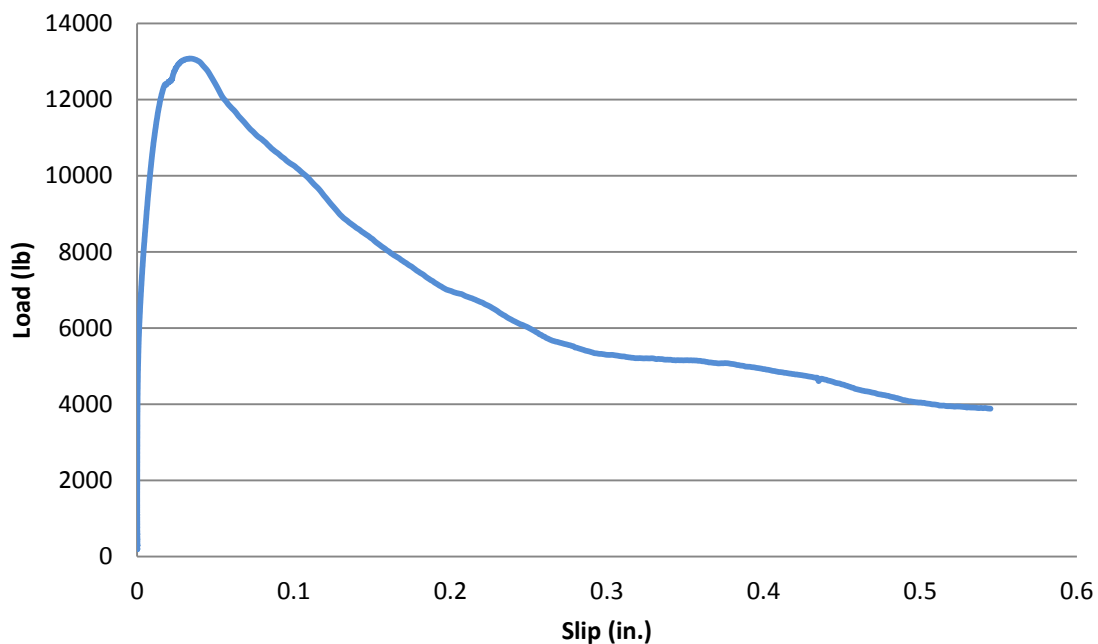


Figure 5.4: Typical Plot of Slip versus Applied Load

Conversion: 1 in. = 25.4 mm

1 lb. = 4.45 N

Table 5.3: Testing Matrix for Beam Splice Specimens

Mix	Bottom Reinforcement	Top Reinforcement	Number of Beams
Control	3 #6	2 #4	3
RAC-50	3 #6	2 #4	3
RAC-100	3 #6	2 #4	3

Throughout the testing of the beam splice specimens, the midspan deflection, applied total load, and strain in the steel were recorded. When all testing was complete, the maximum applied load (peak load) of each beam was determined. Additionally, the

maximum strain in the steel was taken as the average of the maximum strains in each of the strain gauges. Then, using the modulus of elasticity of the steel as determined in the tension testing of the reinforcing bars, the average maximum stress in the steel was determined. This value was compared with the yield stress of the steel found in the tension testing of the bars to ensure that the steel did not yield during beam splice testing. The experimentally determined yield stress of the steel was found to be 74.9 ksi. Upon comparing the maximum stress in the steel to the yield stress, it was observed that none of the specimens experienced steel yield prior to bond rupture failure.

Table 5.4 shows the results from the beam splice testing. Within each of the specimen names, VAC represents virgin aggregate concrete (the control), RAC50 represents recycled aggregate concrete designed with 50% RCA replacement, and RAC100 represents recycled aggregate concrete designed with 100% RCA replacement. The final number in the specimen name indicates which of the three tests that specimen was identified as. The coefficient of variation (COV) of both the peak load carried and the peak stress developed in the longitudinal reinforcement of each set of data is also given in **Table 5.4**. For each test set, the variation is relatively low; the maximum within all of the collected test data is 7.8%. These low COV values indicate consistency in the results and reliability in the test as a measure of bond performance. Plots of the maximum applied loads for VAC, RAC-50, and RAC-100 specimens are shown in **Figures 5.5, 5.6, and 5.7**, respectively. Likewise, plots of the maximum developed stresses for VAC, RAC-50, and RAC-100 specimens are shown in **Figures 5.8, 5.9, and 5.10**, respectively.

Table 5.4: Beam Splice Test Results

Mix	Specimen	Peak Load (kips)	Peak Load COV	Steel Stress at Failure (ksi)	Peak Stress COV
VAC	VAC-1	62.0	4.2%	63.0	7.6%
	VAC-2	67.3		70.8	
	VAC-3	65.9		61.6	
RAC-50	RAC50-1	54.4	5.7%	56.5	1.7%
	RAC50-2	48.8		55.2	
	RAC50-3	50.1		54.8	
RAC-100	RAC100-1	48.8	7.3%	47.3	7.8%
	RAC100-2	50.7		49.9	
	RAC100-3	56.1		55.1	

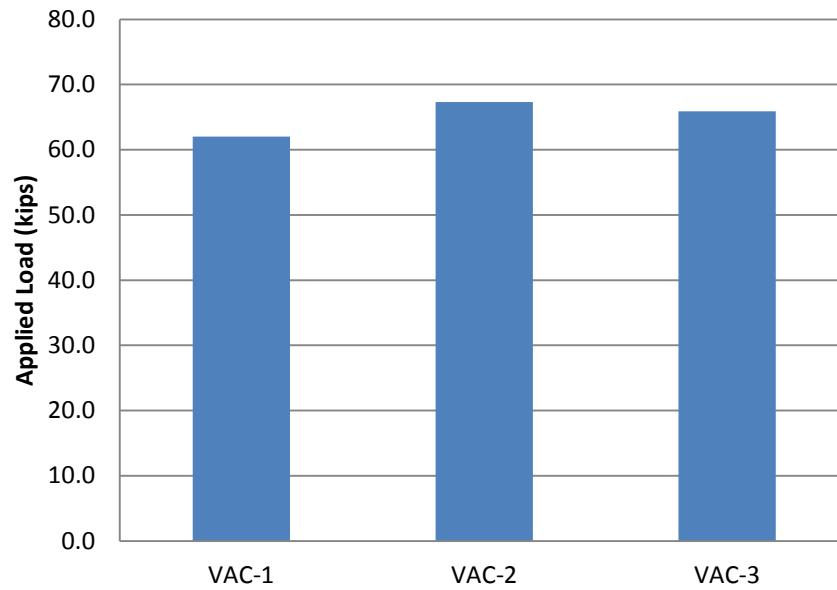


Figure 5.5: Peak Loads for VAC Beam Splice Specimens
 Conversion: 1 kip = 4.45 kN

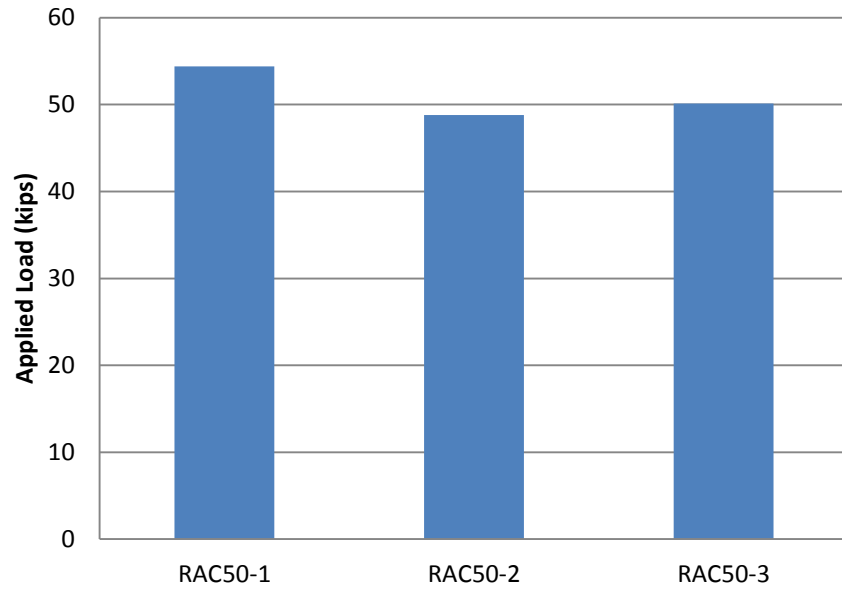


Figure 5.6: Peak Loads for RAC-50 Beam Splice Specimens
Conversion: 1 kip = 4.45 kN

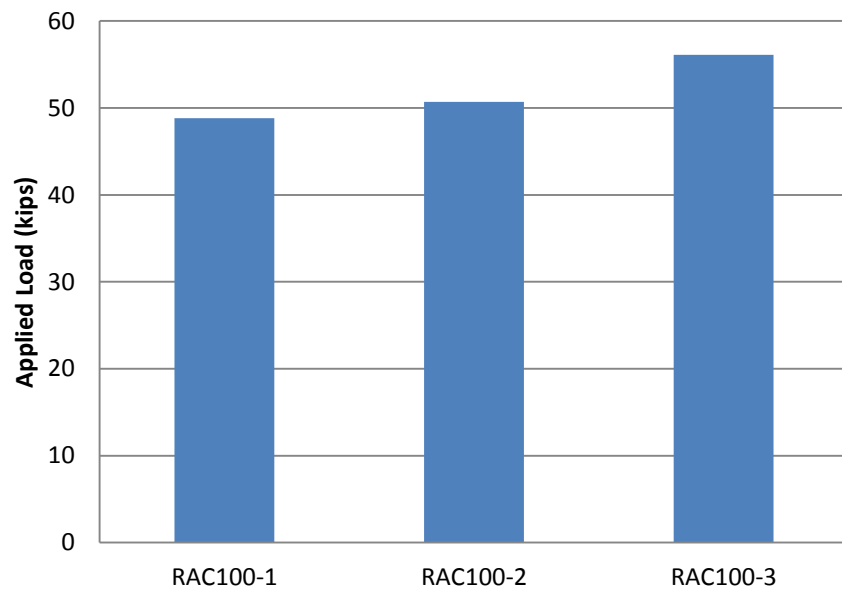


Figure 5.7: Peak Loads for RAC-100 Beam Splice Specimens
Conversion: 1 kip = 4.45 kN

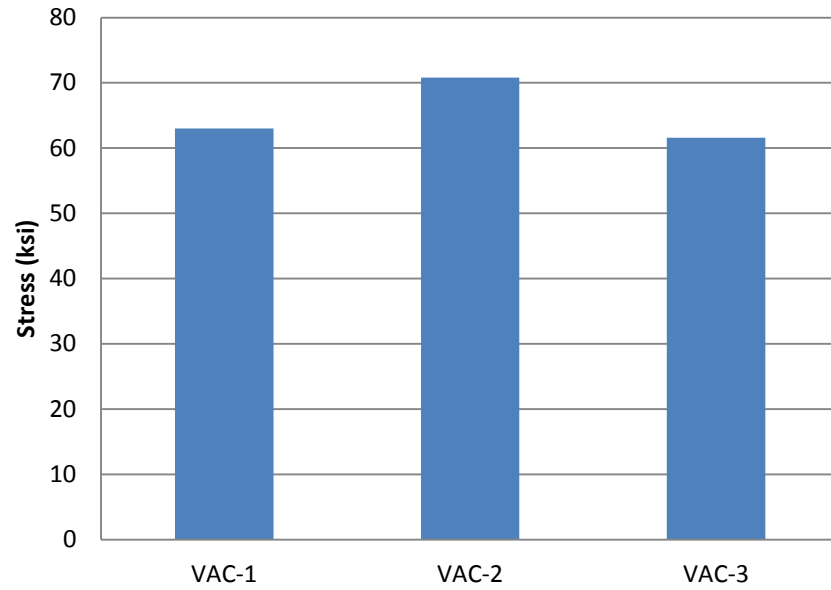


Figure 5.8: Peak Stresses for VAC Beam Splice Specimens
Conversion: 1 ksi = 6.9 MPa

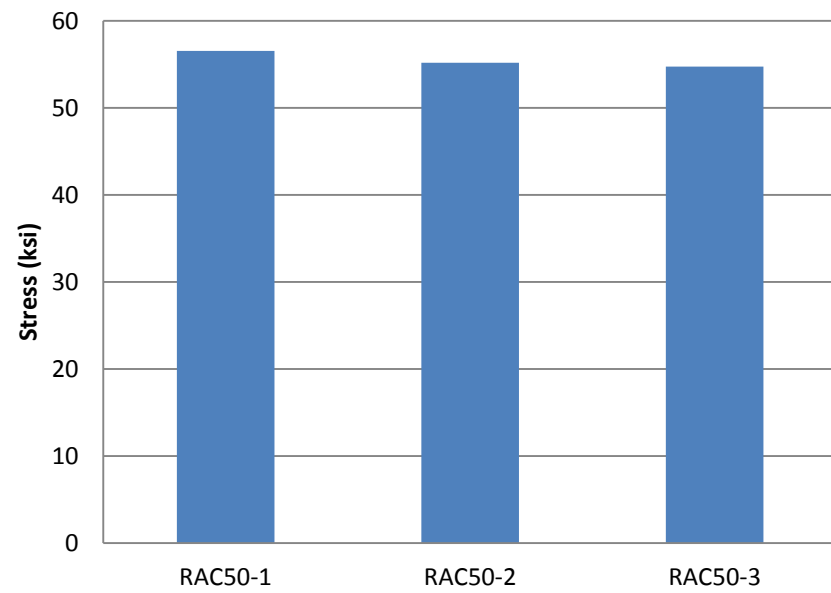


Figure 5.9: Peak Stresses for RAC-50 Beam Splice Specimens
Conversion: 1 ksi = 6.9 MPa

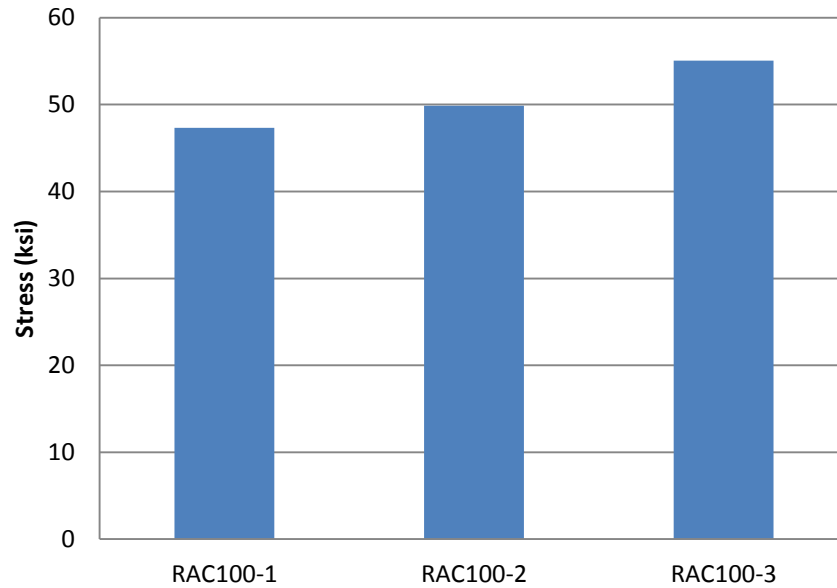


Figure 5.10: Peak Stresses for RAC-100 Beam Splice Specimens
Conversion: 1 ksi = 6.9 MPa

In order to better evaluate and compare the response of the beam splice specimens, the deflection and steel strain data were plotted against the total applied load for each beam. A typical plot of load versus deflection is shown in **Figure 5.11**, and a typical plot of load versus strain is shown in **Figure 5.12**. The plots shown are from specimen VAC-3. Both plots indicate that flexural cracking began to occur in specimen VAC-3 around 15 kips (66.7 kN), as evidenced by the change in slope of the plots at this load. From the constant linear-elastic nature of the load versus strain and load versus deflection plots of the specimens, it was again verified that the steel did not reach yield in any of the test specimens. The load versus deflection and load versus strain plots for each of the tested specimens are included in Appendix B.

At their failure loads, all specimens experienced a bond rupture type of failure. This failure type was indicated by the abrupt audible and visible signs of splitting crack development at the peak load. A typical crack pattern at failure is shown from specimen

RAC50-1 in **Figure 5.13**. The corresponding bottom view at midspan of specimen RAC50-1 is shown in **Figure 5.14**. In both pictures, the splitting cracks at the spliced longitudinal reinforcement are evident. In some beam splice tests, the splitting cracks were so pronounced that the concrete cover within the spliced region spalled off of the specimen. Images of crack patterns of all tested specimens at failure are shown in Appendix C.

5.3. REINFORCING BAR TENSION TEST RESULTS

In order to determine the ultimate stress, yield stress, and modulus of elasticity of the reinforcing bars used in the beam splice specimens, tension tests were performed in accordance with ASTM E8-09 *Standard Test Methods for Tension Testing of Metallic Materials* (ASTM E9-09). This test was performed on three 30 in. (76.2 cm) lengths of #6 reinforcing bars. Each specimen was clamped at each end in a 200 kip (890kN) capacity load frame and loaded until rupture. Throughout testing, both strain and load were recorded. For each specimen, the yield stress of the bar was determined from the 0.5% strain offset of the stress versus strain plot. The modulus of elasticity was also determined for each bar using both the 0.5% offset stress and strain value and the stress and strain value at 40% of the yield stress. **Table 5.5** shows the results of the #6 reinforcing bar tension test.

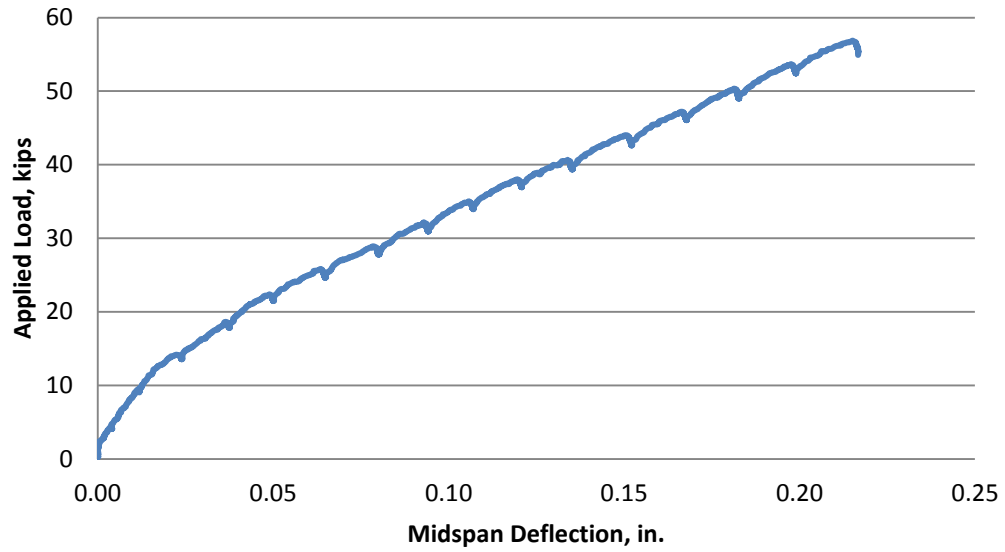


Figure 5.11: Typical Load versus Deflection Plot (VAC-3)

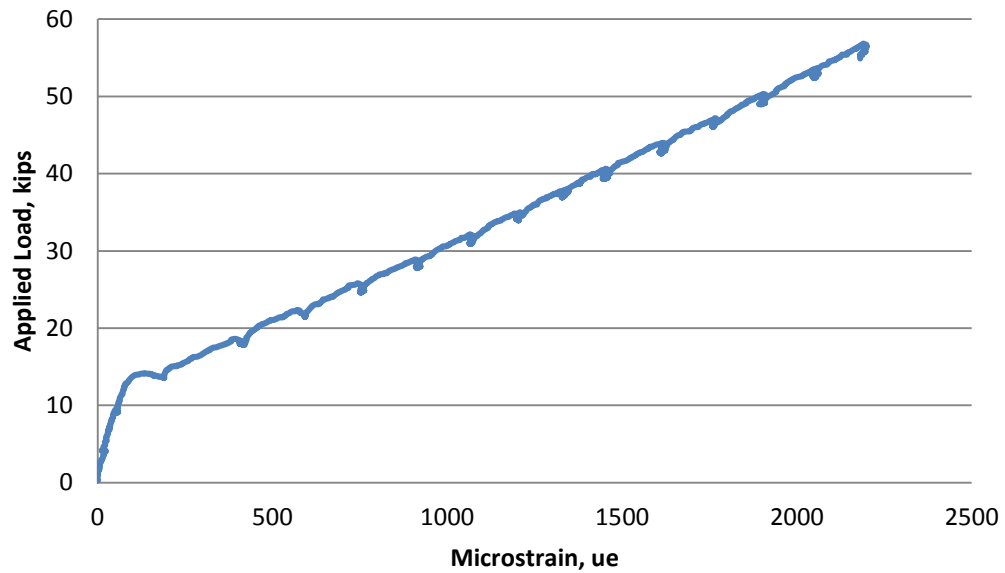


Figure 5.12: Typical Load versus Strain Plot (VAC-3)

5.4. ANALYSIS OF RESULTS

5.4.1. Methodology. In order to directly compare the test results across mix designs, the data was normalized to account for the different test day strengths of the concrete. For the beam splice specimens, the data was also normalized to account for the design strength of the beams. Two different normalization techniques were used to compare the results. The first normalization technique was based on the development length equations provided in ACI 318-11 (ACI 318, 2011), shown in **Equation 5.1**, and AASHTO LRFD-07 (AASHTO, 2007), shown in **Equation 5.2**. Both development length equations are indirectly proportional to the square root of the concrete compressive strength. Thus, in order to normalize the results with varying compressive strengths, peak bond stresses in the direct pull-out tests were divided by the square root of the corresponding compressive strength as shown in **Equation 5.3**. Furthermore, to account for the different design strengths of the concrete used in developing the splice length of the beam splice specimens, the results from these tests were normalized by multiplying the peak stresses by the square root of the design concrete strength. Thus, the developed stress in the steel was multiplied by the square root of the ratio of design strength to actual test-day strength as shown in **Equation 5.4**.

$$l_d = \left[\frac{3}{40} \frac{f_y}{\lambda \sqrt{f'_c}} \frac{\Psi_t \Psi_e \Psi_s}{\left(\frac{c_b + K_{tr}}{d_b} \right)} \right] * d_b \quad (5.1)$$

where,

- l_d = development length
- f_y = specified yield strength of reinforcement
- λ = lightweight concrete modification factor
- f'_c = specified compressive strength of concrete
- Ψ_t = reinforcement location modification factor
- Ψ_e = reinforcement coating modification factor
- Ψ_s = reinforcement size modification factor

c_b = smallest of distance from center of a bar to nearest concrete surface or one-half the center-to-center bar spacing
 K_{tr} = transverse reinforcement index
 d_b = nominal diameter of the reinforcing bar

$$l_{db} = \frac{1.25 A_b f_y}{\sqrt{f'_c}} \geq 0.4 d_b f_y \quad (5.2)$$

where, l_{db} = tension development length
 A_b = area of the reinforcing bar
 f_y = specified yield strength of reinforcement
 f'_c = specified compressive strength of concrete
 d_b = the nominal diameter of the reinforcing bar

$$\text{Normalized Stress} = \frac{\text{Failure Stress}}{\sqrt{\text{Test-Day Concrete Strength}}} \quad (5.3)$$

$$\text{Normalized Stress} = \text{Failure Stress} * \sqrt{\frac{\text{Design Concrete Strength}}{\text{Test-Day Concrete Strength}}} \quad (5.4)$$

The second normalization technique is a fourth root normalization as recommended by ACI 408R (2003) and Zuo and Darwin (2000). Zuo and Darwin observed from a large international database of beam splice specimens that $f'_c^{1/4}$ best represents the effect of concrete strength on development and splice length. This observation was based on 171 beam specimens with bottom-cast bars not confined by transverse reinforcement (Zuo and Darwin 2000). Using this relationship with bond strength and concrete compressive strength, the peak bond stresses of direct pull-out specimens were divided by the fourth root of the test-day concrete compressive strength as shown in **Equation 5.5**. Similarly, the peak stress developed in the beam splice specimens was normalized by the fourth root of the ratio of the design concrete compressive strength and the actual test-day strength as shown in **Equation 5.6**.

$$\text{Normalized Stress} = \frac{\text{Failure Stress}}{\sqrt[4]{\text{Test-Day Concrete Strength}}} \quad (5.5)$$

$$\text{Normalized Stress} = \text{Failure Stress} * \sqrt[4]{\frac{\text{Design Concrete Strength}}{\text{Test-Day Concrete Strength}}} \quad (5.6)$$

For the VAC control beam splice specimens, the design strength used was 4000 psi (27.58 MPa). For the RCA-50 and RCA-100 beam splice specimens, the design strength was 5500 psi (37.92 MPa). These design strengths were determined from trial batching of the mix designs prior to beam splice specimen construction. On test day, the actual concrete compressive strengths were determined from companion cylinder specimens, and the resulting values are shown in **Tables 5.6**.

Table 5.6: Beam Splice Test Day Compressive Strengths

Cylinder Break	VAC	RAC-50	RAC-100
1	4012	3666	4861
2	4166	3436	4750
3	3823	3571	4919
Average	4000	3558	4843
COV	4.3%	3.2%	1.8%

Conversion: 1 psi = 6.9 kPa

5.4.2. Analysis and Interpretation of Direct Pull-Out Results. The normalized results from the direct pull-out tests are shown in **Table 5.7** below. The table shows the test-day compressive strength used to normalize the peak bond stress prior to pull-out failure for each set of specimens. For the #4 (No. 13) specimens, the average square root and fourth root normalized results for each RCA replacement level are shown in **Figures 5.15** and **5.17**, respectively. For the #6 (No. 19) specimens, the average square root and fourth root normalized results for each RCA replacement level are shown in **Figures 5.19**

and **5.21**, respectively. Boxplots indicating the spread of the data for each normalization technique are shown in **Figures 5.16** and **5.18** for the #4 (No.13) specimens and **Figures 5.20** and **5.22** for the #6 (No.19) specimens.

A comparison of the average square root normalized data for the #4 (No.13) specimens indicates that there was essentially no change in peak bond stress between the VAC and RAC-50 specimens. However, there was a 6.0% increase in the RAC-100 over the VAC specimens. Using the average fourth root normalized data for the #4 (No.13) specimens, there was a slight increase in peak bond stress between the control and both RCA replacement levels. The bond stress increased 7.9% in RAC-50 specimens and 12.9% in the RAC-100 specimens.

A comparison of the average square root normalized data for the #6 (No.19) specimens indicates that there was a 1% decrease in peak bond stress in the RAC-50 specimens over the controls. However, there was a very slight increase in peak bond stress of 0.5% in the RAC-100 specimens over the VAC specimens. Using the average fourth root normalized data for the #6 (No. 19) specimens, there was a slight increase in peak bond stress between the control and both RCA replacement levels. In both RAC-50 and RAC-100 specimens, the average peak bond stress was 7.1% higher than the control.

A parametric statistical analysis was performed on the normalized peak bond stresses between both RCA replacement levels and the control specimens for both normalization techniques. The analysis used an independent, two-sample, student's t-test assuming unequal variances and a 95% confidence interval. An analysis of the square root normalized bond stresses in the #4 (No. 13) pull-out specimens showed that both the 50% and 100% RCA specimens were statistically the same as the control #4 (No.13)

specimens. Likewise, an analysis of the fourth root normalized bond stresses in the #4 (No. 13) pull-out specimens showed that both the 50% and 100% RCA specimens were statistically the same as the control #4 (No.13) specimens. This analysis helps verify that the slight percent increase in bond stress was within the test variability. An analysis of the square root normalized bond stresses in the #6 (No. 19) pull-out specimens showed that both the 50% and 100% RCA specimens were statistically the same as the control #6 (No.13) specimens. Likewise, an analysis of the fourth root normalized bond stresses in the #6 (No. 13) pull-out specimens showed that the 50% RCA specimens were statistically the same as the control #6 (No.13) specimens. However, the student's t-test shows that the percent increase between the 100% RCA specimens and the controls is statistically significant.

Because the data sets are small, a non-parametric analysis was also performed to verify the student's t-test. The Mann-Whitney test was utilized to compare the normalized peak bond stresses between both RCA pull-out sets and the control set with a 95% confidence interval. Analyzing the square root normalized peak bond stresses, this test showed that there was no significant difference from the control in either the 50% RCA specimens or 100% RCA specimens for both #4 (No.13) and #6 (No.19) bars. Likewise, analyzing the fourth root normalized peak bond stresses, this test showed that there was no significant difference from the control in either the 50% RCA specimens or 100% RCA specimens for both #4 (No.13) and #6 (No.19) bars. This analysis reveals that while there was a slight increase in peak bond stress, this increase was not significantly large. A summary of these statistical analyses are provided in Appendix D.

Table 5.7: Normalized Bond Stresses for Pull-Out Specimens

Mix	Bar Size	Specimen	Max. Applied Load (lb)	Bond Stress (psi)	Test Day Strength (psi)	Normalized Bond Stress (Square Root)	Average of Normalized Bond Stress (Square Root)	Normalized Bond Stress (Fourth Root)	Average of Normalized Bond Stress (Fourth Root)
VAC	#4 (No. 13)	VAC-PO4-1	10344	2634	4000	42	43	331	343
		VAC-PO4-2	10435	2657		42		334	
		VAC-PO4-3	11379	2898		46		364	
	#6 (No. 19)	VAC-PO6-1	27172	3075		49	47	387	373
		VAC-PO6-2	25869	2928		46		368	
		VAC-PO6-3	25563	2893		46		364	
RAC-50	#4 (No. 13)	RAC50-PO4-1	12760	3249	5460	44	43	378	370
		RAC50-PO4-2	13083	3332		45		388	
		RAC50-PO4-3	11657	2968		40		345	
	#6 (No. 19)	RAC50-PO6-1	31109	3521		48	46	410	399
		RAC50-PO6-2	28430	3218		44		374	
		RAC50-PO6-3	31440	3558		48		414	
RAC-100	#4 (No. 13)	RAC100-PO4-1	13968	3557	5147	50	46	420	387
		RAC100-PO4-2	12236	3116		43		368	
		RAC100-PO4-3	12451	3171		44		374	
	#6 (No. 19)	RAC100-PO6-1	30302	3429		48	47	405	400
		RAC100-PO6-2	29597	3350		47		395	
		RAC100-PO6-3	29804	3373		47		398	

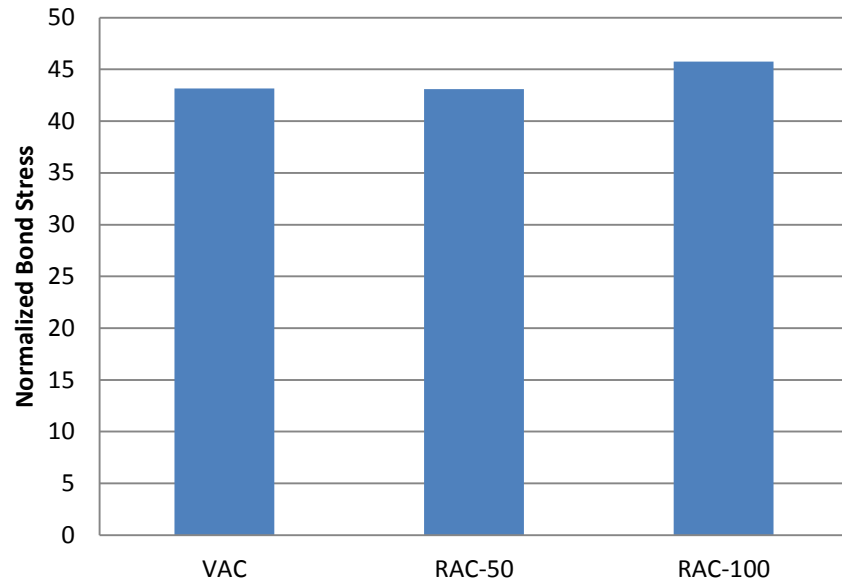


Figure 5.15: Average #4 Pull-Out Bond Stresses by Square Root Normalization

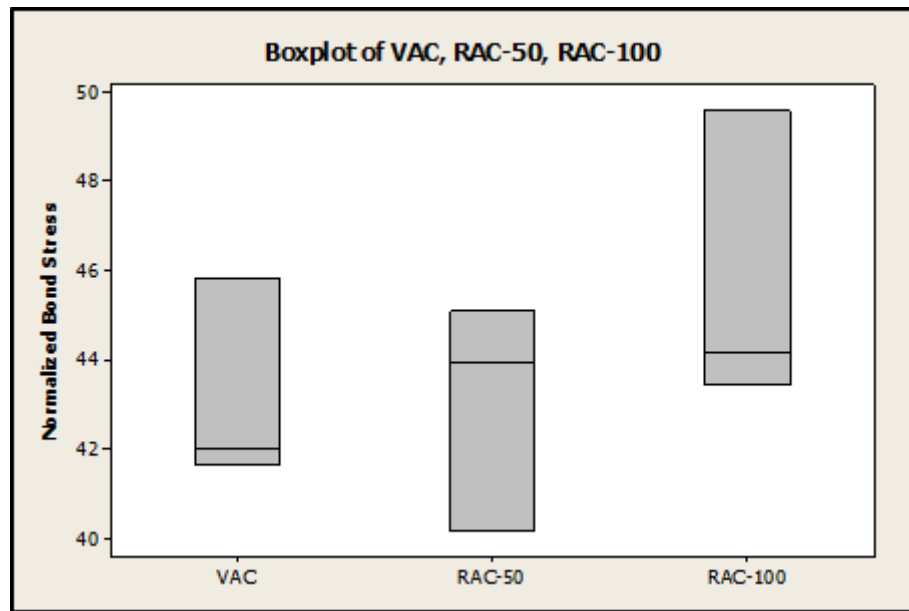


Figure 5.16: Boxplot of #4 Pull-Out Bond Stresses by Square Root Normalization

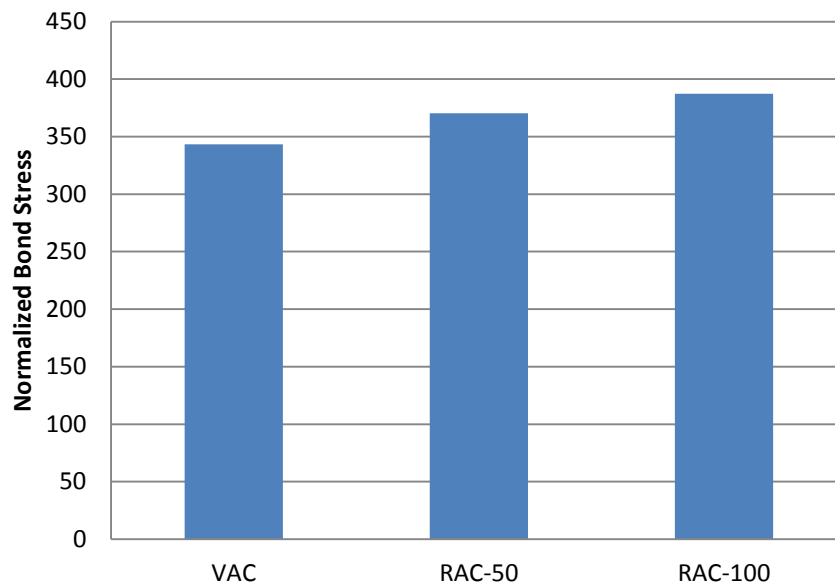


Figure 5.17: Average #4 Pull-Out Bond Stresses by Fourth Root Normalization

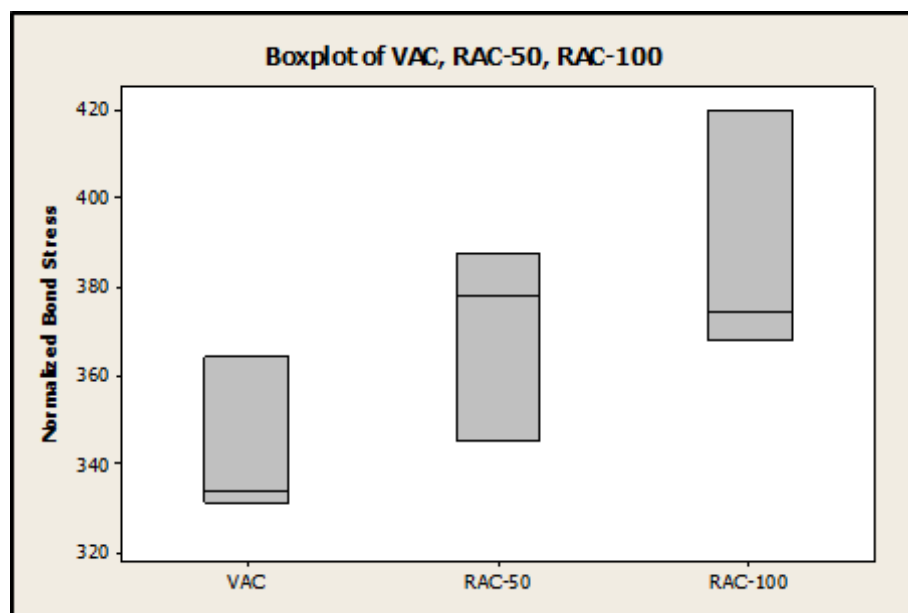


Figure 5.18: Boxplot of #4 Pull-Out Bond Stresses by Fourth Root Normalization

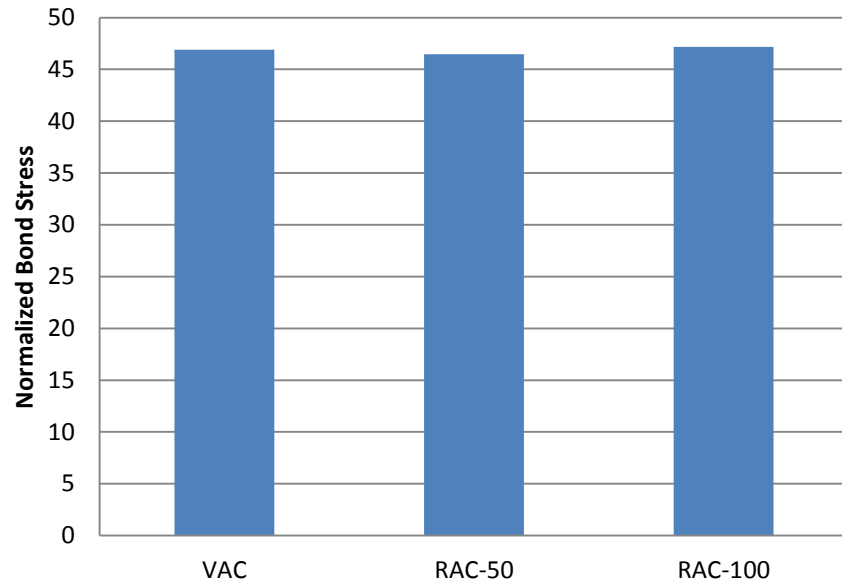


Figure 5.19: Average #6 Pull-Out Bond Stresses by Square Root Normalization

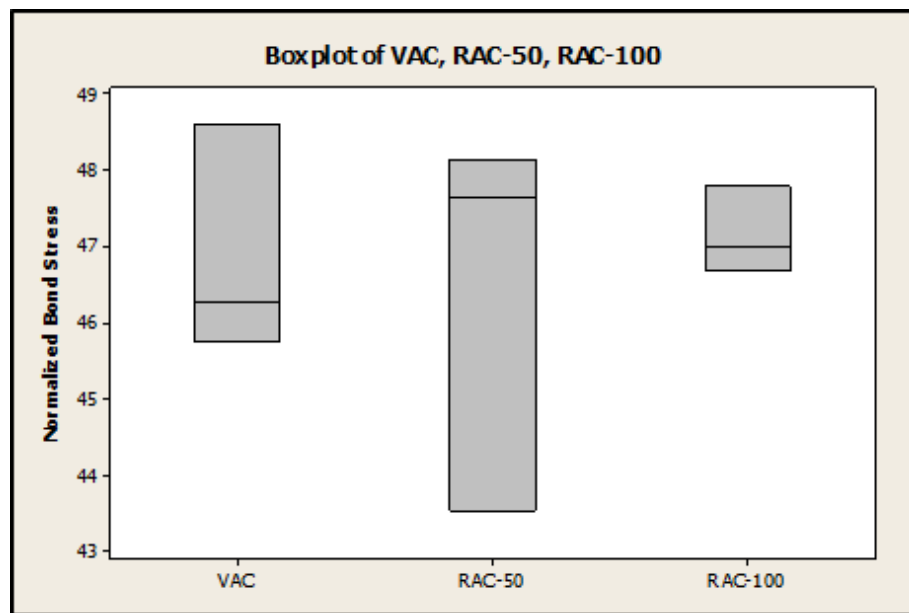


Figure 5.20: Boxplot of #6 Pull-Out Bond Stresses by Square Root Normalization

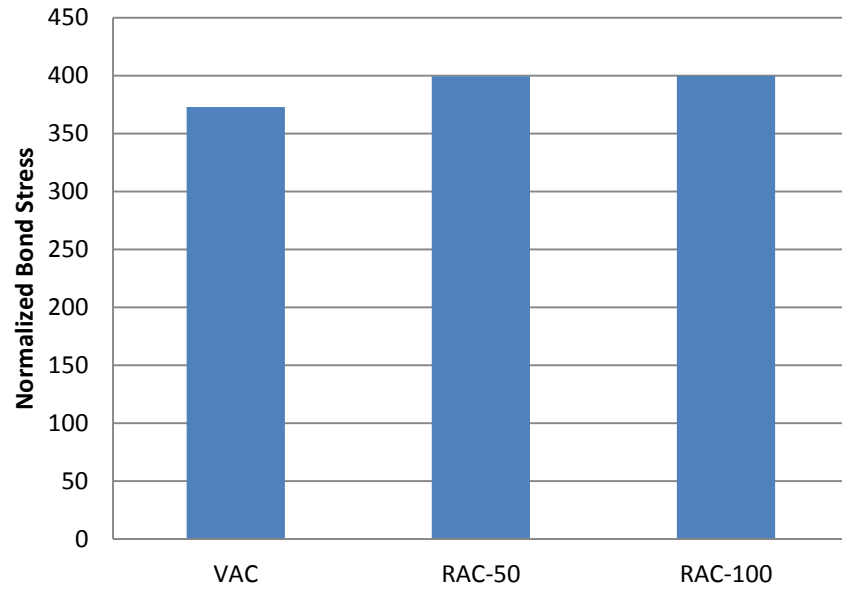


Figure 5.21: Average #6 Pull-Out Bond Stresses by Fourth Root Normalization

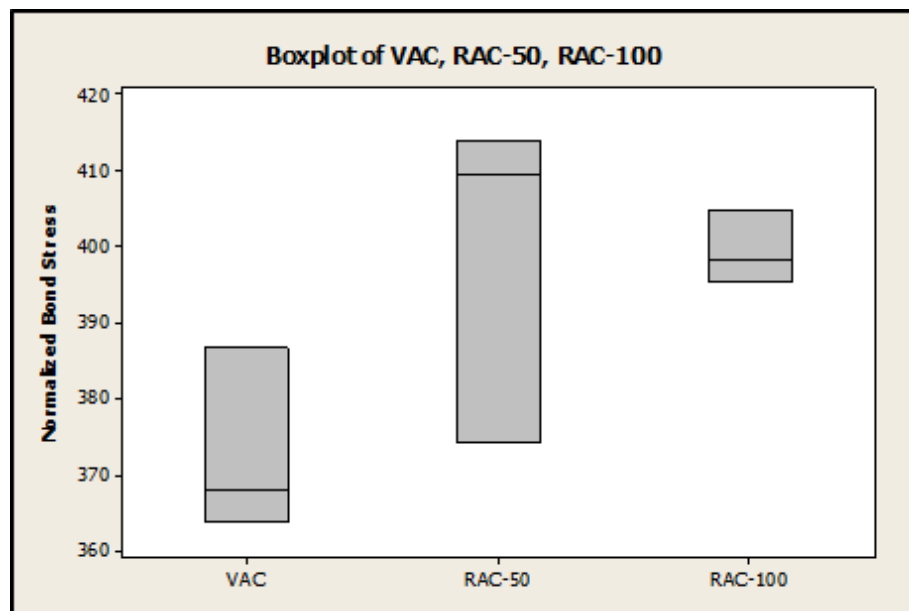


Figure 5.22: Boxplot of #6 Pull-Out Bond Stresses by Fourth Root Normalization

To evaluate the effect of bar size, the average normalized peak bond stresses were compared between the #4 (No. 13) and #6 (No. 19) specimens. In all RCA replacement levels, the #6 (No. 19) specimens exhibited higher bond stresses than the #4 specimens. However, as RCA replacement increases, the percent difference between decreased. The percent difference between #4 (No. 13) and #6 (No. 19) was 8.6%, 7.8%, and 3.1% for the VAC, RAC-50, and RAC-100, respectively. This comparison is shown in **Figure 5.23** for the square root normalized bond stresses and in **Figure 5.24** for the fourth root normalized bond stresses.

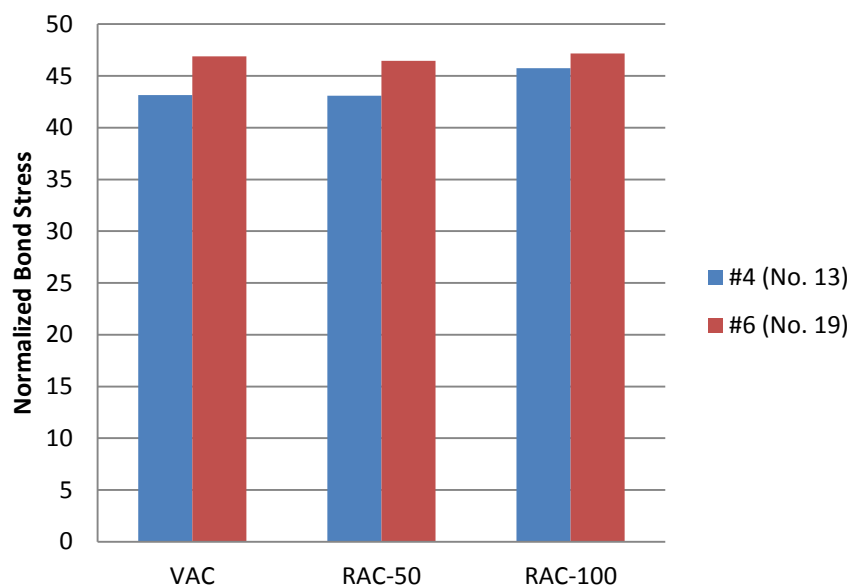


Figure 5.23: Comparison of #4 (No.13) and #6 (No. 19) Square Root Normalized Pull-out Results

5.4.3. Analysis and Interpretation of Beam Splice Results. The normalized results from the beam splice tests are shown in **Table 5.8**. The table shows the test day compressive strength for each set of beams as well as the design strength of the beams. These values were used to normalize the peak stresses developed in the beams prior to bond rupture. The average square root normalized stresses for each set of beams are also plotted in **Figure 5.25**. A boxplot indicating the spread of the square root normalized

beam splice results is provided in **Figure 5.26**. Likewise, the average fourth root normalized stresses for each set of beam are plotted in **Figure 5.27**, and a boxplot indicating the spread of the data is shown in **Figure 5.28**.

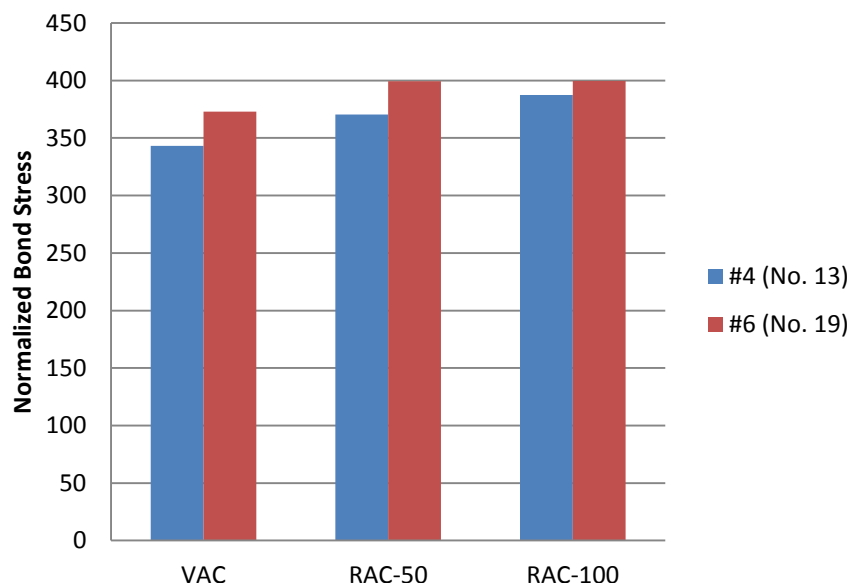


Figure 5.24: Comparison of #4 (No.13) and #6 (No. 19) Fourth Root Normalized Pull-out Results

A comparison of the square root normalized results indicates that 50% RCA beams had a slight increase in developed stress in the steel of 5.9% over the VCA control. However, the 100% RCA beams had a decrease in stress of 16.9% over the VCA control. A comparison of the fourth root normalized results shows that generally, both RCA beam sets had a lower stress in the steel. The 50% RCA beams decreased by 5.0%, and the 100% RCA beams decreased by 19.5%.

A parametric statistical analysis was performed on the normalized peak stresses between both RCA mix beams and the control beams for both normalization techniques. The analysis used an independent, two-sample, student's t-test assuming unequal variances and a 95% confidence interval. For the square root normalized results, the t-test

showed that the 50% RCA beam results are statistically the same as the control beam results. However, the same student's t-test showed that the 100% RCA beam results are different from the control beams under square root normalization. This statistical analysis verifies that the slight percent increase between the 50% RCA beams and the control beams is well within the test variability, whereas the 100% RCA beams exhibited diminished bond strength over the control beams. For the fourth root normalization, the t-test likewise showed that the 50% RCA beam results are statistically the same as the control beam results, and the 100% RCA beam results are different from the control beams. This statistical analysis verifies that the percent difference between the 50% RCA beams and control beams is within the test variability, whereas the 100% RCA beams exhibited diminished bond strength over the control beams. A summary of this parametric statistical analysis is provided in Appendix D.

Given that the data set for each set of beams was small, a non-parametric statistical analysis was performed to validate the student's t-test. The Mann-Whitney test was utilized to compare the normalized peak stresses between both RCA beam sets and the control beam set with a 95% confidence interval. This test verified the results from the student's t-test that there was no difference between the 50% RCA and the control beams under both normalization techniques. However, the test showed that the difference between the 100% RCA and control beams under both normalization techniques was just barely insignificant. A summary of this non-parametric statistical analysis is provided in Appendix D.

Table 5.8: Normalized Developed Stresses for Beam Splice Specimens

Mix	Specimen	Design Strength (psi)	Test Day Strength (psi)	Peak Stress (ksi)	Square Root Normalized Stress (ksi)	Average of Square Root Normalized Stress (ksi)	Fourth Root Normalized Stress (ksi)	Average of Fourth Root Normalized Stress (ksi)
VAC	VAC-1	4000	4000	63.0	63.01	65.13	63.01	65.13
	VAC-2			70.8	70.79		70.79	
	VAC-3			61.6	61.58		61.58	
RAC-50	RAC50-1	5500	3560	56.5	70.28	68.98	63.04	61.87
	RAC50-2			55.2	68.61		61.54	
	RAC50-3			54.8	68.05		61.04	
RAC-100	RAC100-1	5500	4840	47.3	50.46	54.10	48.87	52.40
	RAC100-2			49.9	53.14		51.47	
	RAC100-3			55.1	58.69		56.85	

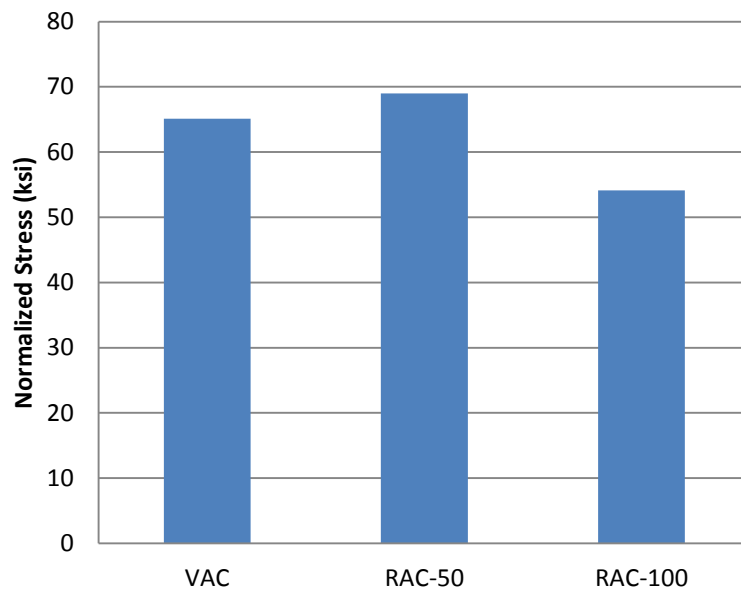


Figure 5.25: Average Beam Splice Peak Stresses by Square Root Normalization

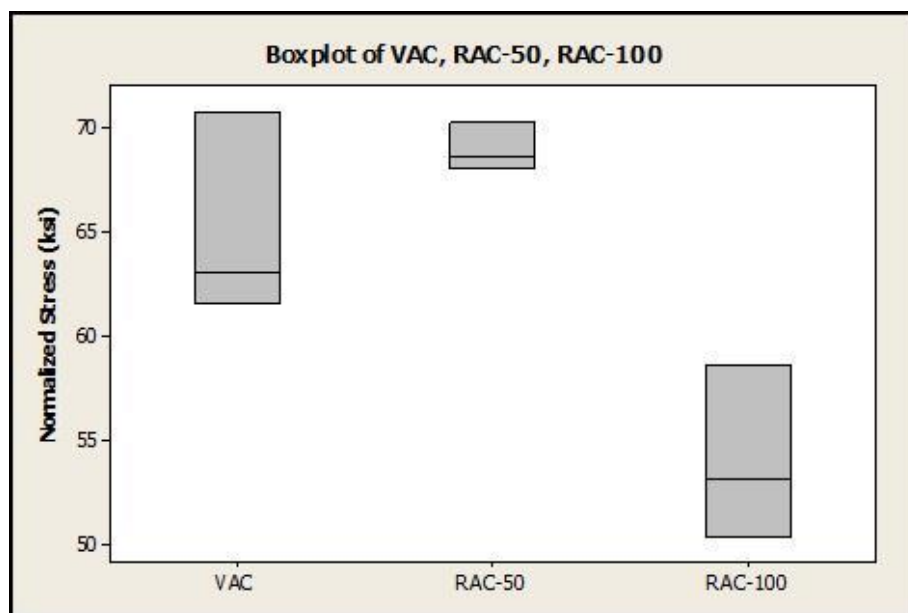


Figure 5.26: Boxplot of Peak Stresses by Square Root Normalization

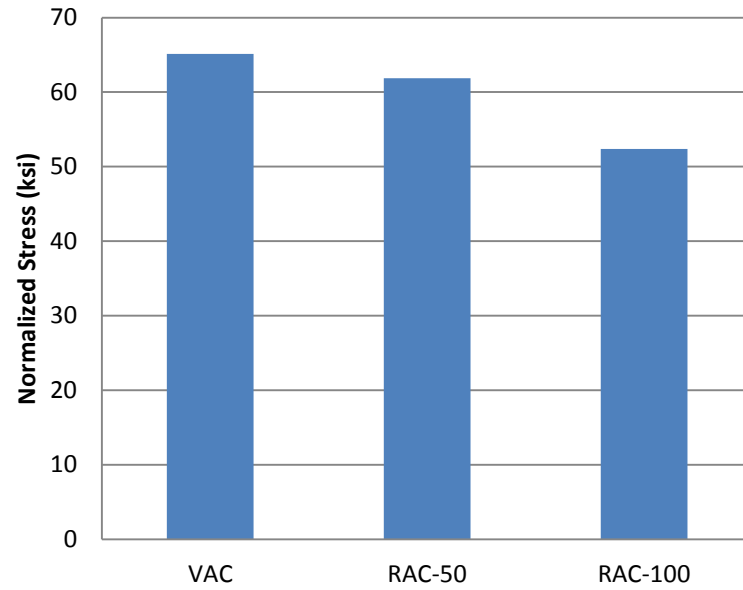


Figure 5.27: Average Beam Splice Peak Stresses by Fourth Root Normalization

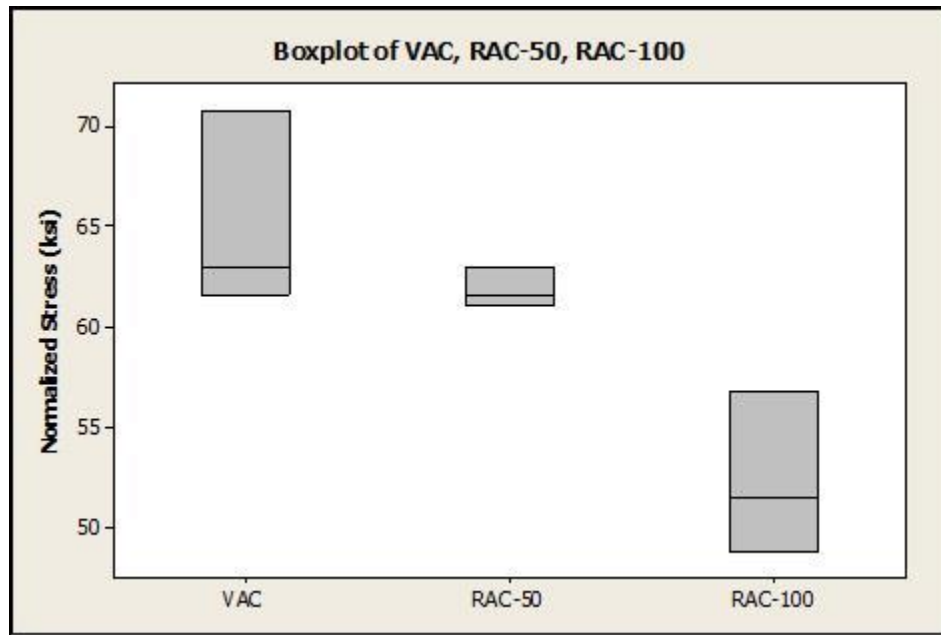


Figure 5.28: Boxplot of Peak Stresses by Fourth Root Normalization

The stress developed in the longitudinal steel was compared to the theoretical values from moment-curvature calculations of the section. This was done in order to further evaluate the validity of the test results and to evaluate the applicability of stress-strain relationships to the 50% and 100% RCA mixes. To calculate the theoretical stress in the longitudinal reinforcement, the moment-curvature program *Response-2000* (Bentz and Collins 2000) was used to evaluate the section under the peak applied moment observed in the specimens. These applied moments were calculated from the average peak loads carried by the beams. Two different stress-strain models were used to describe the concrete. The first was Hognestad's stress-strain relationship, which is recommended by ACI 408R (2003). The second was Popovic, Thorenfeldt and Collins' stress-strain relationship. **Table 5.9** shows the summary of measured and theoretically calculated stress values.

Table 5.9 also shows the ratio of measured to theoretically calculated stress. This ratio provides an indication of how well the measured values were predicted by the theoretical models. The theoretical values slightly underestimated the measured results, as indicated by the ratio values slightly over unity. Despite this small underestimation, the measured stresses were fairly accurately predicted. This analysis indicates that both Hognestad's stress-strain relationship as well as the Popovic, Thorenfeldt and Collins' stress-strain relationship for concrete may be acceptable for use with concrete containing up to 100% RCA replacement for coarse aggregates.

Table 5.9: Comparison of Measured to Theoretical Stress in Beam Splice Specimens

Table reports stress values in ksi

Conversion: 1 ksi = 6.9 MPa

Mix	Specimen	Measured ^a	Average Measured ^a	M- ϕ ^b	Average M- ϕ ^b	$f_{s(\text{measured})}/f_{s(\text{M-}\phi)}$ ^b	M- ϕ ^c	Average M- ϕ ^c	$f_{s(\text{measured})}/f_{s(\text{M-}\phi)}$ ^c
VAC	VAC-1	63.01	65.13	58.5	61.53	1.06	58.5	61.37	1.06
	VAC-2	70.79		63.6			63.5		
	VAC-3	61.58		62.5			62.1		
RAC-50	RAC50-1	56.54	55.50	51.7	48.57	1.14	51.5	48.40	1.15
	RAC50-2	55.20		46.4			46.3		
	RAC50-3	54.75		47.6			47.4		
RAC-100	RAC100-1	47.33	50.75	45.8	48.60	1.04	45.8	49.17	1.03
	RAC100-2	49.85		47.5			47.6		
	RAC100-3	55.06		52.5			54.1		

^a Strain (average from strain gages) multiplied by modulus of elasticity

^b Hognestad stress-strain model (ACI 408R-03 recommended method)

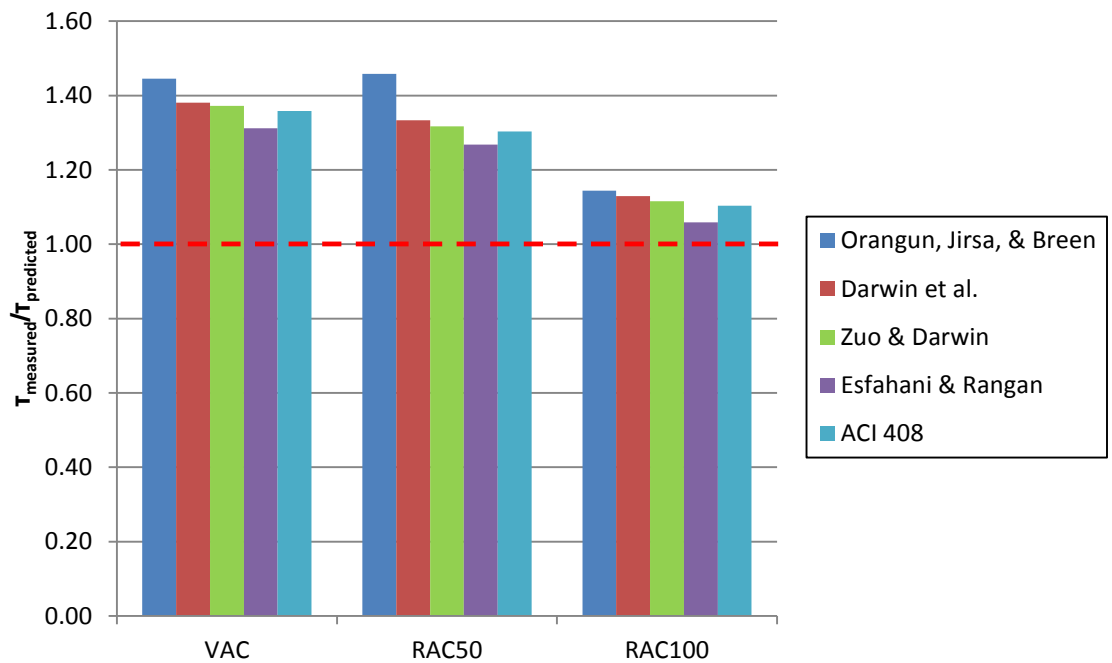
^c Popovic, Thorenfeldt, & Collins stress-strain model

The beam splice results were compared to the bond strength prediction equations summarized in ACI 408R 2003. This was done in order to evaluate if the trend of decreasing bond strength with increasing replacement with RCA could be observed under the normalization techniques used in all of these formulae. Further, this analysis was performed to evaluate how closely RCA concrete bond behavior could be predicted by these equations developed for conventional concrete. The prediction ratios were calculated as the measured bond stress over the calculated bond stress. The measured stresses in the steel were normalized as per the technique adopted by each descriptive equation. These ratios are provided in **Table 5.10**. A graphical representation is provided in **Figure 5.29**.

As shown in **Figure 5.29**, the bond stress generally decreases as the amount of RCA increases. Furthermore, all equations underestimate the bond strength for both VAC and RAC-50 on average, whereas RAC-100 is not as conservatively predicted. The equation in ACI 318 2011 for development and splice length of straight reinforcement in tension is based on the equations provided by Orangun, Jirsa, and Breen (1977). For all three levels of RCA replacement, their technique was the most conservative as it underestimated average bond strengths.

Table 5.10: Prediction Ratios for Beam Splice Results

Specimen	Orangun, Jirsa, & Breen (1977)	Darwin et al. (1992)	Zuo & Darwin (2000)	Esfahani & Rangan (1998)	ACI 408 (2003)
VAC-1	1.40	1.34	1.33	1.27	1.31
VAC-2	1.57	1.50	1.49	1.43	1.48
VAC-3	1.37	1.31	1.30	1.24	1.28
Average	1.45	1.38	1.37	1.31	1.36
RAC50-1	1.49	1.36	1.34	1.29	1.33
RAC50-2	1.45	1.33	1.31	1.26	1.30
RAC50-3	1.44	1.32	1.30	1.25	1.29
Average	1.46	1.33	1.32	1.27	1.30
RAC100-1	1.07	1.05	1.04	0.99	1.03
RAC100-2	1.12	1.11	1.10	1.04	1.08
RAC100-3	1.24	1.23	1.21	1.15	1.20
Average	1.14	1.13	1.12	1.06	1.10

**Figure 5.29: Comparison of Prediction Ratios for Beam Splice Results**

The beam splice results were compared to the bond database 10-2001 provided by ACI Committee 408 (ACI 408R, 2003) in **Figure 5.30**. The plot below shows those beam splice tests results from similar bond specimens with bottom-cast bars and no transverse confinement in the spliced region. This comparison helps validate the test method from this study as falling within the range of data provided by previous bond researchers. For a given compressive strength of concrete, the beam splice results fit well within the scatter of the data. However, due to the large scatter of this historical bond data, it is difficult to draw a conclusion about the trend of bond strength with concrete compressive strength.

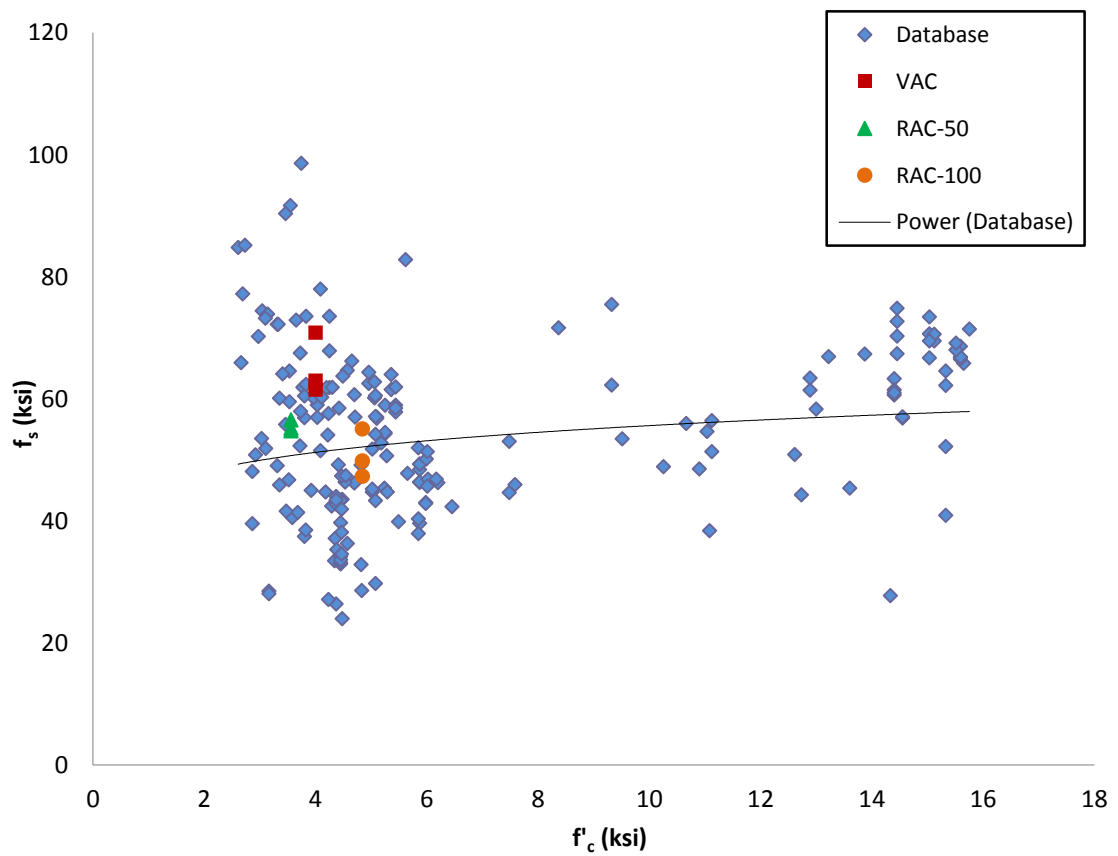


Figure 5.30: Comparison of Beam Splice Results to Database
Conversion: 1 ksi = 6.9 MPa

6. FINDINGS, CONCLUSIONS AND RECOMMENDATIONS

6.1. INTRODUCTION

The objective of this study was to determine the effect of replacing coarse natural aggregates with RCA on the bond strength between deformed steel bars and surrounding concrete. The following section presents the findings, conclusions, and recommendations of this study. The testing program compared mix designs at three different RCA replacement levels, 0%, 50%, and 100%. A standard Missouri Department of Transportation (MoDOT) Class B mix design was used as a baseline mix throughout the study. Two test methods were used to evaluate bond performance. The first method was the direct pull-out test based on the RILEM 7-II-128 *RC6: Bond test for reinforcing steel* (RILEM, 1994). The second method was a full-scale spliced beam tested under third point loading. While the direct pull-out test is a widely used test method for comparing bond performance, the full-scale beam splice specimens are regarded as the most realistic stress state response in evaluating bond performance.

6.2. FINDINGS

6.2.1. Material Properties Testing. All concrete material properties were negatively impacted with increasing replacement of coarse natural aggregates with RCA. The most drastic decreases were seen in splitting tensile strength and fracture energy. The splitting tensile strength decreased 12% and 29% for 50% RCA replacement and 100% RCA replacement, respectively. The fracture energy decreased 14% and 22% for 50% RCA replacement and 100% RCA replacement, respectively.

6.2.2. Direct Pull-Out Testing. A total of 18 direct pull-out specimens were constructed and tested in this study. For each RCA replacement level, three specimens were constructed with a #4 (No. 13) deformed bar and three specimens were constructed with a #6 (No. 19) deformed bar. Comparing average square root normalized data for the #4 (No.13) specimens indicates that there was essentially no difference in peak bond stress between the VAC and RAC-50 specimens and a slight increase of 6.0% in the RAC-100 over the VAC specimens. A comparison of the average square root normalized data for the #6 (No.19) specimens indicates that there was a 1% decrease in peak bond stress in the RAC-50 specimens over the controls and essentially no difference in peak bond stress between the RAC-100 specimens and the VAC specimens.

Comparing the fourth root normalized data for the #4 (No.13) specimens, there was a slight increase in peak bond stress between the control and both RCA replacement levels. The bond stress increased 7.9% in RAC-50 specimens and 12.9% in the RAC-100 specimens. Likewise, comparing the fourth root normalized data for the #6 (No. 19) specimens, there was a slight increase in peak bond stress between the control and both RCA replacement levels. In both RAC-50 and RAC-100 specimens, the average peak bond stress was 7.1% higher than the control.

In all RCA replacement levels, the #6 (No. 19) specimens exhibited higher bond stresses than the #4 specimens. However, as RCA replacement increases, the percent difference between decreased. The percent difference between #4 (No. 13) and #6 (No. 19) was 8.6%, 7.8%, and 3.1% for the VAC, RAC-50, and RAC-100, respectively.

6.2.3. Beam Splice Testing. Three beam splice specimens were constructed and tested for each RCA replacement level. Deformed #6 (No. 19) steel bars were used as

longitudinal reinforcement and no confinement was provided in the spliced region. All beams were cast with longitudinal reinforcement in the bottom of the beam. A comparison of the square root normalized results indicates that 50% RCA beams had a slight increase in developed stress in the steel of 5.9% over the VAC control. However, the 100% RCA beams had a decrease in stress of 16.9% over the VAC control. A comparison of the fourth root normalized results shows that generally, both RCA beam sets had a lower stress in the steel. The 50% RCA beams decreased by 5.0%, and the 100% RCA beams decreased by 19.5%.

6.3. CONCLUSIONS

6.3.1. Direct Pull-Out Testing. Analysis of the direct pull-out data indicates that both 50% and 100% RCA mixes performed comparably or had a slight improvement in bond capacity over the controls. However, a statistical analysis indicates that all mixes performed comparably when normalized by the square root of concrete compressive strength for both #4 (No. 13) and #6 (No. 19) specimens. When normalized by the fourth root of concrete compressive strength, #4 (No. 13) specimens performed comparably across all three mixes, and #6 (No. 19) specimens were comparable between the 50% RCA and control mixes. Only the #6 (No. 19) specimens had a statistically significant difference between the 100% RCA and control mixes, with the 100% RCA showing a 7.1% increase in bond strength.

6.3.2. Beam Splice Testing. Analysis of the beam splice data indicates that both 50% and 100% RCA specimens exhibited diminished bond strength over the control specimens. A statistical analysis indicates that when normalized by either the square root

or fourth root of concrete compressive strength, the 50% RCA specimens performed comparably to the control specimens. However, the 100% RCA specimens exhibited a statistically significant decrease in bond strength from the control specimens, 16.9% based on the square root normalization and 19.5% based on the fourth root normalization. This decrease in bond strength parallels the decrease in splitting tensile strength, 29%, and fracture energy, 22%, both of which are related to the tensile response of the concrete, which governs bond failures where splitting cracks control. These findings indicate that replacing more than 50% of the coarse natural aggregates with RCA may require some modification to the bond and development length to achieve sufficient bond strength between deformed steel reinforcing bars and the surrounding concrete.

6.4. RECOMMENDATIONS

Due to the limited number of studies into the bond behavior of RCA, further research is needed to make comparisons and conclusions across a larger database. To better understand the influence of RCA replacement on the bond behavior of reinforced concrete, additional variables important to design must also be investigated. A list of the testable variables relating to the structural characteristics and bar properties of the reinforced member is given below:

- Perform tests with wider variation in bar sizes to investigate bar size effect
- Perform tests with smooth bars and deformed bars with different rib heights to develop relationship between rib height and bond strength
- Perform tests with different surface deterioration and cleanliness
- Perform tests with epoxy or zinc coated bars

- Perform studies with transverse reinforcement provided in the spliced region to investigate effect of confinement
- Perform studies with splice region cast with more than 12 in. (30.5 cm) of concrete below to investigate “top bar” effect
- Perform tests with noncontact lap splices to evaluate performance with contact lap splices

Testable variables relating to the RCA material itself are listed below:

- Perform studies on RCA from different source structures (pavements, building structures, bridge structures, etc.)
- Perform studies on RCA from different source locations (different geographical regions of the United States)
- Perform studies on RCA from different parent rock material
- Perform studies with varied amounts of chloride contamination
- Perform studies with varied amounts of organic impurities
- Perform studies with varied amounts of fine RCA

APPENDIX A: DIRECT PULL-OUT TEST DATA PLOTS

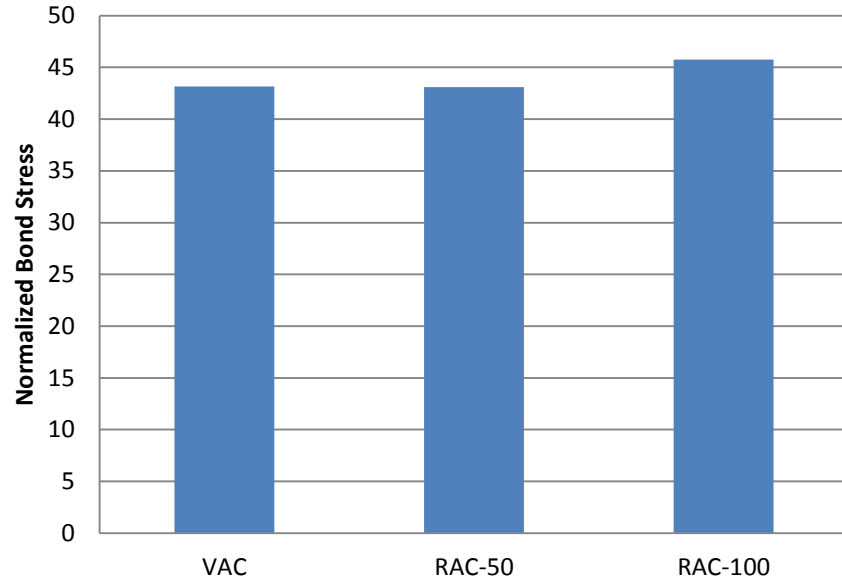


Figure A.1: Bond Stresses for #4 Pull-Out Specimens, Square Root Normalization

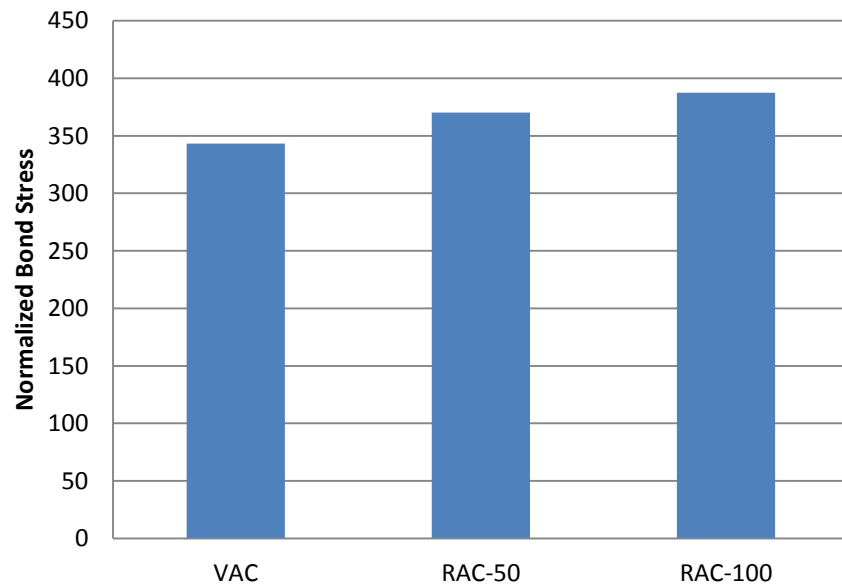


Figure A.2: Bond Stresses for #4 Pull-Out Specimens, Fourth Root Normalization

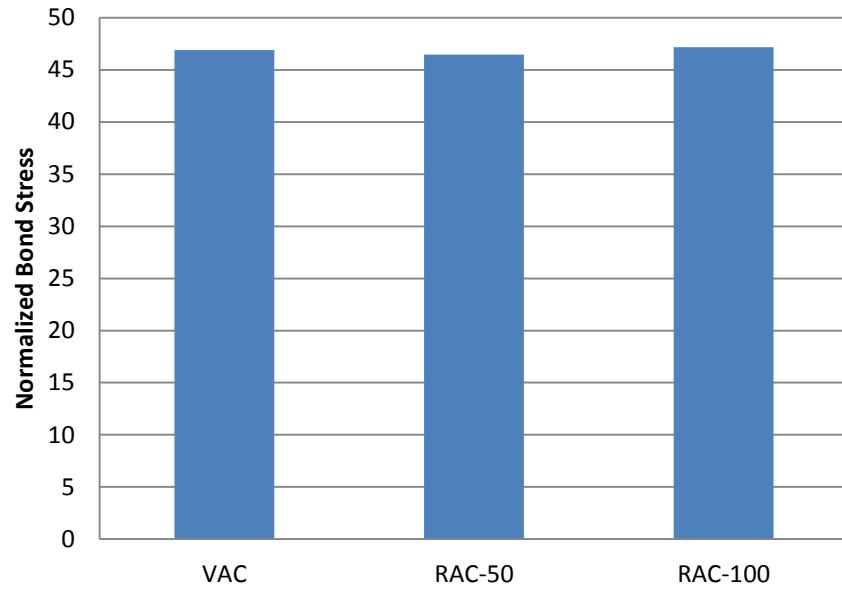


Figure A.3: Bond Stresses for #6 Pull-Out specimens, Square Root Normalization

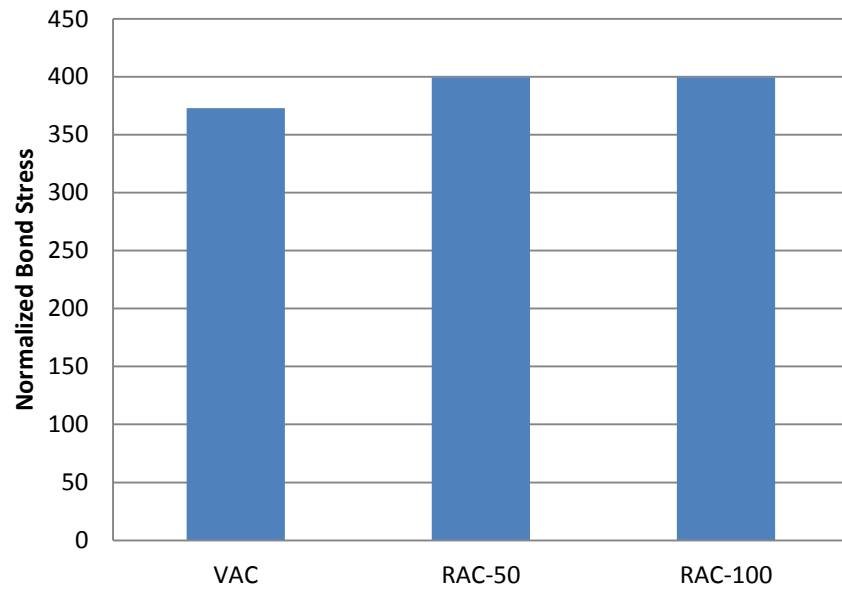


Figure A.4: Bond Stresses for #6 Pull-Out Specimens, Fourth Root Normalization

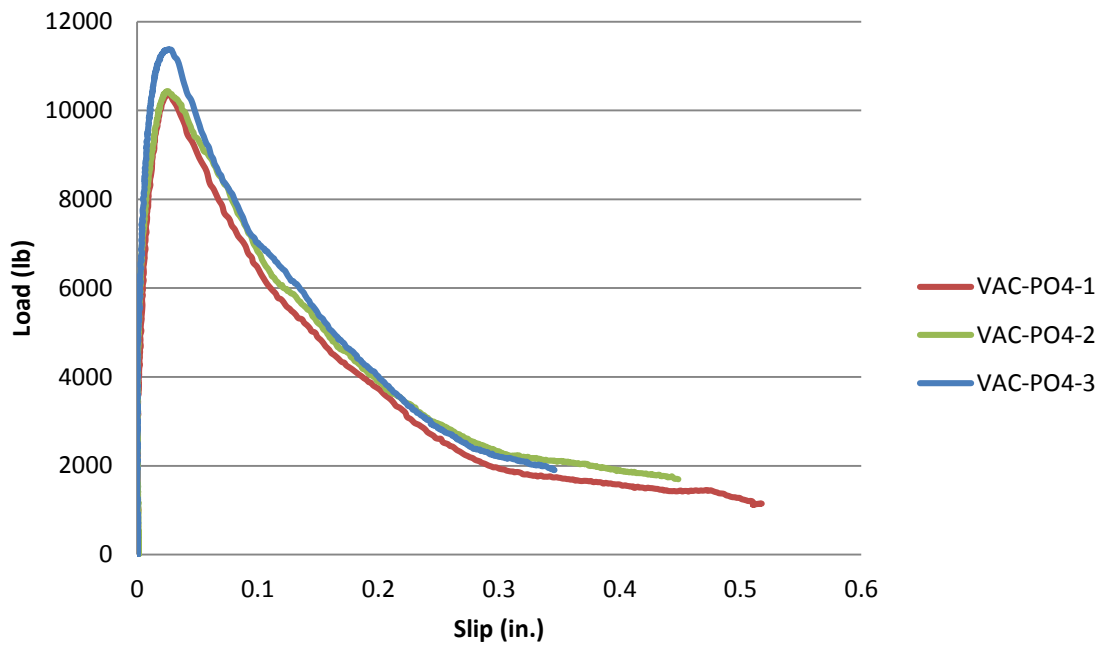


Figure A.5: Applied Load vs. Slip Plot for #4 (No. 13) VAC-PO4
Conversion: 1 in. = 25.4 mm
1 lb. = 4.45 N

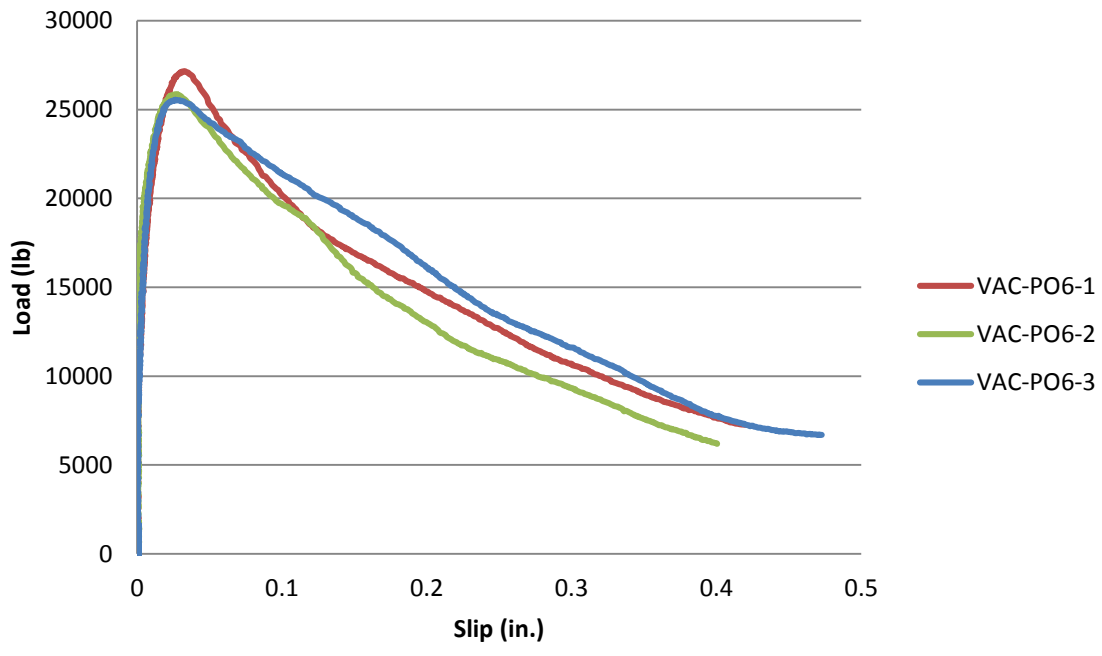


Figure A.6: Applied Load vs. Slip Plot for #6 (No. 19) VAC-PO6
Conversion: 1 in. = 25.4 mm
1 lb. = 4.45 N

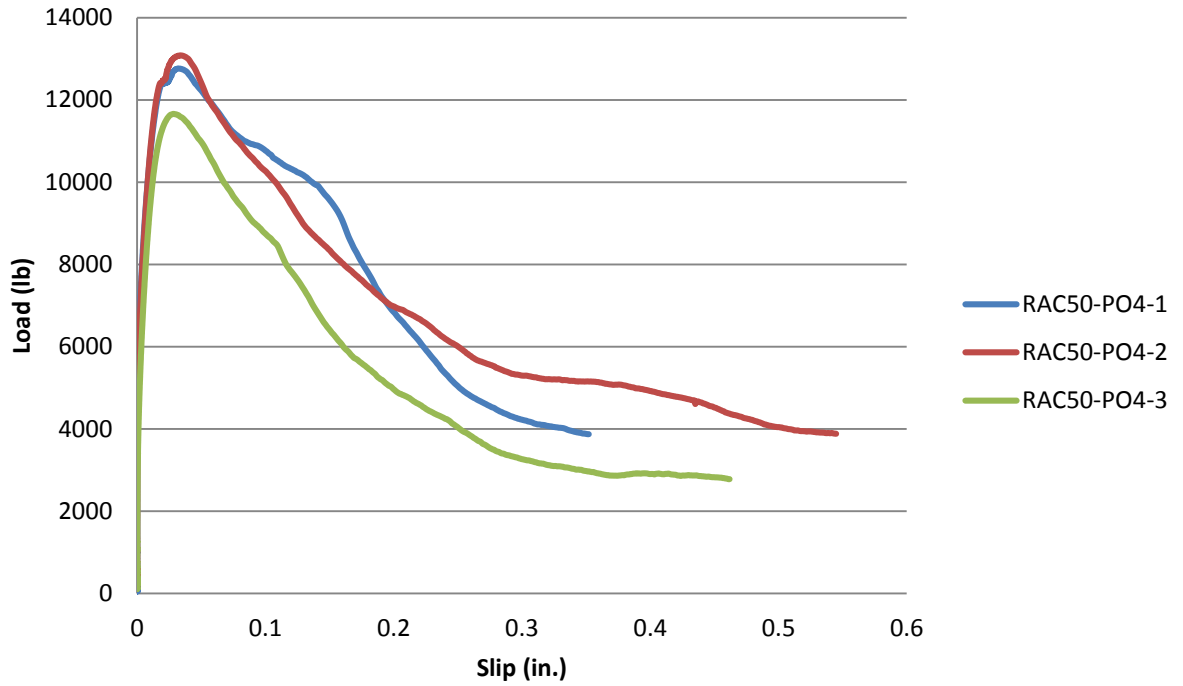


Figure A.7: Applied Load vs. Slip Plot for #4 (No. 13) RCA50-PO4
 Conversion: 1 in. = 25.4 mm
 1 lb. = 4.45 N

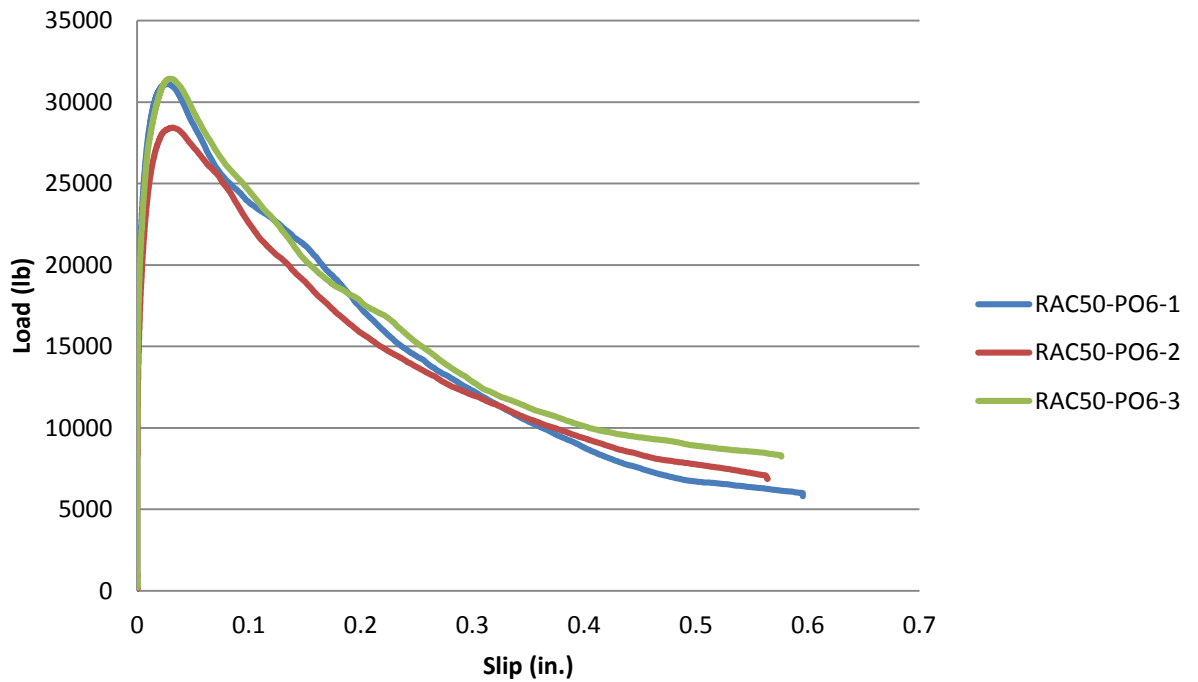


Figure A.8: Applied Load vs. Slip Plot for #6 (No. 19) RCA50-PO6
 Conversion: 1 in. = 25.4 mm
 1 lb. = 4.45 N

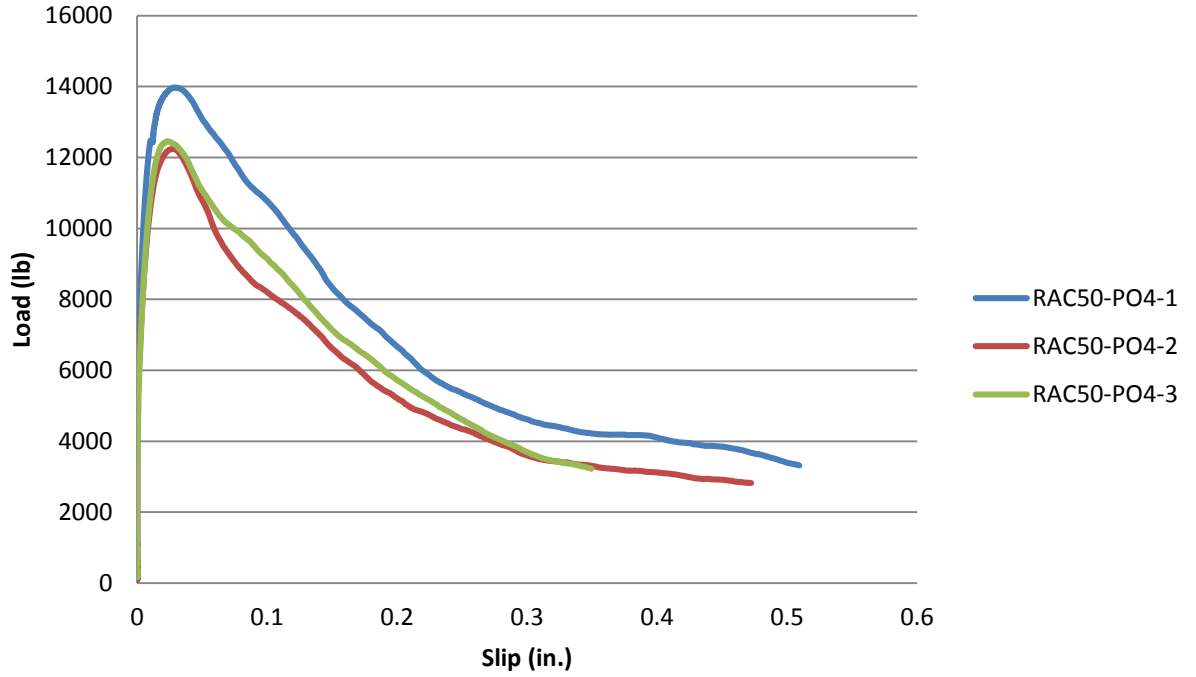


Figure A.9: Applied Load vs. Slip Plot for #4 (No. 13) RCA100-PO4

Conversion: 1 in. = 25.4 mm

1 lb. = 4.45 N

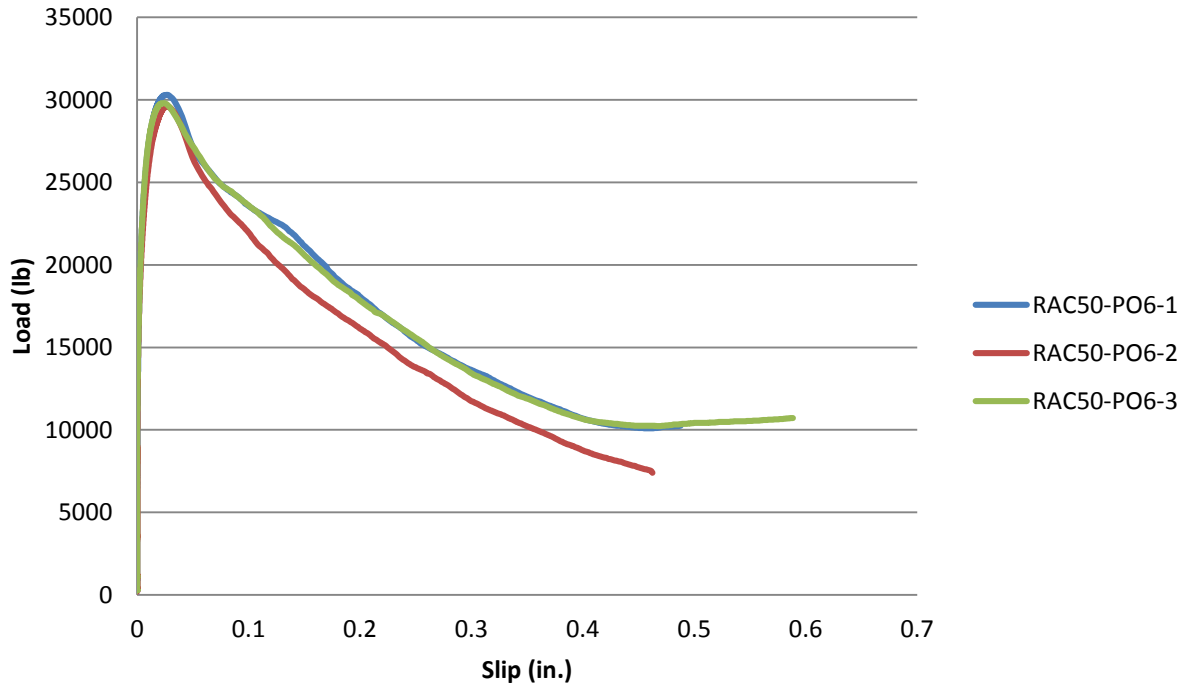


Figure A.10: Applied Load vs. Slip Plot for #6 (No. 19) RCA100-PO6

Conversion: 1 in. = 25.4 mm

1 lb. = 4.45 N

APPENDIX B: BEAM SPLICE TEST DATA PLOTS

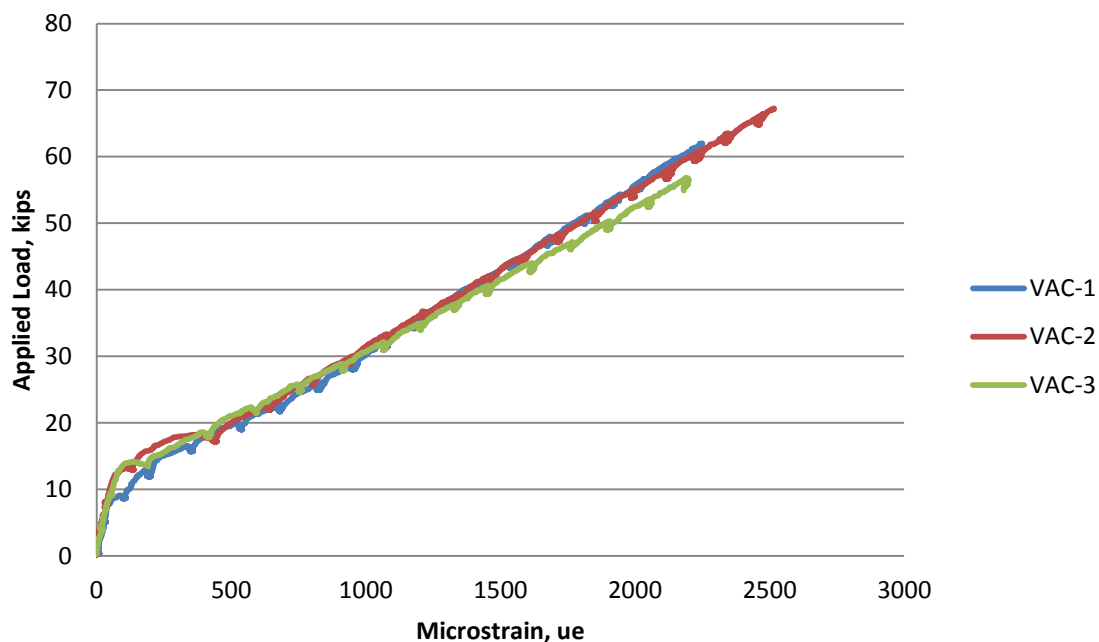


Figure B.1: Applied Load vs. Strain for VAC Specimens

Conversion: 1 kip = 4.45 kN

Note: Average of all gauges per specimen.

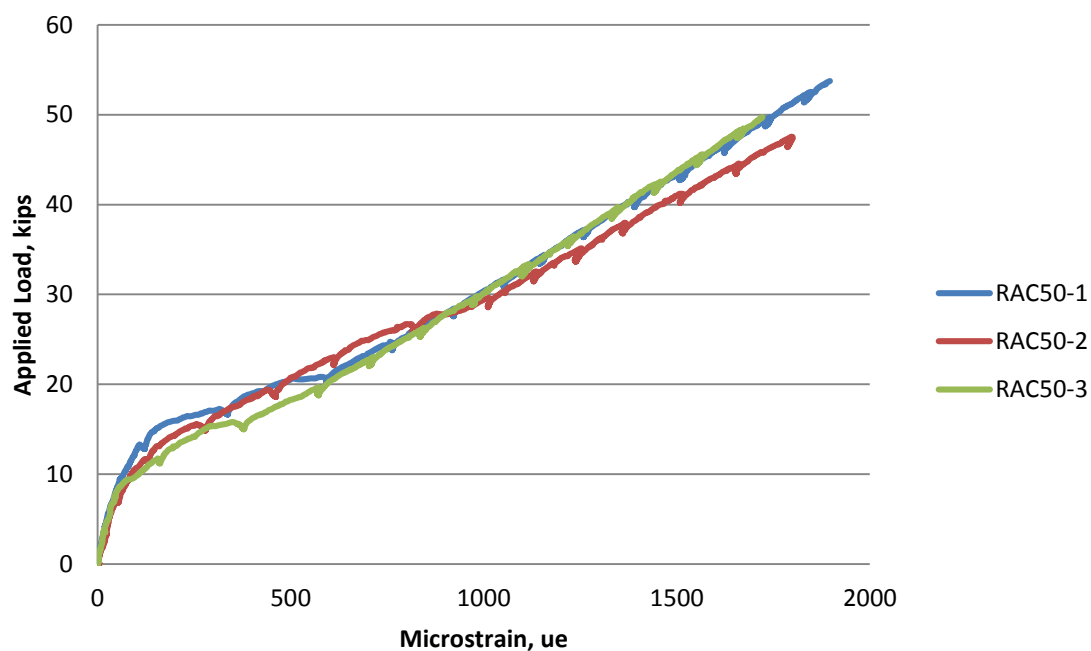


Figure B.2: Applied Load vs. Strain for RAC-50 Specimens

Conversion: 1 kip = 4.45 kN

Note: Average of all gauges per specimen.

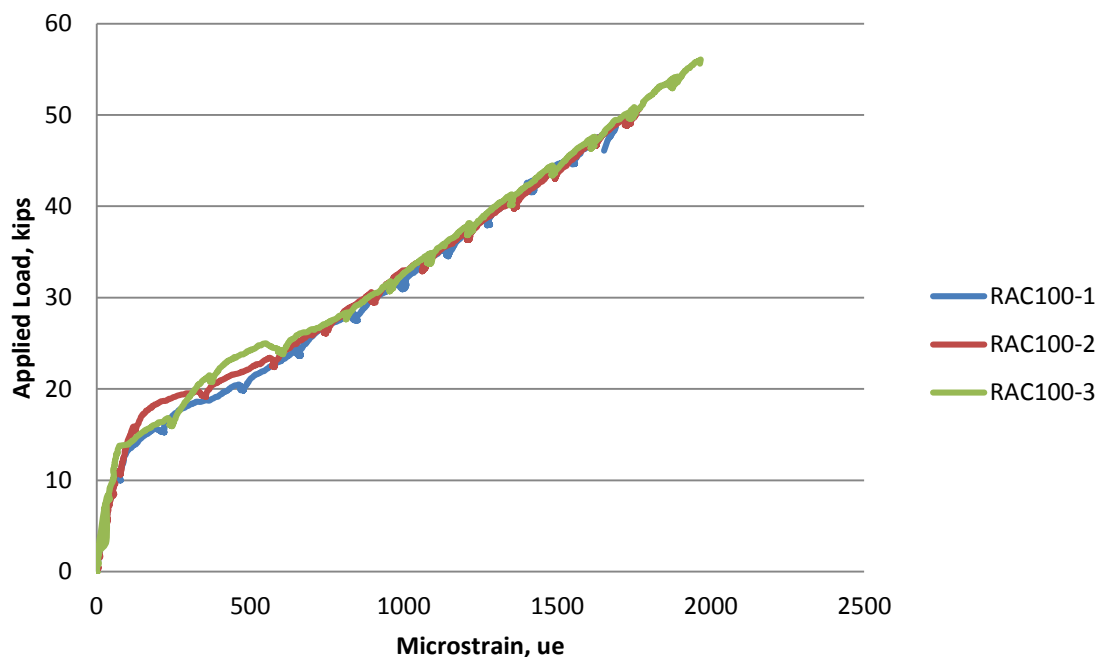


Figure B.3: Applied Load vs. Strain for RAC-100 Specimens

Conversion: 1 kip = 4.45 kN

Note: Average of all gauges per specimen.

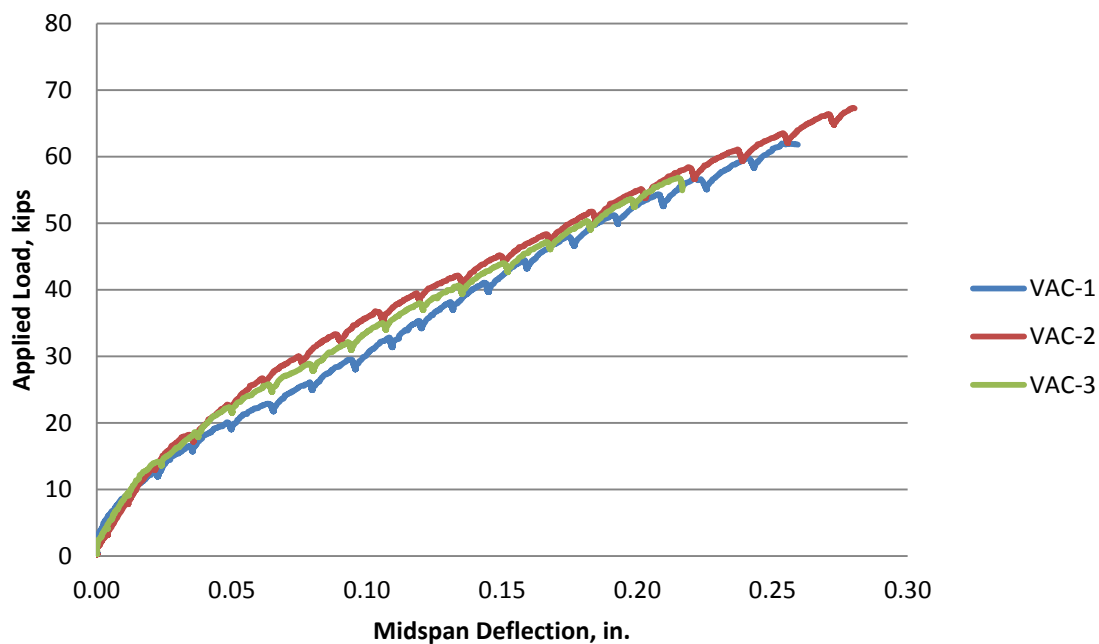


Figure B.4: Applied load vs. Midspan Deflection for VAC

Conversion: 1 in. = 25.4 mm

1 kip = 4.45 kN

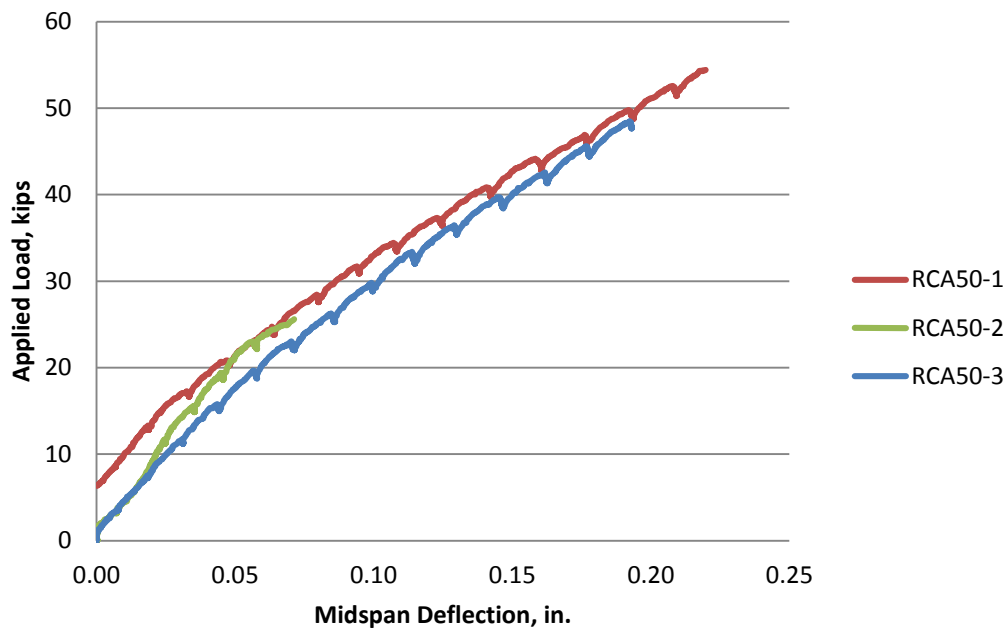


Figure B.5: Applied load vs. Midspan Deflection for RAC-50

Conversion: 1 in. = 25.4 mm

1 kip = 4.45 kN

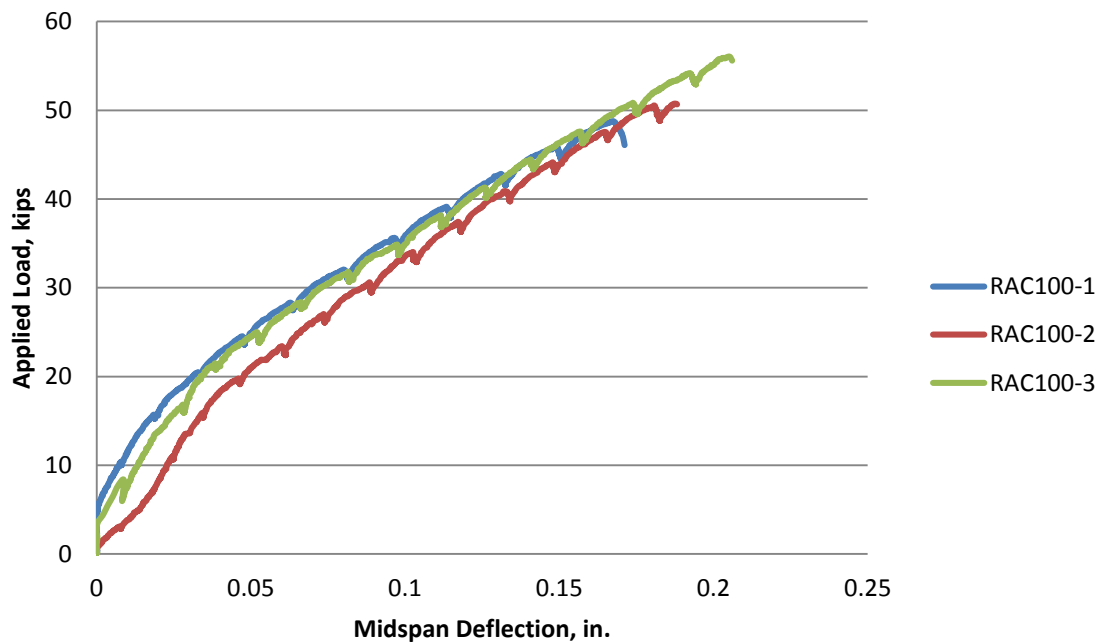


Figure B.6: Applied load vs. Midspan Deflection for RAC-100

Conversion: 1 in. = 25.4 mm

1 kip = 4.45 kN

APPENDIX C: PHOTOGRAPHS OF BEAM SPLICE FAILURES



Figure C.3: Side View of VAC-2



Figure C.4: Bottom View of VAC-2



Figure C.5: Side View of VAC-3



Figure C.6: Bottom View of VAC-3

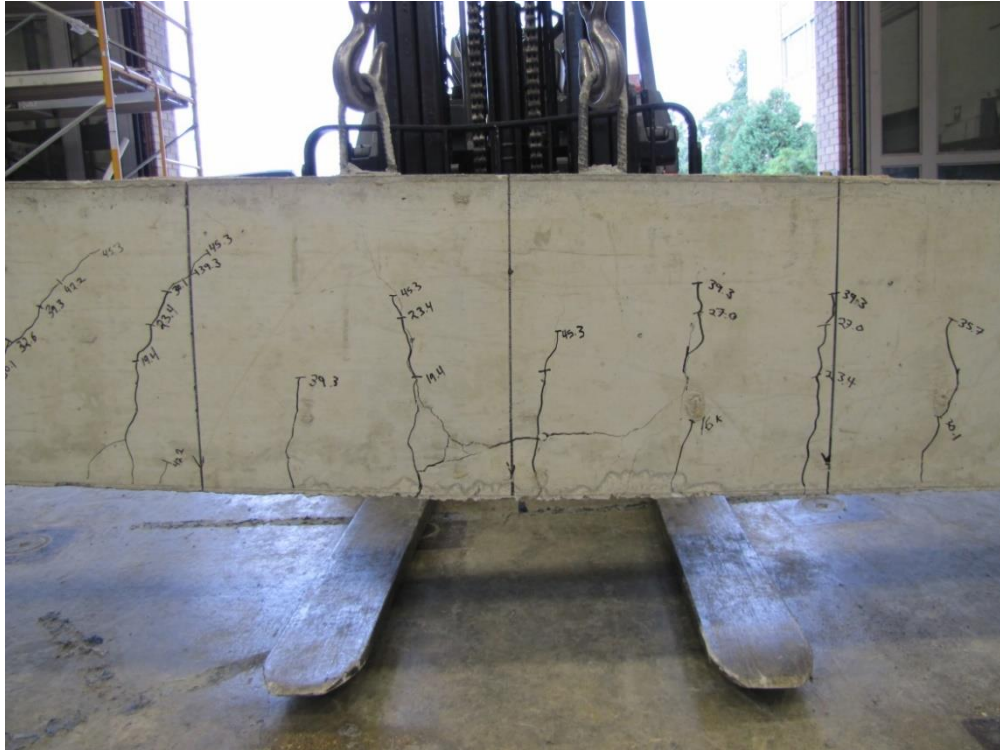




Figure C.9: Side View of RAC50-2



Figure C.10: Bottom View of RAC50-2



Figure C.11: Side View of RAC50-3



Figure C.12: Bottom View of RAC50-3



Figure C.13: Side View of RAC100-1



Figure C.14: Bottom View of RAC100-1



Figure C.15: Side View of RAC100-2



Figure C.16: Bottom View of RAC100-2



Figure C.17: Side View of RAC100-3



Figure C.18: Bottom View of RAC100-3

APPENDIX D: STATISTICAL ANALYSIS OF RESULTS

Table D.1: Parametric Analysis of #4 (No.13) Pull-Out Results with Square Root Normalization between VAC and RAC-50

t-Test: Two-Sample Assuming Unequal Variances

	VAC	RAC-50
Mean	43.15965	43.07783
Variance	5.324474	6.639769
Observations	3	3
Hypothesized Mean Difference	0	
df	4	
t Stat	0.040971	
P(T<=t) one-tail	0.484641	
t Critical one-tail	2.131847	
P(T<=t) two-tail	0.969283	
t Critical two-tail	2.776445	

Table D.2: Non-parametric Analysis of #4 (No.13) Pull-Out Results with Square Root Normalization between VAC and RAC-50

Mann-Whitney Test and CI: VAC, RAC-50	
N Median	
VAC	3 42.015
RAC-50	3 43.974
Point estimate for ETA1-ETA2 is 0.729	
91.9 Percent CI for ETA1-ETA2 is (-3.438,5.645)	
W = 11.0	
Test of ETA1 = ETA2 vs ETA1 not = ETA2 is significant at 1.0000	

Table D.3: Parametric Analysis of #4 (No.13) Pull-Out Results with Square Root Normalization between VAC and RAC-100

t-Test: Two-Sample Assuming Unequal Variances

	<i>VAC</i>	<i>RAC-100</i>
Mean	43.15965	45.73487
Variance	5.324474	11.22826
Observations	3	3
Hypothesized Mean Difference	0	
df	4	
t Stat	-1.09633	
P(T<=t) one-tail	0.167254	
t Critical one-tail	2.131847	
P(T<=t) two-tail	0.334509	
t Critical two-tail	2.776445	

Table D.4: Non-parametric Analysis of #4 (No.13) Pull-Out Results with Square Root Normalization between VAC and RAC-100

Mann-Whitney Test and CI: VAC, RAC-100	
	N Median
VAC	3 42.015
RAC-100	3 44.194
Point estimate for ETA1-ETA2 is -2.180	
91.9 Percent CI for ETA1-ETA2 is (-7.932,2.384)	
W = 8.0	
Test of ETA1 = ETA2 vs ETA1 not = ETA2 is significant at 0.3827	

Table D.5: Parametric Analysis of #6 (No.19) Pull-Out Results with Square Root Normalization between VAC and RAC-50

t-Test: Two-Sample Assuming Unequal Variances

	VAC	RAC-50
Mean	46.88684	46.44951
Variance	2.337816	6.39148
Observations	3	3
Hypothesized Mean Difference	0	
df	3	
t Stat	0.256377	
P(T<=t) one-tail	0.407118	
t Critical one-tail	2.353363	
P(T<=t) two-tail	0.814236	
t Critical two-tail	3.182446	

Table D.6: Non-Parametric Analysis of #6 (No.19) Pull-Out Results with Square Root Normalization between VAC and RAC-50

Mann-Whitney Test and CI: VAC, RAC-50	
N	Median
VAC 3	46.292
RAC-50 3	47.648
Point estimate for ETA1-ETA2 is 0.469	
91.9 Percent CI for ETA1-ETA2 is (-2.410,5.080)	
W = 11.0	
Test of ETA1 = ETA2 vs ETA1 not = ETA2 is significant at 1.0000	

Table D.7: Parametric Analysis of #6 (No.19) Pull-Out Results with Square Root Normalization between VAC and RAC-100

t-Test: Two-Sample Assuming Unequal Variances

	VAC	RAC-100
Mean	46.88684	47.17004
Variance	2.337816	0.32679
Observations	3	3
Hypothesized Mean Difference	0	
df	3	
t Stat	-0.30049	
P(T<=t) one-tail	0.391712	
t Critical one-tail	2.353363	
P(T<=t) two-tail	0.783424	
t Critical two-tail	3.182446	

Table D.8: Non-Parametric Analysis of #6 (No.19) Pull-Out Results with Square Root Normalization between VAC and RAC-100

Mann-Whitney Test and CI: VAC, RAC-100	
N	Median
VAC 3	46.292
RAC-100 3	47.017
Point estimate for ETA1-ETA2 is -0.725	
91.9 Percent CI for ETA1-ETA2 is (-2.057,1.933)	
W = 9.0	
Test of ETA1 = ETA2 vs ETA1 not = ETA2 is significant at 0.6625	

Table D.9: Parametric Analysis of #4 (No.13) Pull-Out Results with Fourth Root Normalization between VAC and RAC-50

t-Test: Two-Sample Assuming Unequal Variances

	VAC	RAC-50
Mean	343.236	370.2985
Variance	336.7493	490.6246
Observations	3	3
Hypothesized Mean Difference	0	
df	4	
t Stat	-1.62959	
P(T<=t) one-tail	0.089261	
t Critical one-tail	2.131847	
P(T<=t) two-tail	0.178522	
t Critical two-tail	2.776445	

Table D.10: Non-parametric Analysis of #4 (No.13) Pull-Out Results with Fourth Root Normalization between VAC and RAC-50

Mann-Whitney Test and CI: VAC, RAC-50	
N	Median
VAC 3	334.13
RAC-50 3	378.00
Point estimate for ETA1-ETA2 is -23.21	
91.9 Percent CI for ETA1-ETA2 is (-56.36,19.04)	
W = 7.0	
Test of ETA1 = ETA2 vs ETA1 not = ETA2 is significant at 0.1904	

Table D.11: Parametric Analysis of #4 (No.13) Pull-Out Results with Fourth Root Normalization between VAC and RAC-100

t-Test: Two-Sample Assuming Unequal Variances

	VAC	RAC-100
Mean	343.236	387.3789
Variance	336.7493	805.5445
Observations	3	3
Hypothesized Mean Difference	0	
df	3	
t Stat	-2.26221	
P(T<=t) one-tail	0.054352	
t Critical one-tail	2.353363	
P(T<=t) two-tail	0.108704	
t Critical two-tail	3.182446	

Table D.12: Non-parametric Analysis of #4 (No.13) Pull-Out Results with Fourth Root Normalization between VAC and RAC-100

Mann-Whitney Test and CI: VAC, RAC-100	
N	Median
VAC	3 334.13
RAC-100	3 374.33
Point estimate for ETA1-ETA2 is -40.20	
91.9 Percent CI for ETA1-ETA2 is (-88.70,-3.51)	
W = 6.0	
Test of ETA1 = ETA2 vs ETA1 not = ETA2 is significant at 0.0809	

Table D.13: Parametric Analysis of #6 (No.19) Pull-Out Results with Fourth Root Normalization between VAC and RAC-50

t-Test: Two-Sample Assuming Unequal Variances

	VAC	RAC-50
Mean	372.8773	399.2816
Variance	147.8565	472.2781
Observations	3	3
Hypothesized Mean Difference	0	
df	3	
t Stat	-1.83651	
P(T<=t) one-tail	0.081803	
t Critical one-tail	2.353363	
P(T<=t) two-tail	0.163606	
t Critical two-tail	3.182446	

Table D.14: Non-Parametric Analysis of #6 (No.19) Pull-Out Results with Fourth Root Normalization between VAC and RAC-50

Mann-Whitney Test and CI: VAC, RAC-50	
N	Median
VAC 3	368.15
RAC-50 3	409.59
Point estimate for ETA1-ETA2 is -27.25	
91.9 Percent CI for ETA1-ETA2 is (-50.14,12.37)	
W = 7.0	
Test of ETA1 = ETA2 vs ETA1 not = ETA2 is significant at 0.1904	

Table D.15: Parametric Analysis of #6 (No.19) Pull-Out Results with Fourth Root Normalization between VAC and RAC-100

t-Test: Two-Sample Assuming Unequal Variances

	VAC	RAC-100
Mean	372.8773	399.5349
Variance	147.8565	23.44476
Observations	3	3
Hypothesized Mean Difference	0	
df	3	
t Stat	-3.52778	
P(T<=t) one-tail	0.01935	
t Critical one-tail	2.353363	
P(T<=t) two-tail	0.038701	
t Critical two-tail	3.182446	

Table D.16: Non-Parametric Analysis of #6 (No.19) Pull-Out Results with Fourth Root Normalization between VAC and RAC-100

Mann-Whitney Test and CI: VAC, RAC-100	
N	Median
VAC	3 368.15
RAC-100	3 398.24
Point estimate for ETA1-ETA2 is -30.09	
91.9 Percent CI for ETA1-ETA2 is (-41.10,-8.79)	
W = 6.0	
Test of ETA1 = ETA2 vs ETA1 not = ETA2 is significant at 0.0809	

Table D.17: Parametric Analysis of Beam Splice Results with Square Root Normalization between VAC and RAC-50

t-Test: Two-Sample Assuming Unequal Variances

	VAC	RAC-50
Mean	65.12762	68.98221
Variance	24.56742	1.342879
Observations	3	3
Hypothesized Mean Difference	0	
df	2	
t Stat	-1.3116	
P(T<=t) one-tail	0.159997	
t Critical one-tail	2.919986	
P(T<=t) two-tail	0.319993	
t Critical two-tail	4.302653	

Table D.18: Non-Parametric Analysis of Beam Splice Results with Square Root Normalization between VAC and RAC-50

Mann-Whitney Test and CI: VAC, RAC-50	
N	Median
VAC 3	63.010
RAC-50 3	68.611
Point estimate for ETA1-ETA2 is -5.602	
91.9 Percent CI for ETA1-ETA2 is (-8.700,2.736)	
W = 9.0	
Test of ETA1 = ETA2 vs ETA1 not = ETA2 is significant at 0.6625	

Table D.19: Parametric Analysis of Beam Splice Results with Square Root Normalization between VAC and RAC-100

t-Test: Two-Sample Assuming Unequal Variances

	<i>VAC</i>	<i>RAC-100</i>
Mean	65.12762	54.09878
Variance	24.56742	17.64037
Observations	3	3
Hypothesized Mean Difference	0	
df	4	
t Stat	2.940316	
P(T<=t) one-tail	0.021188	
t Critical one-tail	2.131847	
P(T<=t) two-tail	0.042376	
t Critical two-tail	2.776445	

Table D.20: Non-Parametric Analysis of Beam Splice Results with Square Root Normalization between VAC and RAC-100

Mann-Whitney Test and CI: VAC, RAC-100		
	N	Median
VAC	3	63.01
RAC-100	3	53.14
Point estimate for ETA1-ETA2 is 11.12		
91.9 Percent CI for ETA1-ETA2 is (2.89,20.33)		
W = 15.0		
Test of ETA1 = ETA2 vs ETA1 not = ETA2 is significant at 0.0809		

Table D.21: Parametric Analysis of Beam Splice Results with Fourth Root Normalization between VAC and RAC-50

t-Test: Two-Sample Assuming Unequal Variances

	VAC	RAC-50
Mean	65.12762	61.8741
Variance	24.56742	1.08039
Observations	3	3
Hypothesized Mean Difference	0	
df	2	
t Stat	1.112727	
P(T<=t) one-tail	0.190821	
t Critical one-tail	2.919986	
P(T<=t) two-tail	0.381643	
t Critical two-tail	4.302653	

Table D.22: Non-Parametric Analysis of Beam Splice Results with Fourth Root Normalization between VAC and RAC-50

Mann-Whitney Test and CI: VAC, RAC-50	
N	Median
VAC 3	63.010
RAC-50 3	61.541
Point estimate for ETA1-ETA2 is 1.468	
91.9 Percent CI for ETA1-ETA2 is (-1.459,9.748)	
W = 13.0	
Test of ETA1 = ETA2 vs ETA1 not = ETA2 is significant at 0.3827	

Table D.23: Parametric Analysis of Beam Splice Results with Fourth Root Normalization between VAC and RAC-100

t-Test: Two-Sample Assuming Unequal Variances

	VAC	RAC-100
Mean	65.12762	52.39721
Variance	24.56742	16.54813
Observations	3	3
Hypothesized Mean Difference	0	
df	4	
t Stat	3.438744	
P(T<=t) one-tail	0.013162	
t Critical one-tail	2.131847	
P(T<=t) two-tail	0.026324	
t Critical two-tail	2.776445	

Table D.24: Non-Parametric Analysis of Beam Splice Results with Fourth Root Normalization between VAC and RAC-100

Mann-Whitney Test and CI: VAC, RAC-100		
	N	Median
VAC	3	63.01
RAC-100	3	51.47
Point estimate for ETA1-ETA2 is 12.71		
91.9 Percent CI for ETA1-ETA2 is (4.73,21.92)		
W = 15.0		
Test of ETA1 = ETA2 vs ETA1 not = ETA2 is significant at 0.0809		

BIBLIOGRAPHY

- AASHTO (2007). AASHTO LRFD Bridge Design Specification. Fourth Edition, Washington, D.C.
- Abbas, A., et al. (2008). "Proposed Method for Determining the Residual Mortar Content of Recycled Concrete Aggregates," Journal of ASTM International, Vol. 5, Issue 1, pp. JAI101087.
- ACI 408R (2003). Bond and Development of Straight Reinforcing Bars in Tension. American Concrete Institute, Farmington Hills, MI.
- ACI 318 (2011). Building Code Requirement for Structural Concrete, Farmington Hills, MI.
- ASTM C 29 (2009). Standard Test Method for Bulk Density (Unit Weight) and Voids in Aggregate. American Society for Testing and Materials. West Conshohocken, PA.
- ASTM C 39 (2011). Standard Test Method for Compressive Strength of Cylindrical Concrete Specimens. American Society for Testing and Materials. West Conshohocken, PA.
- ASTM C 78 (2010). Standard Test Method for Flexural Strength of Concrete (Using Simple Beam with Third-Point Loading). American Society for Testing and Materials. West Conshohocken, PA.
- ASTM C 127 (2012). Standard Test Method for Density, Relative Density (Specific Gravity), and Absorption of Coarse Aggregate. American Society for Testing and Materials. West Conshohocken, PA.
- ASTM C 136 (2006). Standard Test Method for Sieve Analysis of Fine and Coarse Aggregates. American Society for Testing and Materials. West Conshohocken, PA.
- ASTM C 138 (2010). Standard Test Method for Density (Unit Weight), Yield, and Air Content (Gravimetric) of Concrete. American Society for Testing and Materials. West Conshohocken, PA.
- ASTM C 143 (2010). Standard Test Methods for Slump of Hydraulic Cement Concrete. American Society for Testing and Materials. West Conshohocken, PA.
- ASTM C 231 (2010). Standard Test Method for Air Content of Freshly Mixed Concrete by the Pressure Method. American Society for Testing and Materials. West Conshohocken, PA.

- ASTM C 469 (2010). Standard Test Method for Static Modulus of Elasticity and Poisson's Ratio of Concrete in Compression. American Society for Testing and Materials. West Conshohocken, PA.
- ASTM C 496 (2011). Standard Test Method for Splitting Tensile Strength of Cylindrical Concrete Specimens. American Society for Testing and Materials. West Conshohocken, PA.
- ASTM E8 (2009). Standard Test Methods for Tension Testing of Metallic Materials. American Society for Testing and Materials. West Conshohocken, PA.
- Bentz, E., Collins, M. (2000). Response-2000 Reinforced Concrete Sectional Analysis. Version 1.0.5. Toronto, Canada.
- Butler, L. et al. (2011). "The effect of recycled concrete aggregate properties on the bond strength between RCA concrete and steel reinforcement," *Cement and Concrete Research*, Vol. 41, Issue 10, pp. 1037-1049
- CEB-FIP Model Code for Concrete Structures (1990). "Evaluation of the Time Dependent Behaviour of Concrete," *Bulletin d'Information No. 199*, Comite European du Béton/Fédération Internationale de la Précontrainte, Lausanne, 1991, pp. 201
- Fathifazl, G. (2008). "Structural performance of steel reinforced recycled concrete members." Ph.D. Thesis, Department of Civil and Environmental Engineering, Carleton University, Ottawa, Ontario, Canada
- Federal Highway Administration. (2004). *Transportation Application of Recycled Concrete Aggregate: Federal Highway Administration State of Practice National Review*, <<http://www.fhwa.dot.gov/pavement/recycling/applications.pdf>>
- Kim, S.W. (2012). "Influence of recycled coarse aggregates on the bond behavior of deformed bars in concrete," *Engineering Structures*, Vol. 48, pp. 133
- Looney, T. (2012). "Bond Behavior of High-Volume Fly Ash and Self-Consolidation Concrete." M.S. Thesis, Missouri University of Science and Technology, Rolla, MO.
- RILEM 7-II-28. (1994). "Bond Test for Reinforcing Steel. 2. Pull-out test." E & FN Spon, London.
- RILEM, TC 50-FMC, (1985). *Fracture Mechanics of Concrete*, "Determination of the Fracture Energy of Mortar and Concrete by Means of Three-Point Bend Tests on Notched Beams," RILEM Recommendation, *Materials and Structures*, V. 18, No. 16, pp. 287-290.

- Shayan, A., and Xu, A. (2003). "Performance and Properties of Structural Concrete Made with Recycled Concrete Aggregate," *ACI Mater. J.*, Vol. 100, No. 5, pp. 371–380.
- Shi-Cong Kou, Chi-Sun Poon , Hui-Wen Wan, Properties of concrete prepared with low-grade recycled aggregates, *Construction and Building Materials* 36 (2012) 881–889.
- Wolfe, M. (2011). "Bond Strength of High-Volume Fly Ash Concrete." M.S. Thesis, Missouri University of Science and Technology, Rolla, MO.
- Zuo, J., and Darwin, D. (2000). "Splice Strength of Conventional and High Relative Rib Area Bars in Normal and High Strength Concrete," *ACI Structural Journal*, V. 97, No.4, July-Aug., pp.630-641

APPENDIX D

FINAL Report D

TRyy1317

**Project Title: Recycled Concrete Aggregate (RCA) for
Infrastructure Elements**

Report D: Shear Behavior of RCA Concrete

Prepared for
Missouri Department of Transportation
Construction and Materials

Missouri University of Science and Technology, Rolla, Missouri

May 2014

The opinions, findings, and conclusions expressed in this publication are those of the principal investigators and the Missouri Department of Transportation. They are not necessarily those of the U.S. Department of Transportation, Federal Highway Administration. This report does not constitute a standard or regulation.

ABSTRACT

Sustainability is at the forefront of our society. Unfortunately, concrete, our most common construction material uses a significant amount of non-renewable resources. Consequently, many researchers have investigated the use of recycled materials in the production of concrete such as recycled aggregate.

Most research to date has consisted only of the evaluation of the strength and durability of recycled aggregate concrete (RAC) mixtures, while only a limited number of studies have implemented full-scale testing of specimens constructed with RAC to determine its potential use in the industry. For this research, a laboratory testing program was developed to investigate the shear performance of reinforced concrete (RC) beams constructed with RAC. The experimental program consisted of 18 tests performed on full-scale RC beams. The principal parameters investigated were: (1) concrete type (RAC or conventional concrete (CC)) and (2) amount of longitudinal (flexural) reinforcement. The full-scale test results were compared to the theoretical results using design approaches contained in several codes common to North America as well as a shear database of CC specimens.

Analysis of the test data indicates that replacing more than 50% of coarse natural aggregates with RCA results in diminished shear strength. This result suggests that the existing equations for shear capacity as reported in AASHTO LRFD and ACI 318 may require additional modification factors to account for diminished shear strength when aggregate replacement levels exceed 50%. This diminished shear strength is likely the result of a double interfacial transition zone when using recycled concrete as aggregate.

TABLE OF CONTENTS

	Page
ABSTRACT	ii
LIST OF ILLUSTRATIONS	v
LIST OF TABLES	vii
NOMENCLATURE	viii
1. INTRODUCTION	1
1.1. BACKGROUND	1
1.2. CONCERNS WITH RECYCLED AGGREGATE CONCRETE	3
1.3. OBJECTIVE AND SCOPE OF WORK	4
1.4. RESEARCH METHODOLOGY	5
1.5. REPORT OUTLINE	7
2. LITERATURE REVIEW ON RECYCLED AGGREGATE	9
2.1. GENERAL	9
2.2. USE OF RECYCLED AGGREGATE AS COARSE AGGREGATE	9
2.3. PREVIOUS STUDIES RELATED TO RAC	10
2.4. CONCLUDING REMARKS	12
3. LITERATURE REVIEW ON SHEAR	13
3.1. GENERAL	13
3.2. FACTORS AFFECTING SHEAR BEHAVIOR	13
3.3. BASIC SHEAR TRANSFER MECHANISMS	16
3.4. SHEAR DESIGN PRINCIPLES	17
3.4.1. Truss Model	17
3.4.2. Strut and Tie Model	23
3.4.3. Modified Compression Field Theory	29
3.4.4. Fracture Mechanics Approach	40
3.4.5. Truss Model and Modified Compression Field Theory Comparison	53
3.4.6. Summary of Shear Design	53
3.5. DESIGN CODES REVIEW	54
3.5.1. American Concrete Institute, ACI 318-08	54

3.5.2. AASHTO LRFD Bridge Design Specifications.....	56
3.5.3. Canadian Standards Association, CSA A23.3-04	59
4. EXPERIMENTAL PROGRAM.....	61
4.1. GENERAL.....	61
4.2. TEST BEAMS	61
4.3. MATERIALS.....	63
4.3.1. Concrete.....	63
4.3.2. Steel Reinforcement	65
4.4. BEAM FABRICATION	66
4.5. TEST SET-UP	67
4.6. INSTRUMENTATION	70
4.6.1. Local Deformations and Strains.....	70
4.6.2. Global Deformations	71
5. TEST RESULTS, BEHAVIOR & ANALYSIS.....	73
5.1. GENERAL.....	73
5.2. TEST RESULTS & BEHAVIOR OF FULL-SCALE SPECIMENS.....	73
5.3. COMPARISON OF REINFORCEMENT STRAINS FROM EXPERIMENT AND AASHTO LRFD (2010).....	78
5.4. STATISTICAL DATA ANALYSIS	78
5.4.1. Parametric Test.....	78
5.4.2. Nonparametric Test.....	80
5.5. COMPARISON OF TEST RESULTS WITH SHEAR PROVISIONS OF SELECTED STANDARDS.....	81
5.6. COMPARISON OF TEST RESULTS WITH SHEAR TEST DATABASE...	83
5.7. MATERIAL PROPERTY TEST RESULTS AND COMPARISON WITH SHEAR BEHAVIOR.....	86
6. FINDINGS, CONCLUSIONS, AND RECOMMENDATIONS	88
6.1. FINDINGS AND CONCLUSIONS	88
6.2. RECOMMENDATIONS.....	90
BIBLIOGRAPHY.....	92

LIST OF ILLUSTRATIONS

Figure	Page
Figure 1.1: States using RCA as Aggregate.....	2
Figure 1.2: States using RCA as Base Aggregate.....	3
Figure 1.3: States using RCA in PC Concrete	3
Figure 3.1: Ritter’s Truss Analogy for Shear.....	18
Figure 3.2: Truss Model for Beams Postulated by Mörsh	19
Figure 3.3: Equilibrium Conditions for the Truss Model (Collins and Mitchell, 1991)....	20
Figure 3.4: B-Regions and D-Regions (Schlaich et al., 1987).....	24
Figure 3.5: Strut and Tie Model (Nilson et al., 2004).....	26
Figure 3.6: Nodal Zones (Nilson et al., 2004)	26
Figure 3.7: Predicted and Observed Strengths of a Series of RC Beams Tested by Kani (Collins and Mitchell, 1997).....	28
Figure 3.8: Description of Deep and Slender Beams (ACI 318-08).....	30
Figure 3.9: Slender Beams Used in This Study	30
Figure 3.10: Tensile Stress Along a Cracked Strut (Vecchio and Collins, 1986)	31
Figure 3.11: Mohr’s Circle for Average Strains	32
Figure 3.12: Average Concrete Stress in a Cracked Element (Vecchio and Collins, 1986).....	33
Figure 3.13: Mohr Stress Circle for Average Concrete Stresses	33
Figure 3.14: Cross Section, Principal Stresses, and Tension in Web Reinforcement (Collins and Mitchell, 1991).....	34
Figure 3.15: Softening Function and Initial Tangent for Cohesive Crack Model (Einsfeld and Velasco, 2006)	43
Figure 3.16: Softening Stress-Separation Curve of Cohesive Crack Model (Bazant and Becq-Giraudon, 2002)	46
Figure 3.17: Free Body Diagram and Notation Definition (Gastebled and May, 2001) ...	48
Figure 4.1: Cross Sections and Reinforcement Layout of the Beams	62
Figure 4.2: Load Pattern and Location of Strain Gauges on the Test Beams.....	63
Figure 4.3: Reinforcing Cage Assembly.....	66

Figure 4.4: Beam Construction Process.....	67
Figure 4.5: Details of Test Set-Up (1)	68
Figure 4.6: Details of Test Set-Up (2)	69
Figure 4.7: Photograph of Test Set-Up.....	69
Figure 4.8: Data Acquisition System.....	70
Figure 4.9: Location of LVDT to Measure Deflection.....	71
Figure 4.10: Detail of LVDT for Deflection Measurement.....	72
Figure 5.1: Crack Progression for the Beams	75
Figure 5.2: Crack Pattern of the Beams at Shear Failure.....	76
Figure 5.3: Load-Deflection Response of the Beams	77
Figure 5.4: Shear Strength vs. Longitudinal Reinforcement Ratio; Results from Reineck et al. (2003) and Test Results of this Study.....	85
Figure 5.5: Comparison of Mechanical Properties and Shear Strengths of the CC and RAC Beams	87

LIST OF TABLES

Table	Page
Table 3.1: Values of θ and β for Sections With Transverse Reinforcement (AASHTO LRFD, 2010).....	57
Table 3.2: Values of θ and β for Sections With Less Than Minimum Transverse Reinforcement (AASHTO LRFD, 2010).....	58
Table 4.1: Shear Beam Test Matrix	62
Table 4.2: Aggregate Properties	64
Table 4.3: Mix Designs per Cubic Yard	65
Table 4.4: Typical Fresh and Hardened Concrete Properties for CC and RCA Mixes	65
Table 4.5: Mechanical Properties of Steel Reinforcement	65
Table 5.1: Test Results Summary	75
Table 5.2: Comparison of Reinforcement Strain from Experiment and AASHTO LRFD (2010) Equation	79
Table 5.3: Comparison of Shear Strength of Experiment and Codes	82

NOMENCLATURE

Symbol	Description
A	Angular coefficient of linear regression plot (Equation 3-34)
A_c	Area of concrete on flexural tension side
A_p	Area of prestressing steel
A_{ps}	Area of prestressing steel
A_s	Area of longitudinal reinforcement
A'_s	Area of compression reinforcement
A_{sl}	Area of longitudinal reinforcement
A_{sw}	Steel vertical reinforcement area
A_v	Steel vertical reinforcement area
A_{vi}	Cross-sectional area in the i^{th} stirrup crossing the critical crack
$A_{v,min}$	Minimum shear reinforcement area
a	Aggregate size (Equation 3-18)
a	Depth of equivalent rectangular stress block
a	Shear span
\underline{a}	Critical crack length
a/d	Shear span-to-depth ratio
a_0	Notch depth
a_0/d	Notch depth-to-depth ratio
a_c	Critical position of diagonal crack
a_g	Aggregate size (AASHTO LRFD, 2010)

a_s	Shear span
B	Coefficient obtained through linear regression plot (Equation 3-27)
B	Width of cross-section
b	Width of cross-section
b_v	Effective width of cross-section
b_w	Width of cross-section
C_i	Measured initial compliance
C_u	Unloading compliance
c	Distance from extreme compression fiber to the neutral axis
c_v	Concrete cover for transverse reinforcement
c_x	Concrete cover for longitudinal reinforcement
D	Diameter of the cylinder
D_{max}	Aggregate size
d	Characteristic dimension of structure (Equation 3-28)
d	Effective depth of cross-section
d'	Distance from extreme compression fiber to centroid of longitudinal compression reinforcement
d_0	Coefficient determined experimentally (Bazant and Pfeiffer, 1987)
d_{agg}	Aggregate size
d_{bv}	Diameter of transverse steel reinforcement
d_{bx}	Diameter of longitudinal steel reinforcement
d_v	Effective shear depth (AASHTO LRFD, 2010)
E	Modulus of elasticity of the concrete (Equation 3-34)

E_c	Modulus of elasticity of the concrete
E_p	Modulus of elasticity of the prestressing steel
E_s	Modulus of elasticity of the steel
F_c	Concrete compressive force
F_s	Longitudinal reinforcement force
f_1	Principal tensile stress of the concrete
f_2	Principal compressive stress of the concrete
$f_{2,max}$	Maximum principal compressive stress of the concrete
f'_c	Compressive strength of the concrete
f_{ci}	Compressive stress on crack surface
f_{cr}	Concrete stress at cracking
f_{ct}	Tensile strength of the concrete
f_{cx}	Horizontal concrete stress
f_{cy}	Vertical concrete stress
f_{p0}	Parameter to account for level of prestressing (AASHTO LRFD, 2010)
f_t	Splitting tensile strength of the concrete
f'_t	Tensile strength of the concrete
f_v	Tensile stress in the stirrups
f_{vi}	Stress in the i^{th} stirrup crossing the critical crack
f_y	Yield stress of steel
f_{yt}	Yield stress of transverse steel reinforcement
G	Fracture energy consumption (Equation 3-36)
G_F	Fracture energy (Work-of-fracture method)

G_f	Fracture energy (Size effect method)
G_f	Fracture energy (Two parameter method)
G_s	Shear modulus of steel
$g_f(\alpha_0)$	Non-dimensional energy release rate (Equation 3-34)
H	Height of cross-section
H_0	Thickness of clip gauge holder
h	Height of cross-section
jd	Distance between resultants of internal compressive and tensile forces on a cross-section
K_{Ic}	Stress intensity factor
k	Parameter to reflect size effect (Equation 3-27)
k_1	Coefficient that characterizes bond properties of bars (Equations 3-20)
k_3	Empirical coefficient (Equation 3-49)
L	Length of the beam
M_{exp}	Experimentally determined total moment applied to specimen
M_f	Factored shear moment
M_n	Nominal moment capacity
M_u	Factored shear moment
MOR	Modulus of rupture of the concrete
N_h	Tensile force in longitudinal reinforcement
N_u	Factored axial force
n	Curve-fitting factor (Collins and Mitchell, 1997)
n	Number of data points

P	Maximum load at failure
P_{max}	Measured peak load
S	Specimen loading span
s	Center-to-center spacing of steel stirrups
s	Shear crack sliding
s	Standard deviation
s_{mv}	Average spacing of cracks perpendicular to transverse reinforcement
s_{mx}	Average spacing of cracks perpendicular to longitudinal reinforcement
s_x	Crack spacing parameter (AASHTO LRFD, 2010)
s_x	Spacing of longitudinal steel reinforcement
s_{xe}	Effective crack spacing
s_z	Crack spacing parameter (CSA A23.3, 2004)
s_{ze}	Effective crack spacing
s_{θ}	Crack spacing
$T_{n,1}$	Test criterion (ASTM E178 [2008])
V	External shear force
V_c	Concrete contribution to shear strength
V_{cr}	Ultimate shear force
V_{cz}	Uncracked concrete force
V_d	Longitudinal reinforcement dowel force
V_f	Factored shear force
V_i	Interlock forces
V_n	Nominal shear strength

$V_{n,exp}$	Experimentally determined total shear resistance
$V_{n,max}$	Maximum nominal shear strength
V_p	Vertical component of prestressing force
V_r	Nominal shear resistance
V_s	Steel contribution to shear strength
V_{test}	Experimentally determined total shear resistance
V_u	Factored shear force
v	Shear stress
v_{ci}	Shear transferred by aggregate interlock
$v_{ci,max}$	Maximum shear transferred by aggregate interlock
v_{cxy}	Shear stress on concrete layer face
W	Total energy dissipated (Equation 3-26)
W_{ext}	Work of external force (Equation 3-36)
w	Average crack width (Equation 3-18)
w	Crack opening (Einsfeld and Velasco, 2006)
w	Width of idealized prismatic strut
w/c	Water-to-cement ratio
w/cm	Water-to-cementitious material ratio
\bar{x}	Arithmetic average
y	Diagonal crack extent (Equation 3-38)
z	Inner level arm
α_0	Aggregate shape factor (Equation 3-51)
α_0	Relative notch length (Equation 3-35)

α_1	Coefficient for bond characteristics of reinforcement (Vecchio and Collins, 1993)
α_2	Coefficient for type of loading (Vecchio and Collins, 1993)
β	Brittleness number (Equation 3-27)
β	Concrete softening coefficient (Equation 3-14)
β	Shear retention factor (AASHTO LRFD, 2010)
γ_{xy}	Shear strain
δ_e	Variation of unbounded length
δ_s	Unbonded length of reinforcement
ε_0	Concrete strain at peak stress
ε_1	Principal tensile strain in concrete
$\bar{\varepsilon}_1$	Uniaxial tensile strain in the perpendicular direction
ε_2	Principal compressive strain in concrete
ε_c	Compressive strain in the concrete
ε'_c	Compressive strain in the concrete
ε_{cr}	Crack strain in concrete
ε_s	Measured longitudinal strain at the center of gravity at the bottom steel reinforcement
ε_s	Strain in the tension reinforcement
ε'_s	Measured longitudinal strain at the top steel reinforcement
ε'_s	Strain in the compression reinforcement
ε_{sm}	Measured longitudinal strain at the bottom steel reinforcement
ε_{td}	Transverse strain

ε_x	Longitudinal strain (AASHTO LRFD, 2010)
ε_x	Strain in the x-direction
ε_{xx}	Horizontal strain
ε_{xy}	Shear strain
ε_y	Strain in the y-direction
ε_{yield}	Yield strain of steel
ε_{yy}	Vertical strain
θ	Shear crack angle
θ_c	Shear crack angle
ξ	Concrete softening coefficient
$\xi f'_c$	Concrete peak softened stress
$\xi \varepsilon_0$	Concrete softened compressive strain
ρ_L	Longitudinal reinforcement ratio
ρ_s	Longitudinal reinforcement ratio
ρ_v	Transverse reinforcement ratio
ρ_w	Longitudinal reinforcement ratio
ρ_x	Longitudinal reinforcement ratio
σ_N	Nominal stress at failure (Equation 3-27)
Σ_s	Reduced cross section of rebar (Equation 3-38)
\emptyset	Capacity reduction factor
\emptyset_c	Capacity reduction factor
\emptyset_s	Capacity reduction factor
Γ	Fracture energy per unit length of splitting crack extension

1. INTRODUCTION

1.1. BACKGROUND

The construction of buildings, bridges, and roadways continues to increase in the twenty-first century, especially in areas with ever-growing populations. Existing structures and highways require repair or replacement as they reach the end of their service life or simply no longer satisfy their intended purpose due to the growing population. As modern construction continues, two pressing issues will become more apparent to societies: an increasing demand for construction materials, especially concrete and asphalt aggregates, and an increasing production of construction and demolition waste. Already, the Federal Highway Administration (FHWA 2004) estimates that two billion tons of new aggregate are produced each year in the United States. This demand is anticipated to increase to two and a half billion tons each year by 2020. With such a high demand for new aggregates, the concern arises of the depletion of the current sources of natural aggregates and the availability of new sources. Similarly, the construction waste produced in the United States is expected to increase. From building demolition alone, the annual production of construction waste is estimated to be 123 million tons (FHWA 2004). Currently, this waste is most commonly disposed of in landfills.

To address both the concern of increasing demand for new aggregates and increasing production of waste, many states have begun to recognize that a more sustainable solution exists in recycling waste concrete for use as aggregate in new concrete, or recycled concrete aggregates (RCA). The solution helps address the question

of how to sustain modern construction demands for aggregates as well as helps to reduce the amount of waste that enters already over-burdened landfills.

Based on a survey by FHWA in 2002, many states had begun to implement recycled concrete aggregates in some ways in new construction. As shown in **Figure 1.1**, most states had recognized the many uses of RCA as a raw material, such as for rip-rap, soil stabilization, pipe bedding, and even landscape materials. As shown in **Figure 1.2**, many states had gone a step further in integrating RCA into roadway systems for use as aggregate base course material. However, as shown in **Figure 1.3**, only a small number of states had begun using RCA in Portland cement concrete for pavement construction. However, over the intervening 12 years, the use of RCA has increased significantly, particularly within the last 5 years, and the Missouri Department of Transportation (MoDOT) has instituted a very aggressive program to increase the use of recycled materials in transportation-related construction. However, there are currently no acceptable standards or guidelines in the U.S. for utilizing RCA in structural concrete.

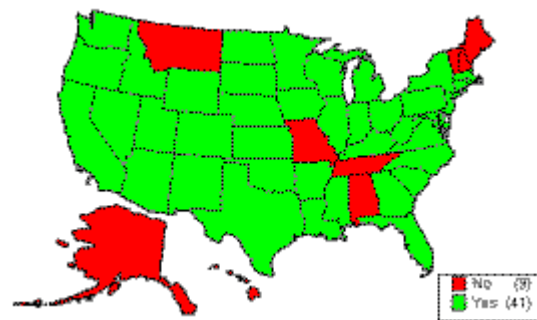


Figure 1.1: States using RCA as Aggregate

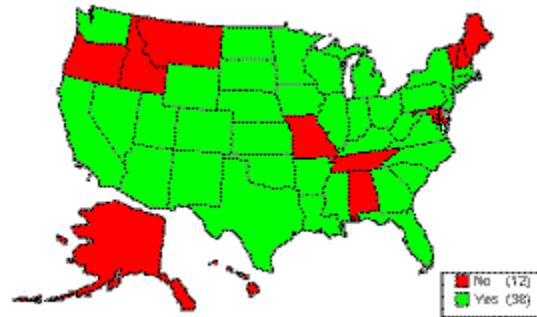


Figure 1.2: States using RCA as Base Aggregate

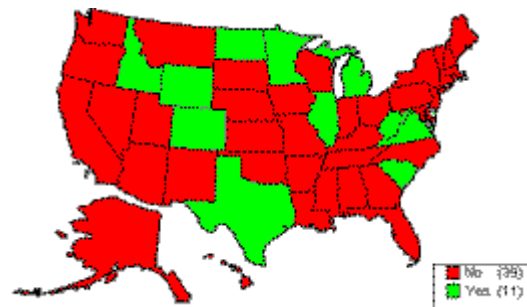


Figure 1.3: States using RCA in PC Concrete

1.2. CONCERNS WITH RECYCLED AGGREGATE CONCRETE

RCAs are composed of both the original, or virgin, aggregate, as well as mortar which remains adhered to the surface of the aggregate. In the production of RCA, the removal of all this residual mortar would prove costly and detrimental to the integrity of the virgin aggregates within the concrete. Therefore, residual mortar is inevitable.

Research has shown that this residual mortar causes high water absorption, low density, low specific gravity, and high porosity in RCAs compared to natural aggregates. These effects in the recycled aggregate can decrease hardened concrete properties of recycled aggregate concrete (RAC). According to Abbas et al. (2008), the amount of residual

mortar on the RCA can significantly affect the mechanical and durability properties of RAC. To reduce the negative impacts of this residual mortar, new mix design methods such as the equivalent mortar volume method can be used.

Due to the variety of sources of RCA and the various functions, environment, and wear of the concrete structures and pavements from which the RCA can be obtained, characterizing this aggregate can be very difficult. Controlled studies must be performed to account for each of these variables on a regional basis, such as for each state's Department of Transportation, so that the aggregates within the area can be adequately characterized.

1.3. OBJECTIVE AND SCOPE OF WORK

The main *objective* of this research study was to evaluate the shear behavior and response of RCA through material, component, and full-scale testing. This objective included a study and evaluation of current analytical models used to predict the shear response of conventional Portland-cement concrete as applied to RCA, including recommended modifications.

The following *scope of work* was implemented in order to achieve the objective of the research study:

- Perform a literature review;
- Develop a research plan;
- Develop mix designs for both conventional and RAC;
- Evaluate the fresh and hardened properties of several RAC and CC mixes;
- Design and construct small and full-scale specimens;

- Test specimens to failure;
- Record and analyze data from tests;
- Compare test results to current guidelines and previous research findings;
- Provide greater insight into the shear resistance mechanisms and quantify their effect;
- Evaluate the applicability of current analytical models to predict the shear behavior and response of RAC;
- Develop conclusions and recommendations; and
- Prepare this report to document the details, results, findings, conclusions, and recommendations of this study.

1.4. RESEARCH METHODOLOGY

The proposed research methodology included six (6) tasks necessary to successfully complete the study. They are as follows:

Task #1: Perform a literature review. The goal of the literature review was to become familiarized with testing methods and results from previous studies. This knowledge was used for a better understanding of the behavior of the specimens, to avoid mistakes, as well as to provide support for comparisons.

Task #2: Develop RAC and CC mix designs. The purpose of this task was to develop RAC mix designs that maximized the percentage of recycled concrete aggregate, but that still fulfilled typical construction needs, such as early strength development. Conventional concrete mix designs served as controls during this study. ACI 211.1-91 formed the basis for developing the mix designs.

Task #3: Perform material and component testing. A number of hardened concrete property tests were completed to evaluate the performance of the RAC mix and determine the validity of using these tests to predict the performance of concretes containing recycled concrete aggregate.

Task #4: Perform full-scale testing. This task was critical as current shear design provisions for reinforced concrete are largely empirical. This task involved the construction and testing of full-scale specimens to confirm the potential of RAC. The full-scale specimens included beam specimens for shear testing only. These specimens were constructed with materials from the local Ready Mix Concrete plant to validate the ability of transferring the mix designs from the laboratory to the field. In order to compare the shear strength of conventional and RAC, full-scale beams were tested in a third point loading configuration. These beams were designed to fail in shear by increasing the flexural reinforcement. Different longitudinal reinforcement ratios were also considered. Strain gauges were applied to the flexural reinforcement, and the maximum load applied to the beam was also recorded and used to calculate the strength of the beams and the different shear components.

Task #5: Analyze test data. The material, component, and full-scale test results were analyzed to evaluate the shear behavior and response of RAC compared to conventional Portland-cement concrete. The test data included: concrete compressive and tensile strength, modulus of rupture (MOR), shear force-deflection plots, crack formation and propagation, and reinforcement strains.

Task #6: Develop findings, conclusions, and recommendations. This task synthesized the results of the previous tasks into findings, conclusions, and recommendations on the shear behavior and response of RAC.

1.5. REPORT OUTLINE

This report includes six chapters. This section will discuss the information that will be presented in more detail throughout this document.

Chapter 1 acts as an introduction to the report. This introduction contains a brief background of recycled aggregate. It also discusses the research objective, scope of work, and research plan.

Chapter 2 includes information from previous research performed on the characterization of recycled aggregate and its applications as a coarse aggregate in concrete.

Chapter 3 presents information from previous research performed on shear design including the different methods and approaches formulated to address this phenomenon. Four different approaches are presented: truss model, Strut and Tie Model (STM), Modified Compression Field Theory (MCFT), and fracture mechanics approach. A collection of three design code philosophies that can be found in North America are also presented in this chapter.

Chapter 4 includes information about the experimental program. The experimental program consisted of 12 tests performed on full-scale reinforced concrete beams as well as material and component testing to determine hardened concrete properties such as compressive strength, splitting tensile strength, and flexural strength.

This chapter also describes the fabrication process, test set-up, and instrumentation for the full-scale testing.

Chapter 5 presents the test results and the different analyses used to investigate the shear resistance mechanisms. The overall behavior of the specimens is described first, with a focus on crack patterns, failure modes, and shear strength.

Chapter 6 concludes this document, summarizing the findings and conclusions of this study and proposing recommendations and future research.

2. LITERATURE REVIEW ON RECYCLED AGGREGATE

2.1. GENERAL

Conventional Portland-cement concrete is produced more than any other material in the world. It is used in every civil engineering field for applications such as pavements, dams, bridges, and buildings because of its versatility, strength, and durability. In this chapter, a brief review is presented of the research performed on concrete mixtures containing recycled aggregate as coarse aggregate.

Concrete with recycled aggregate can be produced to achieve desired strengths at various ages, with a given water-cementitious ratio, aggregate size, air content, and slump as it is done for conventional concrete.

2.2. USE OF RECYCLED AGGREGATE AS COARSE AGGREGATE

Recently, there has been an increasing trend toward the use of sustainable materials. Sustainability helps the environment by reducing the consumption of non-renewable natural resources. Concrete – the second most consumed material in the world after water – uses a significant amount of non-renewable resources. As a result, numerous researchers have investigated the use of recycled materials in the production of concrete such as fly ash and recycled aggregate.

Unfortunately, global data on concrete waste generation is not available, but construction and demolition waste accounts for around 900 million tonnes every year just in Europe, the US, and Japan (WBCSD 2012). Recycling concrete not only reduces using virgin aggregate but also decreases the amount of waste in landfills.

In general, RCA has lower specific gravity and unit weight and considerably higher absorption and porosity compared to natural aggregates. These factors need to be taken into account when designing concrete mixes containing RCA.

2.3. PREVIOUS STUDIES RELATED TO RAC

Comprehensive research has been done on both the fresh and hardened properties of recycled aggregate concrete (RAC), but limited, and often contradictory, research has been performed on the structural behavior of RAC. The early research on structural performance of RAC was published in Japan (Kikuchi et al.1988). Maruyama et al. (2004) tested beams with different longitudinal reinforcement ratios ranging between 2.4% and 4.2%. They also investigated three different water/cementitious material ratios, w/cm, (0.30, 0.45, and 0.60) for their mix designs. They reported that the crack patterns and failure modes of the RAC beams were identical with the conventional concrete (CC) beams. The RAC beams without stirrups showed 10-20% lower shear strength compared with the CC beams.

Gonzalez-Fonteboa et al. (2007) tested eight beams with 3% longitudinal reinforcement ratio and 50% recycled coarse aggregate. Results of their study showed that in terms of both deflection and ultimate shear strength, no significant difference was observed between the RAC and CC beams, but they observed notable splitting cracks along the tension reinforcement. They concluded that existing code provisions for shear can be used for the RAC beams. Gonzalez-Fonteboa et al. (2009) repeated the previous study except for adding 8% silica fume to the mix designs. They observed that notable

splitting cracks along the tension reinforcements were mitigated by the addition of silica fume.

Fathifazl et al. (2009) used the equivalent mortar volume (EMV) method for their mix designs. They used both limestone (63.5% recycled aggregate replacement) and river gravel (74.3% recycled aggregate replacement) as a coarse aggregate for their mix designs. They tested beams with four different shear span-to-depth ratios ranging between 1.5 and 4, and also with four different effective depths (250, 375, 450, and 550 mm) to investigate size effect. They reported superior shear strength for the RAC beams. They also concluded that current code provisions for shear conservatively predicted the capacities of the RAC beams.

Choi et al. (2010) evaluated the shear strength of 20 reinforced concrete beams with different span-to-depth ratios (1.50, 2.50, and 3.25), longitudinal reinforcement ratios (0.53%, 0.83%, and 1.61%), and RCA replacement ratios (0%, 30%, 50%, and 100%). Results of their study showed that the shear strength of the RAC beams was lower than that of the CC beams with the same reinforcement ratio and shear span-to-depth ratio. They reported that beams with smaller span-to-depth ratios and higher percentage of recycled aggregate showed a higher reduction in shear strength.

Schubert et al. (2012) studied 14 slabs (0.2 x 0.5 x 2.3 m) with 100% recycled coarse aggregate under four point load condition. They concluded that RAC slabs can be designed using the same design equations as for CC.

Xiao et al. (2012) tested 32 shear push-off specimens with different percentages of recycled coarse aggregate replacement. They reported no significant difference observed in terms of shear stress-slip curves, crack propagation path, and shear transfer

performance across cracks between the RAC and CC specimens. They also concluded that recycled aggregate replacement up to 30% did not affect ultimate shear load, but for higher percentages of RCA replacement, the ultimate shear load decreased.

2.4. CONCLUDING REMARKS

The literature review reported different results (in some cases contradictory) in terms of shear strength when recycled aggregate was used in concrete. Some research showed using recycled aggregate instead of virgin aggregate in concrete had no effect on shear strength of RAC. Other researchers reported RAC showed lower shear strength and only Fathifazl et al. (2009) used the EMV method and reported superior shear strength for RAC compared with CC.

3. LITERATURE REVIEW ON SHEAR

3.1. GENERAL

The main subject of this document is the shear behavior of reinforced concrete (RC) beams composed of RAC. The current shear design methods and guidelines are presented in this chapter. Four different approaches are presented: truss model, Strut and Tie Model (STM), Modified Compression Field Theory (MCFT), and fracture mechanics approach. A collection of three design code philosophies that can be found in North America will also be used in the evaluation of the shear strength. Some of these guidelines rely on empirical formulas, such as the ACI 318-11, while others, such as the AASHTO LRFD-10 and CSA A23.3-04, rely more on concrete models such as the MCFT.

3.2. FACTORS AFFECTING SHEAR BEHAVIOR

Shear strength is controlled by the presence of web reinforcement, longitudinal reinforcement, coarse aggregate size, presence of axial loads, depth of the member, tensile strength of the concrete, and shear span to depth ratio (a/d). Some of these parameters are included in design equations and others are not.

Web reinforcement, typically called stirrups, is used to increase the shear strength of concrete beams and to ensure flexural failure. This is necessary due to the explosive and sudden nature of shear failures, compared with flexural failures which tend to be more ductile. Web reinforcement is normally provided as vertical stirrups and is spaced at varying intervals along a beam depending on the shear requirements. Alternatively, this reinforcement may be provided as inclined longitudinal bars. In general, small sized bars

such as #3 and #4 are used in a U-shaped configuration that may be open or closed, or used as multiple legs.

Shear reinforcement has very little effect prior to the formation of diagonal cracks. However after cracking, the web reinforcement enhances the beam in the following ways (Nilson et al., 2004):

- The stirrups crossing the crack help in resisting the shear force.
- The stirrups restrict the growth of the cracks and reduce their penetration further into the compression zone.
- The stirrups oppose widening of the cracks, which helps to maintain aggregate interlock within the concrete.
- The presence of stirrups provides extra restraint against the splitting of concrete along the longitudinal bars due to their confinement effect.

The longitudinal reinforcement ratio (ρ_L) affects the extent and the width of the flexural cracks. If this ratio is small, the flexural cracks extend higher into the beam and open wider. When the crack width increases, the components of shear decrease, because they are transferred either by dowel action or by shear stresses on the crack surfaces.

The coarse aggregate type and size noticeably affect the shear capacity, especially for beams without stirrups. Lightweight aggregate has a lower tensile strength than normal aggregate. The shear capacity of a concrete beam with no stirrups is directly related to the tensile strength, therefore, the failure due to mortar cracking, which is more desirable, could be preceded by aggregate failure instead. The aggregate size also affects the amount of shear stresses transferred across the cracks. Large diameter aggregate

increases the roughness of the crack surfaces, allowing higher shear stresses to be transferred (Wight and MacGregor, 2009).

Researchers have concluded that axial compression serves to increase the shear capacity of a beam while axial tension greatly decreases the strength. As the axial compressive force is increased, the onset of flexural cracking is delayed, and the flexural cracks do not penetrate as far as into the beam (Wight and MacGregor, 2009).

The size of the beam affects the shear capacity at failure. If the overall depth of a beam is increased, it could result in a smaller shear force at failure. The reasoning is that when the overall depth of a beam increases, so do the crack width and crack spacing, causing loss of aggregate interlock. This condition is known as a size effect.

The tensile strength of the concrete (f_{ct}) also affects the shear strength. Because of the low tensile strength of the concrete, diagonal cracking develops along planes perpendicular to the planes of principal tensile stress. The shear strength of an RC beam increases as the concrete material strength increases. The tensile strength of the concrete is known to have a great influence on the shear strength, but the concrete compressive strength (f'_c) is used instead in most shear strength formulas. This approach is used because tensile tests are more difficult to conduct and usually show greater scatter than compression tests.

The shear span to depth ratio (a/d) does not considerably affect the diagonal cracking for values larger than 2.5. The shear capacity increases as the shear span to depth ratio decreases. This phenomenon is quite significant in deep beams ($a/d \leq 2.5$) because a portion of shear is transmitted directly to the support by an inclined strut or

arch action. For deep beams, the initial diagonal cracking develops suddenly along almost the entire length of the test region (Wight and MacGregor, 2009).

3.3. BASIC SHEAR TRANSFER MECHANISMS

The 1973 ASCE-ACI Committee 426 Report concluded that shear is transferred by the following four mechanisms: shear stress in the uncracked concrete, interface shear transfer, dowel action, and arch action. In a RC beam, after the development of flexural cracks, a certain amount of shear is carried by the concrete in the compression zone. The shear force carried by the uncracked concrete in the compression zone can be represented by the compressive strength of concrete and the longitudinal reinforcement ratio. Shear may continue to be transferred across a crack in the concrete by interface shear transfer, also known as aggregate interlock. Since the flexural crack width is approximately proportional to the strain of the tension reinforcement, the crack width at failure becomes smaller as the longitudinal reinforcement ratio is increased. It is also expected that the interlocking force will be increased when the compressive strength of the concrete is high. If longitudinal reinforcing bars cross a crack, dowel forces in the bars will resist shear displacement. The dowel force induces tension in the surrounding concrete that may produce splitting cracks along the longitudinal reinforcement. Although there is some contribution in dowel action by the number and arrangement of longitudinal bars, spacing of flexural cracks, and the concrete cover, the main factors influencing this mechanism are the flexural rigidity of the longitudinal bars and the strength of the surrounding concrete. Arch action occurs where shear flow cannot be transmitted. Arch action is dominant in deep beams. For this mechanism to be developed, a tie is required

to restrain the thrust developed as a result of the arch. For deep beams, failure is often due to anchorage failure of the bars restraining this thrust.

Shear can be carried through beam action, arch action or any combination of the two. When shear is carried through beam action, the tensile force in the reinforcement varies through bond stresses and plane sections remain plane. These are the normal assumptions of elastic beam theory.

The 1998 ASCE-ACI Committee 445 Report highlights a new mechanism, residual tensile stresses, which are transmitted directly across cracks. The basic explanation of residual tensile stresses is that when concrete first cracks, small pieces of concrete bridge the crack and continue to transmit tensile force as long as cracks do not exceed 0.00197-0.0059 in. in width. The application of fracture mechanics to shear design is based on the premise that residual tensile stress is the primary mechanism of shear transfer.

3.4. SHEAR DESIGN PRINCIPLES

3.4.1. Truss Model. The truss method of analysis has for some time been accepted as an appropriate method for the design of structural concrete members comprising both reinforced and prestressed concrete elements, and it now forms the basis of many design standard recommendations. The truss model was presented by the Swiss engineer Ritter (1899) to explain the flow of forces in cracked reinforced concrete. The principle of the truss model is based on the following assumptions: (1) the longitudinal tension reinforcement acts as a tension chord of the truss while the flexural compressive zone of the beam acts as the compression chord, and (2) the diagonal compressive

stresses (green lines in **Figure 3.1**) act as diagonal members, and the stirrups (blue lines in **Figure 3.1**) are considered as vertical tension members.

Mörsch (1902), a German engineer, pointed out that the compression diagonals do not need to extend from the top of one stirrup to the bottom of the next stirrup, and that the stirrups represent a continuous field of stresses rather than the discrete diagonal compressive struts formed by the concrete. Mörsch and Ritter neglected the tensile stress in cracked concrete assuming that only after cracking the diagonal compression stresses would remain at 45 degrees. Mörsch also proposed truss models to explain the behavior of beams detailed with bent-up longitudinal reinforcing bars. He also used the principal stress trajectories as an indication of how tensile reinforcement should be proportioned and detailed in a region where the internal stress flow is complex. **Figure 3.2** presents the model proposed by Mörsch.

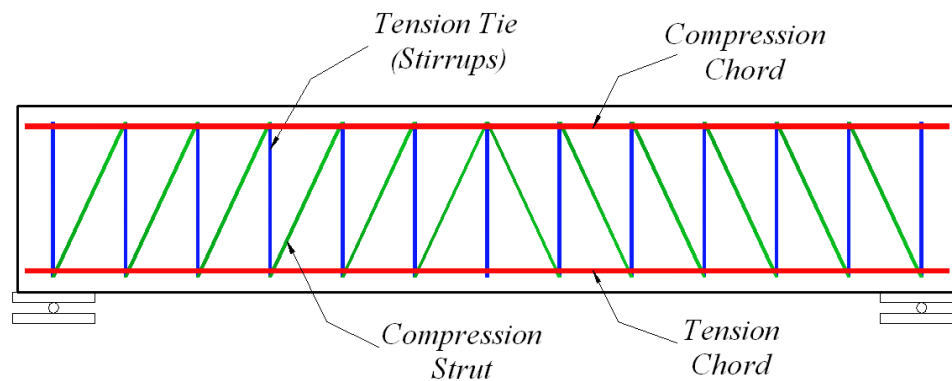


Figure 3.1: Ritter's Truss Analogy for Shear

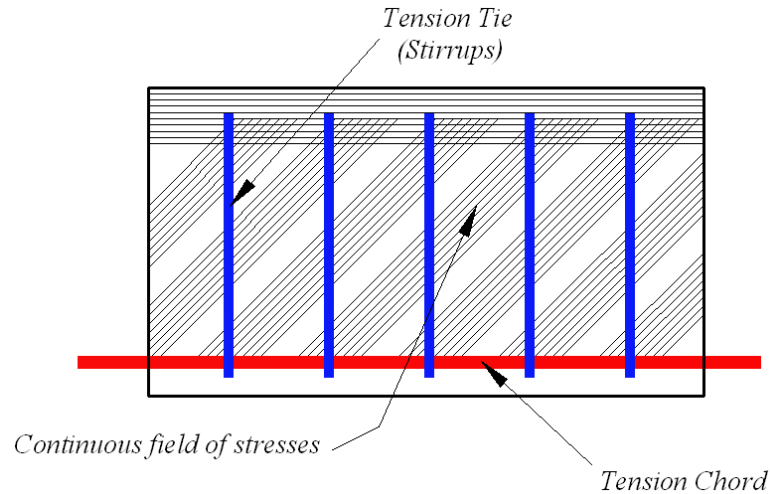


Figure 3.2: Truss Model for Beams Postulated by Morsch

The truss model is derived using the equilibrium condition between the external and internal forces as presented in **Figure 3.3**. The shear stresses are assumed to be uniformly distributed over an effective shear area b_w wide and d deep. Between the external shear force, V , and the total diagonal compressive force, **Equation 3.1** can be written, from which the principal compressive stress (f_2) can be determined assuming a crack angle of 45 degrees.

The longitudinal component of the diagonal compressive force is considered equal to the external shear force. The tensile stress in the stirrups is determined considering **Equation 3.2**. Allowing only the use of the 45 degrees crack angle the method is robust and gives conservative results, and it is widely used by designers because of its simplicity.

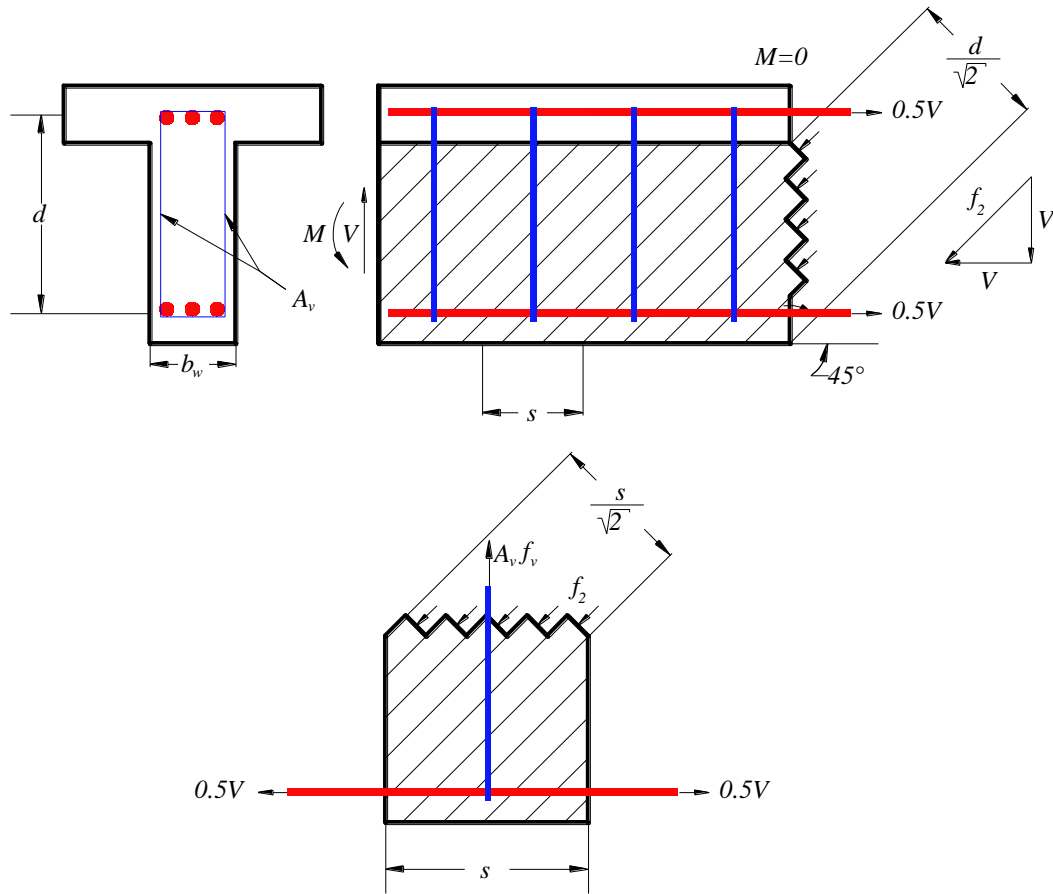


Figure 3.3: Equilibrium Conditions for the Truss Model (Collins and Mitchell, 1991)

$$\frac{f_2 b_w d}{\sqrt{2}} = \sqrt{2} V \quad (3.1)$$

$$\frac{A_v f_v}{s} = \frac{V}{d} \quad (3.2)$$

The variable-angle truss model is derived from the Mörsh truss model. This model adds a concrete contribution to shear strength to compensate for the conservative nature of the model based on a variable angle of the crack (θ). The principle is very similar to the one presented in **Figure 3.3**. In this model, the required magnitude of the principal compressive stress (f_2) is determined from the equality between the resultant of the diagonal stresses and the diagonal projection of the shear force, as stated in **Equation 3.3**. The tensile force in the longitudinal reinforcement (N_h) due to shear will be equal to

the horizontal projection of the shear force, as stated in **Equation 3.4**. The tensile stress in the stirrups is multiplied by the factor $\tan \theta$, as stated in **Equation 3.5**.

$$f_2 = \frac{V}{b_w d} (\tan \theta + \cos \theta) \quad (3.3)$$

$$N_h = V \cos \theta \quad (3.4)$$

$$\frac{A_v f_v}{s} = \frac{V}{d} \tan \theta \quad (3.5)$$

Since there are only three equations of equilibrium (**Equations 3.3, 3.4, and 3.5**), and there are four unknowns (f_2 , N_h , f_v , and θ), the stresses in a beam caused by a given shear force cannot be explicitly determined. For design considerations, the shear force can be predicted assuming the crack angle at 45 degrees and the tensile stress in the stirrups as the tensile strength of steel (f_y). Another approach could be assuming the compressive stress in the concrete to determine the crack angle (**Equation 3.3**) and the shear force (**Equation 3.5**). Other approaches to solving the variable angle truss model have been developed based on subsequent test data. For instance, it has been suggested that the effective compressive strength should be taken as $0.6f'_c$, and that the factor $\tan \theta$ should be less than 0.5 (Collins and Mitchell, 1991).

Proportioning and detailing of the transverse reinforcement in members with a complex flow of internal stresses was a main aspect of structural concrete research in central Europe during the 1960s and 1970s. Leonhardt, from the University of Stuttgart in Germany, and Thürlimann and Müller, from the Swiss Federal Institute of Technology in Zürich, were instrumental in the development of analysis and design methods for structural concrete regions with complex internal stress flows. Leonhardt focused mainly

on the analysis and design of deep beams and anchorage end regions in post-tensioned beams. In most of his work, the detailing of the reinforcing steel closely followed the principal tensile stress trajectories found from an elastic analysis of a homogeneous isotropic element. Thürlimann focused mainly on the application of the theory of plasticity in reinforced and prestressed concrete, with practical applications to the design for shear and torsion.

In the mid-1970s, Park and Paulay, from the University of Canterbury, extended many of the analytical and design concepts developed by Leonhardt to include, for the first time, the detailing of regions having a complex flow of stresses and subjected to cyclic load reversals caused by earthquake excitation (Park and Paulay, 1975). One of these regions is the joint between the beam and column in a moment resisting frame. In the analysis and design of beam-column joints, Park and Paulay deviated from Leonhardt's method by proposing a simple mechanism of shear transfer that did not follow the principal tensile stress trajectories shown by an elastic analysis. This model requires vertical and horizontal reinforcement to sustain the diagonal compressive field introduced into the joint as a result of bond forces from the outermost longitudinal column and beam bars.

The truss model is also the starting point of the shear friction model, also known as Loov's theory (1998), in which the shear forces are carried by stirrups and shear friction across the concrete crack. The method comprises the calculation of the shear capacity from all possible crack angles by identifying the weakest plane of failure. The force that holds the two surfaces together is equal to the yield stress multiplied by the cross-sectional area of any steel crossing the crack for bars perpendicular to the failure

plane. In addition to the friction of the failure plane surface, the model accounts for shearing of the reinforcement and the dowel action that they generate. The main drawback to the use of the shear friction models for beam shear is that the critical failure plane is typically unknown, so an interactive approach must be conducted to find the weakest or most critical failure plane.

3.4.2. Strut and Tie Model. The Strut and Tie Model (STM) was developed in the late 1980s. It was formalized and popularized by Schlaich et al. in a comprehensive paper published in 1987. Reinforced concrete theory hinges on various assumptions of simple beam theory such as plane sections remaining plane. However, regions near a discontinuity do not satisfy this assumption and are called D-regions, which stands for disturbed regions that do not follow simple beam theory. These regions extend approximately a distance h away from the discontinuity which may include concentrated loads, openings, or changes in the cross section. Entire beams consisting of a D-region are called deep beams. Regions in between these areas are subjected to typical beam behavior and are called B-regions. **Figure 3.4** shows the distribution of D- and B-regions, where D stands for discontinuity or disturbed, and B stands for beam or Bernoulli. The STM was developed based on the truss model to account for these D-regions. They consist of struts, ties, and nodal zones. **Figure 3.5** shows how each are combined within a beam.

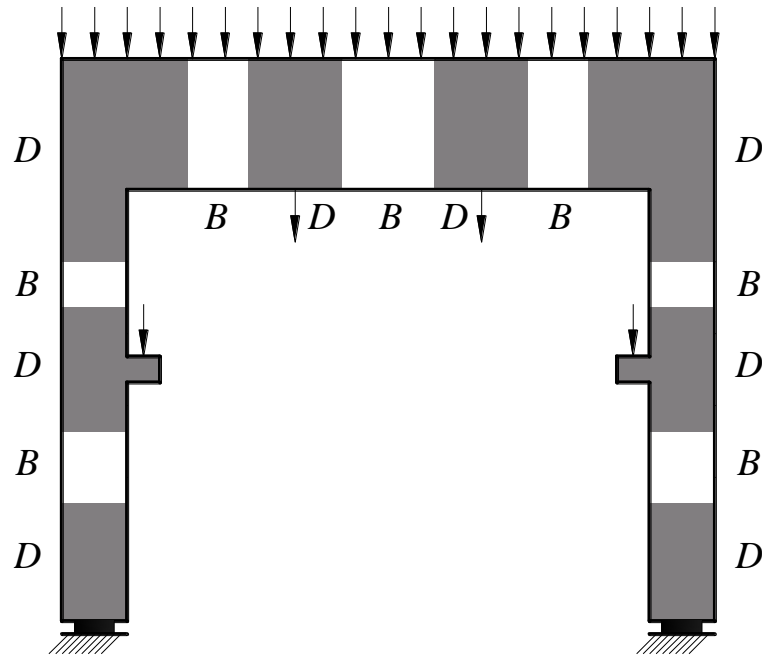


Figure 3.4: B-Regions and D-Regions (Schlaich et al., 1987)

Struts are internal concrete compression members which may be rectangular or bottle-shaped. Bottle-shaped struts swell throughout their depth, and are wider at the center than at the ends. The STM shown in **Figure 3.5** features a rectangular strut, but the bottle-shaped strut is depicted with dashed lines. Ties are tension members within the model and consist of steel reinforcement, plus the portion of concrete surrounding the steel. However, the model assumes that the steel carries all of the tension force. Nodal zones are regions where struts, ties, and concentrated loads meet. Nodes are classified by the types of forces passing into them, which create four types: (a) C-C-C, (b) C-C-T, (c) C-T-T, and (d) T-T-T, where C represents compression and T represents tension. **Figure 3.6** presents each node type.

The following procedure is used to develop a STM:

- Defining of the D-region; borders and forces within these boundaries.
- Drawing a STM based on the assumed node geometry.

- Solving for the truss member forces.
- Calculating the reinforcement layout providing the required tied capacity and enough anchorage length for the bars to ensure the correct behavior at the nodes.
- Dimensioning nodes using truss member forces obtained previously.
- Repeating analysis for the new geometry in order to find a converged solution.

The STM method is not always trouble-free and has many uncertainties. There are four major problems in developing a STM, and these are:

- Uncertainties in obtaining dimensions, stiffness, and effective strength of strut, ties, and nodes for the truss models.
- Need to select the optimal STM and iteratively adjust and refine the truss geometry.
- Need to combine different load cases.
- Multiple potential solutions for statically indeterminate models.

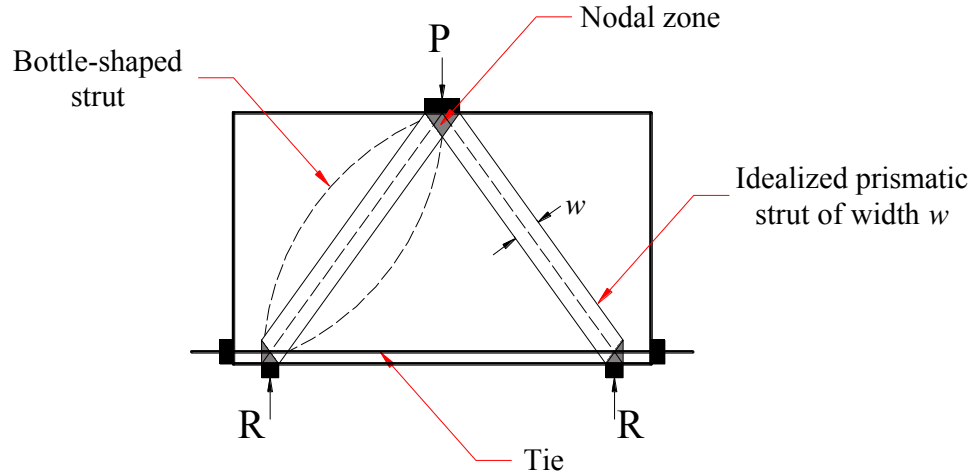


Figure 3.5: Strut and Tie Model (Nilson et al., 2004)

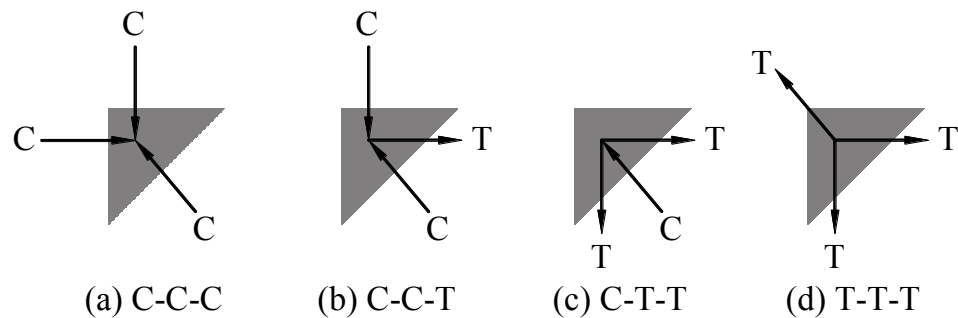


Figure 3.6: Nodal Zones (Nilson et al., 2004)

The creation of the strut and tie model offers no unique solution, and more than one admissible model may be valid for a given problem. The STM must be statically admissible, thus, in equilibrium with the external loads, reactions and nodes. Design takes place by selecting the amount of steel for the tension ties, effective width of the strut, and shape of the nodal zone such that the strength is adequate.

Previous researchers (Kani, 1967) have found that beams with shear span-to-depth ratios greater than 2.5 are governed by conditions away from the disturbed regions adjacent to the support and the loads. In this range, the strength of the beam is not influenced by details such as the size of the bearing plates, and the strength decreases by

only a small amount as the shear span increases. Collins and Mitchell (1997) presented an example of the use of the strut and tie model illustrated in **Figure 3.7**, which shows how the shear strength of a simply supported reinforced concrete beam loaded with two point loads changes as the shear span changes. This study shows that a beam can resist a higher shear force if the shear is produced by a load that is closer to the support. This series of beams was tested by Kani (1967), and based on the observation of the results, it was concluded that the shear strength was reduced by a factor of about 6 as the shear span-to-depth ratio decreased from 1 to 7 (Collins and Mitchell, 1997). This result can be explained by the fact that deep beams carry the load by strut-and-tie action, and as the applied load moves closer to the support, the angle of the compression strut increases, reducing the force (stress) in the strut, and thus increasing the capacity of a given cross section. A typical failure mode of these beams involves crushing of the concrete strut.

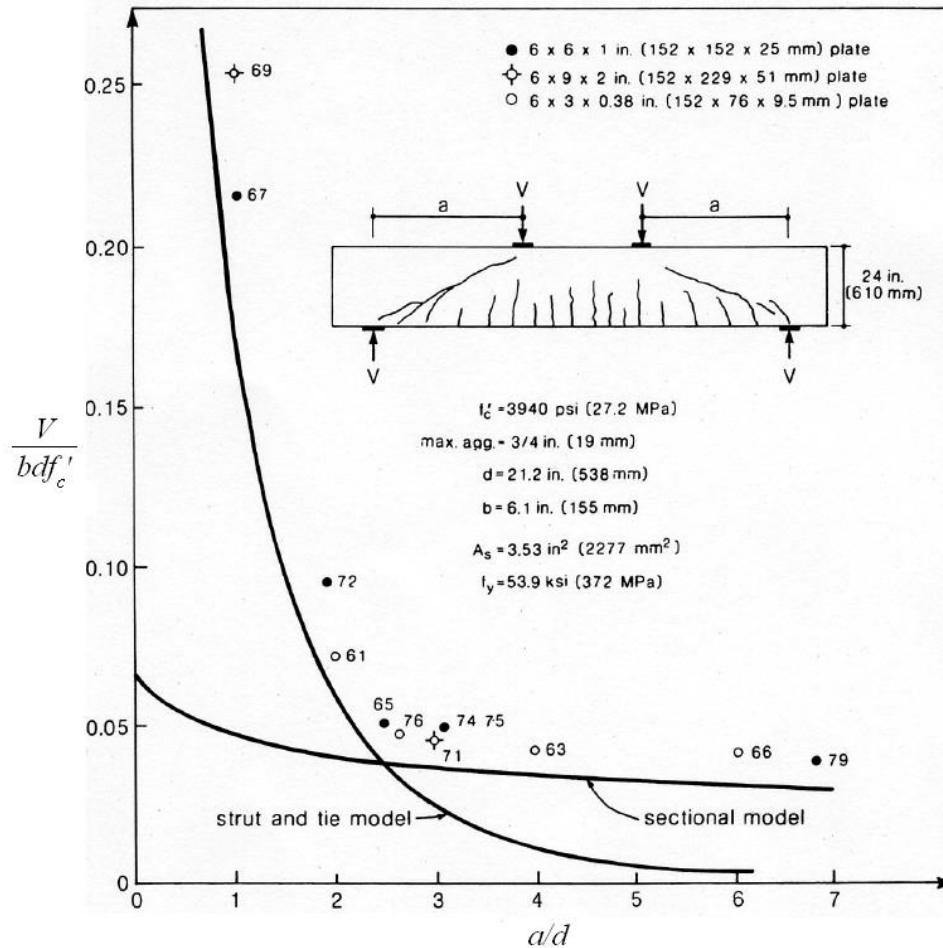


Figure 3.7: Predicted and Observed Strengths of a Series of RC Beams Tested by Kani (Collins and Mitchell, 1997)

The STM approach is rapidly gaining popularity for the analysis and design of deep beams, and has been adopted in several North American codes, such as the American Concrete Institute (ACI) Building Code Requirements for Structural Concrete (ACI 318-08) and the Canadian Standard Association (CSA) Design of Concrete Structures (CSA A23.3-04). Appendix A of ACI 318-08 provides guidance for sizing struts, nodes, and ties. The code addresses the performance of highly stressed compression zones that may be adjacent to or crossed by cracks in a member, the effect of stresses in nodal zones, and the requirements for bond and anchorage of ties. However,

ACI 318-08 provides no clear guidance to indicate when a strut should be considered as rectangular or bottle-shaped.

Furthermore, as shown in **Figure 3.8**, structural elements may consist of B-regions, D-regions, or a combination of both depending on several factors. ACI 318-08 states that if there is a B-region located between D-regions in a shear span, as shown in **Figure 3.8(b)**, the strength of the shear span is governed by the strength of the B-region if the B- and D-regions have similar geometry and reinforcement. This is because the shear strength of a B-region is less than the shear strength of a comparable D-region. Shear spans containing B-regions are designed for shear using traditional truss model approaches.

Figure 3.9 presents the layout and dimensions of the beam specimens tested in the current study. Based on the previous discussion, the presence of B-regions within the shear span precludes the application of a STM approach in determining the capacity of this section. Instead, these beams are governed by the traditional truss model approach.

3.4.3. Modified Compression Field Theory. The Modified Compression Field Theory (MCFT) was developed by Vecchio and Collins in 1986, and is a further development of the Compression Field Theory (CFT) derived by Collins and Mitchell in 1980. In the CFT it is assumed that the principal tensile stress (f_1) is zero after the concrete has cracked while in the MCFT the effect of the residual stress in the concrete between the cracks is taken into account. Tensile stresses across the diagonal struts increase from zero at the cracks to a maximum in the middle of the strut as shown in **Figure 3.10**.

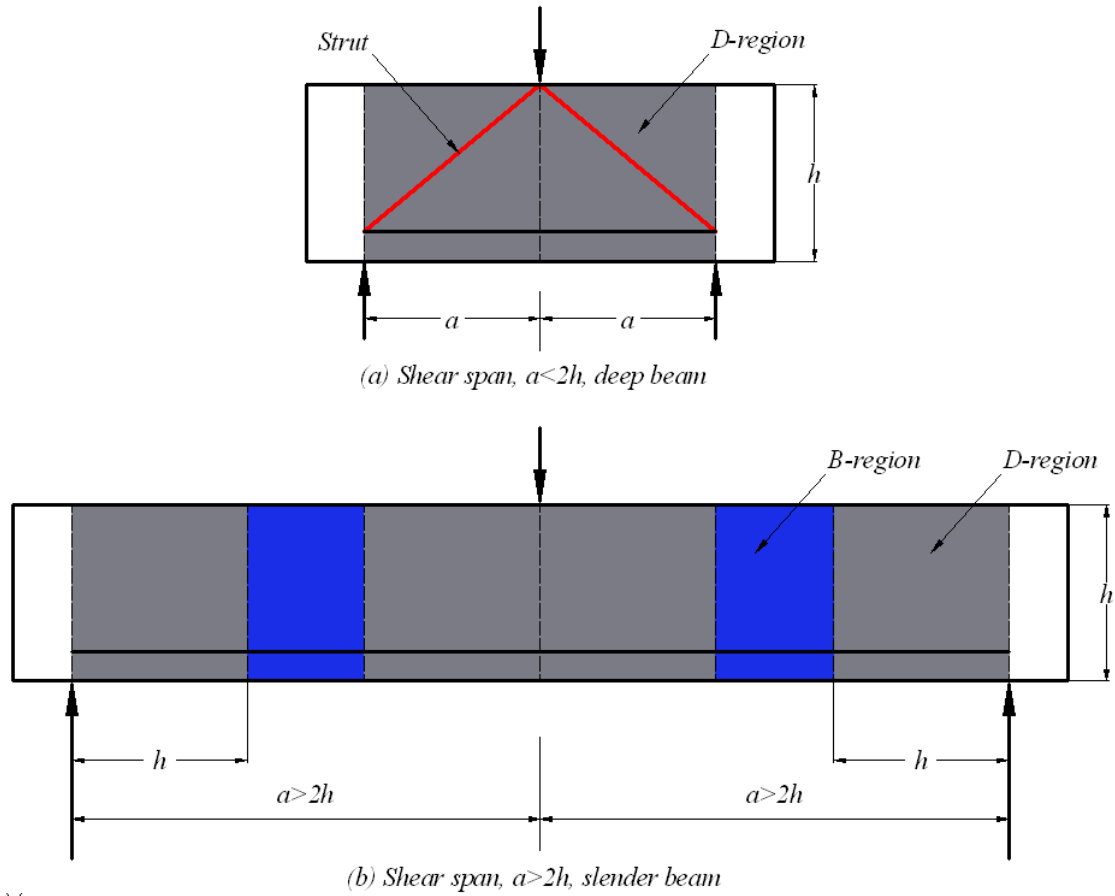


Figure 3.8: Description of Deep and Slender Beams (ACI 318-08)

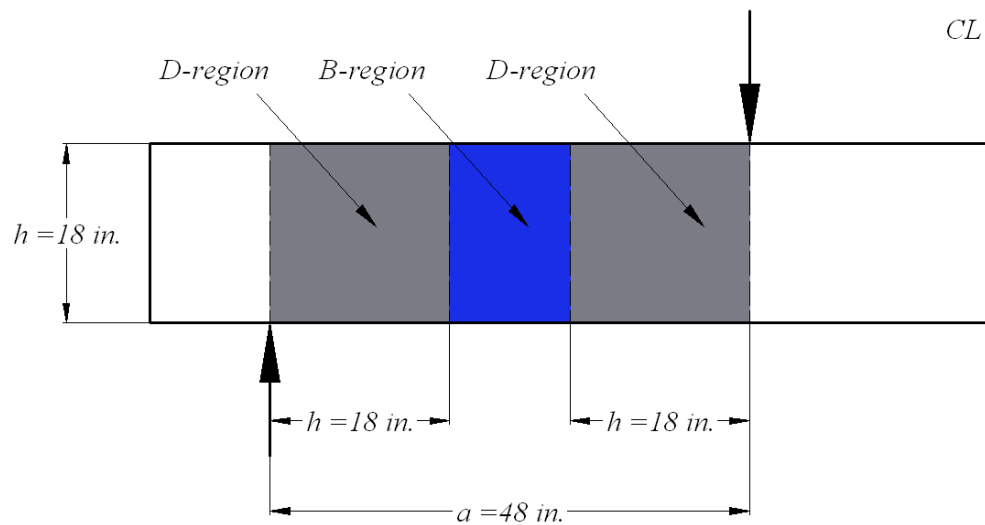


Figure 3.9: Slender Beams Used in This Study

The MCFT model consists of strain compatibility and equilibrium equations which can be used to predict the complete shear deformation response. All the compatibility equations are expressed in terms of average strains measured over base lengths long enough to include several cracks. The compatibility equations for both the CFT and the MCFT are given in **Equations 3.6, 3.7, and 3.8**, which are obtained from the Mohr's circle shown in **Figure 3.11**.

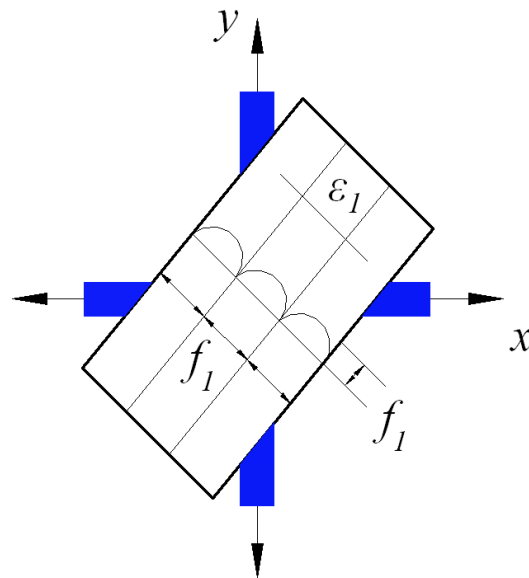


Figure 3.10: Tensile Stress Along a Cracked Strut (Vecchio and Collins, 1986)

$$\gamma_{xy} = \frac{2(\varepsilon_x - \varepsilon_2)}{\tan \theta} \quad (3.6)$$

$$\varepsilon_1 + \varepsilon_2 = \varepsilon_x + \varepsilon_y \quad (3.7)$$

$$\tan^2 \theta = \frac{\varepsilon_x - \varepsilon_2}{\varepsilon_y - \varepsilon_2} = \frac{\varepsilon_1 - \varepsilon_y}{\varepsilon_1 - \varepsilon_x} \quad (3.8)$$

where γ_{xy} is the shear strain, ϵ_x is the strain in the x-direction, ϵ_y is the strain in the y-direction, ϵ_1 is the principal tensile strain in concrete (positive value), and ϵ_2 is the principal compressive strain in concrete (negative value).

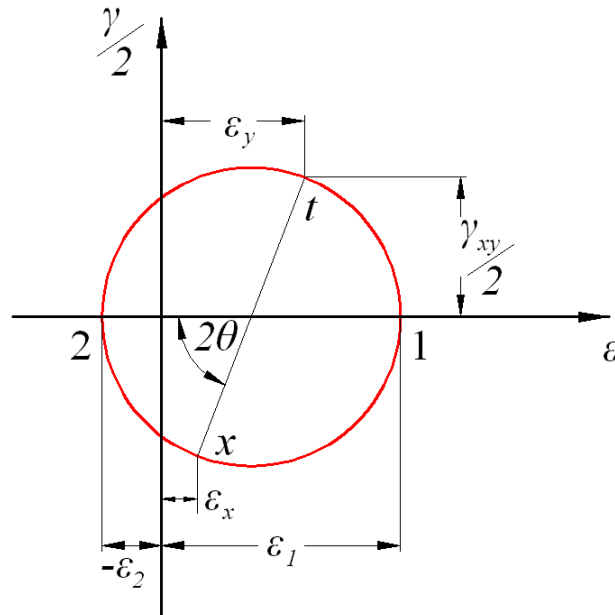


Figure 3.11: Mohr's Circle for Average Strains

The concrete element shown in **Figure 3.12** will resist concrete shear forces (v_{cxy}), horizontal concrete stresses (f_{cx}), and vertical concrete stresses (f_{cy}). All three forces combine to form the principal tensile stress (f_1), and the principal compressive stress (f_2). Converting these stresses into a Mohr's circle of stress, as shown in **Figure 3.13**, the equilibrium **Equations 3.9** and **3.10** can be derived.

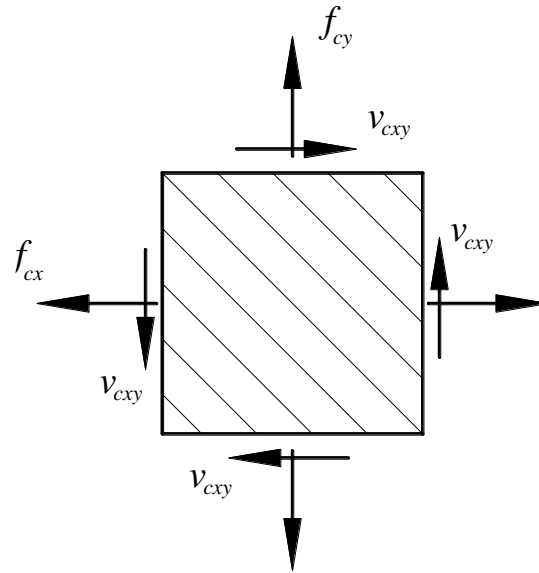


Figure 3.12: Average Concrete Stress in a Cracked Element (Vecchio and Collins, 1986)

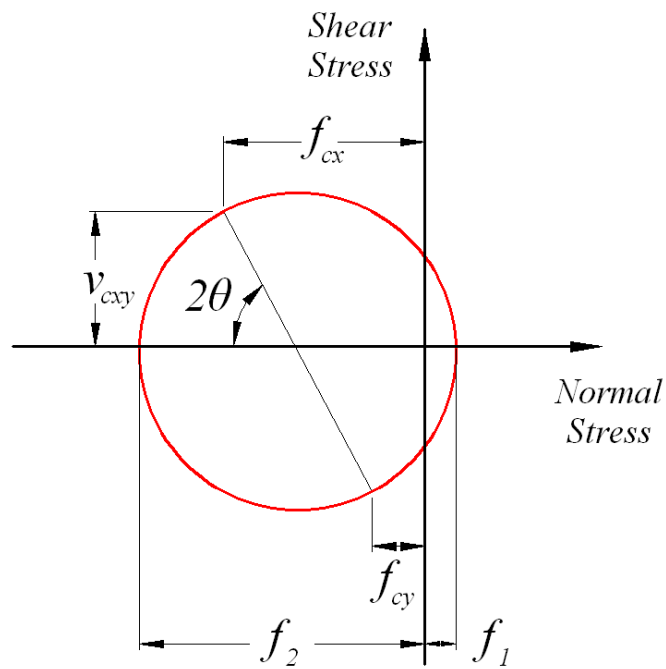


Figure 3.13: Mohr Stress Circle for Average Concrete Stresses

$$f_{cx} = f_1 - \frac{v_{cxy}}{\tan \theta} \quad (3.9)$$

$$f_{cy} = f_1 - v_{cxy} \tan \theta \quad (3.10)$$

The Mohr's circle can also be used to derive an equation for relating the principal compressive stress (f_2) and tensile stresses as shown in **Equation 3.11**.

$$f_2 = (\tan \theta + \cot \theta)v - f_1 \quad (3.11)$$

where, $v = \frac{V}{b_w jd}$ and jd is the distance between the resultants of the internal compressive and tensile forces on a cross section.

The equilibrium conditions for a symmetrical cross section subjected to pure shear are shown in **Figure 3.14**. These conditions can be expressed as shown in **Equation 3.12**.

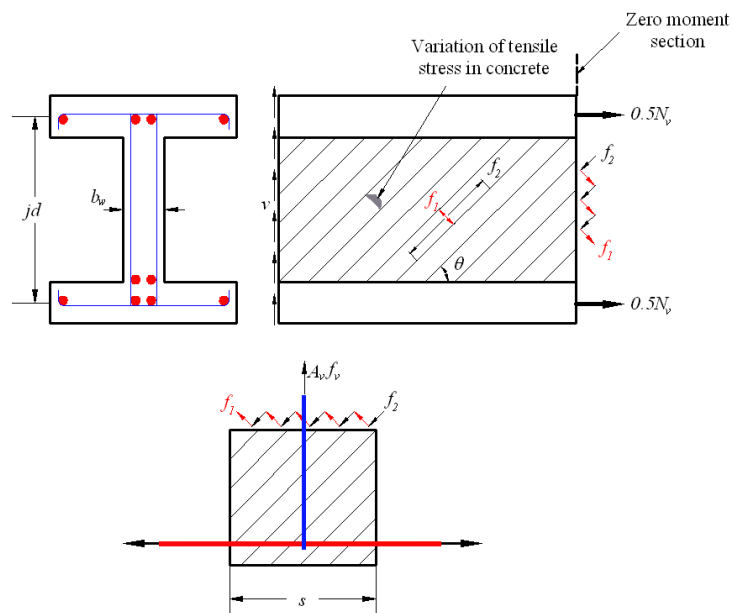


Figure 3.14: Cross Section, Principal Stresses, and Tension in Web Reinforcement (Collins and Mitchell, 1991)

$$A_v f_v = (f_2 \sin^2 \theta - f_1 \cos^2 \theta) b_w s \quad (3.12)$$

where A_v is the steel vertical reinforcement area and f_v is the stress in the stirrups.

Substituting **Equation 3.11** into **3.12** generates the expression in **Equation 3.13**.

$$V = f_1 b_w j d \cot \theta + \frac{A_v f_v}{s} j d \cot \theta \quad (3.13)$$

Collins and Mitchell (1991) noted that **Equation 3.13** expresses shear resistance in terms of the sum of the concrete and steel contributions, as the traditional or classical method. The concrete contribution depends on the average tensile stresses in the concrete, and the steel contribution depends on the tensile stresses in the stirrups. It must be clarified that although the MCFT and the truss model approaches might seem to be similar, the concrete contribution from the concrete suggested by the MCFT is not constant as assumed in the classical truss model. The shear contribution of the concrete (V_c) in the MCFT is not equal to the shear strength of a similar member without shear reinforcement. According to the MCFT, the contribution of the concrete is a function primarily of the crack width. Increasing the number of stirrups reduces the crack spacing, this decreases the crack width and thus increases the concrete contribution (Cladera, 2002).

One of the most important features of the MCFT is the average strain-stress relationships derived from the tests of reinforced panels subjected to pure shear (Vecchio and Collins, 1986). The concrete compressive strength is reduced to take into account softening due to transverse tensile strain (ε_1). Initially, a parabolic relationship for

cracked concrete in compression subjected to high tensile strains in the direction normal to the compression was suggested, as shown in **Equation 3.14**.

$$f_2 = f_{2,max} \left[2 \left(\frac{\varepsilon_2}{\varepsilon'_c} \right) - \left(\frac{\varepsilon_2}{\varepsilon'_c} \right)^2 \right] \quad (3.14)$$

where ε'_c is the strain in the concrete, and for the MCFT, $\beta = \frac{f_{2,max}}{f'_c} =$

$$\frac{1}{0.8 - 0.34 \frac{\varepsilon_1}{\varepsilon'_c}} \leq 1.0$$

This relationship for the concrete softening (β) was derived for the MCFT in which the crack slip is not taken into account. According to Vecchio and Collins (1993), concrete strength can also have an influence in concrete softening. Moreover, size effects can also have an effect. For concrete in tension, the curve proposed in Vecchio and Collins (1986) is given by **Equations 3.15** and **3.16**.

$$\text{If } \varepsilon_1 \leq \varepsilon_{cr} \text{ then } f_1 = E_c \varepsilon_1 \quad (3.15)$$

$$\text{If } \varepsilon_1 > \varepsilon_{cr} \text{ then } f_1 = \frac{f_{cr}}{1 + \sqrt{200\varepsilon_1}} \quad (3.16)$$

where ε_{cr} is the crack strain, E_c is the modulus of elasticity of the concrete, and f_{cr} is the stress in the concrete at cracking.

Equation 3.16 was updated by Vecchio and Collins (1993) to include two new parameters (α_1 and α_2) to account for the bond characteristics of the reinforcement and the type of loading. The updated equation is presented in **Equation 3.17**.

$$f_1 = \frac{\alpha_1 \alpha_2 f_{cr}}{1 + \sqrt{500 \varepsilon_1}} \quad (3.17)$$

$$\text{where, } f_{cr} = 0.33 \sqrt{f'_c}$$

The stress and strain formulations adopted in the MCFT use average values, so local variations are not considered. In this methodology, a check must be done to ensure that the reinforcement can take the increment in tensile stress at the crack. In order to make this check, a value of the stress along the crack must be assumed. The shear transfer at the cracks by aggregate interlock action is estimated using the relationship in **Equation 3.18**. This equation was developed based on Walraven's (1980) experiments.

The MCFT can provide accurate predictions of shear strength and deformation. The first and most important assumption made in the MCFT is that of a rotating crack model in which previous cracks are assumed to be inactive. The MCFT assumes that the angles of the axes for the principal strains and principal stresses coincide (θ). The crack in which all the checks are performed is assumed to be oriented at the same angle, θ , as the compressive stress field.

$$v_{ci} = 0.18v_{ci,max} + 1.64f_{ci} - 0.82 \frac{f_{ci}^2}{v_{ci,max}} \quad (3.18)$$

$$\text{where, } v_{ci,max} = \frac{\sqrt{f'_c}}{0.31 + \frac{24w}{a+16}}$$

In the expression above, a is the maximum aggregate size in millimeters, and w is the average crack width over the crack surface which is estimated as the product of the

principal tensile strain (ε_1) and the crack spacing (s_θ). The spacing of shear cracks is considered to be dependent on the crack spacing in the longitudinal and transverse reinforcement directions. The crack spacing can be calculated by using **Equation 3.19**. In this equation s_{mx} is the average spacing of cracks perpendicular to the longitudinal reinforcement, and s_{mv} is the average spacing of cracks perpendicular to the transverse reinforcement. Finally, s_{mx} and s_{mv} are estimated using the formulas given by **Equations 3.20 and 3.21**.

$$s_\theta = \frac{1}{\frac{\sin \theta}{s_{mx}} + \frac{\cos \theta}{s_{mv}}} \quad (3.19)$$

$$s_{mx} = 2 \left(c_x + \frac{s_x}{10} \right) + 0.25k_1 \frac{d_{bx}}{\rho_x} \quad (3.20)$$

$$s_{mv} = 2 \left(c_y + \frac{s}{10} \right) + 0.25k_1 \frac{d_{bv}}{\rho_v} \quad (3.21)$$

where c_x and c_y are the concrete covers for the longitudinal and transverse reinforcement respectively; s_x and s are the spacing of the longitudinal and transverse reinforcement respectively; d_{bx} and d_{bv} are the bar diameters of the longitudinal and transverse reinforcement respectively; ρ_x and ρ_v are the ratios for the longitudinal and transverse reinforcement respectively; and k_1 equals 0.4 for deformed bars and 0.8 for plain bars.

The MCFT has been criticized from a practical perspective since it requires the use of a computer in order to solve the system of equations. This problem was addressed

by Bentz and Collins by providing two free software packages, called RESPONSE 2000 and MEMBRANE 2000, to solve these equations.

Bentz et al. (2006) developed simplified versions of the MCFT which can be used in order to predict the maximum shear capacity rather than the complete load-deformation response. **Equations 3.22** and **3.23** present these expressions that are also incorporated in the Canadian Code CSA A23.3 (2004).

$$V_r = V_c + V_s \leq 0.25\phi_c f'_c b_w d_v \quad (3.22)$$

$$V_r = \phi_c \beta \sqrt{f'_c} b_w d + \phi_s \frac{A_{sw}}{s} f_y d_v \cot \theta \quad (3.23)$$

where ϕ_c and ϕ_s are the capacity reduction factors, b_w is the width of the web, d_v is the effective shear depth ($d_v = 0.9d$), A_s is the area of longitudinal reinforcement on the flexural tension side. The parameter β represents the shear retention factor that can be defined as the ability of cracked concrete to transmit shear by means of aggregate interlock, while θ is the angle of inclination of the strut. These two parameters are estimated in terms of the longitudinal strain at the mid-depth of the section using **Equations 3.24** and **3.25**.

$$\beta = \frac{0.40}{1+1500\varepsilon_x} \cdot \frac{1300}{1000+s_{xe}} \quad (3.24)$$

$$\theta = 29 + 7000\varepsilon_x \quad (3.25)$$

$$\text{where, } \varepsilon_x = \frac{M_f + V_f d}{2E_s A_s l}$$

The parameters V_f and M_f are the factored shear force and moment at the section. The effective crack spacing (s_{xe}) is taken as 11.8 in. for members with at least minimum stirrups and for members without stirrups, $s_{xe} = \frac{35s_x}{15+a_g} \geq 0.85s_x$. The crack spacing parameter (s_x) is the longitudinal spacing between cracks, measured at mid-depth of the member. For members without horizontal reinforcement at the web, s_x is usually taken as d_v .

3.4.4. Fracture Mechanics Approach. Although fracture mechanics was developed by Griffith in 1920, for half a century, it was considered inappropriate for concrete. The reason that it took so long to apply this method to concrete is that the traditional fracture mechanics approach was developed for homogeneous materials, such as steel. However, the existence of a size effect observed in experimental results obtained during previous research (Bazant and Kim, 1984) prompted several researchers to apply fracture mechanics to shear failures. The use of fracture mechanics in design could increase the safety and reliability of concrete structures. Numerous analytical and numerical tools have been developed to simulate the fracture behavior of concrete structures, and in connection with these developments, researchers are focused on designing experimental methods to measure the different parameters required for these models. The ACI 446.1R (1999) document highlights five compelling reasons to use a fracture mechanics approach. The first one is the energy required for crack formation. This reason states that the actual formation of cracks requires energy, called fracture energy, which represents the surface energy of a solid. The second one is the objectivity

of the calculations. Any physical theory must be objective and the result of the calculations must not depend on subjective aspects such as choice of coordinates, mesh, etc. Objectivity should come ahead of experimental verification. The third reason is the lack of yield plateau. Based on load-deflection diagrams, there are two distinguishable basic types of structural failure, plastic and brittle. Plastic failures typically develop a single-degree-of-freedom mechanism such that the failure proceeds simultaneously in various parts of the structure. These failures are characterized by the presence of a long yield plateau on the load-deflection diagram. If this diagram does not have such a plateau, the failure is brittle or brittle-ductile. The fourth reason is capability to absorb energy, as related to ductility. The area under the complete load-deflection diagram of a concrete or reinforced concrete member represents the energy which the element will absorb during failure, and this energy must be supplied by the loads. The current plastic limit analysis cannot give information on the post-peak decline of the load and energy dissipated in this process. The fifth and most compelling reason for using fracture mechanics is the size effect. ACI 446.1R (1999) defines the size effect through a comparison of geometrically similar structures of different sizes, characterized in terms of the nominal stress at maximum ultimate load. When this nominal stress does not change its value for geometrically similar structures of different sizes, it can be said that there is no size effect.

The study of fracture mechanics of concrete started in 1961 with Kaplan. Later, in 1972, Kesler et al. concluded that the classical linear elastic fracture mechanics (LEFM) approach with only one fracture parameter, either the fracture energy or the fracture

toughness, was not applicable to concrete. Kesler et al. suggested at least two fracture parameters.

The simplest model that describes the progressive fracture process is the cohesive crack model (Hillerborg et al., 1976). Hillerborg et al. proposed the cohesive crack model for simulation of plain concrete, in which concrete fracture energy characterized the softening response of a cohesive crack that could develop anywhere in a concrete structure. The softening curve is the main feature of the cohesive crack model. This curve presents an initial portion with a steep descending slope, followed by a smooth drop when the stress reaches a value approximately equal to $1/3$ of the nominal tensile strength (f'_t), and a long tail asymptotic to the horizontal axis (crack opening, w) as shown in **Figure 3.15**. Geometrically, the area under the complete curve represents the fracture energy. The fracture energy is defined as the amount of energy necessary to create a crack of unit surface area projected in a plane parallel to the crack direction.

Hillerborg (1985) provided a theoretical basis for a concrete fracture energy testing procedure, often referred to as the work-of-fracture method (WFM), in which the fracture energy per unit area of concrete is computed as the area under the experimental load-deflection response curve for a notched concrete beam subjected to three-point bending, divided by the area of fracture concrete.

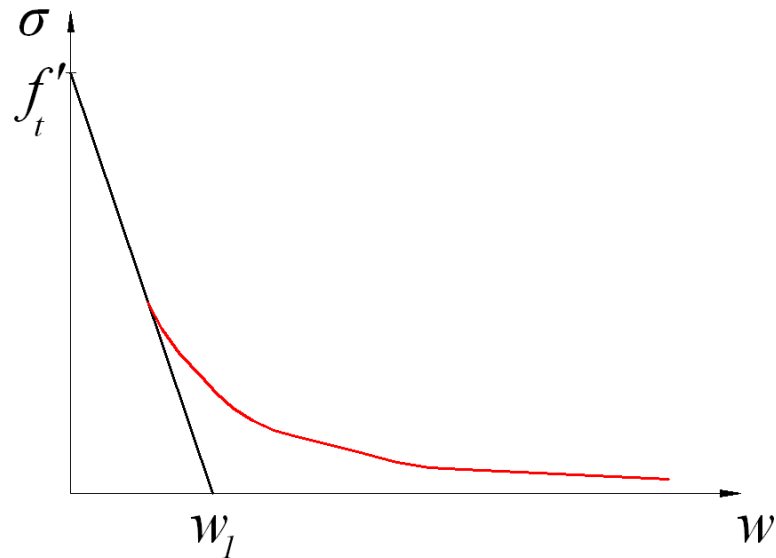


Figure 3.15: Softening Function and Initial Tangent for Cohesive Crack Model (Einsfeld and Velasco, 2006)

For example, when conducting three-point bending tests on notched beams, as the beam splits into two halves, the fracture energy (G_F) can be determined by dividing the total dissipated energy by the total surface area of the crack as shown in **Equation 3.26**.

$$G_F = \frac{W}{b(d-a_0)} \quad (3.26)$$

where W is the total energy dissipated in the test, and b , d , and a_0 are the thickness, height and notch depth of the beam, respectively.

Several additional test methods have been proposed in recent years to determine concrete fracture properties from which fracture energy may be computed.

In 1987, Bazant and Pfeiffer concluded that the cohesive crack model results in fracture characteristics that are ambiguous and size-dependent. As a consequence, different values for the fracture energy could be obtained for specimens of different sizes.

Bazant and Pfeiffer proposed a method where the fracture energy is calculated based on the size effect law. In this approach, the fracture energy is independent of the size of the specimens. This asymptotic approach is known as the size effect method (SEM). Bazant and Pfeiffer suggested the following relationship shown in **Equation 3.27**.

$$\sigma_N = B(1 + \beta^k)^{\frac{1}{2k}} \quad (3.27)$$

where σ_N is the nominal stress at failure, B is the coefficient obtained through the linear regression plot of the results, β is the brittleness number, and k is a parameter to reflect the size effect.

The brittleness number indicates whether the behavior of any structure is related to either the limit state analysis or to LEM analysis. Bazant and Pfeiffer proposed **Equation 3.28** for the brittleness number.

$$\beta = \frac{d}{d_0} \quad (3.28)$$

where d is the characteristic dimension of the structure (for their study, the specimen height), and d_0 is a coefficient determined experimentally. The coefficients B and d_0 are determined by linear regression. In this approach, specimens of different sizes but geometrically similar can be rearranged in a linear regression plot as shown in **Equation 3.29**. **Equations 3.30 to 3.33** present the different relationships for the parameters contained in **Equation 3.29**.

Rupture of a structure of infinite size follows the LEFM theory, since the plastic region around the concrete fracture zone is relatively small. In this case, the fracture energy can be calculated using **Equation 3.34**.

$$y = Ax + C \quad (3.29)$$

$$y = \left(\frac{1}{\sigma_N}\right)^2 \quad (3.30)$$

$$x = d \quad (3.31)$$

$$d_0 = \frac{c}{A} \quad (3.32)$$

$$B = \frac{1}{\sqrt{c}} \quad (3.33)$$

$$G_f = \frac{g_f(\alpha_0)}{AE} \quad (3.34)$$

where E is the modulus of elasticity of the concrete, A is the angular coefficient of the linear regression plot, $g_f(\alpha_0)$ is the non-dimensional energy release rate calculated according to LEFM, and α_0 is the relative notch length defined in **Equation 3.35**.

$$\alpha_0 = \frac{a_0}{d} \quad (3.35)$$

The fracture energy normally associated with WFM is different from the one calculated through SEM. They are usually differentiated as G_F for values calculated with WFM, and G_f for values calculated using SEM. The values obtained with WFM are

sensitive to the specimen size and shape. On the other hand, values obtained with SEM are independent of the structure size as well as geometry (Einsfeld and Velasco, 2006).

While G_F corresponds to the area under the complete softening stress-separation curve of the cohesive crack model, G_f corresponds to the area under the initial tangent of the stress-separation curve as shown in **Figure 3.16**.

Bazant and Kim (1984) and Bazant and Sun (1987) developed a set of equations to describe the dependence of the diagonal shear strength on the size, shape, and longitudinal reinforcement ratio of beams failing in diagonal shear. The shear strength in this model is assumed to result from the combination of the arching action and the composite beam action. The summation of the two components resulted in an expression similar to that of the ACI building code. However, this expression failed to explain the structural behavior.

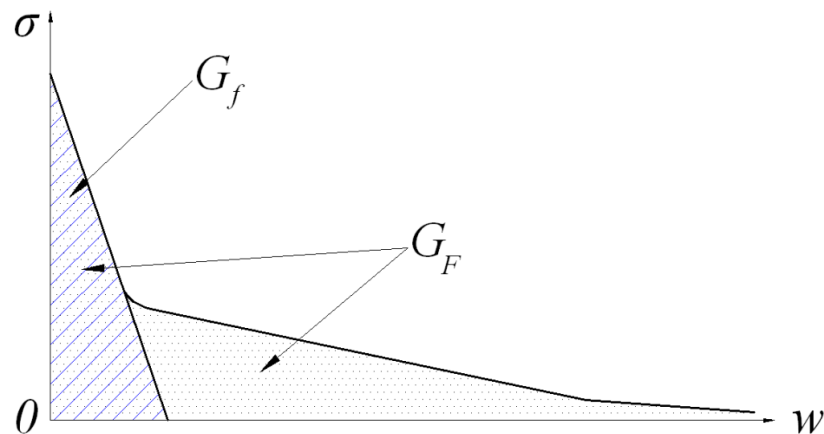


Figure 3.16: Softening Stress-Separation Curve of Cohesive Crack Model (Bazant and Becq-Giraudon, 2002)

Gustafsson and Hillerborg in 1988 investigated the diagonal shear strength of members without stirrups using the cohesive crack concept, with the objective to show that a size effect can be predicted theoretically. This model assumes that a single

polygonal cohesive crack with linear softening is formed, while the bulk of the concrete remains linear elastic. The behavior of the steel is assumed to be linear elastic. The failure criterion adopted is crushing of the concrete. Using this approach Gustafsson and Hillerborg analyzed the influence of the size, longitudinal reinforcement ratio, and the shear span-to-depth ratio.

Jenq and Shah (1989) adopted a more physical approach applying a two-parameter nonlinear fracture mechanics model to the shear failure. In this model, the ultimate shear capacity is assumed to be the summation of the contributions from the reinforcement and the concrete. The concrete contribution is derived using the fracture mechanics model. The steel contribution is estimated by considering the average ultimate bond stress, which is assumed to be proportional to the embedded length.

In 1993, So and Karihaloo criticized Jenq and Shah's approach pointing out that their approach was oversimplified and ignored the influence of the reinforcement on the fracture behavior of the concrete. Large discrepancies between the predicted and measured capacities confirmed their criticism. Karihaloo introduced a failure criterion for longitudinal splitting using Van der Veen's model (Van der Veen, 1990) to derive the maximum bond stress. Finally, Karihaloo concluded that the bond-slip relationship, the dowel action, and the aggregate interlock must be taken into account to accurately predict the shear capacity using Jenq and Shah's approach. The only weak point of Karihaloo's model is the significant use of empirical equations.

In 2001, Gasteblet and May proposed a fracture mechanics model for the flexural-shear failure of reinforced concrete beams without stirrups. This model was developed assuming that the ultimate shear load is reached when the splitting crack starts

to propagate. The critical load is calculated considering the energy balance of the system during splitting crack propagation. The position of the critical diagonal crack is obtained using Kim and White's semi-empirical formula proposed in 1991. Gastebled and May used the empirical formula for the assessment of the fracture energy proposed by the CEB-FIP Model Code.

The formulation of this model is based on the fundamental relation of LEFM presented in **Equation 3.36**, where G is the fracture energy consumption and W_{ext} is the work of the external force. The external load is produced by the rotation under constant load about the tip of the diagonal crack. In order to calculate the energy release, the rotational stiffness of the beam must be determined. This stiffness depends on the axial and dowel stiffness of the longitudinal reinforcement. The stiffness is calculated based on the free body diagram (FBD) presented in **Figure 3.17**.

$$\delta G = \frac{1}{2} \delta W_{ext} \quad (3.36)$$

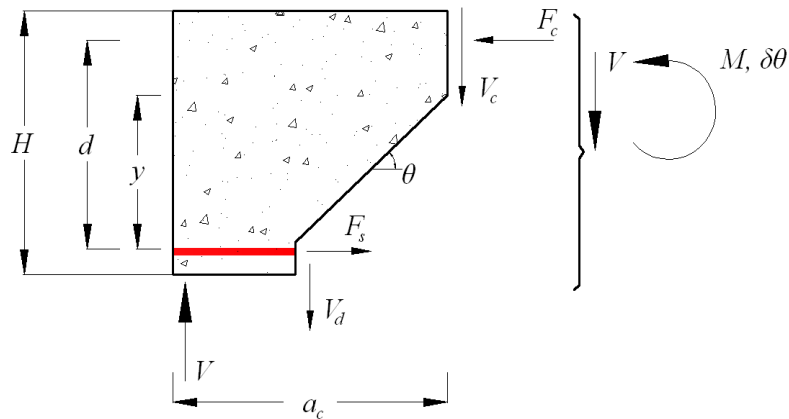


Figure 3.17: Free Body Diagram and Notation Definition (Gastebled and May, 2001)

The axial and shear force in the steel bar crossing the diagonal crack were linked to the angle of rotation (θ) using the elastic properties of the bar and the geometry of the deformation mechanism as shown in **Equation 3.37**. The beam bending theory for a circular cross section is also used to derive the dowel force as shown in **Equation 3.38**.

$$F_s = \frac{E_s A_s}{\delta_s} y \theta \quad (3.37)$$

$$V_d = \frac{G_s \Sigma_s}{\delta_s} y \theta = \frac{9}{26} \cdot \frac{E_s A_s}{\delta_s} y \theta \quad (3.38)$$

where F_s is the longitudinal reinforcement force, δ_s is the unbounded length of the reinforcement, y is the diagonal crack extent, θ is the rotation, V_d is the longitudinal reinforcement dowel force, G_s is the shear modulus of steel, and Σ_s is the reduced cross section of the bar (taken as $0.9A_s$).

The equilibrium of the FBD presented in **Figure 3.17** is reached when the following relationships shown in **Equations 3.39** to **3.41** are maintained (horizontal, vertical, and moment equilibrium, respectively). Assuming that the diagonal crack extent and the internal moment arm (jd) are proportional to the height of the beam as shown in **Equations 3.42** and **3.43**, **Equation 3.41** can be rewritten and is presented in **Equation 3.44**. **Equation 3.44** provides the rotational stiffness.

$$F_s = F_c \quad (3.39)$$

$$V_c + V_d = V \quad (3.40)$$

$$F_s jd + V_d y = V a_c \quad (3.41)$$

$$y = \beta H \quad (3.42)$$

$$jd = \gamma H \quad (3.43)$$

$$\beta \left(\frac{9}{26} \beta + \gamma \right) \frac{E_s A_s}{\delta_s} H^2 \theta = V a_c \quad (3.44)$$

After differentiating **Equation 3.44** and using the fundamental relation of fracture mechanics as a criterion for splitting failure as shown in **Equation 3.36**, **Equations 3.45** and **3.46** are derived to obtain the expression for the critical shear load.

$$a_c V_{cr} \delta \theta = 2 \Gamma \delta_e \quad (3.45)$$

$$V_{cr} = \sqrt{\frac{9}{13} + 2 \frac{\gamma}{\beta} \cdot \frac{\beta H}{a_c}} \cdot \sqrt{\Gamma A_s E_s} \quad (3.46)$$

where δ_e is the variation of the unbonded length, and Γ is the fracture energy necessary to extend the splitting crack by a unit length. For simplicity of calculations and based on experimental observations, γ and β can be taken as 0.9 and 0.8 respectively. The units for this model have been set as follows: V_{cr} in kN, Γ in kN-m/m, A_s in mm^2 , and E_s in GPa.

This model uses the equation given by the CEB-FIP Model Code for the assessment of the fracture energy and is presented in **Equation 3.47**. The maximum aggregate size (d_{agg}) is assumed in Gastebled and May's model as 0.75 in. Based on all

the previous assumptions and assuming a dynamic mode of failure, **Equation 3.46** can be simplified and is presented in **Equation 3.48**.

$$G_f = (0.0469d_{agg}^2 - 0.5d_{agg} + 26) \left(\frac{f'_c}{10} \right)^{0.7} \quad (3.47)$$

$$V_{cr} = 4.517 \cdot \frac{H}{a_c} \cdot (f'_c)^{0.35} \sqrt{A_s E_s b} \quad (3.48)$$

The units for this model have been set as follows: V_{cr} in kN, f'_c in MPa, A_s in m^2 , and E_s in GPa, and b in mm.

The only problem in this model is the determination of the location of the critical diagonal crack. Kim and White (1991) postulated the same failure mechanism and adopted a mixed approach, partly physical and partly empirical, to predict the flexural-shear cracking and the position of the critical diagonal crack. **Equation 3.49** presents the model to calculate the location of the critical diagonal crack.

$$a_c = k_3 a_s \left(\frac{\rho_s \left(\frac{d}{a_s} \right)^2}{(1 - \sqrt{\rho_s})^2} \right)^{\frac{1}{3}} \quad (3.49)$$

where k_3 is an empirical coefficient determined through statistical analysis and has a value of 3.3, a_s is the shear span, ρ_s is the geometrical reinforcement ratio, and d is the effective depth of the beam. Limited experimental data was available to check the position of the critical diagonal crack, however, Kim and White found 14 experimental results to perform the statistical analysis and determine a value for the coefficient k_3 . Significant scatter was reported by the authors.

The final expression is obtained by substituting **Equation 3.49** into **Equation 3.48** and is shown in **Equation 3.50**. In this expression, the first term corresponds to the size effect, the second term takes into account the slenderness of the beam, the third and fourth terms reflect the reinforcement ratio influence, and the fifth term corresponds to the influence of the concrete strength.

$$V_{cr} = \frac{1.109}{\sqrt{H}} \cdot \left(\frac{H}{a_s}\right)^{\frac{1}{3}} \cdot (1 - \sqrt{\rho_s})^{\frac{2}{3}} \cdot \rho_s^{\frac{1}{6}} \cdot f'_c{}^{0.35} \cdot \sqrt{E_s} \cdot bH \quad (3.50)$$

where H is the height of the beam, a_s is the shear span, ρ_s is the geometrical reinforcement ratio, f'_c is the concrete compressive strength, E_s is the steel modulus of elasticity, and b is the width of the beam.

Bazant and Becq-Giraudon (2002) formulated the empirical expression shown in **Equation 3.51** to compute fracture energy for specimens with rounded aggregate. This equation was calibrated using 161 RILEM work-of-fracture tests whereas the equation proposed by CEB-FIP was calibrated using much less data. Bazant and Becq-Giraudon also reported that G_F data computed from work-of-fracture testing have significantly more scatter than G_f data computed using other test methods and suggested that this scatter was due to errors in measurement of the tail of the load-displacement response curve.

$$G_f = 0.0143\alpha_0 \left(\frac{f'_c}{8.41}\right)^{0.40} \left(1 + \frac{D_{max}}{0.0763}\right)^{0.43} \left(\frac{w}{c}\right)^{-0.18} \quad (3.51)$$

where α_0 is an aggregate shape factor ($\alpha_0 = 1$ for rounded aggregate, and $\alpha_0 = 1.12$ for angular aggregate), f'_c is the compressive strength of the concrete, D_{max} is the

maximum aggregate size, and $\frac{w}{c}$ is the water-to-cement ratio of the concrete. The units of this model have been set as follows: f'_c in psi, and D_{max} in inches.

3.4.5. Truss Model and Modified Compression Field Theory Comparison.

The MCFT can be explained as a truss model in which the shear strength is the sum of the steel and concrete contributions. The main difference from a classic truss model with concrete contribution is that the concrete contribution in the MCFT is the vertical component of the shear stress transferred across the crack (v_{ci}) and not the diagonal cracking strength.

Cladera (2002) highlighted the main differences between the truss model and the MCFT concrete contributions:

- The truss model concrete contribution is considered equal to the shear strength of a similar beam without shear reinforcement. The MCFT takes into account a concrete contribution based on the actual collapse mechanism of a RC beam.
- The truss model concrete contribution does not vary with the amount of the transverse reinforcement. The MCFT concrete contribution depends on the crack width. The more shear reinforcement, the smaller the crack width, and the greater the concrete contribution.

3.4.6. Summary of Shear Design. Shear design in structural concrete has been a challenging topic for many years. The truss analogy first proposed by Ritter (1899) and then improved by Mörsh (1902) has been a powerful tool in understanding the shear transfer mechanism in a RC beam. However, progress has been made since those early truss models. Three different groups of approaches have been developed: (1) 45 degrees

truss model, (2) compression field theories, and (3) fracture mechanics approaches. Predictions of the shear provided by these approaches have improved considerably from early formulations, which were based on empirical results. As reported by Collins et al. (2008), early design equations for shear have been proven to be unsafe since the experimental data used in calibrating the models corresponded to rather small specimens. The MCFT offers a rational approach in which the shear transmitted along the crack is limited according to the crack width and aggregate size. The STM which was developed by Schaich et al. (1987) is often claimed as a transparent method for designing and detailing discontinuity regions. It has been highlighted that the method requires several simplifications regarding geometry assumed for the truss elements or the effective strength of the struts. Finally, it is clear that several difficulties can be faced in developing a STM, such as uniqueness of the model, combinations with other load cases or dealing with statically indeterminate systems.

3.5. DESIGN CODES REVIEW

There are a variety of design code philosophies that can be found around the world for shear design. Some of these rely on empirical formulas for estimating the shear strength, such as the ACI 318-08 (2008), while others such as the AASHTO LRFD (2010) rely more on concrete models such as the MCFT. This section will detail three selected design codes.

3.5.1. American Concrete Institute, ACI 318-08. The ACI 318-08 method is most commonly used for shear design in the United States, and is based on a 45 degree truss model. The shear strength is based on an average shear stress distribution across the

entire cross section, and is composed of a concrete component (V_c) and a steel component (V_s). The basic equations for normal-weight, non-prestressed reinforced concrete are listed in **Equations 3.52** to **3.56**.

$$V_u \leq \phi V_n = \phi(V_c + V_s) \quad (3.52)$$

$$V_c = \left(1.9\sqrt{f'_c} + 2500\rho_w \frac{V_u d}{M_u}\right) b_w d \leq 3.5\sqrt{f'_c} b_w d \quad (3.53)$$

$$\text{Simplified version: } V_c = 2\sqrt{f'_c} b_w d \quad (3.54)$$

$$A_{v,min} = 0.75\sqrt{f'_c} \frac{b_w s}{f_{yt}} \geq 50 \frac{b_w s}{f_{yt}} \quad (3.55)$$

$$V_s = \frac{A_v f_{yt} d}{s} \quad (3.56)$$

where, V_u is the factored shear force on the section, ϕ is the strength reduction factor equal to 0.75, V_n is the nominal shear strength, $\rho_w = \frac{A_s}{b_w d}$, A_s is the area of longitudinal reinforcement, b_w is the width of the web, d is the distance from the extreme compression fiber to the center of gravity of the steel, M_u is the factored moment at the section, f'_c is the concrete compressive strength (psi), f_{yt} is the yield strength of the transverse reinforcement (psi), s is the spacing of the transverse reinforcement, and A_v is the area of shear reinforcement. The following condition must be maintained $\frac{V_u d}{M_u} \leq 1.0$.

The ACI 318-08 presents a procedure for calculating the failure shear strength for concrete beams without shear reinforcement. The simplified method is presented in **Equation 3.54**. Some research data indicate that **Equation 3.53** overestimates the

influence of f'_c and underestimates the influence of ρ_w and $\frac{V_u d}{M_u}$. This is why, for most designs, it is convenient to assume that the second term of this equation equals to $0.1\sqrt{f'_c}$ and use **Equation 3.54** to calculate the shear contribution of the concrete.

3.5.2. AASHTO LRFD Bridge Design Specifications. The AASHTO LRFD (2010) method is known as the Sectional Design Model, and is based on the MCFT. The nominal shear resistance (V_n) can be computed by **Equations 3.57 to 3.61**.

$$V_n = V_c + V_s + V_p \quad (3.57)$$

$$V_{n,max} = 0.25f'_c b_v d_v + V_p \quad (3.58)$$

$$V_c = 0.0316\beta\sqrt{f'_c} b_v d_v \quad (3.59)$$

$$V_s = \frac{A_v f_y d_v \cot \theta}{s} \quad (3.60)$$

$$A_{v,min} \geq 0.0316\sqrt{f'_c} \frac{b_v s}{f_y} \quad (3.61)$$

where, V_p is the vertical component of the prestressing force, b_v is the effective width of the web taken as the minimum web width within the depth, d_v is the effective shear depth taken as the greater of $0.9d$ or $0.72h$, β is the factor indicating the ability of diagonal cracked concrete to transmit tension, θ is the angle of inclination of the diagonal compressive struts, f'_c is the concrete compressive strength (ksi), and f_y is the yield strength of the transverse reinforcement (ksi).

For sections containing at least the minimum amount of transverse reinforcement, the values of β and θ may be found using **Table 3.1**. The designer selects the row

corresponding to the shear design stress ratio $\frac{v}{f'_c} = \frac{V_u}{b_v d_v f'_c}$, and selects the column

corresponding to the longitudinal strain (ϵ_x) at mid-depth. The longitudinal strain may be computed using **Equation 3.62**.

Table 3.1: Values of θ and β for Sections With Transverse Reinforcement (AASHTO LRFD, 2010)

$\frac{V_u}{f'_c}$		$\epsilon_x \times 1000$										
		≤ -0.20	≤ -0.10	≤ -0.05	≤ 0	≤ 0.125	≤ 0.25	≤ 0.50	≤ 0.75	≤ 1.00	≤ 1.50	≤ 2.00
≤ 0.075	θ	22.3°	20.4°	21.0°	21.8°	24.3°	26.6°	30.5°	33.7°	36.4°	40.8°	43.9°
	β	6.32	4.75	4.10	3.75	3.24	2.94	2.59	2.38	2.23	1.95	1.67
≤ 0.100	θ	18.1°	20.4°	21.4°	22.5°	24.9°	27.1°	30.8°	34.0°	36.7°	40.8°	43.1°
	β	3.79	3.38	3.24	3.14	2.91	2.75	2.50	2.32	2.18	1.93	1.69
≤ 0.125	θ	19.9°	21.9°	22.8°	23.7°	25.9°	27.9°	31.4°	34.4°	37.0°	41.0°	43.2°
	β	3.18	2.99	2.94	2.87	2.74	2.62	2.42	2.26	2.13	1.90	1.67
≤ 0.150	θ	21.6°	23.3°	24.2°	25.0°	26.9°	28.8°	32.1°	34.9°	37.3°	40.5°	42.8°
	β	2.88	2.79	2.78	2.72	2.60	2.52	2.36	2.21	2.08	1.82	1.61
≤ 0.175	θ	23.2°	24.7°	25.5°	26.2°	28.0°	29.7°	32.7°	35.2°	36.8°	39.7°	42.2°
	β	2.73	2.66	2.65	2.60	2.52	2.44	2.28	2.14	1.96	1.71	1.54
≤ 0.200	θ	24.7°	26.1°	26.7°	27.4°	29.0°	30.6°	32.8°	34.5°	36.1°	39.2°	41.7°
	β	2.63	2.59	2.52	2.51	2.43	2.37	2.14	1.94	1.79	1.61	1.47
≤ 0.225	θ	26.1°	27.3°	27.9°	28.5°	30.0°	30.8°	32.3°	34.0°	35.7°	38.8°	41.4°
	β	2.53	2.45	2.42	2.40	2.34	2.14	1.86	1.73	1.64	1.51	1.39
≤ 0.250	θ	27.5°	28.6°	29.1°	29.7°	30.6°	31.3°	32.8°	34.3°	35.8°	38.6°	41.2°
	β	2.39	2.39	2.33	2.33	2.12	1.93	1.70	1.58	1.50	1.38	1.29

$$\epsilon_x = \frac{\frac{M_u}{d_v} + 0.5N_u + 0.5(V_u - V_p) \cot \theta - A_{ps} f_{po}}{2(E_s A_s + E_p A_p)} \quad (3.62)$$

For sections containing less than the minimum amount of transverse reinforcement, the values of β and θ may be found using **Table 3.2**. The designer selects the row corresponding to an equivalent spacing parameter (s_{xe}), and selects the column corresponding to the longitudinal strain at mid-depth. The equivalent spacing may be

computed using **Equation 3.63**. The longitudinal strain for this case may be computed using **Equation 3.64**.

Table 3.2: Values of θ and β for Sections With Less Than Minimum Transverse Reinforcement (AASHTO LRFD, 2010)

s_{xe} (in.)		$\epsilon_x \times 1000$										
		≤ -0.20	≤ -0.10	≤ -0.05	≤ 0	≤ 0.125	≤ 0.25	≤ 0.50	≤ 0.75	≤ 1.00	≤ 1.50	≤ 2.00
≤ 5	θ	25.4°	25.5°	25.9°	26.4°	27.7°	28.9°	30.9°	32.4°	33.7°	35.6°	37.2°
	β	6.36	6.06	5.56	5.15	4.41	3.91	3.26	2.86	2.58	2.21	1.96
≤ 10	θ	27.6°	27.6°	28.3°	29.3°	31.6°	33.5°	36.3°	38.4°	40.1°	42.7°	44.7°
	β	5.78	5.78	5.38	4.89	4.05	3.52	2.88	2.50	2.23	1.88	1.65
≤ 15	θ	29.5°	29.5°	29.7°	31.1°	34.1°	36.5°	39.9°	42.4°	44.4°	47.4°	49.7°
	β	5.34	5.34	5.27	4.73	3.82	3.28	2.64	2.26	2.01	1.68	1.46
≤ 20	θ	31.2°	31.2°	31.2°	32.3°	36.0°	38.8°	42.7°	45.5°	47.6°	50.9°	53.4°
	β	4.99	4.99	4.99	4.61	3.65	3.09	2.46	2.09	1.85	1.52	1.31
≤ 30	θ	34.1°	34.1°	34.1°	34.2°	38.9°	42.3°	46.9°	50.1°	52.6°	56.3°	59.0°
	β	4.46	4.46	4.46	4.43	3.39	2.82	2.19	1.84	1.60	1.30	1.10
≤ 40	θ	36.6°	36.6°	36.6°	36.6°	41.2°	45.0°	50.2°	53.7°	56.3°	60.2°	63.0°
	β	4.06	4.06	4.06	4.06	3.20	2.62	2.00	1.66	1.43	1.14	0.95
≤ 60	θ	40.8°	40.8°	40.8°	40.8°	44.5°	49.2°	55.1°	58.9°	61.8°	65.8°	68.6°
	β	3.50	3.50	3.50	3.50	2.92	2.32	1.72	1.40	1.18	0.92	0.75
≤ 80	θ	44.3°	44.3°	44.3°	44.3°	47.1°	52.3°	58.7°	62.8°	65.7°	69.7°	72.4°
	β	3.10	3.10	3.10	3.10	2.71	2.11	1.52	1.21	1.01	0.76	0.62

$$s_{xe} = \frac{1.38s_x}{a_g + 0.63} \quad (3.63)$$

$$\epsilon_x = \frac{\frac{M_u}{d_v} + 0.5N_u + 0.5(V_u - V_p) \cot \theta - A_{ps}f_{po}}{E_s A_s + E_p A_p} \quad (3.64)$$

If either value computed for ϵ_x is negative, the user should use **Equation 3.65** to compute the longitudinal steel strain instead.

$$\epsilon_x = \frac{\frac{M_u}{d_v} + 0.5N_u + 0.5(V_u - V_p) \cot \theta - A_{ps}f_{po}}{2(E_c A_c + E_s A_s + E_p A_p)} \quad (3.65)$$

where, A_c is the area of concrete on the flexural tension side, A_p is the area of prestressing steel on the flexural tension side, A_s is the area of non-prestressed steel on the flexural tension side, f_{po} is computed by the modulus of elasticity of the prestressing tendons (E_p) times the locked difference in strain at ultimate load between the prestressing tendons and the surrounding concrete, N_u is the factored axial force, s_x is the crack spacing parameter, and a_g is the maximum aggregate size in inches.

A simplified procedure is presented in the AASHTO LRFD (2010) where the values of β and θ can be calculated using the following expressions shown in **Equations 3.66** and **3.67**. The parameter s_{xe} can be calculated using **Equation 3.63**.

$$\beta = \frac{4.8}{1+750\varepsilon_x} \cdot \frac{51}{39+s_{xe}} \quad (3.66)$$

$$\theta = 29 + 3500\varepsilon_x \quad (3.67)$$

3.5.3. Canadian Standards Association, CSA A23.3-04. The Canadian Standards Association method, also based on MCFT, gives the following **Equations 3.68** to **3.76** to calculate the shear strength of a section using their general method. Note that the equations are given in psi and in. units, with the same notation defined in previous sections.

$$V_n = V_c + V_s + V_p \quad (3.68)$$

$$V_{n,max} = 0.25f'_c b_v d_v + V_p \quad (3.69)$$

$$V_c = \beta \sqrt{f'_c} b_v d_v \quad (3.70)$$

$$\beta = \frac{0.40}{1+1500\varepsilon_x} \cdot \frac{1300}{1000+s_{ze}} \quad (3.71)$$

$$s_{ze} = \frac{35s_z}{15+a_g} \quad (3.72)$$

The term a_g should be taken as zero if f'_c exceeds 10,150 psi. The crack spacing parameter s_z can be taken as d_v or as the maximum distance between layers of distributed longitudinal reinforcement, whichever is less. Each layer of reinforcement must have an area at least equal to $0.003b_v s_z$. However, $s_{ze} \geq 0.85s_z$.

$$\varepsilon_x = \frac{\frac{M_u}{d_v} + 0.5N_u + V_u - V_p - A_p s f_{po}}{2(E_s A_s + E_p A_p)} \quad (3.73)$$

$$V_s = \frac{A_v f_y d_v \cot \theta}{s} \quad (3.74)$$

$$\theta = 29 + 7000\varepsilon_x \quad (3.75)$$

$$A_{v,min} \geq 0.06 \sqrt{f'_c} \frac{b_v s}{f_y} \quad (3.76)$$

4. EXPERIMENTAL PROGRAM

4.1. GENERAL

The objective of this study was to investigate the shear performance of reinforced concrete (RC) beams composed of RCA. The experimental program consisted of 18 tests performed on full-scale RC beams. The principal parameters investigated were:

- (1) concrete type – recycled aggregate concrete (RAC) or conventional concrete (CC), and
- (2) amount of longitudinal reinforcement.

Also, as part of this study, small scale testing was performed to determine hardened concrete properties such as compressive strength, flexural strength, and splitting tensile strength.

4.2. TEST BEAMS

The reinforcement for the beams was designed in accordance with the AASHTO LRFD Bridge Design Specifications (AASHTO LRFD, 2010). Each beam measured 14 ft. in length with a cross section of 12 in. x 18 in. The cross section was selected to maintain a slender beam with a shear span-to-depth ratio larger than 3.0, thus avoiding any deep beam effects. The longitudinal reinforcement was selected to ensure a shear failure prior to a flexural failure yet still remain below the maximum amount allowed by code. Each beam had two test regions, with each region measuring approximately 4 ft. in length. All of the specimens had #3 stirrups spaced at 2 in. within the bearing area to prevent premature failure as well as #3 stirrups spaced at 7 in. within the middle region to

support the reinforcing cage and prevent any premature failure outside of the shear test regions.

Table 4.1 summarizes the test matrix used in this study. The beam designation included a combination of letters and numbers: NS stands for no stirrups within the test region. The numbers 4, 6, and 8 indicate the number of #7 longitudinal reinforcement bars within the tension area of the beam section. For example, NS-6 indicates a beam with no stirrups within the test region and 6 #7 bars within the bottom of the beam. Two beams were constructed and tested for each combination of variables shown in **Table 4.1**. The cross sections for these specimens are shown in **Figure 4.1**. **Figure 4.2** shows the load pattern and location of strain gauges on the test beams.

Table 4.1: Shear Beam Test Matrix

Section	Bottom reinforcement	Top reinforcement	ρ	Stirrups
NS-4	4#7	2#4	0.0127	-
NS-6	6#7	2#4	0.0203	-
NS-8	8#7	2#7	0.0271	-

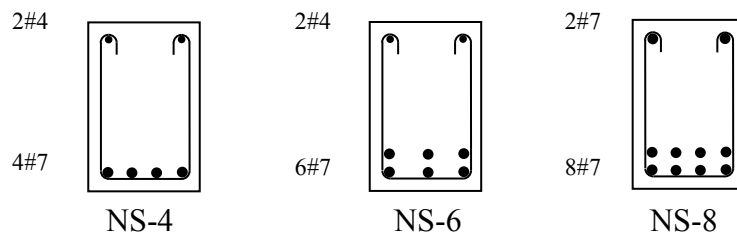


Figure 4.1: Cross Sections and Reinforcement Layout of the Beams

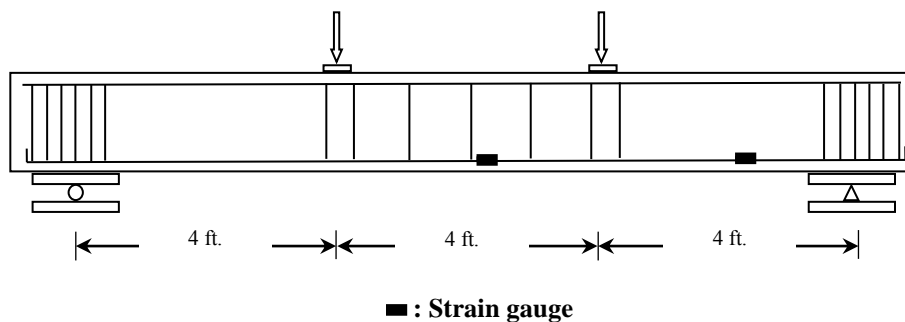


Figure 4.2: Load Pattern and Location of Strain Gauges on the Test Beams

4.3. MATERIALS

4.3.1. Concrete. For this study, three mix designs were produced and evaluated for shear performance. A MoDOT Class B air-entrained mix design was used as a baseline for reference throughout the study and also as the parent material for the recycled concrete aggregate. The specified cement content in this mix was 535 lb., the water-to-cement ratio was 0.40, the target slump was 6 in., and the design air content was 6%. The specified amount of fine aggregate as a volume of total aggregates was 40%. For this mix, the typical dosage range of the MoDOT-approved air entrainment MB-AE 90 was 0.25-4.0 fl.oz./100 lb. of cement. The typical dosage of the Type A water reducer Glenium 7500 was 5.0 – 8.0 fl.oz./100 lb. of cement.

For the CC mix, the coarse aggregate consisted of crushed limestone with a maximum nominal aggregate size of 1 in. from the Potosi Quarry (Potosi, MO) while the fine aggregate was natural sand from Missouri River Sand (Jefferson City, MO). For the RAC mixes, the coarse aggregate consisted of RCA ground from the CC mix to a nominal maximum aggregate size of 1 in., with either 50% replacement or 100% replacement of the Potosi limestone. Test results for the coarse aggregate used in the CC mix design as well as the resulting RCA are shown in **Table 4.2**. As expected, the RCA

had lower specific gravity and unit weight and considerably higher absorption. The Los Angeles abrasion test results were virtually identical.

Table 4.2: Aggregate Properties

Property	CC	RCA
Bulk Specific Gravity, Oven-Dry	2.72	2.35
Dry-Rodded Unit Weight, (lb/ft ³)	99.8	89.8
Absorption (%)	0.98	4.56
LA Abrasion (% Loss)	43	41

Tables 4.3 and **4.4** present the mix designs and representative fresh and hardened strength properties, respectively, of the CC and RAC mixes. The first mix incorporating RCA was a 50% direct replacement design. Half of the total volume of coarse aggregate in the control MoDOT Class B mix was directly substituted with the laboratory-produced RCA and is subsequently referred to as RAC-50. The second mix incorporating RCA was a 100% direct replacement design. The total volume of coarse aggregate in the control MoDOT Class B mix was directly substituted with the laboratory-produced RCA and is subsequently referred to as RAC-100. In order to maintain consistency with the control specimens, the MoDOT Class B mix specifications were used to design the RAC mixes. However, during laboratory trial batching, it was noticed from the slump test that the RAC-100 mix lacked cohesion. To remedy this situation, the mix was modified by increasing the amount of fine aggregate volume by 5% of total aggregates, which noticeably improved the cohesion of the mix.

Table 4.3: Mix Designs per Cubic Yard

	CC	RAC-50	RAC-100
Cement (Type I) (lb)	535	535	535
w/cm	0.40	0.40	0.40
Natural Coarse Aggregate (lb)	1958	979	-
Recycled Coarse Aggregate (lb)	-	846	1650
Fine Aggregate (lb)	1253	1253	1442
HRWR (fl. oz)	55	50	42
AE (fl. oz)	20	14	7

Table 4.4: Typical Fresh and Hardened Concrete Properties for CC and RCA Mixes

Property	CC	RAC-50	RAC-100
Slump (in.)	5.5	6.5	8
Air content (%)	8.5	8	6.5
Unit weight (lb/ft ³)	145.4	139.8	136.0
Split cylinder strength (psi)	505	417	370
Flexural strength (psi)	500	425	410
Fracture Energy (lb/in.)	0.82	0.71	0.57
Compressive strength (psi)	5400	4150	4350

4.3.2. Steel Reinforcement. Shear reinforcement for the test specimens consisted of A615, Grade 60 #3 reinforcing bars. Longitudinal reinforcement for the test specimens consisted of A615, Grade 60 #4 and #7 reinforcing bars. All the steel reinforcement was tested in accordance with ASTM A370 (2011) “Standard Test Methods and Definitions for Mechanical Testing of Steel Products” to obtain the mechanical properties, which are summarized in **Table 4.5**. These results are the average of three replicate specimens.

Table 4.5: Mechanical Properties of Steel Reinforcement

Bar size	Yield strength (psi)
#3	71,650
#4	73,970
#7	65,120

4.4. BEAM FABRICATION

All the test beams were fabricated in either the Structural Engineering High-Bay Research Laboratory (SERL) at Missouri S&T or the Donald G. Fears Structural Engineering Laboratory at the University of Oklahoma. Steel formwork was used to cast the beams. The steel cage was assembled from reinforcement that was bent in the laboratory to the desired geometry. Due to the dimension of the beams, it was possible to cast three beams at a time. After casting, the top surface of the beams was covered with burlap and plastic sheeting, and a wet surface was maintained for three days to retain moisture for proper curing. Cylinders were cured in the same environment as the test beams by placing them next to the beams. The sheeting and burlap were then removed, and the beams were allowed to air cure in the lab environment. Photographs showing the reinforcing cages and the construction process are shown in **Figures 4.3** and **4.4**, respectively.



Figure 4.3: Reinforcing Cage Assembly



(a) Formwork



(b) Concrete placement



(c) Concrete consolidation



(d) Concrete finishing

Figure 4.4: Beam Construction Process**4.5. TEST SET-UP**

All the specimens were tested as simply supported and subjected to third-point loading. The maximum compression capacity of the actuators available in SERL, when working individually, were insufficient to cause specimen failure. Therefore, the test set-up required the simultaneous action of two actuators as shown in **Figure 4.5**.

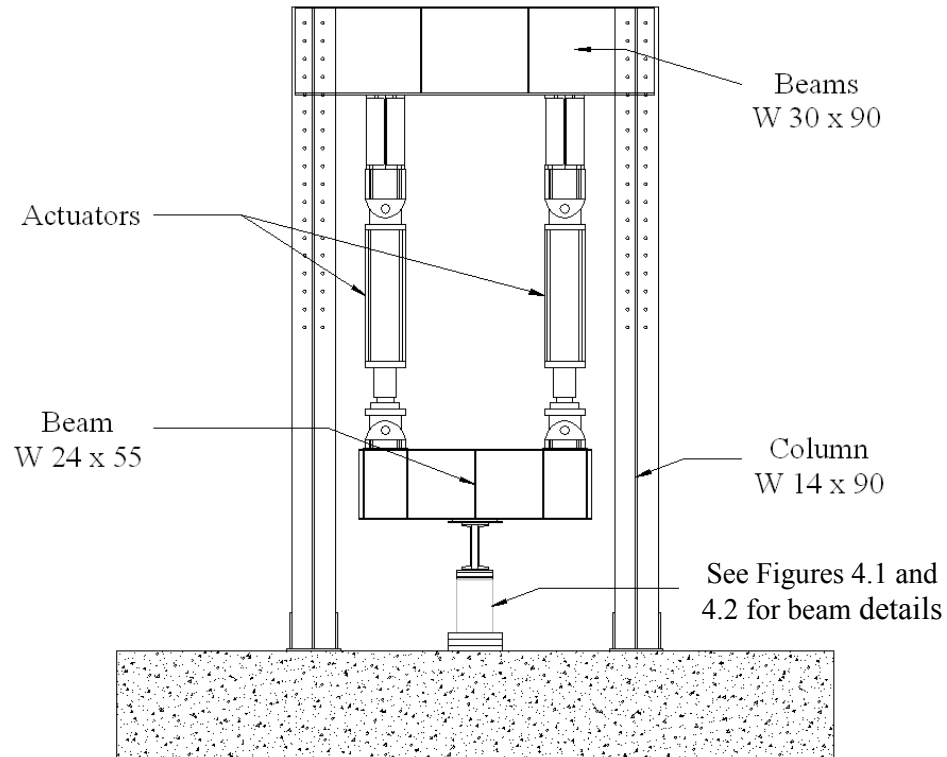


Figure 4.5: Details of Test Set-Up (1)

Two actuators, each with a 140-kip compressive capacity, were used to apply load to the beam specimens, as shown in **Figure 4.6**. The actuators applied load by pushing the steel beam downward to distribute the load onto two points of the test specimen. The loading frame assembly was designed to withstand at least two times the anticipated maximum load applied to fail the beams. Each test was performed under displacement control, and the load was applied in a series of loading steps of 0.05 in., which corresponded to a load of approximately 8 kips, until failure. Electronic measurements of strain and deformation were recorded throughout the entire loading history of the specimens, while hand measurements of strain and crack pattern formations were taken at the end of each load step while the load was paused. Each beam consisted of two test regions. The total beam length was 14 ft, with a simply supported span length of 12 ft.

The load was applied at 4 ft from each support, representing a shear span-to-depth ratio between 3.00 and 3.30 depending on the specimen, as measured from center of support to center of load. **Figure 4.7** shows a photograph of the test set-up.

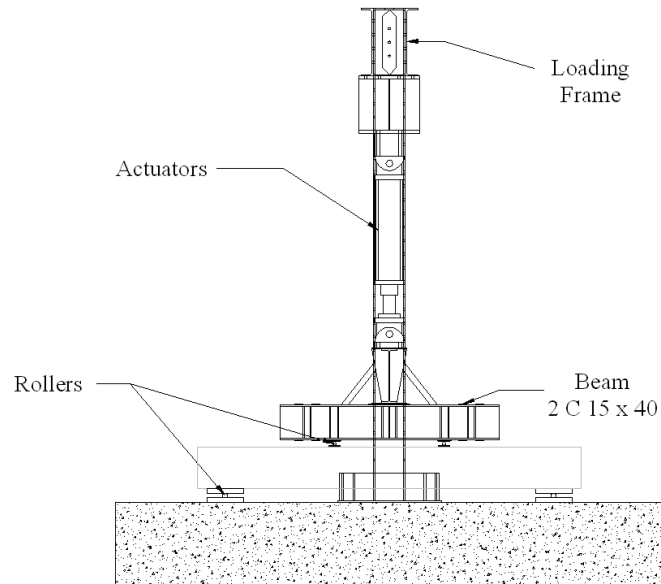


Figure 4.6: Details of Test Set-Up (2)



Figure 4.7: Photograph of Test Set-Up

4.6. INSTRUMENTATION

The specimens were instrumented with several measurement devices in order to monitor global and local deformations and strains. The load was directly measured from the load cell of the actuators. All devices were connected to a data acquisition system capable of reading up to 120 channels and all the data was recorded as shown in **Figure 4.8**.



Figure 4.8: Data Acquisition System

4.6.1. Local Deformations and Strains. Electrical resistance gauges were used to monitor local strains in the longitudinal steel reinforcement of the test region. The strain gauges were purchased from Vishay Precision Group. They were made of constantan foil with 120 ohm resistance and had a linear pattern (uniaxial) with a gauge

length of $\frac{1}{4}$ in. Two strain gauges were installed on longitudinal steel reinforcement in the test region as shown in **Figure 4.2**. The strain values obtained from the strain gauges are localized measurements at the point where the gauge is installed. The first one was located at the midpoint of the shear test region, while the second was located at mid-span.

4.6.2. Global Deformations. One Linear Variable Displacement Transducer (LVDT) was used to monitor vertical deflection of the test specimen. The LVDT was located at the midpoint of the test specimen, 3 in. below the top of the beam as shown in **Figures 4.9** and **4.10**.

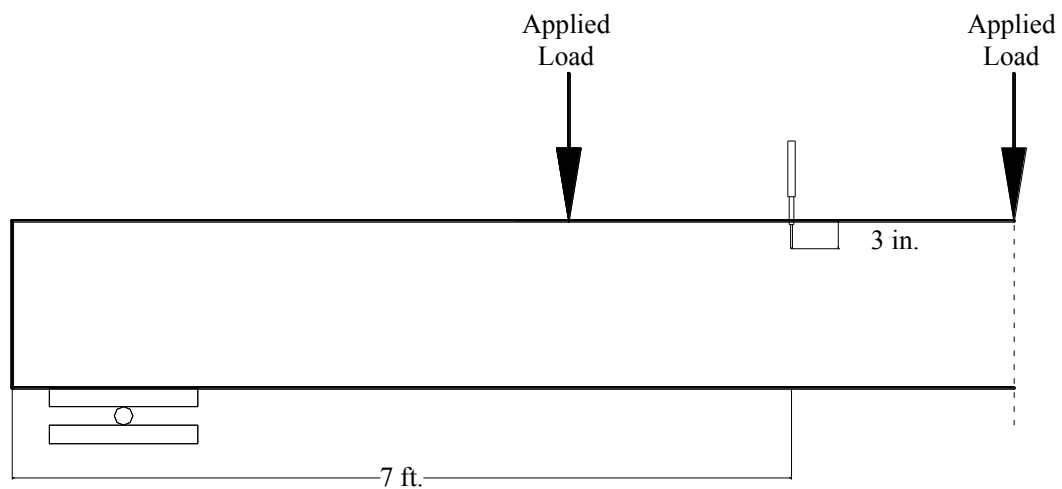


Figure 4.9: Location of LVDT to Measure Deflection



Figure 4.10: Detail of LVDT for Deflection Measurement

5. TEST RESULTS, BEHAVIOR & ANALYSIS

5.1. GENERAL

The purpose of this study was to evaluate the shear behavior of full-scale reinforced concrete (RC) beams constructed from RCA, which has not been fully investigated in previous research studies. The objectives of this section are to: (1) discuss the overall behavior of the specimens, (2) discuss the crack morphology and progression, (3) discuss the load-deflection response, (4) evaluate the failure mechanism including reinforcement strains, (5) compare the test results with predicted capacities based on applicable design standards, (6) compare the RAC test results with the control specimen results, and (7) compare the test results with a shear test database of conventional concrete specimens.

5.2. TEST RESULTS & BEHAVIOR OF FULL-SCALE SPECIMENS

Table 5.1 summarizes the compressive strength at time of testing, shear force at failure, V_{test} , average shear stress at failure, V_{test}/b_wd , and ratio of the average shear stress to square root of the compressive strength, $v_{\text{test}}/\sqrt{f'_c}$. A useful comparison is to compare the last column in **Table 5.1** with ACI 318 (2011) Equation 11-3, rewritten in terms of average shear stress for normal weight concrete and shown as **Equation 5.1**. As shown in **Table 5.1**, comparison between the experimental shear strength and ACI 318 (2011) shear provisions shows this equation overestimates the shear strength of two beams (one for the RAC-50 mix and one for the RAC-100 mix) with low longitudinal reinforcement ratios, which has also been reported by other researchers (Collins and Kuchma 1999).

$$v_c = 2\sqrt{f'_c} \quad (5.1)$$

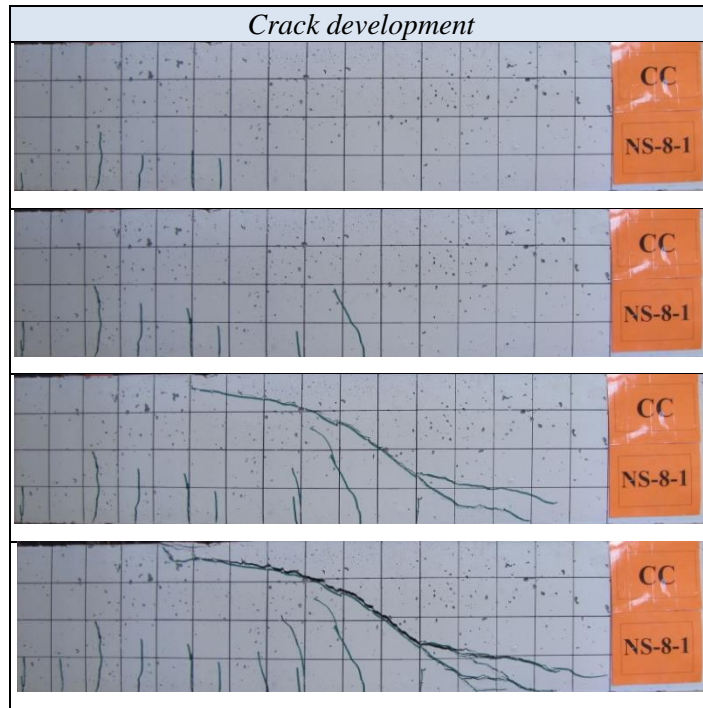
In addition to studying the behavior of the specimens, the crack patterns experienced by the beams were also evaluated. During testing, cracks within the test region were marked using a permanent marker after each load step. Typical crack pattern progressions are shown in **Figure 5.1**. Furthermore **Figure 5.2** shows the crack pattern for the CC and RAC-100 beams with different percentages of longitudinal reinforcement. Cracks typically began on the tension face of the beam near the loading points. As the loading progressed, the flexural cracks in the shear test region formed inclined flexure-shear cracks. The formation of the inclined flexure-shear crack did not result in immediate failure, and additional load was required prior to failure. In general, the failure crack typically extended from the beam support to the loading point on the top side of the beam.

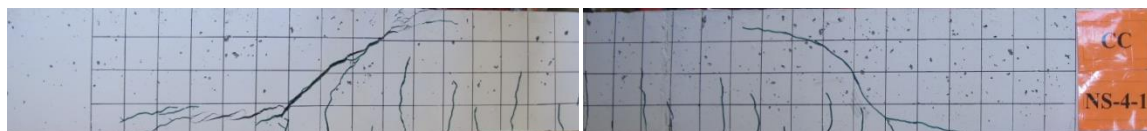
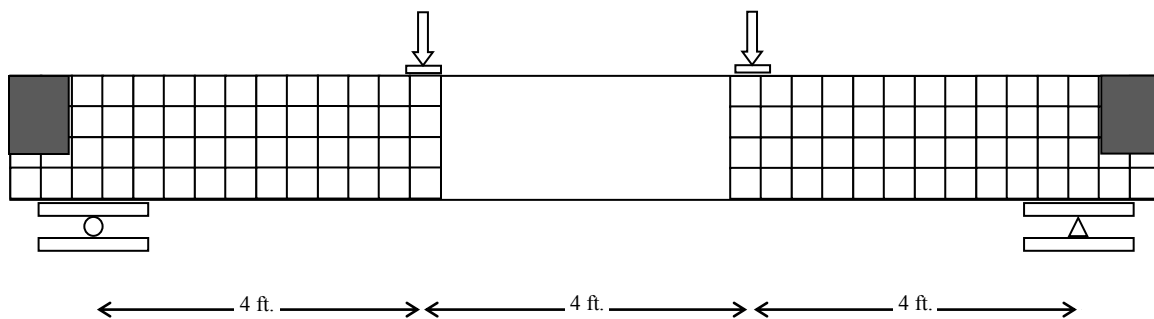
Figure 5.3 shows the load-deflection behavior for the beams with different longitudinal reinforcement ratios (the deflection was measured at midspan). Before the first flexural cracks occurred (point A), all of the beams displayed a steep linear elastic behavior. After additional application of load, the beams eventually developed the critical flexure-shear crack, which resulted in a drop in load. As expected, sections with a higher percentage of longitudinal reinforcement generally had a higher shear capacity, which can be attributed to a combination of additional dowel action (Taylor 1972, 1974), tighter shear cracks and thus an increase in aggregate interlock, and a larger concrete compression zone due to a downward shift of the neutral axis.

Table 5.1: Test Results Summary

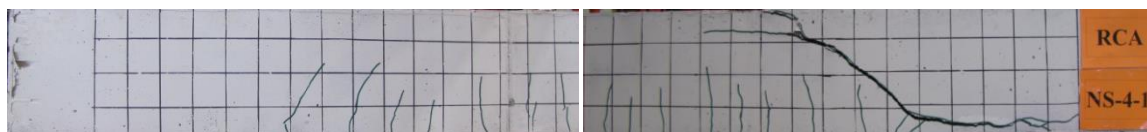
Mix Design	Section		f'_c psi	V^*_{test} kips	$v_{test}=V_{test}/b_wd$ psi	$v_{test} / \sqrt{f'_c}$
CC	NS-4	1	5400	27.2	144.4	2.0
		2	4960	29.2	155.0	2.2
	NS-6	1	5400	32.2	181.9	2.5
		2	4960	37.5	211.9	3.0
	NS-8	1	5400	39.0	220.3	3.0
		2	4960	38.4	216.9	3.1
RAC-50	NS-4	1	4650	26.4	140.1	2.1
		2	5170	25.1	133.2	1.9
	NS-6	1	4650	34.0	192.1	2.8
		2	5170	33.4	188.7	2.6
	NS-8	1	4650	38.6	218.1	3.2
		2	5170	37.9	214.1	3.0
RAC-100	NS-4	1	4350	25.8	136.9	2.1
		2	4950	25.4	134.8	1.9
	NS-6	1	4350	32.2	181.9	2.8
		2	4950	27.9	157.6	2.2
	NS-8	1	4350	29.5	166.7	2.5
		2	4950	31.5	178.0	2.5

*: Includes part of the load frame not registered by the load cells and also the beam self weight at a distance d from the interior face of the support plate.

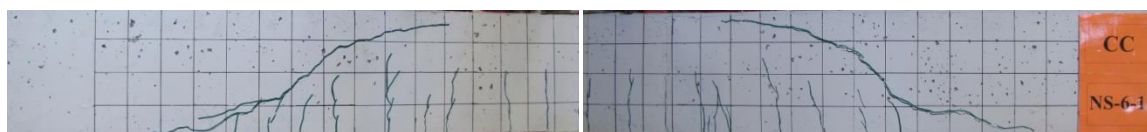
**Figure 5.1: Crack Progression for the Beams**



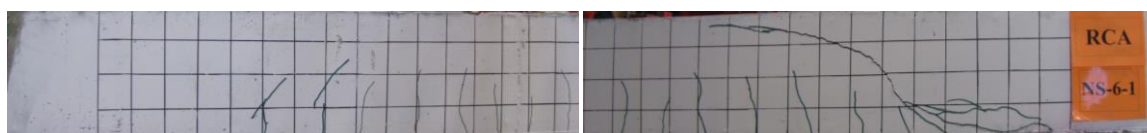
CC-NS-4-1



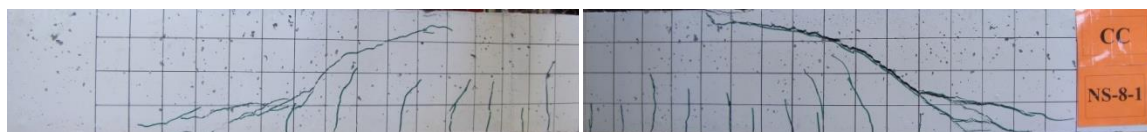
RAC-100-NS-4-1



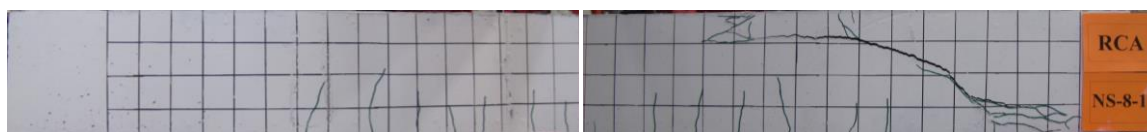
CC-NS-6-1



RAC-100-NS-6-1

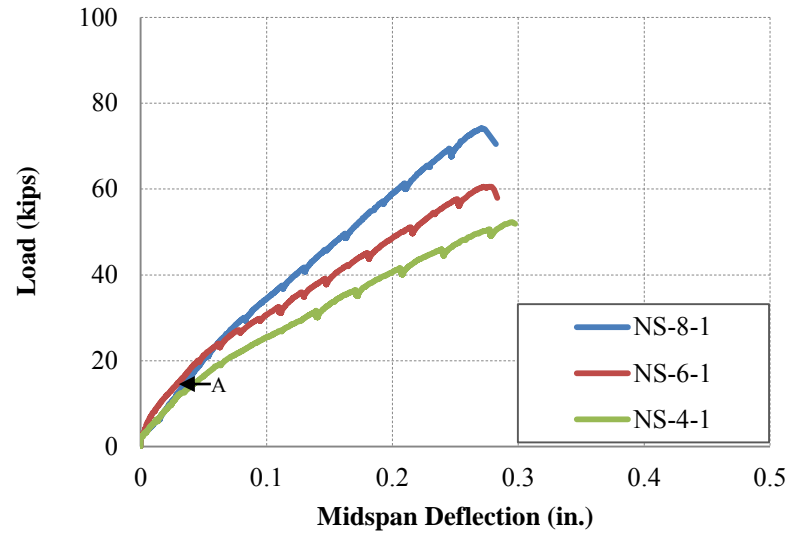


CC-NS-8-1

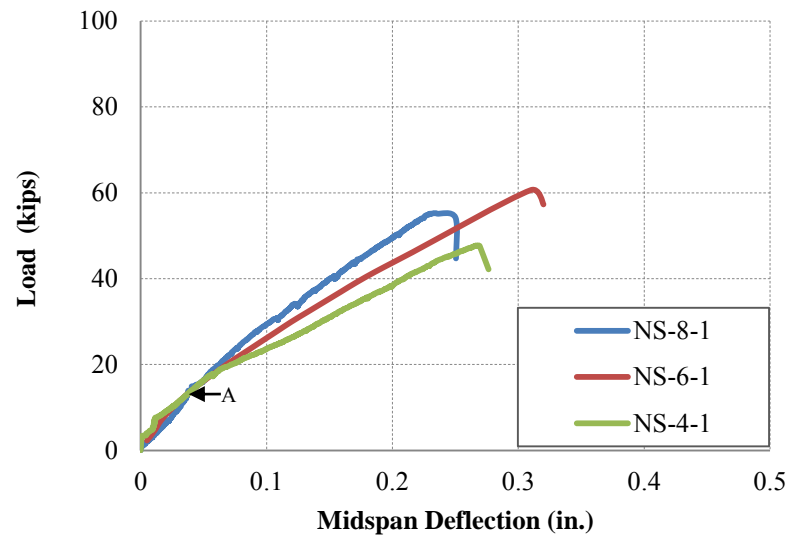


RAC-100-NS-8-1

Figure 5.2: Crack Pattern of the Beams at Shear Failure



a) CC Beams



b) RAC-100 Beams

Figure 5.3: Load-Deflection Response of the Beams

5.3. COMPARISON OF REINFORCEMENT STRAINS FROM EXPERIMENT AND AASHTO LRFD (2010)

According to the AASHTO LRFD standard (2010), strain in the longitudinal tension reinforcement can be determined by

$$\varepsilon_s = \frac{\left(\frac{|M_u|}{d_v} + |V_u| \right)}{E_s A_s} \quad (5.2)$$

Table 5.2 presents the tensile strain in the longitudinal tension reinforcement at the quarter-point of the span (middle of the shear test region) obtained from both the experiments (strain gauges) and the AASHTO LRFD (2010) equation. The AASHTO LRFD equation showed good agreement with experimental results for both the CC and RAC beams.

5.4. STATISTICAL DATA ANALYSIS

Statistical tests were used to evaluate whether there is any statistically significant difference between the normalized shear strength of the CC and the RAC beams. Both parametric and nonparametric statistical tests were performed.

5.4.1. Parametric Test. The paired t-test is a statistical technique used to compare two population means. This test assumes that the differences between pairs are normally distributed. If this assumption is violated, the paired t-test may not be the most powerful test. The hypothesis for the paired t-test is as follows:

H_{01} : The means of the normalized shear capacity of the CC is equal to the RAC-50 beams.

Table 5.2: Comparison of Reinforcement Strain from Experiment and AASHTO LRFD (2010) Equation

Section			ϵ_s quarter-point Experiment	ϵ_s quarter-point Equation	$\frac{\epsilon_{s-Ex.}}{\epsilon_{s-Eq.}}$	
CC	NS-4	1	1039	1236	0.84	
		2	1063	1136	0.94	
	NS-6	1	1065	1032	1.03	
		2	1105	1064	1.04	
	NS-8	1	860	872	0.99	
		2	858	783	1.10	
	Ave.					0.99
	RAC-50	NS-4	1	1001	1154	0.87
			2	912	973	0.94
NS-6		1	1080	1064	1.01	
		2	1095	1087	1.00	
NS-8		1	897	821	1.09	
		2	834	768	1.09	
Ave.					1.00	
RAC-100		NS-4	1	950	1000	0.95
			2	1123	984	1.14
	NS-6	1	837	872	0.96	
		2	790	752	1.05	
	NS-8	1	586	598	0.98	
		2	414	640	0.65	
	Ave.					0.95

H_{02} : The means of the normalized shear capacity of the CC is higher than the RAC-100 beams.

$H_{a1,2}$: The means of the normalized shear capacity of the CC is not higher than the RAC-100 beams.

The statistical computer program Minitab 15 was employed to perform these statistical tests. Both Kolmogorov-Smirnov and Anderson-Darling tests showed the data, the differences between the shear capacities of the CC and the RAC beams, follows a normal distribution. Therefore, the paired t-tests could be performed. The result of the paired t-test showed that the p-values were 0.778 and 0.924 (>0.05) for the first and second hypothesis, respectively. This confirms the null hypothesis at the 0.05 significance level. In other words, the means of the normalized shear capacity of the CC was equal to the RAC-50 beams; however, it was statistically higher than the RAC-100 beams.

5.4.2. Nonparametric Test. Unlike the parametric tests, nonparametric tests are referred to as distribution-free tests. These tests have the advantage of requiring no assumption of normality, and they usually compare medians rather than means. The Wilcoxon signed-rank test is usually identified as a nonparametric alternative to the paired t-test. The hypothesis for this test is the same as those for the paired t-test. The Wilcoxon signed-rank test assumes that the distribution of the difference of pairs is symmetrical. This assumption can be checked; if the distribution is normal, it is also symmetrical. As mentioned earlier, the data follows normal distribution and the Wilcoxon signed-rank test can be used. The p-values for the Wilcoxon signed rank were 0.675 and 0.957 (>0.05) for the first and second hypothesis, respectively. That confirmed

the null hypothesis at the 0.05 significance level. Interestingly, the p-values for both the paired t-tests (parametric test) and the Wilcoxon signed rank test (nonparametric test) are very close to each other.

Overall, results of the statistical data analyses showed that the CC beams had almost the same normalized shear strength as the RAC-50 beams and higher normalized shear capacity than the RAC-100 beams.

5.5. COMPARISON OF TEST RESULTS WITH SHEAR PROVISIONS OF SELECTED STANDARDS

In the following section, the experimental shear strengths of the beams are compared with the shear provisions of the following standards: AASHTO LRFD (2010), ACI 318 (2011), and CSA (2004). For this comparison, all of the safety factors of the standards were set equal to one and all ultimate moments and shear forces were calculated without load factors.

Table 5.3 presents the ratios of experimental-to-code predicted capacity ($V_{\text{test}}/V_{\text{code}}$) for the selected design standards for all of the beams. In general, the ratios are lower for the AASHTO and CSA design code provisions compared with the ACI approach. As discussed in Chapter 3, the AASHTO and CSA design codes are based on a modified compression field theory while the ACI approach is entirely empirical. For the CC beams, the ratios range from 0.80 to 1.54, while the ratios range from 0.83 to 1.68 for the RAC-50 specimens and 0.76 to 1.27 for the RAC-100 beams. For both concrete types, ACI 318-11 offered the most conservative results.

Table 5.3: Comparison of Shear Strength of Experiment and Codes

Section		AASHTO	ACI	CSA		
CC	NS-4	1	0.82	0.98	0.80	
		2	0.95	1.10	0.93	
	NS-6	1	0.94	1.24	0.92	
		2	1.23	1.51	1.20	
	NS-8	1	1.11	1.50	1.09	
		2	1.13	1.54	1.11	
	Ave.		1.03	1.31	1.01	
	COV (%)		14.7	18.2	14.8	
	RAC-50	NS-4	1	0.91	1.10	0.89
			2	0.85	1.00	0.83
NS-6		1	1.16	1.49	1.13	
		2	1.13	1.39	1.10	
NS-8		1	1.22	1.68	1.20	
		2	1.19	1.56	1.17	
Ave.		1.08	1.37	1.05		
COV (%)		14.5	19.5	14.7		
RAC-100		NS-4	1	0.85	1.04	0.83
			2	0.78	0.96	0.76
	NS-6	1	1.05	1.38	1.03	
		2	0.81	1.12	0.79	
	NS-8	1	0.84	1.27	0.83	
		2	0.86	1.27	0.85	
	Ave.		0.87	1.17	0.85	
	COV (%)		11.0	13.6	11.2	

In looking closer at the results, the code comparisons offer some very important information. First, the design codes tend to overestimate the shear capacities of the CC, RAC-50, and RAC-100 beams at low reinforcement ratios (i.e., the ratios are less than one), which has also been reported by other researchers (Collins and Kuchma 1999). However, at higher reinforcement ratios, the ratio of experimental-to-code predicted capacity for the AASHTO and CSA provisions is greater than one for CC and RAC-50 yet less than one for the RAC-100 specimens. For AASHTO, the averages are 1.10, 1.18 and 0.89 for the CC, RAC-50, and RAC-100 specimens, and for CSA, the averages are 1.09, 1.15, and 0.88 for the CC, RAC-50, and RAC-100 test results. This result indicates that existing code provisions overestimated the shear capacity for the specimens that used 100% replacement of virgin aggregate with recycled aggregate but offer good agreement for those with aggregate replacement levels up to 50%.

5.6. COMPARISON OF TEST RESULTS WITH SHEAR TEST DATABASE

The four key parameters that affect concrete contribution to shear strength include depth of member or size effect (d), shear span to depth ratio (a/d), compressive strength of concrete ($f'c$), and longitudinal reinforcement ratio (ρ) (Reineck et al. 2003). To evaluate the effect of the aforementioned parameters on shear strength of the beams, the results of this study were compared with the wealth of shear test data available in the literature for CC (Reineck et al. 2003). **Figure 5.4(a-d)** presents the shear stress versus $f'c$, ρ , d , and a/d , respectively. Given the significant scatter of the database of previous shear test results, it is somewhat difficult to draw definitive conclusions on the current test values. Nonetheless, visually, **Figure 5.4(a-d)** seems to indicate that the CC and

RAC test results fall within the central portion of the data and follow the same general trend of the database. Furthermore, statistical analysis of the data indicates that the test results fall within a 95% confidence interval of a nonlinear regression curve fit of the database (using regression analysis to draw the best fit and 95% confidence intervals).

Figure 5.4(e) shows normalized shear strength (based on square root of compressive strength of concrete) versus longitudinal reinforcement ratio for the beams of this study and the shear database. As mentioned previously, since span-to-depth ratio plays a significant role in the shear strength of beams, **Figure 5.4(f)** shows the normalized shear strength for the beams of this study with the portion of the database that had similar span-to-depth ratios of the current study (span-to-depth ratio $\pm 5\%$ [2.9-3.4]). Similar to **Figure 5.4(a - d)**, it can be seen from **Figure 5.4 (e)** and **(f)** that the test results of this current study are also within a 95% confidence interval of a nonlinear regression curve fit of the shear database and subset of the database. As a result, it would again appear that only the RAC-100 beams show slightly lower shear strength compared with the CC beams.

Although both the RAC-50 and RAC-100 test specimen results fall within the central portion of the plots and within a 95% confidence interval, the RAC-100 test results plot consistently lower, indicating decreased capacity for the specimens constructed with 100% replacement of virgin aggregate with recycled concrete.

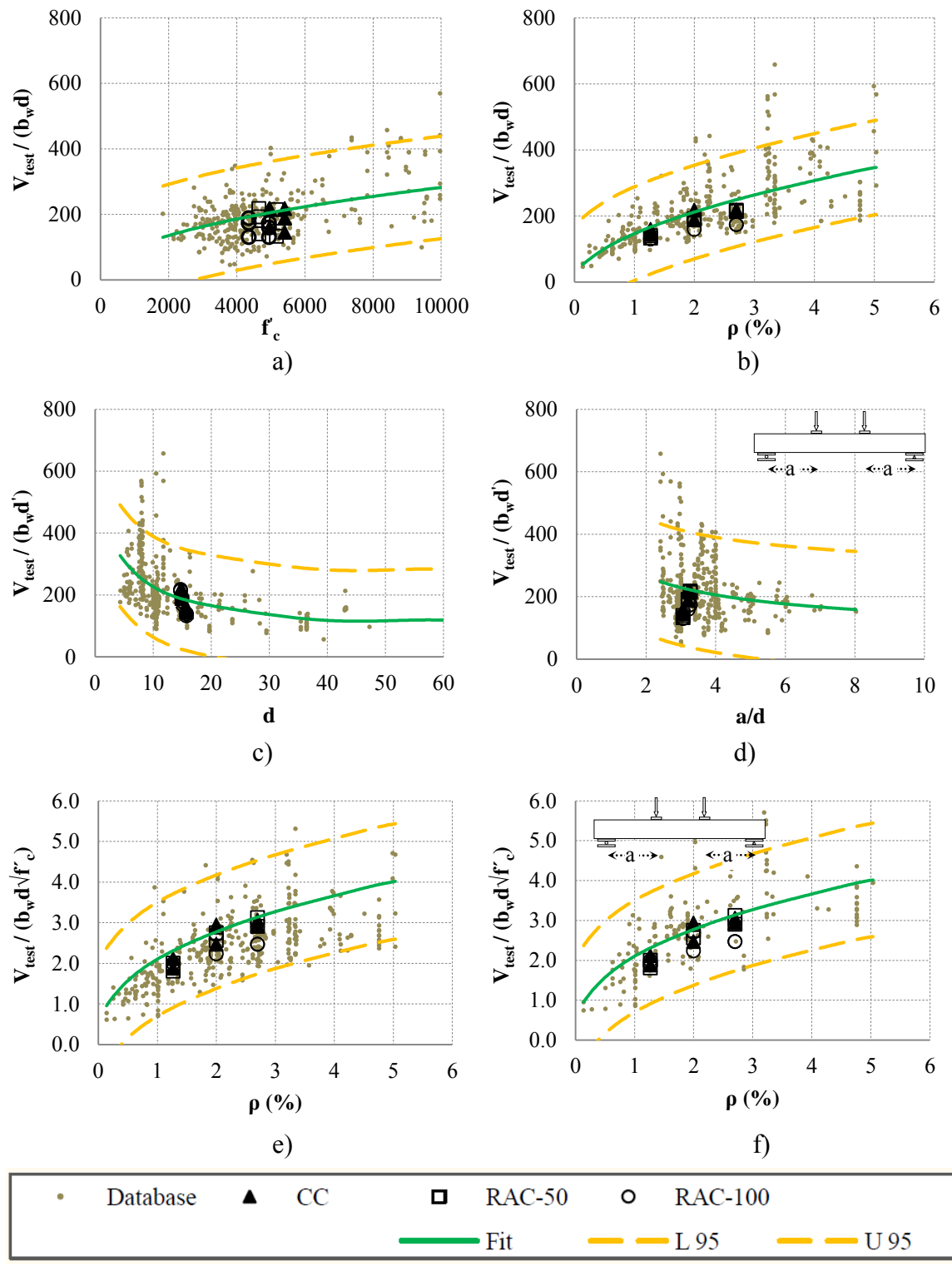


Figure 5.4: Shear Strength vs. Longitudinal Reinforcement Ratio; Results from Reineck et al. (2003) and Test Results of this Study

5.7. MATERIAL PROPERTY TEST RESULTS AND COMPARISON WITH SHEAR BEHAVIOR

Previous research and reports (ASCE-ACI Task Committee 426, 1973 and ACI Committee 445, 2009) showed that splitting tensile strength, flexural strength, and fracture energy are important parameters affecting shear strength of concrete. For this reason, the following section compares the relationship between these parameters and shear strengths for the three mixes studied in this project. To compare the shear strengths of the CC and RAC beams, the test results must be adjusted to reflect the different compressive strengths. ACI 318 (2011) provisions use the square root of the compressive strength of concrete to determine the splitting tensile strength (**Equation 5.3**), flexural strength (**Equation 5.4**), and shear strength (**Equation 5.1**) of a beam. In terms of fracture energy, Bazant's equation (**Equation 5.5**) uses a 0.46 power of the compressive strength of concrete to calculate the fracture energy of concrete. Therefore, to normalize the data for comparison, the splitting tensile strengths, flexural strengths, and shear strengths were divided by the square root of the compressive strengths of the respective concretes; however, fracture energies were divided by the compressive strengths to the power of 0.46.

$$f_{ct} = 6.7\sqrt{f'_c} \quad (5.3)$$

$$f_{ct} = 7.5\sqrt{f'_c} \quad (5.4)$$

$$G_F = 2.5 \alpha_o \left(\frac{f'_c}{0.051} \right)^{0.46} \left(1 + \frac{d_a}{11.27} \right)^{0.22} \left(\frac{w}{c} \right)^{-0.30} \quad (5.5)$$

Figure 5.5 offers a comparison of the splitting tensile strength, flexural strength, fracture energy, and shear strength for the three different concretes tested in this study.

For the RAC-50 test beams, the splitting tensile strength, flexural strength, and fracture energy decreased between 1% and 6% compared to the CC, with the shear strength of the RAC-50 specimens experiencing a decrease of only 1%. However, for the RAC-100 test beams, the splitting tensile strength, flexural strength, and fracture energy decreased between 9% and 22% compared to the CC, with a corresponding reduction in shear strength of 11%. In other words, the RAC-50 mix exhibited a slight decrease in basic mechanical properties and a corresponding slight decrease in shear capacity, while the RAC-100 mix exhibited a larger decrease in basic mechanical properties and a corresponding larger decrease in shear strength.

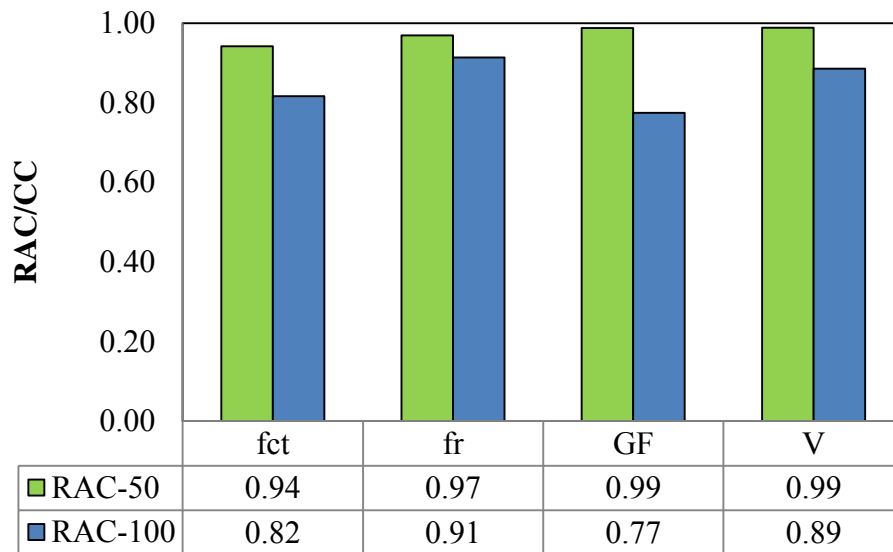


Figure 5.5: Comparison of Mechanical Properties and Shear Strengths of the CC and RAC Beams

6. FINDINGS, CONCLUSIONS, AND RECOMMENDATIONS

The main objective of this research study was to evaluate the shear behavior and response of RAC through material, component, and full-scale testing. The main feature of the experimental program consisted of 18 tests performed on full-scale reinforced concrete beams. The principal parameters investigated were: (1) concrete type – RAC vs. CC, and (2) amount of longitudinal (flexural) reinforcement. The behavior of the RAC was examined in terms of crack morphology and progression, load-deflection response, failure mechanism including critical crack angle and reinforcement strains, comparison with predicted strengths from design standards, comparison with identical CC test specimens (including statistical analyses), comparison with a shear test database of CC specimens, and, finally, comparison of basic mechanical properties related to shear strength. This section contains the findings of the test program as well as conclusions and recommendations.

6.1. FINDINGS AND CONCLUSIONS

Based on the results of this research study, the following findings are presented with regard to shear behavior and the use of recycled concrete as aggregate:

- In terms of crack morphology, crack progression, and load-deflection response, the behavior of the CC and RAC beams was virtually identical.
- Statistical data analyses – both parametric and nonparametric – showed that there was no statistically significant difference between the normalized shear capacities of the CC and the RAC-50 specimens.

- Statistical data analyses – both parametric and nonparametric – showed that there was a statistically significant difference between the normalized shear capacities of the CC and RAC-100 specimens, and as a result, the RAC-100 specimens had, on average, 11% lower shear capacity than the CC.
- Existing design standards (AASHTO, ACI, CSA) overestimated the shear capacities of the RAC-100 beams in most of the cases studied.
- Existing design standards (AASHTO, ACI, CSA) overestimated the shear capacities of all beams at low reinforcement ratios, except for the ACI code for specimens CC-NS-4-1 and RAC100-NS-4-2.
- The CC and RAC test results fall within a 95% confidence interval of a nonlinear regression curve fit of the CC shear test database.
- For the RAC-50 test beams, the splitting tensile strength, flexural strength, and fracture energy decreased between 1% and 6% compared to the CC, with the shear strength of the RAC-50 specimens experiencing a decrease of only 1%.
- For the RAC-100 test beams, the splitting tensile strength, flexural strength, and fracture energy decreased between 9% and 22% compared to the CC, with a corresponding reduction in shear strength of 11%.
- The AASHTO LRFD equation accurately estimated the reinforcement strain for both the CC and RAC beams.

Based on the findings of this research study, the following conclusions are drawn with regard to shear behavior and the use of recycled concrete as aggregate:

- Beams containing 50% replacement of virgin aggregate with RCA had normalized shear strengths comparable to conventional concrete.
- Beams containing 100% replacement of virgin aggregate with RCA had normalized shear strengths 11% lower, on average, than conventional concrete.
- The decrease in shear capacity is most likely due to the double interfacial transition zone that exists when using recycled concrete as an aggregate, and the effect is more pronounced as the percentage replacement increases.
- The decrease in basic mechanical properties (splitting tensile strength, fracture energy) for the RAC parallels the decrease in full-scale shear behavior and can be used as a predictor in mixes containing recycled concrete as aggregate.
- Although limited based on the number of variables tested in this study, it would appear that replacing more than 50% of the virgin aggregate with RCA will result in a noticeable decrease in shear capacity, 11% for the mixes studied in this investigation.

6.2. RECOMMENDATIONS

Due to the limited number of studies of the shear behavior of RAC, further research is needed to make comparisons and conclusions across a larger database. However, based on the findings and conclusions developed in this current study, the following preliminary recommendations are presented:

- Limit the percentage replacement of virgin aggregate with RCA to 50%, which should not result in any noticeable decrease in overall structural behavior compared to conventional concrete.
- Perform detailed material and full-scale specimen testing of any mixes containing more than 50% replacement of virgin aggregate with RCA.
- Additional testing is required to definitively determine whether RAC has decreased shear capacity compared to CC. This testing should investigate additional mix design variations, aggregate type and content, cross section aspect ratio, and type of loading. This database will then provide a basis for modifications to existing design standards.

BIBLIOGRAPHY

- Abbas, A., Fathifazl, G., Isgor, O.B., Razaqpur, A.G., Fournier, B., and Foo, S. (2006). "Proposed Method for Determining the Residual Mortar Content of Recycled Concrete Aggregates." CSCE 2006 Annual Conference, Calgary, Alberta, Canada.
- AASHTO LRFD, (2010). Bridge Design Specifications and Commentary (4th Ed.). American Association of State and Highway Transportation Officials. Washington, DC.
- AASHTO T 318 (2002). Water Content of Freshly Mixed Concrete Using Microwave Oven Drying. American Association of State Highway and Transportation Officials, Washington D.C.
- ACI Committee 211, (1991). Standard Practice for Selecting Proportions for Normal, Heavyweight, and Mass Concrete (ACI 211.1-91). American Concrete Institute, Farmington Hills, MI.
- ACI Committee 318, (2011). Building Code Requirements for Structural Concrete and Commentary (ACI 318-08). American Concrete Institute, Farmington Hills, MI.
- ACI Committee 445, (2009). Recent Approaches to Shear Design of Structural Concrete (ACI 445R-99). American Concrete Institute, Farmington Hills, MI.
- ACI Committee 446, (1999). Fracture Mechanics of Concrete: Concepts, Models and Determination of Material Properties (ACI 446.1R). American Concrete Institute, Farmington Hills, MI.
- ASCE-ACI Task Committee 426, (1973). The Shear Strength of Reinforced Concrete Members. ASCE Journal of the Structural Division, Vol. 99, No. 6, pp. 1091-1187.
- ASCE-ACI Task Committee 445, (1998). Recent Approaches to Shear Design of Structural Concrete. ASCE Journal of Structural Engineering, Vol. 124, No. 12, pp. 1375-1417.
- ASTM A370, (2011). "Standard Test Methods and Definitions for Mechanical Testing of Steel Products." American Society for Testing Materials (ASTM International).
- ASTM A615/A615M, (2009). "Standard Specification for Deformed and Plain Carbon-Steel Bars for Concrete Reinforcement." ASTM, West Conshohocken, PA, 6 pp.

- ASTM C127, (2007). “Standard Test Method for Density, Relative Density (Specific Gravity), and Absorption of Coarse Aggregate.” American Society for Testing Materials (ASTM International).
- ASTM C128, (2007). “Standard Test Method for Density, Relative Density (Specific Gravity), and Absorption of Fine Aggregate.” American Society for Testing Materials (ASTM International).
- ASTM C138, (2010). “Standard Test Method for Density (Unit Weight), Yield, and Air Content (Gravimetric) of Concrete.” American Society for Testing Materials (ASTM International).
- ASTM C192, (2007). “Standard Practice for Making and Curing Concrete Test Specimens in the Laboratory.” American Society for Testing Materials (ASTM International).
- ASTM C231, (2010). “Standard Test Method for Air Content of Freshly Mixed Concrete by the Pressure Method.” American Society for Testing Materials (ASTM International).
- ASTM C39/C39M, (2011). “Standard Test Method for Compressive Strength of Cylindrical Concrete Specimens.” American Society for Testing Materials (ASTM International).
- ASTM C469, (2002). “Standard Test Method for Static Modulus of Elasticity and Poisson’s Ratio of Concrete in Compression.” American Society for Testing Materials (ASTM International).
- ASTM C496, (2004). “Standard Test Method for Splitting Tensile Strength of Cylindrical Concrete Specimens.” American Society for Testing Materials (ASTM International).
- ASTM C566, (1997). “Standard Test Method for Total Evaporable Moisture Content of Aggregate by Drying.” American Society for Testing Materials (ASTM International).
- ASTM C617, (2009). “Standard Practice for Capping Cylindrical Concrete Specimens.” American Society for Testing Materials (ASTM International).
- ASTM C78, (2009). “Standard Test Method for Flexural Strength of Concrete (Using Simple Beam with Third-Point Loading).” American Society for Testing Materials (ASTM International).
- ASTM E178, (2008). “Standard Practice for Dealing with Outlying Observations.” American Society for Testing Materials (ASTM International).

- Bazant, Z.P., and Becq-Giraudon, E., (2002). "Statistical Prediction of Fracture Parameters of Concrete and Implications for Choice of Testing Standards." *Cement and Concrete Research Journal*, Vol. 32, No. 4, pp. 529-556.
- Bazant, Z.P., and Kim, J.K., (1984). "Size Effect in Shear Failure of Longitudinally Reinforced Beams." *ACI Journal Proceedings*, Vol. 81, pp. 456-468.
- Bazant, Z.P., and Pfeiffer, P.A., (1987). "Determination of Fracture Energy from Size Effect and Brittleness Number." *ACI Materials Journal*, Vol. 84, No. 6, pp. 463-480.
- Bazant, Z.P., and Sun, H.H., (1987). "Size Effect in Diagonal Shear Failure: Influence of Aggregate Size and Stirrups." *ACI Journal Proceedings*, Vol. 84, pp. 259-272.
- Bazant, Z. P., and Yu, Q., (2005). "Design against Size Effect on Shear Strength of Reinforced Concrete Beams without Stirrups," *Journal of Structural Engineering*, ASCE, V. 131, No. 12, pp. 1877-1885.
- Bentz, E.C., Vecchio, F.J., and Collins, M.P., (2006). "Simplified Modified Compression Field Theory for Calculating Shear Strength of Reinforced Concrete Elements." *ACI Structural Journal*, Vol. 103, No. 4, pp. 614-624.
- Boresi, A.P., and Schmidt, R.J., (2003). *Advanced Mechanics of Materials* (6th Ed.). John Wiley & Sons.
- Choi, H. B., Yi, C. K., Cho, H. H., & Kang, K. I. (2010). "Experimental Study on the Shear Strength of Recycled Aggregate Concrete Beams." *Magazine of Concrete Research*, V.62 (2), pp.103-114.
- Cladera, A., (2002). *Shear Design of Reinforced High-Strength Concrete Beams*. PhD Thesis. Universitat Politècnica de Catalunya. Barcelona, Spain.
- Collins, MP, Kuchma D. (1999). "How Safe are Our Large, Lightly Reinforced Concrete Beams, Slabs, and Footings?" *ACI Structural Journal*, V.96, No. 4, pp. 482-90
- Collins, M.P., and Mitchell, D., (1991). *Prestressed Concrete Structures*. Response Publications.
- Collins, M.P., Bentz, E.C., and Sherwood, E.G., (2008). "Where is Shear Reinforcement Required? Review of Research Results and Design Procedures." *ACI Structural Journal*, Vol. 105, No. 5, pp. 590-600.
- Collins, M.P., Mitchell, D., and Bentz, E.C., (2008). "Shear Design of Concrete Structures." *The Structural Engineer*, Vol. 86, No. 10, pp. 32-39.

- Comite Euro-International du Beton, (1990). CEB-FIP Model Code 1990, Redwood Books, Wiltshire, England.
- Coronado, C., (2006). Characterization, Modeling and Size Effect of Concrete-Epoxy Interfaces. PhD Thesis. Pennsylvania State University. United States of America.
- CSA Committee A23.3, (2004). Design of Concrete Structures (CSA A23.3-04). Canadian Standards Association. Rexdale, ON, Canada.
- Dahl, H., and Brincker, R., (1989). "Fracture Energy of High-Strength Concrete in Compression." International Conference on Fracture of Concrete and Rock: Cardiff. Elsevier Science, pp. 523-536.
- Duthinh, D., (1999). "Sensitivity of Shear Strength of Reinforced Concrete and Prestressed Concrete Beams to Shear Friction and Concrete Softening According to Modified Compression Field Theory." ACI Structural Journal, Vol. 96, No. 4, pp. 495-508.
- Einsfeld, R.A., and Velasco, M.S.L., (2006). "Measurement of the Ratio G_F/G_f for Numerical Analysis of Concrete Structures." Latin American Journal of Solids and Structures, Vol. 3, pp. 361-376.
- Eurocode 2, (2004). Design of Concrete Structures – Part 1.1: General Rules and Rules for Buildings. EN 1992-1-1. Brussels. Belgium.
- Fathifazl, G., Razaqpur, A. G., Isgor, O. B., Abbas, A., Fournier, B., & Foo, S. (2009). "Flexural performance of steel-reinforced recycled concrete beams." ACI Structural Journal, V. 106, No. 6, pp. 858-867.
- FHWA State of the Practice National Review (2004). "Transportation Applications of Recycled Concrete Aggregate".
- Gastebled, O.J., and May, I.M., (2001). "Fracture Mechanics Model Applied to Shear Failure of Reinforced Concrete Beams without Stirrups." ACI Structural Journal, Vol. 98, No. 2, pp. 184-190.
- Ghaemmaghami, A., and Ghaemian, M., (2004). "Specific Fracture Energy Approximation of Dam Concrete." 13th World Conference on Earthquake Engineering. Paper No. 69. Vancouver, BC. Canada.
- Griffith, A.A., (1920). The Phenomena of Rupture and Flow in Solids. Philosophical Transactions, Series A, Vol. 221, pp. 163-198.
- Guinea, G.V., Planas, J., and Elices, M., (1992). "Measurement of the Fracture Energy Using Three-Point Bend Tests: Part 1 – Influence of Experimental Procedures." Materials and Structures. Materials and Structures, Vol. 25, pp. 212-218.

- Gonzalez-Fonteboa, B., & Martinez-Abella, F. (2007). "Shear Strength of Recycled Concrete Beams." *Construction and Building materials*, 21(4), 887-893.
- González-Fonteboa, B., Martínez-Abella, F., Martínez-Lage, I., & Eiras-López, J. (2009). "Structural Shear Behaviour of Recycled Concrete with Silica Fume." *Construction and Building Materials*, 23(11), 3406-3410.
- Gustafsson, P.J., and Hillerborg, A., (1988). "Sensitivity in Shear Strength of Longitudinally Reinforced Concrete Beams to Fracture Energy of Concrete." *ACI Journal Proceedings*, Vol. 85, pp. 286-294.
- Hillerborg, A., (1985). "Theoretical Basis of a Method to Determine the Fracture Energy G_F of Concrete." *Materials and Structures*, Vol. 18, No. 106, pp. 291-296.
- Hillerborg, A., Modeer, M., and Petersson, P.E., (1976). "Analysis of Crack Formation and Crack Growth in Concrete by Means of Fracture Mechanics and Finite Elements." *Cement and Concrete Research Journal*, Vol. 6, pp. 773-782.
- Hsu, T.T.C., (1993). *Unified Theory of Reinforced Concrete*. CRC Press.
- Hsu, T.T.C., and Mo, Y.L., (2010). *Unified Theory of Concrete Structures*. John Wiley & Sons.
- Irwin, G.R., Kies, J.A., and Smith, H.L., (1958). "Fracture Strength Relative to Onset and Arrest of Crack Propagation." *Proceedings ASTM*, Vol. 58, pp. 640-657.
- Jenq, Y.S., and Shah, S.P., (1989). "Shear Resistance of Reinforced Concrete Beams – A Fracture Mechanics Approach." *ACI Special Publication*, Vol. 118, pp. 237-258.
- Kaplan, M.F., (1961). "Crack Propagation and the Fracture of Concrete. *ACI Journal Proceedings*," Vol. 58, pp. 591-610.
- Kellermann, W.F., (1933). "Effect of Size of Specimen, Size of Aggregate and Method of Loading upon the Uniformity of Flexural Strength Results." *Public Roads*, Vol. 13, No. 11, pp. 177-184.
- Kesler, C.E., Naus, D.J., and Lott, J.L., (1972). "Fracture Mechanics – Its Applicability to Concrete." *Proceedings of the International Conference on the Mechanical Behavior of Materials*, Vol. IV, pp. 113-124, Kyoto, Japan.
- Kikuchi, M., Mukai, T., & Koizumi, H. (1988). "Properties of Concrete Products Containing Recycled Aggregate." In *Proc., 2nd Int. Symp. on Demolition and Reuse of Concrete and Masonry*, Vol. 2, pp. 595-604.

- Kim, J.K., and Park, Y.D., (1996). "Prediction of Shear Strength of Reinforced Concrete Beams without Web Reinforcement." *ACI Materials Journal*, Vol. 93, No. 3, pp. 213-222.
- Kim, W., and White, R.N., (1991). "Initiation of Shear Cracking in Reinforced Concrete Beams with No Web Reinforcement." *ACI Structural Journal*, Vol. 88, No. 3, pp. 301-308.
- Kuchma, D., (2009). "Contribution of Stirrups to Shear Resistance." *Structures Congress 2009: Don't Mess with Structural Engineers*, ASCE, pp. 1587-1594.
- Laskar, A., Hsu, T.T.C., and Mo, Y.L.C., (2010). "Shear Strengths of Prestressed Concrete Beams Part 1: Experiments and Shear Design Equations." *ACI Structural Journal*, Vol. 107, No. 3, pp. 330-339.
- Loov, R.E., (1998). "Review of A23.3-94 Simplified Method of Shear Design and Comparison with Results using Shear Friction." *Canadian Journal of Civil Engineering*, Vol. 25, No. 3, pp. 437-450.
- Marotta, T.W., Coffey, J.C., LaFleur, C.B., and LaPlante, C., (2011). *Basic Construction Materials* (8th Ed.). Pearson-Prentice Hall.
- Martin, J., Stanton, J., Mitra, N., and Lowes, L.N., (2007). "Experimental Testing to Determine Concrete Fracture Energy Using Simple Laboratory Test Setup." *ACI Materials Journal*, Vol. 104, No. 6, pp. 575-584.
- Maruyama, I., Sogo, M., Sogabe, T., Sato, R., & Kawai, K. (2004). "Flexural Properties of Reinforced Recycled Concrete Beams." In *Internacional RILEM conference on the Use of Recycled Materials in Buildings and Structures*, Paper No.315, Barcelona, Spain.
- Mindess, S., Young, J.F., and Darwin, D., (2003). *Concrete* (2nd Ed.). Prentice Hall.
- Mörsch, E., (1902). *Der Eisenbetonbau, Seine Theorie und Anwendung*. Stuttgart, Germany.
- Neville, A.M., (1997). *Properties of Concrete* (4th Ed.). John Wiley & Sons.
- Nielsen, K.E.C., (1954). "Effect of Various Factors on the Flexural Strength of Concrete Tests Beams." *Magazine of Concrete Research*, No. 15, pp. 105-114.
- Nilson, A.H., Darwin, D., and Dolan, C.W., (2004). *Design of Concrete Structures* (13th Ed.). McGraw Hill.
- Park, R., and Paulay, T., (1975). *Reinforced Concrete Structures*. John Wiley & Sons.

- Rangan, B.V., (1991). "Web Crushing Strength of Reinforced and Prestressed Concrete Beams." *ACI Structural Journal*, Vol. 88, No. 1, pp. 12-16.
- Reineck, KH, Kuchma, DA, Kim, KS; and Marx, S., (2003). "Shear Database for Reinforced Concrete Members without Shear Reinforcement," *ACI Structural Journal*, V. 100, No. 2, pp. 240-249.
- Raphael, J.M., (1984). "Tensile Strength of Concrete." *Concrete International*, Vol. 81, No. 2, pp. 158-165.
- RILEM TC 89-FMT Fracture Mechanics of Concrete-Test Methods, (1990). Determination of Fracture Parameters (K_{IC} and $CTOD_C$) of Plain Concrete Using Three-Point Bend Tests. *Materials and Structures*, Vol. 23, pp. 457-460.
- RILEM TC 89-FMT Fracture Mechanics of Concrete-Test Methods, (1990). Size Effect Method for Determining Fracture Energy and Process Zone Size of Concrete. *Materials and Structures*, Vol. 23, pp. 461-465.
- Ritter, W., (1899). *Die Bauweise Hennebique*. Schweizerische Bauzeitung. Zurich, Switzerland.
- Schlaich, J., Schäfer, K., and Jennewein, M., (1987). "Towards a Consistent Design of Structural Concrete." *PCI Journal*, Vol. 32, No. 3, pp. 74-150.
- Schubert, S., Hoffmann, C., Leemann, A., Moser, K., & Motavalli, M. (2012). "Recycled Aggregate Concrete: Experimental Shear Resistance of Slabs without Shear Reinforcement." *Engineering Structures*, 41, 490-497.
- Shah, S.G., Bhasya, V., and Chandra Kishen, J.M., (2011). "Tension-Softening Properties for Concrete-Concrete Interfaces." *ACI Structural Journal*, Vol. 108, No. 6, pp. 725-734.
- Shah, S.P., and Carpinteri, A., (1991). *Fracture Mechanics Test Methods for Concrete: Report of Technical Committee 89-FMT (1st Ed.)*. Chapman and Hall.
- So, K.O., and Karihaloo, B.L., (1993). "Shear Capacity of Longitudinally Reinforced Beams – A Fracture Mechanics Approach." *ACI Structural Journal*, Vol. 90, No. 6, pp. 591-600.
- Taylor, HPJ. (1972). "Shear Strength of Large Beams," *Journal of the Structural Division, ASCE*, V. 98, No. ST11, Nov., pp. 2473-2489.
- Taylor, HPJ. (1974). "The Fundamental Behavior of Reinforced Concrete Beams in Bending and Shear," *American Concrete Institute, Shear in Reinforced Concrete*, SP-42, pp. 43-77.

- Tureyen, A.K., (2001). Influence of Longitudinal Reinforcement Type on the Shear Strength of Reinforced Concrete Beams without Transverse Reinforcement. PhD Thesis. Purdue University. United States of America.
- Tureyen, A.K, and Frosch, R.J., (2003). "Concrete Shear Strength: Another Perspective." ACI Structural Journal, Vol. 100, No. 5, pp. 609-615.
- Van der Veen, C., (1990). Cryogenic Bond Stress-Slip Relationship. MS Thesis. Delft University. Delft, Netherlands.
- Vecchio, F.J., and Collins, M.P., (1986). "The Modified Compression Field Theory for Reinforced Concrete Elements Subjected to Shear." ACI Journal Proceedings, Vol. 83, No. 2, pp. 219-231.
- Vecchio, F.J., and Collins, M.P., (1993). "Compression Response of Cracked Reinforced Concrete." Journal of Structural Engineering, Vol. 119, No. 12, pp. 3590-3610.
- Walraven, J.C., (1980). Aggregate Interlock: a Theoretical and Experimental Analysis. PhD Thesis. Delft University of Technology. Delft, Netherlands.
- Whitney, C.S., (1937). "Design of Reinforced Concrete Members under Flexure or Combined Flexure and Direct Compression." ACI Journal Proceedings, Vol. 33, No. 3, pp. 483-498.
- Wight, J.K., and MacGregor, J.G., (2009). Reinforced Concrete Mechanics and Design (5th Ed.). Pearson-Prentice Hall.
- World Business Council for Sustainable Development (WBCSD) Report (2012). "Recycling concrete" <http://www.wbcscement.org/index.php/key-issues/sustainability-with-concrete/54>, Accessed date: August 2013.
- Wright, P.J.F, (1955). "Comments on an Indirect Tensile Test on Concrete Cylinders." Magazine of Concrete Research, Vol. 7, No. 20, pp. 87-96.
- Xiao, J., Xie, H., & Yang, Z. (2012). "Shear Transfer Across a Crack in Recycled Aggregate Concrete." Cement and Concrete Research, V. 42, pp. 700-709.
- Zakaria, M., Ueda, T., Wu, Z., and Meng, L., (2009). "Experimental Investigation on Shear Cracking Behavior in Reinforced Concrete Beams with Shear Reinforcement." Journal of Advanced Concrete Technology, Vol. 7, No. 1, pp. 79-96.

APPENDIX E

FINAL Report E

TRyy1317

**Project Title: Recycled Concrete Aggregate (RCA) for
Infrastructure Elements**

Report E: Flexural Behavior of RCA Concrete

Prepared for
Missouri Department of Transportation
Construction and Materials

Missouri University of Science and Technology, Rolla, Missouri

May 2014

The opinions, findings, and conclusions expressed in this publication are those of the principal investigators and the Missouri Department of Transportation. They are not necessarily those of the U.S. Department of Transportation, Federal Highway Administration. This report does not constitute a standard or regulation.

ABSTRACT

Sustainability is at the forefront of our society. Unfortunately, concrete, our most common construction material uses a significant amount of non-renewable resources. Consequently, many researchers have investigated the use of recycled materials in the production of concrete such as recycled aggregate.

Most research to date has consisted only of the evaluation of the material strength and durability of recycled aggregate concrete (RAC) mixtures, while only a limited number of studies have implemented full-scale testing of specimens constructed with RAC to determine its potential use in the industry. For this research, a laboratory testing program was developed to investigate the flexural performance of reinforced concrete (RC) beams constructed with RAC. The experimental program consisted of eight tests performed on full-scale RC beams. The principal parameters investigated were: (1) concrete type (RAC or conventional concrete (CC)) and (2) amount of longitudinal (flexural) reinforcement. The cracking, yielding, and ultimate capacities of the beams were compared with existing design code provisions. Furthermore, the experimental flexural strengths of the beams were compared with a flexural test database of CC specimens.

Results of this study indicate that the RAC beams have comparable ultimate flexural strengths and approximately 13% higher deflections compared to CC.

TABLE OF CONTENTS

	Page
ABSTRACT	ii
LIST OF ILLUSTRATIONS	v
LIST OF TABLES	vi
NOMENCLATURE	vii
1. INTRODUCTION	1
1.1. BACKGROUND	1
1.2. CONCERNS WITH RECYCLED AGGREGATE CONCRETE	3
1.3. OBJECTIVE AND SCOPE OF WORK	4
1.4. RESEARCH METHODOLOGY	5
1.5. REPORT OUTLINE	6
2. LITERATURE REVIEW ON RECYCLED AGGREGATE	8
2.1. GENERAL	8
2.2. USE OF USE OF RECYCLED AGGREGATE AS COARSE AGGREGATE	8
2.3. PREVIOUS STUDIES RELATED TO RAC	9
2.4. CONCLUDING REMARKS	10
3. EXPERIMENTAL PROGRAM	11
3.1. GENERAL	11
3.2. TEST BEAMS	11
3.3. MATERIALS	13
3.3.1. Concrete	13
3.3.2. Steel Reinforcement	15
3.4. BEAM FABRICATION	15
3.5. TEST SET-UP	16
3.6. INSTRUMENTATION	19
3.6.1. Local Deformations and Strains	19
3.6.2. Global Deformations	20
4. TEST RESULTS, BEHAVIOR & ANALYSIS	21

4.1. INTRODUCTION	21
4.2. GENERAL BEHAVIOR	21
4.3. LOAD-DEFLECTION BEHAVIOR	23
4.4. COMPARISON OF CC AND RAC RESULTS WITH CODE PROVISIONS	23
4.5. COMPARISON OF TEST RESULTS WITH FLEXURAL TEST DATABASE.....	25
5. FINDINGS, CONCLUSIONS, AND RECOMMENDATIONS	28
5.1. FINDINGS AND CONCLUSIONS	28
5.2. RECOMMENDATIONS.....	30
BIBLIOGRAPHY	31

LIST OF ILLUSTRATIONS

Figure	Page
Figure 1.1: States using RCA as Aggregate.....	2
Figure 1.2: States using RCA as Base Aggregate.....	3
Figure 1.3: States using RCA in PC Concrete	3
Figure 3.1: Cross Sections and Reinforcement Layout of the Beams	12
Figure 3.2: Load Pattern and Location of Strain Gauges on the Test Beams	12
Figure 3.3: Beam Construction Process.....	16
Figure 3.4: Details of Test Set-Up (1)	17
Figure 3.5: Details of Test Set-Up (2)	18
Figure 3.6: Photograph of Test Set-Up.....	18
Figure 3.7: Data Acquisition System.....	19
Figure 3.8: Location of LVDT to Measure Deflection	20
Figure 3.9: Detail of LVDT for Deflection Measurement.....	20
Figure 4.1: Crack Pattern of the Test Beams at Flexural Failure.....	22
Figure 4.2: Load-Deflection of the Test Beams.....	24
Figure 4.3: Normalized Flexural Strength vs. Normalized Longitudinal Reinforcement Ratio; Results from (Leet et al., 1997) and Test Results of this Study.....	27

LIST OF TABLES

Table	Page
Table 3.1: Flexural Beam Test Matrix	12
Table 3.2: Aggregate Properties	14
Table 3.3: Mix Designs per Cubic Yard	14
Table 3.4: Typical Fresh and Hardened Concrete Properties for CC and RAC Mixes	14
Table 3.5: Mechanical Properties of Steel Reinforcement	15
Table 4.1: Test Results Summary	25

NOMENCLATURE

Symbol	Description
A_s	Area of longitudinal reinforcement
b	Width of cross-section
b_v	Effective width of cross-section
b_w	Width of cross-section
d	Effective depth of cross-section
E_c	Modulus of elasticity of the concrete
E_s	Modulus of elasticity of the steel
F_c	Concrete compressive force
F_s	Longitudinal reinforcement force
f'_c	Compressive strength of the concrete
f_{ci}	Compressive stress on crack surface
f_{cr}	Concrete stress at cracking
f_{ct}	Tensile strength of the concrete
f_t	Splitting tensile strength of the concrete
f'_t	Tensile strength of the concrete
f_v	Tensile stress in the stirrups
f_y	Yield stress of steel
h	Height of cross-section
I_g	Moment of inertia of gross concrete section about centroidal axis

jd	Distance between resultants of internal compressive and tensile forces on a cross-section
L	Length of the beam
M_{cr}	Cracking moment
M_{exp}	Experimentally determined total moment applied to specimen
M_n	Nominal moment capacity
MOR	Modulus of rupture of the concrete
P_{max}	Measured peak load
w/cm	Water-to-cementitious material ratio
\bar{x}	Arithmetic average
y_t	Distance from centroidal axis of gross section
z	Inner level arm
ϵ_0	Concrete strain at peak stress
ϵ_c	Compressive strain in the concrete
ϵ_s	Strain in the tension reinforcement
ρ_l	Longitudinal reinforcement ratio

1. INTRODUCTION

1.1. BACKGROUND

The construction of buildings, bridges, and roadways continues to increase in the twenty-first century, especially in areas with ever-growing populations. Existing structures and highways require repair or replacement as they reach the end of their service life or simply no longer satisfy their intended purpose due to the growing population. As modern construction continues, two pressing issues will become more apparent to societies: an increasing demand for construction materials, especially concrete and asphalt aggregates, and an increasing production of construction and demolition waste. Already, the Federal Highway Administration (FHWA 2004) estimates that two billion tons of new aggregate are produced each year in the United States. This demand is anticipated to increase to two and a half billion tons each year by 2020. With such a high demand for new aggregates, the concern arises of the depletion of the current sources of natural aggregates and the availability of new sources. Similarly, the construction waste produced in the United States is expected to increase. From building demolition alone, the annual production of construction waste is estimated to be 123 million tons (FHWA, 2004). Currently, this waste is most commonly disposed of in landfills.

To address both the concern of increasing demand for new aggregates and increasing production of waste, many states have begun to recognize that a more sustainable solution exists in recycling waste concrete for use as aggregate in new concrete, or recycled concrete aggregates (RCA). The solution helps address the question

of how to sustain modern construction demands for aggregates as well as helps to reduce the amount of waste that enters already over-burdened landfills.

Based on a survey by FHWA in 2002, many states had begun to implement recycled concrete aggregates in some ways in new construction. As shown in **Figure 1.1**, most states had recognized the many uses of RCA as a raw material, such as for rip-rap, soil stabilization, pipe bedding, and even landscape materials. As shown in **Figure 1.2**, many states had gone a step further in integrating RCA into roadway systems for use as aggregate base course material. However, as shown in **Figure 1.3**, only a small number of states had begun using RCA in Portland cement concrete for pavement construction. However, over the intervening 12 years, the use of RCA has increased significantly, particularly within the last 5 years, and the Missouri Department of Transportation (MoDOT) has instituted a very aggressive program to increase the use of recycled materials in transportation-related construction. However, there are currently no acceptable standards or guidelines in the U.S. for utilizing RCA in structural concrete.

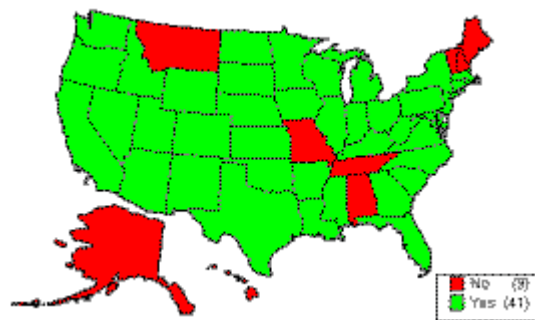


Figure 1.1: States using RCA as Aggregate

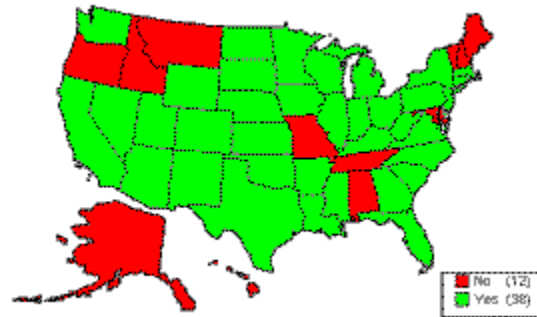


Figure 1.2: States using RCA as Base Aggregate

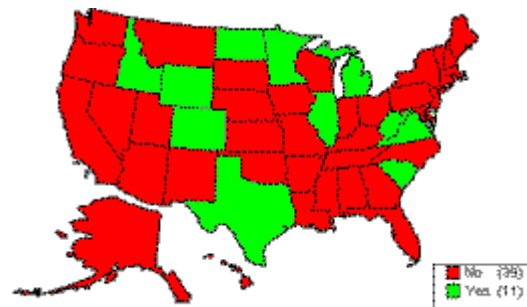


Figure 1.3: States using RCA in PC Concrete

1.2. CONCERNS WITH RECYCLED AGGREGATE CONCRETE

RCAs are composed of both the original, or virgin, aggregate, as well as mortar which remains adhered to the surface of the aggregate. In the production of RCA, the removal of all this residual mortar would prove costly and detrimental to the integrity of the virgin aggregates within the concrete. Therefore, residual mortar is inevitable.

Research has shown that this residual mortar causes high water absorption, low density, low specific gravity, and high porosity in RCAs compared to natural aggregates. These effects in the recycled aggregate can decrease hardened concrete properties of recycled aggregate concrete (RAC). According to Abbas et al. (2008), the amount of residual

mortar on the RCA can significantly affect the mechanical and durability properties of RAC. To reduce the negative impacts of this residual mortar, new mix design methods such as the equivalent mortar volume method can be used.

Due to the variety of sources of RCA and the various functions, environment, and wear of the concrete structures and pavements from which the RCA can be obtained, characterizing this aggregate can be very difficult. Controlled studies must be performed to account for each of these variables on a regional basis, such as for each state's Department of Transportation, so that the aggregates within the area can be adequately characterized.

1.3. OBJECTIVE AND SCOPE OF WORK

The main *objective* of this research study was to evaluate the flexural behavior and response of RCA through material, component, and full-scale testing. This objective included a study and evaluation of current analytical models used to predict the flexural response of conventional Portland-cement concrete as applied to RCA, including recommended modifications.

The following *scope of work* was implemented in order to achieve the objective of the research study:

- Perform a literature review;
- Develop a research plan;
- Develop mix designs for both conventional and RAC;
- Evaluate the fresh and hardened properties of several RAC and CC mixes;
- Design and construct small and full-scale specimens;

- Test specimens to failure;
- Record and analyze data from tests;
- Compare test results to current guidelines and previous research findings;
- Develop conclusions and recommendations; and
- Prepare this report to document the details, results, findings, conclusions, and recommendations of this study.

1.4. RESEARCH METHODOLOGY

The proposed research methodology included six (6) tasks necessary to successfully complete the study. They are as follows:

Task #1: Perform a literature review. The goal of the literature review was to become familiarized with testing methods and results from previous studies. This knowledge was used for a better understanding of the behavior of the specimens, to avoid mistakes, as well as to provide support for comparisons.

Task #2: Develop RAC and CC mix designs. The purpose of this task was to develop RAC mix designs that maximized the percentage of recycled concrete aggregate, but that still fulfilled typical construction needs, such as early strength development. Conventional concrete mix designs served as controls during this study. ACI 211.1-91 formed the basis for developing the mix designs.

Task #3: Perform material and component testing. A number of hardened concrete property tests were completed to evaluate the performance of the RAC mix and determine the validity of using these tests to predict the performance of concretes containing recycled concrete aggregate.

Task #4: Perform full-scale testing. This task involved the construction and testing of full-scale specimens to confirm the potential of RAC. The full-scale specimens included beam specimens for flexural testing only. These specimens were constructed with materials from the local ready mix concrete plant to validate the ability of transferring the mix designs from the laboratory to the field. In order to compare the flexural strength of conventional and RAC, full-scale beams were tested in a third point loading configuration. These beams were designed to fail in flexure. Different longitudinal reinforcement ratios were also considered. Strain gauges were applied to the flexural reinforcement, and the maximum load applied to the beam was also recorded and used to calculate the strength of the beams.

Task #5: Analyze test data. The material, component, and full-scale test results were analyzed to evaluate the flexural behavior and response of RAC compared to conventional Portland-cement concrete. The test data included: concrete compressive and tensile strength, modulus of rupture (MOR), flexural force-deflection plots, crack formation and propagation, and reinforcement strains.

Task #6: Develop findings, conclusions, and recommendations. This task synthesized the results of the previous tasks into findings, conclusions, and recommendations on the flexural behavior and response of RAC.

1.5. REPORT OUTLINE

This report includes six chapters. This section will discuss the information that will be presented in more detail throughout this document.

Chapter 1 acts as an introduction to the report. This introduction contains a brief background of recycled aggregate. It also discusses the research objective, scope of work, and research plan.

Chapter 2 includes information from previous research performed on the characterization of recycled aggregate and its applications as a coarse aggregate in concrete.

Chapter 3 includes information about the experimental program. The experimental program consisted of eight tests performed on full-scale reinforced concrete beams as well as material and component testing to determine hardened concrete properties such as compressive strength, splitting tensile strength, and flexural strength. This chapter also describes the fabrication process, test set-up, and instrumentation for the full-scale testing.

Chapter 4 presents the test results and the different analyses used to investigate the flexural resistance mechanisms. The overall behavior of the specimens is described first, with a focus on crack patterns, failure modes, and flexural strength.

Chapter 5 concludes this document, summarizing the findings and conclusions of this study and proposing recommendations and future research.

2. LITERATURE REVIEW ON RECYCLED AGGREGATE

2.1. GENERAL

Conventional Portland-cement concrete is produced more than any other material in the world. It is used in every civil engineering field for applications such as pavements, dams, bridges, and buildings because of its versatility, strength, and durability. In this chapter, a brief review is presented of the research performed on concrete mixtures containing recycled aggregate as coarse aggregate.

Concrete with recycled aggregate can be produced to achieve desired strengths at various ages, with a given water-cementitious ratio, aggregate size, air content, and slump as it is done for conventional concrete.

2.2. USE OF RECYCLED AGGREGATE AS COARSE AGGREGATE

Recently, there has been an increasing trend toward the use of sustainable materials. Sustainability helps the environment by reducing the consumption of non-renewable natural resources. Concrete – the second most consumed material in the world after water – uses a significant amount of non-renewable resources. As a result, numerous researchers have investigated the use of recycled materials in the production of concrete such as fly ash and recycled aggregate.

Unfortunately, global data on concrete waste generation is not available, but construction and demolition waste accounts for around 900 million tonnes every year just in Europe, the US, and Japan (WBCSD, 2012). Recycling concrete not only reduces using virgin aggregate but also decreases the amount of waste in landfills.

In general, RCA has lower specific gravity and unit weight and considerably higher absorption and porosity compared to natural aggregates. These factors need to be taken into account when designing concrete mixes containing RCA.

2.3. PREVIOUS STUDIES RELATED TO RAC

Comprehensive research has been done on both the fresh and hardened properties of recycled aggregate concrete (RAC), but limited research has been performed on the structural behavior of RAC. The early research on structural performance of RAC was published in Japan (Kikuchi et al., 1988). Maruyama et al. (2004) tested beams with 1.06% longitudinal reinforcement ratio and three different water-to-cement (w/c) ratios (0.30, 0.45, and 0.60). They reported that flexural cracks in the RCA beams were wider and spaced closer compared with the conventional concrete (CC) beams. The RCA beams also had larger deflections than the CC beams because of a lower modulus of elasticity. They also observed no significance difference between the flexural capacity of the RCA and CC beams.

Sato et al. (2007) tested 37 beams with three different longitudinal reinforcement ratios (0.59%, 1.06%, and 1.65%). They used 100% recycled aggregate for their mix designs. Results of their study showed that the RCA beams had larger deflections compared with the CC beams. In terms of crack spacing, no significant difference was observed between the RCA and CC beams; however, the RCA beams had wider cracks compared with the CC beams. They also reported almost the same ultimate moment for the RCA and CC beams.

Ajdukiewicz et al. (2007) summarized the test results of flexural tests from the period of 1998-2006 in Poland. Their mixtures used partial or full recycled aggregate. All the beams were rectangular, measuring 200 x 300 mm in cross section and 2600 mm in length with two longitudinal reinforcement ratios (0.90% and 1.60%). They reported that the RCA beams had slightly lower moment capacity (3.5% on average) and larger deflections compared with the CC beams.

Fathifazl et al. (2009) used the equivalent mortar volume (EMV) method for their mix designs. They used both limestone (63.5% recycled aggregate) and river gravel (74.3% recycled aggregate) as a coarse aggregate for their mix designs. Their beams had three different longitudinal reinforcement ratios ranging between 0.49% and 3.31%. They reported comparable and even superior flexural behavior for RCA beams at both service and ultimate states. They concluded that the flexural provisions in current codes can be used for RCA beams.

Ignjatovic et al. (2012) studied nine full scale beams with 0%, 50%, and 100% recycled coarse aggregate and 0.28%, 1.46%, and 2.54% longitudinal reinforcement ratios. They reported no noticeable difference between load-deflection behavior, service load deflection, and ultimate flexural strength of RCA and CC beams, but they observed that the beams with a higher range of recycled aggregate showed higher levels of concrete destruction at failure.

2.4. CONCLUDING REMARKS

The literature review reported no significance difference in terms of crack morphology, crack patterns, and also failure modes between CC and RAC beams: however, they reported higher deflection for RAC beams compared with CC beams.

3. EXPERIMENTAL PROGRAM

3.1. GENERAL

The objective of this study was to investigate the flexural performance of reinforced concrete (RC) beams composed of RCA. The experimental program consisted of eight tests performed on full-scale RC beams. The principal parameters investigated were:

- (1) concrete type – recycled aggregate concrete (RAC) or conventional concrete (CC), and
- (2) amount of longitudinal reinforcement.

Also, as part of this study, small scale testing was performed to determine hardened concrete properties such as compressive strength, flexural strength, and splitting tensile strength.

3.2. TEST BEAMS

The reinforcement for the beams was designed in accordance with the AASHTO LRFD Bridge Design Specifications (AASHTO LRFD, 2010). The beams measured 10 ft. in length, had a cross section of 12 in. x 18 in., and were constructed with two different longitudinal reinforcement ratios – 0.47% and 0.64%. The beam design included shear reinforcement to ensure a flexural failure. All of the specimens had #3 stirrups spaced at 2 in. within the bearing area to prevent premature bearing failure as well as #3 stirrups spaced at 7 in. within the rest of the beam to avoid any shear failure.

Table 3.1 summarizes the test matrix used in this study. The beam designation included a combination of letters and numbers: F stands for flexural beams and numbers 6 and 7 indicate the size of longitudinal reinforcement bars within the tension area of the beam section. For example, F-6 indicates a beam with 2#6 within the bottom of the beam. Two beams were constructed and tested for each combination of variables shown in **Table 3.1** as well as each concrete type. The cross sections for these specimens are shown in **Figure 3.1**. **Figure 3.2** shows the load pattern and location of strain gauges on the test beams.

Table 3.1: Flexural Beam Test Matrix

Section	Bottom reinforcement	Top reinforcement	ρ
F-6	2#6	2#4	0.0047
F-7	2#7	2#4	0.0064



Figure 3.1: Cross Sections and Reinforcement Layout of the Beams

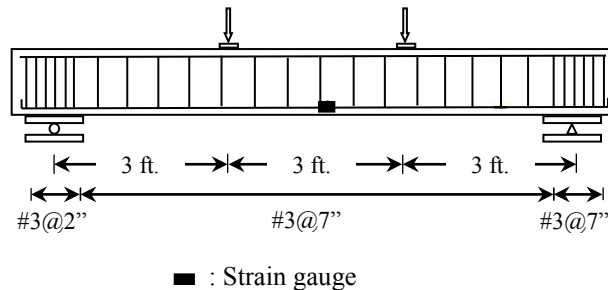


Figure 3.2: Load Pattern and Location of Strain Gauges on the Test Beams

3.3. MATERIALS

3.3.1. Concrete. For this study, two mix designs were produced and evaluated for flexural performance. A MoDOT Class B air-entrained mix design was used as a baseline for reference throughout the study and also as the parent material for the recycled concrete aggregate. The specified cement content in this mix was 535 lb., the water-to-cement ratio was 0.40, the target slump was 6 in., and the design air content was 6%. The specified amount of fine aggregate as a volume of total aggregates was 40%. For this mix, the typical dosage range of the MoDOT-approved air entrainment MB-AE 90 was 0.25-4.0 fl.oz./100 lb. of cement. The typical dosage of the Type A water reducer Glenium 7500 was 5.0 – 8.0 fl.oz./100 lb. of cement.

For the CC mix, the coarse aggregate consisted of crushed limestone with a maximum nominal aggregate size of 1 in. from the Potosi Quarry (Potosi, MO) while the fine aggregate was natural sand from Missouri River Sand (Jefferson City, MO). For the RAC mixes, the coarse aggregate consisted of RCA ground from the CC mix to a nominal maximum aggregate size of 1 in., with 100% replacement of the Potosi limestone. Test results for the coarse aggregate used in the CC mix design as well as the resulting RCA are shown in **Table 3.2**. As expected, the RCA had lower specific gravity and unit weight and considerably higher absorption. The Los Angeles abrasion test results were virtually identical.

Tables 3.3 and **3.4** present the mix designs and representative fresh and hardened strength properties, respectively, of the CC and RAC mixes. The mix incorporating RCA was a 100% direct replacement design. The total volume of coarse aggregate in the control MoDOT Class B mix was directly substituted with the laboratory-produced RCA

and is subsequently referred to as RAC-100. In order to maintain consistency with the control specimens, the MoDOT Class B mix specifications were used to design the RAC. However, during laboratory trial batching, it was noticed from the slump test that the RAC-100 mix lacked cohesion. To remedy this situation, the mix was modified by increasing the amount of fine aggregate volume by 5% of total aggregates, which noticeably improved the cohesion of the mix.

Table 3.2: Aggregate Properties

Property	CC	RCA
Bulk Specific Gravity, Oven-Dry	2.72	2.35
Dry-Rodded Unit Weight, (lb/ft ³)	99.8	89.8
Absorption (%)	0.98	4.56
LA Abrasion (% Loss)	43	41

Table 3.3: Mix Designs per Cubic Yard

Constituent	CC	RAC-100
Cement (Type I) (lb)	535	535
w/cm	0.40	0.40
Natural Coarse Aggregate (lb)	1958	-
Recycled Coarse Aggregate (lb)	-	1650
Fine Aggregate (lb)	1253	1442
HRWR (fl. oz)	55	42
AE (fl. oz)	20	7

Table 3.4: Typical Fresh and Hardened Concrete Properties for CC and RAC Mixes

Property	CC	RAC-100
Slump (in.)	5.5	8
Air content (%)	8.5	6.5
Unit weight (lb/ft ³)	145.4	136.0
Split cylinder strength (psi)	505	370
Flexural strength (psi)	500	410
Compressive strength (psi)	5400	4350

3.3.2. Steel Reinforcement. Shear reinforcement for the test specimens consisted of A615, Grade 60 #3 reinforcing bars. Longitudinal reinforcement for the test specimens consisted of A615, Grade 60 #4, #6, and #7 reinforcing bars. All the steel reinforcement was tested in accordance with ASTM A370 (2011) “Standard Test Methods and Definitions for Mechanical Testing of Steel Products” to obtain the mechanical properties, which are summarized in **Table 3.5**. These results are the average of three replicate specimens.

Table 3.5: Mechanical Properties of Steel Reinforcement

Bar size	Yield strength (psi)
#3	71,650
#4	73,970
#6	71,540
#7	65,120

3.4. BEAM FABRICATION

All the test beams were fabricated in the Structural Engineering High-Bay Research Laboratory (SERL) at Missouri S&T. Steel formwork was used to cast the beams. The steel cage was assembled from reinforcement that was bent in the laboratory to the desired geometry. Due to the dimension of the beams, it was possible to cast two beams at a time. After casting, the top surface of the beams was covered with burlap and plastic sheeting, and a wet surface was maintained for three days to retain moisture for proper curing. Cylinders were cured in the same environment as the test beams by placing them next to the beams. The sheeting and burlap were then removed, and the beams were allowed to air cure in the lab environment. Photographs showing the construction process are shown in **Figures 3.3**.



(a) Formwork



(b) Concrete placement



(c) Concrete consolidation



(d) Concrete finishing

Figure 3.3: Beam Construction Process**3.5. TEST SET-UP**

All the specimens were tested as simply supported and subjected to third-point loading with two actuators as shown in **Figure 3.4**. Two actuators, each with a 140-kip compressive capacity, were used to apply load to the beam specimens, as shown in **Figure 3.5**. The actuators applied load by pushing the steel beam downward to distribute the load onto two points of the test specimen. The loading frame assembly was designed to withstand at least two times the anticipated maximum load applied to fail the beams. Each test was performed under displacement control, and the load was applied in a series

of loading steps of 0.05 in., which corresponded to a load of approximately 8 kips, until failure. Electronic measurements of strain and deformation were recorded throughout the entire loading history of the specimens, while hand measurements of strain and crack pattern formations were taken at the end of each load step while the load was paused. The total beam length was 10 ft, with a simply supported span length of 9 ft. The load was applied at 3 ft from each support, as measured from center of support to center of load.

Figure 3.6 shows a photograph of the test set-up.

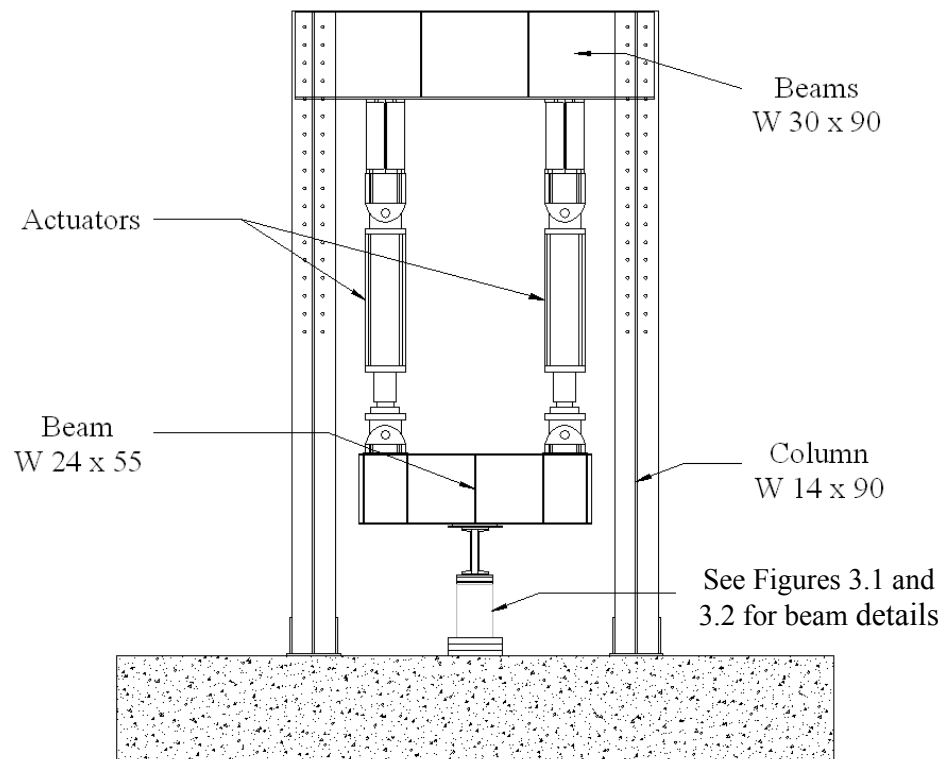


Figure 3.4: Details of Test Set-Up (1)

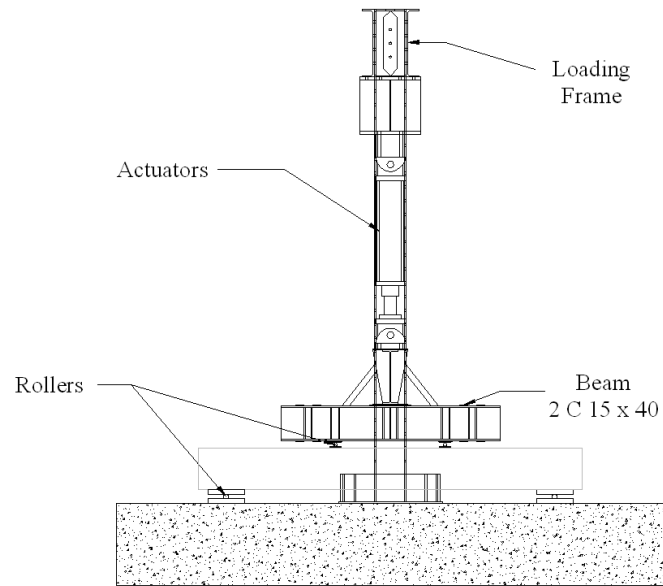


Figure 3.5: Details of Test Set-Up (2)



Figure 3.6: Photograph of Test Set-Up

3.6. INSTRUMENTATION

The specimens were instrumented with several measurement devices in order to monitor global and local deformations and strains. The load was directly measured from the load cell of the actuators. All devices were connected to a data acquisition system capable of reading up to 120 channels and all the data was recorded as shown in **Figure 3.7**.



Figure 3.7: Data Acquisition System

3.6.1. Local Deformations and Strains. Electric resistance gauges were used to monitor local strains in the longitudinal steel reinforcement of the test region. The strain gauges were purchased from Vishay Precision Group. They were made of constantan foil with 120 ohm resistance and had a linear pattern (uniaxial) with a gauge length of $\frac{1}{4}$ in.

One strain gauge was installed on longitudinal steel reinforcement in the test region as shown in **Figure 3.2**. The strain value obtained from the strain gauge is localized measurements at the point where the gauge is installed. It was located at the mid-span of beam.

3.6.2. Global Deformations. One Linear Variable Displacement Transducer (LVDT) was used to monitor vertical deflection of the test specimen. The LVDT was located at the midpoint of the test specimen, 3 in. from the top of the beam as shown in **Figures 3.8** and **3.9**.

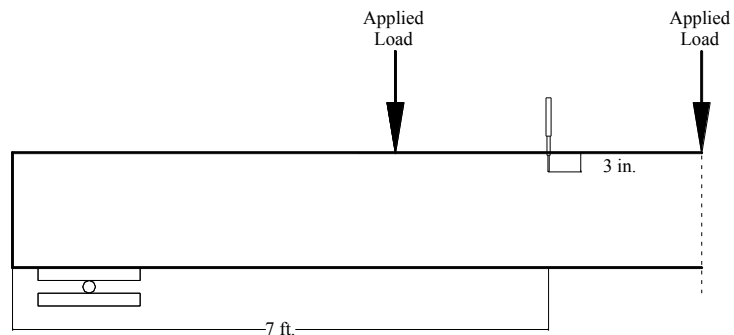


Figure 3.8: Location of LVDT to Measure Deflection



Figure 3.9: Detail of LVDT for Deflection Measurement

4. TEST RESULTS, BEHAVIOR & ANALYSIS

4.1. INTRODUCTION

The purpose of this study was to evaluate the flexural behavior of full-scale reinforced concrete (RC) beams constructed from RCA, which has not been fully investigated in previous research studies. The objectives of this section are to: (1) discuss the general behavior of the specimens with regard to crack progression, crack morphology, and failure mode, (2) compare load-deflection behavior of the test specimens, (3) compare the RAC test specimen results with the control specimen test results, (4) compare the test results with predicted capacities based on applicable design standards, and (5) compare the test results with a flexural test database of conventional concrete specimens.

4.2. GENERAL BEHAVIOR

In terms of crack morphology and crack progression, the behavior of both CC and RAC beams was similar except for crack spacing – flexural cracks for the RAC beams were spaced closer compared to the CC beams. All of the beams failed in flexure. In all of the beams, the longitudinal tension steel yielded first, followed by the concrete crushing, which is a ductile mode of failure, normally called tension failure.

Crack progression in the beams began with the appearance of flexural cracks in the maximum moment region, followed by additional flexural cracks forming between the load and support regions as the load was increased. Upon further increasing the applied load, the majority of the flexural cracks developed vertically and, after that, inclined flexure-shear cracks began to appear. **Figure 4.1** offers a direct visual

comparison of the crack shape and distribution at failure for the beams of both CC and RCA mixes, which are different in terms of crack spacing then has been reported by other researchers (e.g., Maruyama et al., 2004).

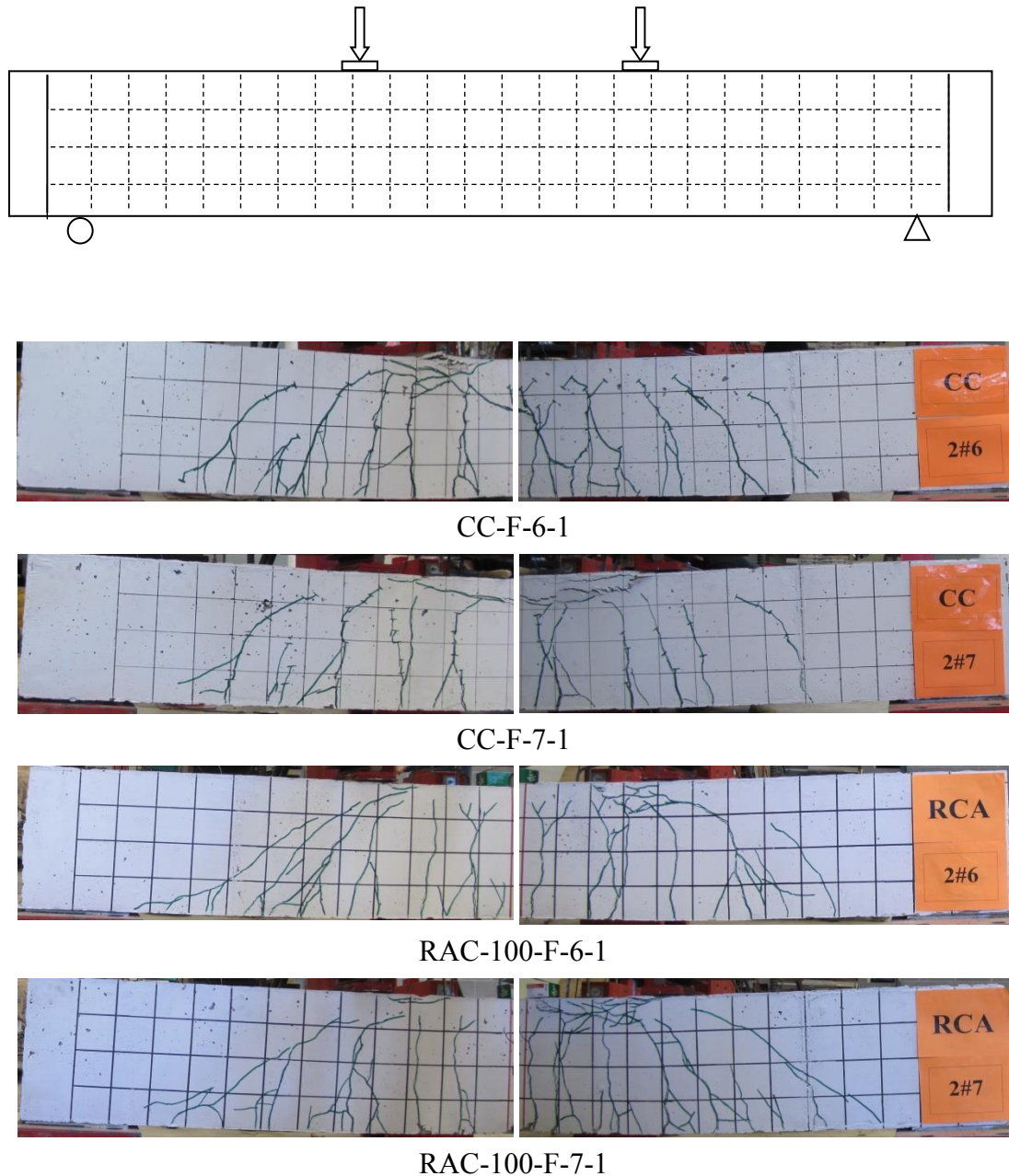


Figure 4.1: Crack Pattern of the Test Beams at Flexural Failure

4.3. LOAD-DEFLECTION BEHAVIOR

Figure 4.2 shows the load-deflection behavior for the test beams (the deflection was measured at midspan). Before the first flexural cracks occurred (point A), all of the beams displayed a steep linear elastic behavior. After additional application of load, the longitudinal steel yielded (point B). The beams then experienced the typical ductile plateau of RC flexural specimens. Eventually, sufficient rotation of the plastic hinge formed causing excessive strains in the compression zone of the beams and caused a crushing failure, resulting in failure of the specimens.

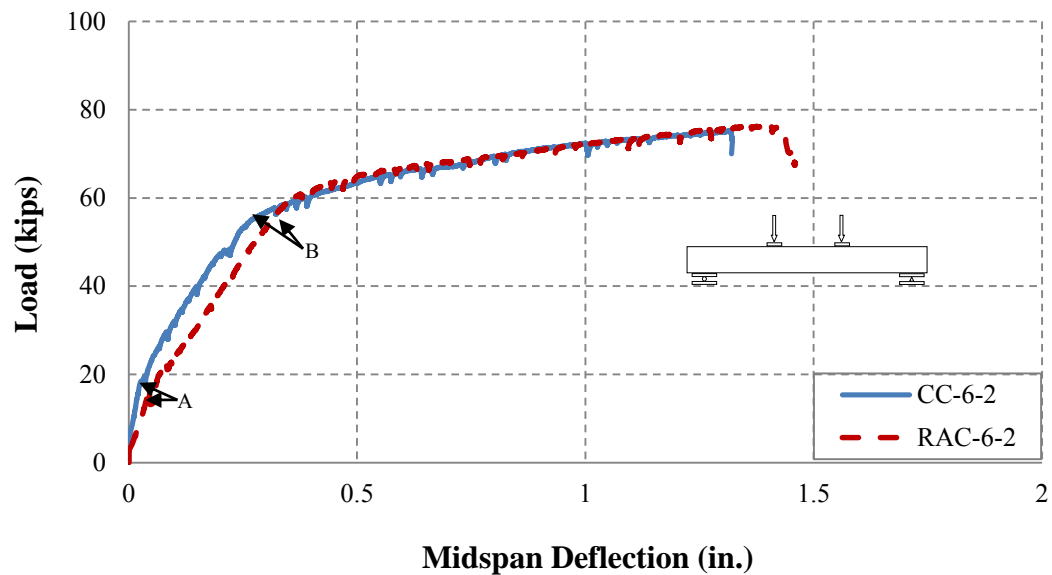
As shown in **Figure 4.2**, the RAC beams displayed lower cracking moment, which may be ascribed to the existence of two types of interfacial transition zones (ITZ) in the RCA beams (the ITZ between virgin aggregate and residual mortar in the RAC and also the ITZ between residual mortar and fresh mortar) compared with only a single ITZ (between virgin aggregate and fresh mortar) in the CC beams. Furthermore, the RAC beams showed lower stiffness after the cracking moments, which can be attributed to lower modulus of elasticity of the RCA mix compared with the CC mix due to the larger effective mortar fraction of the RAC.

4.4. COMPARISON OF CC AND RAC RESULTS WITH CODE PROVISIONS

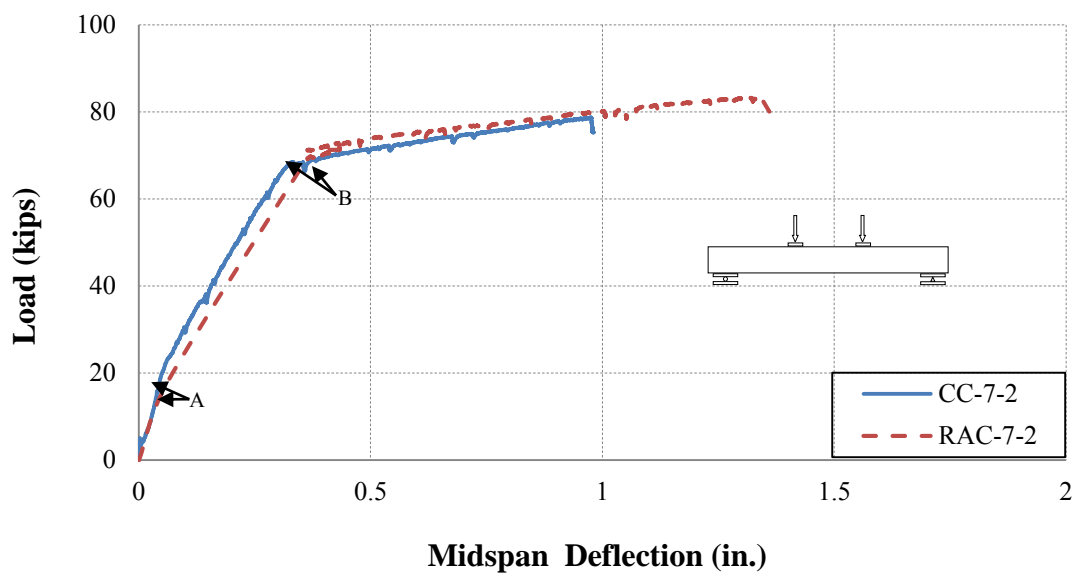
Table 4.1 summarizes the compressive strength of both the CC and RAC beams at time of testing, cracking moment, M_{cr} (**Equation 4.1**), yielding moment, M_y , nominal flexural strength, M_n (**Equation 4.2**), yielding deflection, δ_y , and ultimate deflection, δ_u .

$$M_{cr} = \frac{f_r \times I_g}{y_t} \quad (4.1)$$

$$M_n = \rho f_y b d^2 \left(1 - .59 \rho \frac{f_y}{f_c}\right) \quad (4.2)$$



F-6



F-7

Figure 4.2: Load-Deflection of the Test Beams

Table 4.1: Test Results Summary

Section			f'_c	M_{cr}	M_{cr}	M_y	M_y	M_n	M_n	δ_y	δ_u
			(Test)	(Test)	(Predicted)	(Test)	(Predicted)	(Test)	(Predicted)	(Test)	(Test)
			psi	kips-in.						in.	
CC	F-6	1	5400	32.0	29.8	91.1	88.9	113.7	91.4	0.3	1.3
		2	4960	31.5	28.6	89.6	88.4	116.1	91.1	0.3	1.3
	F-7	1	5400	34.5	29.8	109.1	108.5	126.0	111.7	0.3	1.2
		2	4960	33.5	28.6	108.3	108.1	121.2	111.2	0.3	1.1
RAC-100	F-6	1	4450	25.5	26.9	88.0	88.0	110.4	110.3	0.4	1.4
		2	4550	26.5	27.5	92.5	88.5	114.3	110.7	0.4	1.4
	F-7	1	4450	31.0	26.9	108.8	107.7	127.4	90.4	0.3	1.4
		2	4550	31.5	27.5	109.4	108.1	124.9	90.7	0.3	1.3

The code prescribed equations underestimate the cracking moment for both the CC and RAC beams by 13% and 5%, on average, respectively. Although the equation overestimates the value for RAC-100-F-6 beams by approximately 5%. In terms of ultimate moment, the experimental moments for both the CC and RAC beams are 18% and 20% higher than the code provisions, respectively.

The RAC beams showed higher ultimate deflection compared with the CC beams, approximately 5% for F-6 and 22% for F-7 beams. This phenomena has been reported by other researchers (Maruyama et al., 2004; Sato et al., 2007; Ajdukiewicz et al., 2007) and is generally attributed to lower modulus of elasticity and also lower effective moment of inertia (increased flexural cracking) of the RAC beams compared with the CC beams.

4.5. COMPARISON OF TEST RESULTS WITH FLEXURAL TEST DATABASE

Figure 4.3 presents the normalized flexural strength versus normalized longitudinal reinforcement ratio for the beams of this study as well as the wealth of flexural test data available in the literature for CC (Leet et al., 1997). **Figure 4.3** seems to

indicate that the RAC and CC test results fall within the upper bound and central portion of the data. Furthermore, statistical analysis (regression analysis) of the data indicates that the RAC and CC test results fall within a 95% confidence interval of a nonlinear regression curve fit of the database. This result indicates that the test values are very consistent with the wealth of flexural test data available in the literature and that the RAC beams possess equivalent flexural strength compared to CC beams.

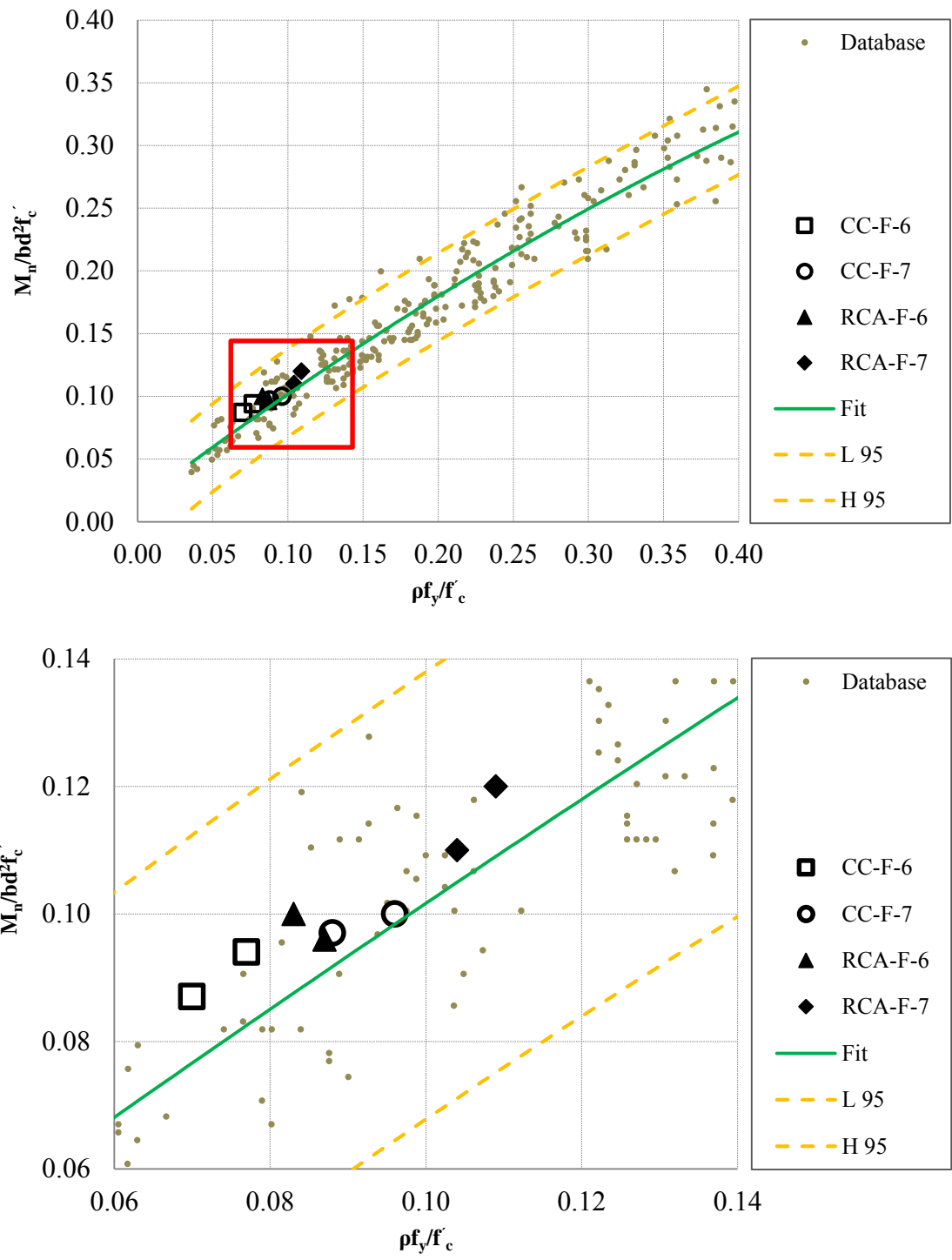


Figure 4.3: Normalized Flexural Strength vs. Normalized Longitudinal Reinforcement Ratio; Results from (Leet et al., 1997) and Test Results of this Study

5. FINDINGS, CONCLUSIONS, AND RECOMMENDATIONS

The main objective of this research study was to evaluate the flexural behavior and response of RAC through material, component, and full-scale testing. The main feature of the experimental program consisted of eight tests performed on full-scale reinforced concrete beams. The principal parameters investigated were: (1) concrete type – RAC vs. CC, and (2) amount of longitudinal (flexural) reinforcement. The behavior of the RAC was examined in terms of crack progression, crack morphology and failure mode; load-deflection response; comparison with identical CC specimens; comparison with predicted strengths from design standards; and comparison with a flexural test database of CC specimens. This section contains the findings of the test program as well as conclusions and recommendations.

5.1. FINDINGS AND CONCLUSIONS

Based on the results of this research study, the following findings are presented with regard to flexural behavior and the use of recycled concrete as aggregate:

- In terms of crack morphology and crack progression, the RAC beams experienced a larger number, and corresponding closer spacing, of flexural cracks compared to the CC beams.
- In terms of load deflection behavior, the RAC beams showed lower stiffness both before and after the cracking moments compared to the CC beams.
- The RAC beams experienced lower cracking moments (around 7%) compared to the CC beams.

- No significant difference was observed between the yielding moments of the RAC and CC beams.
- The RAC beams showed higher ultimate deflection compared with the CC beams.
- The RAC beams showed comparable flexural capacity with the CC beams.
- The CC and RAC test results fall within a 95% confidence interval of a nonlinear regression curve fit of the CC flexural test database.
- Existing design standards conservatively predicted the flexural capacity of the RAC beams.

Based on the findings of this research study, the following conclusions are drawn with regard to flexural behavior and the use of recycled concrete as aggregate:

- The double interfacial transition zone (ITZ) for the RAC results in lower cracking moments compared to CC.
- The double ITZ for the RAC results in a higher number, and thus closer spacing, of flexural cracks compared to CC.
- The higher mortar fraction of the RAC results in a lower modulus of elasticity and thus stiffness compared to the CC, although the reduction is on the order of only 5% for the mixes studied in this investigation.
- Although limited based on the number of variables tested in this study, it would appear that replacing 100% of the virgin aggregate with RCA does not result in any decrease in ultimate flexural capacity compared to CC mixes.

5.2. RECOMMENDATIONS

Due to the limited number of studies of the flexural behavior of RAC, further research is needed to make comparisons and conclusions across a larger database.

However, based on the findings and conclusions developed in this current study, the following preliminary recommendations are presented:

- Do not limit the percentage replacement of virgin aggregate with RCA based on ultimate flexural strength requirements, as it should not result in any noticeable decrease in capacity. Existing code provisions are applicable to concrete containing up to 100% RCA.
- Limit the percentage replacement of virgin aggregate with RCA to 50% where deflections or cracking are a serious design consideration.
- Additional testing is required to definitively determine whether RAC has the same flexural capacity compared to CC. This testing should investigate additional mix design variations, aggregate type and content, cross section aspect ratio, and type of loading. This database will then provide a basis for possible modifications to existing design standards.

BIBLIOGRAPHY

- Abbas, A., Fathifazl, G., Isgor, O.B., Razaqpur, A.G., Fournier, B., and Foo, S. (2006). "Proposed Method for Determining the Residual Mortar Content of Recycled Concrete Aggregates." CSCE 2006 Annual Conference, Calgary, Alberta, Canada.
- AASHTO LRFD, (2010). Bridge Design Specifications and Commentary (4th Ed.). American Association of State and Highway Transportation Officials. Washington, DC.
- AASHTO T 318 (2002). Water Content of Freshly Mixed Concrete Using Microwave Oven Drying. American Association of State Highway and Transportation Officials, Washington D.C.
- ACI Committee 211, (1991). Standard Practice for Selecting Proportions for Normal, Heavyweight, and Mass Concrete (ACI 211.1-91). American Concrete Institute, Farmington Hills, MI.
- ACI Committee 318, (2011). Building Code Requirements for Structural Concrete and Commentary (ACI 318-08). American Concrete Institute, Farmington Hills, MI.
- Ajdukiewicz, A. B., & Kliszczewicz, A. T. (2007). "Comparative tests of beams and columns made of recycled aggregate concrete and natural aggregate concrete." *Journal of Advanced Concrete Technology*, V. 5, No. 2, pp. 259-273.
- ASTM A370, (2011). Standard Test Methods and Definitions for Mechanical Testing of Steel Products. American Society for Testing Materials (ASTM International).
- ASTM A615/A615M (2009). "Standard Specification for Deformed and Plain Carbon-Steel Bars for Concrete Reinforcement" ASTM, West Conshohocken, PA, 6 pp.
- ASTM C127, (2007). Standard Test Method for Density, Relative Density (Specific Gravity), and Absorption of Coarse Aggregate. American Society for Testing Materials (ASTM International).
- ASTM C128, (2007). Standard Test Method for Density, Relative Density (Specific Gravity), and Absorption of Fine Aggregate. American Society for Testing Materials (ASTM International).
- ASTM C138, (2010). Standard Test Method for Density (Unit Weight), Yield, and Air Content (Gravimetric) of Concrete. American Society for Testing Materials (ASTM International).

- ASTM C192, (2007). Standard Practice for Making and Curing Concrete Test Specimens in the Laboratory. American Society for Testing Materials (ASTM International).
- ASTM C231, (2010). Standard Test Method for Air Content of Freshly Mixed Concrete by the Pressure Method. American Society for Testing Materials (ASTM International).
- ASTM C39/C39M, (2011). Standard Test Method for Compressive Strength of Cylindrical Concrete Specimens. American Society for Testing Materials (ASTM International).
- ASTM C469, (2002). Standard Test Method for Static Modulus of Elasticity and Poisson's Ratio of Concrete in Compression. American Society for Testing Materials (ASTM International).
- ASTM C496, (2004). Standard Test Method for Splitting Tensile Strength of Cylindrical Concrete Specimens. American Society for Testing Materials (ASTM International).
- ASTM C566, (1997). Standard Test Method for Total Evaporable Moisture Content of Aggregate by Drying. American Society for Testing Materials (ASTM International).
- ASTM C617, (2009). Standard Practice for Capping Cylindrical Concrete Specimens. American Society for Testing Materials (ASTM International).
- ASTM C78, (2009). Standard Test Method for Flexural Strength of Concrete (Using Simple Beam with Third-Point Loading). American Society for Testing Materials (ASTM International).
- ASTM E178, (2008). Standard Practice for Dealing with Outlying Observations. American Society for Testing Materials (ASTM International).
- Boresi, A.P., and Schmidt, R.J., (2003). Advanced Mechanics of Materials (6th Ed.). John Wiley & Sons.
- Choi, H. B., Yi, C. K., Cho, H. H., & Kang, K. I. (2010). "Experimental Study on the Shear Strength of Recycled Aggregate Concrete Beams." Magazine of Concrete Research, V.62 (2), pp.103-114.
- Fathifazl, G., Razaqpur, A. G., Isgor, O. B., Abbas, A., Fournier, B., & Foo, S. (2009). "Flexural performance of steel-reinforced recycled concrete beams." ACI Structural Journal, V. 106, No. 6, pp. 858-867.
- FHWA State of the Practice National Review (2004). "Transportation Applications Of Recycled Concrete Aggregate".

- Ignjatović, I. S., Marinković, S. B., Mišković, Z. M., & Savić, A. R. (2012) "Flexural behavior of reinforced recycled aggregate concrete beams under short-term Loading." *Materials and Structures*, V. 46, Issue 6, pp 1045-1059.
- Kikuchi, M., Mukai, T., & Koizumi, H. (1988). "Properties of concrete products containing recycled aggregate." In Proc., 2nd Int. Symp. on Demolition and Reuse of Concrete and Masonry, Vol. 2, pp. 595-604.
- Leet Kenneth and Bernal Dionisio (1997) "Reinforced Concrete Design" 3rd edition, McGraw Hill, New York, USA.
- Marotta, T.W., Coffey, J.C., LaFleur, C.B., and LaPlante, C., (2011). *Basic Construction Materials (8th Ed.)*. Pearson-Prentice Hall.
- Maruyama, I., Sogo, M., Sogabe, T., Sato, R., & Kawai, K. (2004) "Flexural properties of reinforced recycled concrete beams." In Internacional RILEM conference on the use of recycled materials in buildings and structures, Paper No. 315, Barcelona, Spain.
- Mindess, S., Young, J.F., and Darwin, D., (2003). *Concrete (2nd Ed.)*. Prentice Hall.
- Neville, A.M., (1997). *Properties of Concrete (4th Ed.)*. John Wiley & Sons.
- Nielsen, K.E.C., (1954). Effect of Various Factors on the Flexural Strength of Concrete Tests Beams. *Magazine of Concrete Research*, No. 15, pp. 105-114.
- Nilson, A.H., Darwin, D., and Dolan, C.W., (2004). *Design of Concrete Structures (13th Ed.)*. McGraw Hill.
- Park, R., and Paulay, T., (1975). *Reinforced Concrete Structures*. John Wiley & Sons.
- Sato, R., Maruyama, I., Sogabe, T., & Sogo, M. (2007) "Flexural behavior of reinforced recycled concrete beams." *Journal of Advanced Concrete Technology*, V. 5, No. 1, pp. 43-61.
- Wight, J.K., and MacGregor, J.G., (2009). *Reinforced Concrete Mechanics and Design (5th Ed.)*. Pearson-Prentice Hall.
- World Business Council for Sustainable Development (WBCSD) Report (2012). "Recycling concrete" <http://www.wbcdcement.org/index.php/key-issues/sustainability-with-concrete/54>, Accessed date: August 2013.